Unravelling the mechanisms of chemotherapy-induced cachexia and the potential of mitoprotective therapeutic strategies

By Dean Campelj (BSc Hons) Victoria University

A thesis presented in total fulfilment for the Degree of Doctor of Philosophy

Primary Supervisor: Dr. Emma Rybalka
Associate supervisors: Dr. Craig Goodman and Prof. Alan Hayes

Abstract

Chemotherapy is an effective first-line cancer-treatment to slow or even cure cancer. Despite it being widely used to treat a variety of cancers, the majority of agents used induce a myriad of serious sequalae. Recently, chemotherapy emerged as a key contributing factor to the induction of devastating wasting condition, cachexia. Cachexia involves the progressive loss of body mass, underscored by severe skeletal muscle wasting and dysfunction (skeletal myopathy). Unravelling the molecular mechanisms involved in the onset and persistence of chemotherapy-induced cachexia represents a complex scientific challenge and is of great clinical interest to identify novel drug targets and efficacious adjuvants.

This thesis characterised the impact of individual chemotherapeutic agents on the skeletal muscular system of mice [doxorubicin (DOX) and irinotecan (IRI), 5-fluorouracil (5FU)] and evaluated the therapeutic efficacy of mitoprotective adjuvant candidates, sodium nitrate (with DOX) and BGP-15 (for 5FU and IRI) to protect body mass and skeletal muscle during chemotherapy. Additionally, since chemotherapeutic agents are usually administered to cancer patients in combination regimens which might escalate cachexia, we also characterised the impact of the '7+3' (cytarabine and daunorubicin) chemotherapy induction regimen (CIR) utilised as standard treatment against acute myeloid leukemia. In this regard, we developed and characterised a novel murine model of AML CIR-induced cachexia. We also used this model to trace the course of cachexia during and after treatment and to evaluate whether voluntary exercise could be protective.

The major findings of thesis were that the onset and severity of chemotherapy-induced cachexia is agent/regimen specific. While DOX, an anthracycline and topoisomerase-II inhibitor, and IRI, a topoisomerase- I inhibitor, induced a cachectic phenotype characterised by diminished body composition indices, and skeletal myopathy, 5FU, an anti-metabolite, did not cause cachexia. Interestingly, the multi-agent CIR induced severe cachexia. The recovery post-CIR was mixed with skeletal muscle mass returning to normal levels, while body and lean mass not completely recuperating in the 2-week recovery period. At the molecular level, the expression of key structural

cytoskeletal proteins, i.e. dystrophin, were impacted by IRI and 5FU whether skeletal myopathy was observed or not. These data suggest that loss of dystrophin might be an early event in the myopathy associated with cachexia. With regard to the adjuvant candidates evaluated, sodium nitrate was not protective against DOX-induced cachexia, despite protecting against early signs of cardiomyopathy. BGP-15 displayed modest protection against IRI-induced cachexia but was not afforded the opportunity when evaluated in combination with 5FU. Alongside the CIR voluntary activity was not protective against cachexia, rather it potentiated CIR-induced cachexia, likely driven through enhanced loss of fat mass. Overall, these findings highlight that further investigation is required regarding the efficacy of mitoprotective adjuvant therapies against chemotherapy-induced cachexia.

Doctor of Philosophy Declaration

I, Dean George Campelj, declare that the PhD thesis entitled "Unravelling the mechanisms of chemotherapy-induced cachexia and the potential of mitoprotective therapeutic strategies" is no more than 80,000 words in length including quotes and exclusive of tables, figures, appendices, bibliography, references and footnotes. This thesis contains no material that has been submitted previously, in whole or in part, for the award of any other academic degree or diploma. Except where otherwise indicated, this thesis is my own work". "I have conducted my research in alignment with the Australian Code for the Responsible Conduct of Research and Victoria University's Higher Degree by Research Policy and Procedures.

Signature: [redacted] Date: 21/05/2021

Acknowledgements

I wish to acknowledge the contribution and support of my supervisors, Dr Emma Rybalka and Dr Craig Goodman throughout my PhD experience, you both helped mould me into the researcher I am today and I have unwavering gratitude for the time and effort you invested into my development. In particular, I extend my sincere appreciation to Emma who despite our ups and downs has supported and challenged me to become a highly capable scientist – I'm not sure I would have made it to the end without you. Also, I would like to thank Craig for stepping up his mentorship duties when Emma went on maternity leave and help open my eyes to the exciting world of molecular biology. I would also like to thank co-supervisor Prof Alan Hayes for all the background support and encouragement given over the journey, you were always someone I could rely on.

I would also like to acknowledge my peers Dr. Cara Alexandrescu, Dr. James Sorensen and Danielle Debruin from the EMU lab for their contribution to my PhD research experience, from hectic experiment days to the odd coffee. Additionally, I would like to thank the lab members of the Professor John Price's CBAM lab, in particular, Charlett Giuliani and Tabitha Cree, who helped me significantly across the ups and downs of my PhD journey, and, taught me patience through adversity when dealing with the dark art of western blotting. Lastly, I would like to thank Anne Luxford. Dr. Steve Holloway and Dr. Margaret Veale, for providing positivity and encouragement in my extended stays at the Werribee campus, and, to Valentina Jovanovska, Dr. Rachel McQuade and Dr. Matthew Cooke, for being supportive mentors throughout my experience.

I wish to express my sincere thanks to my parents, who gave me the foundation to chase my dreams, and, unapologetically, follow the beat to my own drum. To friends and family, who gave me unwavering support and provided an important social outlet throughout my whole PhD journey, thanks! I hope I made you proud and that you don't have to return the favour by reading past this section of my thesis.

VICTORIA UNIVERSITY

DETAILS OF INCLUDED PAPERS: THESIS WITH PUBLICATION

Please list details of each scholarly publication and/or manuscript included in the thesis submission. Copies of published scholarly publications and/or manuscripts submitted and/or final draft manuscripts should also be included in the thesis submission.

This table must be incorporated in the thesis before the Table of Contents.

Chapter No.	Publication Title	Publication Status • Published • Accepted for publication • In revised and resubmit stage • Under review • Manuscript ready for submission	Publication Details • Citation, if published • Title, Journal, Date of acceptance letter and Corresponding editor's email address • Title, Journal, Date of submission
1	Chemotherapy-induced myopathy: The dark side of the cachexia sphere.	Under Review	Campelj DG,Goodman CA, Rybalka E. Chemotherapy-induced myopathy: The dark side of the cachexia sphere. Submitted to Cancers: 20/05/2021. Scimago: Q1; IF: 6.126.
2	Sodium nitrate co-supplementation does not exacerbate low dose metronomic doxorubicin-induced cachexia in healthy mice.	Published	Campelj DG, Debruin DA, Timpani CA, Hayes A, Goodman CA, Rybalka E. Sodium nitrate co-supplementation does not exacerbate low dose metronomic doxorubicin-induced cachexia in healthy mice. Sci Rep. 2020 Sep 24;10(1):15044. doi:
3	The paradoxical effect of PARP inhibitor BGP-15 on irinotecan-induced cachexia and skeletal muscle dysfunction.	Published	Campelj DG, Timpani CA, Petersen AC, Hayes A, Goodman CA, Rybalka E. The Paradoxical Effect of PARP Inhibitor BGP-15 on Irinotecan-Induced Cachexia and Skeletal Muscle Dysfunction. Cancers (Basel). 2020 Dec 17;12(12):3810. doi:
4	Metronomic 5-fluorouracil delivery primes skeletal muscle for myopathy but does not cause cachexia.	Published	Campelj DG, Timpani CA, Cree T, Petersen AC, Hayes A, Goodman CA, Rybalka E. Metronomic 5-Fluorouracil Delivery Primes Skeletal Muscle for Myopathy but Does Not Cause Cachexia. Pharmaceuticals. 2021; 14(5):478.
5	Cachectic muscle wasting in Acute Myeloid Leukemia: A sleeping giant with dire clinical consequences.	Under Review	Campalj DG, Timpani, CA, Rybalka, E. Cachectic muscle wasting in Acute Myeloid Leukemia: A sleeping gian with dire clinical consequences. Journal of Cachexia, Sarcopenia and Muscle. Submitted: 13/05/2021. Scimago: Q1; IF=9.802.
6	The Acute Myeloid Leukemia '7+3' chemotherapy induction regimen induces cachexia and impairs voluntary activity in healthy mice	Manuscript ready for submission	Campelj, DG, Timpani, CA, Goodman, CA, Rybalka, E. The Acute Myeloid Leukemia '7+3' chemotherapy induction regimen induces cachexia and impairs voluntary activity in healthy mice.

Declaration by [candidate name]: Dean Campelj

Signature: Dean Campelj — Digitally signed by Dean Campelj Date: 2021.05.21 13:58:15 +10'00'

Date: 21/05/2021

Updated: September 2020

PRIVACY STATEMENT Victoria University (VU) values your privacy and is committed to handling your personal information in accordance with the Privacy and Data Protection Act 2014 (Vic) and other applicable privacy legislation. The personal information collected on this form will be used primarily for the purposes of assessing and processing this application. VU may also use and disclose your personal information to verify the information provided by you, to comply with government and other reporting requirements and/or to carry out associated activities connected with this application. Your personal information may also be disclosed to Commonwealth and State agencies such as the Department of Education and Training and the Department of Home Affairs in accordance with VU's obligations under the Education Services for Overseas Students Act 2000 (Cth) (ESOS Act), the National Code of Practice for Providers of Education and Training to Overseas Students 2018 (National Code) and other applicable legislation. Your personal information will not otherwise be used or disclosed without your consent, unless permitted by law. By completing and submitting this application, you agree to VU collecting, using and disclosing your personal information as described above and in accordance with VU's Privacy Policy and Student Information Privacy Collection Statement (which provides further detail about the types of personal information VU may collect from you and how it is managed) available on the Privacy page on our website vu.edu.au/privacy You have a right to access your personal information n held by VU. If you have any questions regarding privacy, please refer to the Privacy page on our website, our frequently asked questions at ASKVU or phone us on 9919 6100 or 1300 VIC UNI (or 1300 842 864).

PRIVACY INFORMATION: We collect and protect your personal information in accordance with our Privacy Policy vu.edu.au/privacy.

Victoria University CRICOS Provider No. 00124K (Melbourne) and CRICOS Provider No. 02475D (Sydney). RTO Code: 3113. ABN: 83 776 954 731

Table of Contents

List of Abbreviations

5FU	5-fluorouracil
ACT	Voluntary activity
AML	Acute Myeloid Leukemia
ARA-C	Cytarabine
CIR	Chemotherapy induction regimen
CNS	Central nervous system
CRC	Colorectal cancer
CSA	Cross-sectional area
DAPC	Dystrophin-associated protein complex
DAU	Daunorubicin
DMD	Duchenne Muscular Dystrophy
DOX	Doxorubicin
EDL	*extensor digitorum longus*
EPI FAT	epididymal fat pad
GSN	*gastrocnemius*
H&E	Hematoxylin & Eoisin
HCT	Haematocrit
HGB	Haemoglobin
HRT	Heart
HSCT	Haematopoietic stem-cell transplantation
HSP-70	Heat shock protein-70
IRI	Irinotecan
KIDS	Kidneys
LEU	Leucovorin
LIV	Liver

MAPK	Mitogen-activated protein kinase
MTD	Maximum tolerable dose
NF-κB	Nuclear factor kappa-light-chain-enhancer of activated B cells
OXA	Oxaliplatin
PARP-1	Poly (ADP-ribose) polymerase-1
PLNT	*plantaris*
QOL	Quality of Life
QD	*quadriceps*
RBC	Red blood cell
SED	Sedentary activity
SN	Sodium nitrate
SOL	*soleus*
SPL	Spleen
TA	*tibialis anterior*
VEH	Vehicle

Part I

Investigating the impact of chemotherapeutic agents on skeletal muscle and potential protective adjuvant strategies

Chapter 1

Chemotherapy-induced myopathy: The dark side of the cachexia sphere

Campelj DG, Goodman CA, Rybalka E. Chemotherapy-induced myopathy: The dark side of the cachexia sphere. Submitted: Cancers; 20/05/2021.

VICTORIA UNIVERSITY

THE NEW WAY TO DO UNI

OFFICE FOR RESEARCH TRAINING, QUALITY AND INTEGRITY

DECLARATION OF CO-AUTHORSHIP AND CO-CONTRIBUTION: PAPERS INCORPORATED IN THESIS

This declaration is to be completed for each conjointly authored publication and placed at the beginning of the thesis chapter in which the publication appears.

1. PUBLICATION DETAILS (to be completed by the candidate)

Title of Paper/Journal/Book: Chemotherapy-induced skeletal myopathy: The dark side of the cachexia sphere

Surname: Campelj First name: Dean

Institute: Institute for Health and Sport Candidate's Contribution (%): 80

Status:

Accepted and in press: ☐ Date:

Published: ☐ Date:

2. CANDIDATE DECLARATION

I declare that the publication above meets the requirements to be included in the thesis as outlined in the HDR Policy and related Procedures – policy.vu.edu.au.

Dean Campelj Digitally signed by Dean Campelj Date: 2021.05.21 12:05:38 +10'00'

Signature **Date**

3. CO-AUTHOR(S) DECLARATION

In the case of the above publication, the following authors contributed to the work as follows:

The undersigned certify that:

1. They meet criteria for authorship in that they have participated in the conception, execution or interpretation of at least that part of the publication in their field of expertise;
2. They take public responsibility for their part of the publication, except for the responsible author who accepts overall responsibility for the publication;

3. There are no other authors of the publication according to these criteria;

4. Potential conflicts of interest have been disclosed to a) granting bodies, b) the editor or publisher of journals or other publications, and c) the head of the responsible academic unit; and

5. The original data will be held for at least five years from the date indicated below and is stored at the following **location(s)**:

Victoria University R Drive

Name(s) of Co-Author(s)	Contribution (%)	Nature of Contribution	Signature	Date
Craig A Goodman	10	Conception, supervision, methodological resources, manuscript review and editing	[redacted]	18/05/21
Emma Rybalka	10	Conception, supervision, funding, methodological resources,		18/05/21

Updated: September 2019

cancers

MDPI

Review

Chemotherapy-Induced Myopathy: The Dark Side of the Cachexia Sphere

Dean G. Campelj [1,2], Craig A. Goodman [2,3] and Emma Rybalka [1,2,4,*]

[1] Institute for Health and Sport, Victoria University, Melbourne, VIC 8001, Australia; dean.campelj@live.vu.edu.au
[2] Inherited and Acquired Myopathy Program, Australian Institute for Musculoskeletal Science (AIMSS), Victoria University, St Albans, VIC 3021, Australia; craig.goodman@unimelb.edu.au
[3] Centre for Muscle Research (CMR), Department of Physiology, The University of Melbourne, Parkville, VIC 3010, Australia
[4] Department of Medicine—Western Health, Melbourne Medical School, The University of Melbourne, Melbourne, VIC 3021, Australia
* Correspondence: emma.rybalka@vu.edu.au

Simple Summary: In addition to cancer-related factors, anti-cancer chemotherapy treatment can drive life-threatening body wasting in a syndrome known as cachexia. Emerging evidence has described the impact of several key chemotherapeutic agents on skeletal muscle in particular, and the mechanisms are gradually being unravelled. Despite this evidence, there remains very little research regarding therapeutic strategies to protect muscle during anti-cancer treatment and current global grand challenges focused on deciphering the cachexia conundrum fail to consider this aspect—chemotherapy-induced myopathy remains very much on the dark side of the cachexia sphere. This review explores the impact and mechanisms of, and current investigative strategies to protect against, chemotherapy-induced myopathy to illuminate this serious issue.

Abstract: Cancer cachexia is a debilitating multi-factorial wasting syndrome characterised by severe skeletal muscle wasting and dysfunction (i.e., myopathy). In the oncology setting, cachexia arises from synergistic insults from both cancer–host interactions and chemotherapy-related toxicity. The majority of studies have surrounded the cancer–host interaction side of cancer cachexia, often overlooking the capability of chemotherapy to induce cachectic myopathy. Accumulating evidence in experimental models of cachexia suggests that some chemotherapeutic agents rapidly induce cachectic myopathy, although the underlying mechanisms responsible vary between agents. Importantly, we highlight the capacity of specific chemotherapeutic agents to induce cachectic myopathy, as not all chemotherapies have been evaluated for cachexia-inducing properties—alone or in clinically compatible regimens. Furthermore, we discuss the experimental evidence surrounding therapeutic strategies that have been evaluated in chemotherapy-induced cachexia models, with particular focus on exercise interventions and adjuvant therapeutic candidates targeted at the mitochondria.

Keywords: cachexia; chemotherapy; exercise therapy; mitoprotection; muscle wasting; myopathy; pharmaceutical adjuvants; skeletal muscle

check for updates

Citation: Campelj, D.G.; Goodman, C.A.; Rybalka, E. Chemotherapy-Induced Myopathy: The Dark Side of the Cachexia Sphere. *Cancers* **2021**, *13*, 3615. https://doi.org/10.3390/cancers13143615

Academic Editors: Scott Bowen, Patricia Brum and David Wong

Received: 20 May 2021
Accepted: 14 July 2021
Published: 19 July 2021

1. Introduction

Chemotherapy constitutes a group of anti-neoplastic agents that were progressively discovered throughout the 19th century and became commonplace in oncological treatment as first-line or complementary therapeutic strategies for nearly all cancer types [1]. In general, chemotherapy targets cell cycle arrest through DNA-damage pathways that promote apoptotic cell death, although agents are heterogeneously stratified into different classes depending on their mode of action [2]. Independent of their different mechanisms, chemotherapies remain effective at inducing cancer cytotoxicity to abate the hyper-active

neoplastic cell cycle [3]. Despite exerting anti-cancer efficacy, chemotherapy also elicits detrimental off-target side-effects to otherwise healthy cells due to their non-specific cytotoxicity [4]. Systemic toxicities are pervasive in the blood cell population as well as the central and peripheral nervous, gastrointestinal, cardiovascular, and integumentary systems [5–8]. Over the past decade, interest has developed concerning the non-specific impact of chemotherapy-induced toxicity on the skeletal muscular system [9–11]. Specifically, chemotherapeutic agents reduce body mass concurrent with skeletal muscle atrophy and dysfunction (referred to herein, as cachectic myopathy). These side-effects are clinically evident during patient deconditioning in the oncological setting [12], where weight loss and fatigue are two key debilitating events prominent in metabolic wasting syndrome, cachexia [13].

Cachexia is a multifactorial condition characterised by the loss of body mass and composition (highlighted by lean mass loss, with or without loss of fat mass) and progressive functional impairment [14]. The centrally afflicted organ in cachexia is skeletal muscle, which is driven by a multitude of factors including metabolic dysregulation; anorexia; systemic inflammation; and insulin resistance [15]. Skeletal muscle mass is an integral prognostic marker in cancer cachexia diagnosis—this is because increased adiposity desensitises the utility of body weight and body mass index (a crude indicator of body composition) during cachexia diagnosis [16,17]. Once instigated, cachectic myopathy propagates a vicious cycle involving increased risk of dose-related toxicities, which influences patient risk stratification and clinical decision making [18]. The result is compromised treatment efficacy (i.e., dose-reduction or treatment cessation) that increases the risk of morbidity and mortality [18]. Cachectic myopathy is the result of two synergistic insults from each of: (1) cancer–host interactions and (2) chemotherapy toxicity [15,19]. These effects can be acute, yet are most often life-long [20]. While the number of studies concerning cachexia is increasing exponentially, the proportion of these studies focusing on the impact of chemotherapy is far behind [9].

Overall, cancer cachexia represents a significant burden on patients and clinicians, with estimates suggesting that cachexia affects 50–80% of cancer patients and accounts for up to 20% of cancer deaths [21]. There are no current treatment options outside of standard nutrition interventions for body mass loss, which are largely unsuccessful [22,23]. Thus, cachexia is a significant unmet challenge in need of pre-clinical investigations to identify novel drug-targets and evaluate therapeutic interventions for clinical translation. Herein, we present a review of the literature surrounding experimental chemotherapy-induced cachexia, with particular focus on the skeletal muscle-specific side-effects and underlying mechanisms of myopathy. We also discuss the challenges associated with current experimental approaches used to investigate chemotherapy-induced cachexia and adjuvant strategies to protect against it.

2. Mechanisms of Chemotherapy-Induced Cachectic Myopathy

Chemotherapeutic agents work through different modes of action, which likely influences the degree to which they can induce cachectic myopathy. However, of the agents that do induce myopathy, there are some common underlying mechanisms [9]. It has been proposed that chemotherapy promotes systemic inflammation via the central nervous system, specifically through stimulation of the hypothalamus–pituitary–adrenal axis, to induce an adaptive illness response [24]. This response simultaneously induces the release of glucocorticoids and the production of pro-inflammatory cytokines (e.g., interleukin-1α and β, interleukin-6, and tumour necrosis factor-α (TNF-α)), which are both key events in the induction of skeletal muscle atrophy [25,26]. In particular, over-production of pro-inflammatory cytokines can directly induce skeletal muscle atrophy via engagement of membranous receptors and activation of a pro-catabolic transcription program [9,13]. Braun et al. proposes that instigation of the inflammatory milieu caused by chemotherapy increases activity of the gene, regulated in development and DNA damage response 1 (*REDD1*), which is associated with skeletal muscle atrophy [24]. REDD1 transcription

regulates the adaptive stress response including the activation of stress-sensitive molecular targets, nuclear factor kappa-light-chain-enhancer of activated B cells (NF-κB), and mitogen activated protein kinase (MAPK) [27,28]. These two targets share common signalling pathways during oxidant-induced stress [29]. In particular, MAPK activity promotes phosphorylation of the NF-κB subunit, p65, resulting in NF-κB activation and the induction of skeletal muscle atrophy [29]. This atrophic response is achieved primarily through the ubiquitin-proteasome system (UPS)-mediated transcription of classic atrogenes, the E3 ubiquitin ligases, MuRF-1, and Atrogin-1 [30,31]. Additionally, it has been demonstrated by our laboratory and others that several chemotherapeutic agents can promote reactive oxygen species (ROS) production in C2C12 myotubes, which is associated with impaired myotube morphometry [32–35]. These data suggest that stress-sensitive molecular targets could be common signalling pathways in chemotherapy-induced cachectic myopathy. Furthermore, excessive ROS production is associated with the onset of mitochondrial dysfunction, an event postulated to be the crucial trigger for the induction of skeletal muscle wasting by chemotherapy [36].

As well as through directly targeting differentiated skeletal muscle tissue, chemotherapeutic agents also target myoprogenitor activity (i.e., satellite cell replication), which impacts skeletal muscle growth, repair, and turnover (as reviewed by us previously [37]). Many chemotherapeutic agents arrest cell cycling as their principal mechanisms of action against rampant cancer cell proliferation, resulting in visible side-effects in high-turnover cells including hair, bone marrow, skin, and gastrointestinal epithelium. It has recently emerged that muscle satellite (stem) cells, which normally undergo rapid proliferation and differentiation in response to muscle damage (e.g., inflammation) and growth factors (e.g., growth hormone and androgens) are also impacted, contributing to the net loss of muscle mass observed during cancer-related cachexia [38–40].

The research to date has predominantly focused on three key chemotherapeutic agents to study the mechanisms that govern chemotherapy-induced cachectic myopathy: the anthracycline, doxorubicin (DOX); the platinum-based alkylating agent, cisplatin (cis-diamminedichloroplatinum(II) (CDDP)); and the anti-metabolite, 5-fluorouracil (5FU). As such, we will further explore the current understanding of the connection between these stress-signalling cascades and the induction of cachectic myopathy in the context of specific chemotherapeutic agents and/or regimens.

2.1. Doxorubicin (DOX)

DOX is a member of the anthracycline class of chemotherapies, and, as such, it elicits cytotoxicity via topoisomerase-II inhibition to induce DNA damage and cell cycle arrest [41]. Despite its potent anti-cancer efficacy, DOX is notorious for its cardiotoxic properties, which significantly limits its clinical utility [42]. Subsequently, there has been substantial interest in the effect of DOX on skeletal muscle health (summarised in Figure 1), particularly since skeletal muscle is an active compartment in the metabolism of DOX and its metabolites (e.g., DOX metabolite, doxorubicinol) is retained within skeletal muscle tissue for up to five days post-intravenous delivery [43,44]. The clinical implications of DOX administration are remarkable. Patients often present with debilitating fatigue, muscle weakness, and impaired ambulatory capacity [45,46]. At the cellular level, DOX treatment induces skeletal muscle dysfunction [47,48] characterised by reduced force production, impaired calcium (Ca^{2+}) dynamics, and increased susceptibility to physiological fatigue [47–49]. Importantly, Gilliam et al. highlighted that these symptoms are dependent on the activity of pro-inflammatory cytokine, TNF-α [50]. This pro-inflammatory scenario has been shown to promote pyroptosis, a biological process of programmed cell death, which is characterised by the nucleotide binding oligmerisation domain (NOD), leucine rich repeat-containing proteins (NLR) family member, NRLP3 inflammasome formation, and activation of apoptotic caspases [51,52]. Furthermore, TNF-α mediates skeletal muscle contractile dysfunction through enhanced ROS production [53], although this is considered to be an additive effect to DOX-induced oxidative stress. DOX can directly stimulate ROS

production through redox cycling at NADH dehydrogenase/Complex I of the mitochondrial electron transport chain [54]. As a result, ROS are produced, in particular superoxide anion radicals, via the reduction of DOX's quinone moiety to an unstable semiquinone [54]. This redox cycling significantly elevates skeletal muscle hydrogen peroxide (H_2O_2) emission without perturbing homeostatic antioxidant buffering capacity [55–57] and alters bioenergetic efficiency by impinging on the functionality of respiratory complexes, leading to modifications that promote oxidative damage (e.g., lipid peroxidation) [56,58]. Recent findings from the Hulmi group suggest that DOX-induced skeletal muscle perturbations are predominately influenced by enhanced transcription of *REDD1* as part of the transcriptional program regulated by oxidative stress sensitive tumour suppressor protein, p53, a master regulator of cellular homeostasis [59–61]. Interestingly, there are few data connecting the promotion of inflammatory cytokines and oxidative stress from DOX to increased NF-κB activity in skeletal muscle, which is a downstream target of REDD1 transcription. Supriya et al. showed that DOX potentiated NF-κB activity in the skeletal muscle of diabetic mice [62]. The authors suggested that several mechanisms downstream of REDD1 were likely contributing [62].

Enhanced oxidative damage from DOX administration induces modifications that increase the catabolism of myofibrillar proteins, in particular actin and myosin, two integral proteins of the contractile apparatus [33,63]. The pro-catabolic signalling-cascade potentiated by DOX can activate multiple proteolytic systems including the UPS, autophagy, apoptotic caspases, and Ca^{2+}-dependent proteases (i.e., calpains) [56,63,64]. The pro-catabolic shift in skeletal muscle protein balance has led to the consensus that DOX can cause skeletal muscle mass loss [11]. While DOX mechanisms are largely centred around proteolysis, there is also a rationale to suggest DOX impairs anabolism. This is highlighted by a reduced rate of protein synthesis independent of the classical signalling of mechanistic target of rapamycin complex 1 (mTORC1) [59], a key mediator of protein synthesis (for extensive review see [65]). There is also some evidence that DOX administration can impair the regenerative capacity of muscle through inhibiting satellite cell proliferation [66]. These data implicate alternative pathways that regulate protein synthesis during DOX administration. One such pathway was the activation of the endoplasmic reticulum stress/unfolded protein response signalling cascade, which can negatively regulate protein synthesis [67]. However, there were divergent responses between different types of striated muscle (i.e., heart, diaphragm, and limb skeletal muscles) and the expression of markers involved in this signalling cascade, elicited by DOX [55,68]. Thus, further research is required to enrich the understanding of the processes regulating the skeletal muscle protein balance during DOX treatment.

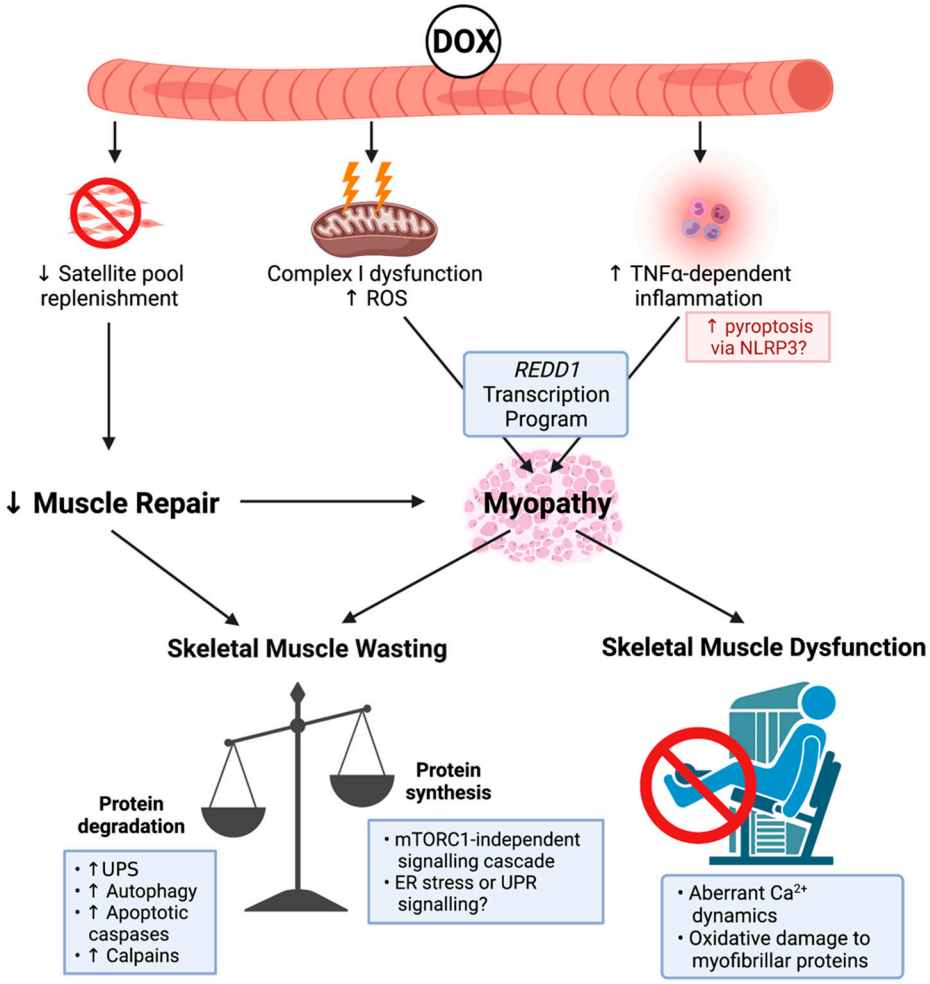

Figure 1. Known mechanisms of doxorubicin (DOX)-induced cachectic myopathy. DOX promotes reactive oxygen species (ROS) production primarily via Complex I dysfunction, which induces mitochondrial dysfunction and tumour-necrosis factor-α (TNF-α)-dependent inflammation, which can promote pyroptosis via increased nucleotide binding oligmerisation domain, leucine rich repeat-containing protein 3 (NLRP3) inflammasome formation, and activation of apoptotic caspases. This stimulates a regulation in the development and DNA damage response 1 (REDD1) transcription program, which overarches DOX-induced cachectic myopathy. DOX also reduces the replenishment of the satellite cell pool, which contributes to cachectic myopathy through impaired muscle repair. Underlying skeletal muscle wasting, DOX increases protein degradation via the ubiquitin-proteasomal system (UPS), autophagy, apoptotic caspases, and the calcium (Ca^{2+})-dependent proteases, calpains, while also reducing protein synthesis in a mammalian target of rapamycin complex 1 (mTORC1)-independent manner. While the exact mechanism has not been fully elucidated, endoplasmic reticulum (ER) stress or the unfolded protein response (UPR) signalling may be contributing factors. DOX also alters Ca^{2+} dynamics and promotes oxidative damage to myofibrillar proteins causing skeletal muscle dysfunction. Created with biorender.com (accessed on 6 July 2021).

2.2. Cisplatin (CDDP)

CDDP is a platinum-based alkylating agent that enhances DNA damage via the aquation of its chloride ligands to form a highly reactive mono-aquated complex. This complex can bind with DNA residues to develop CDDP-DNA adducts, which induce DNA crosslinking and cell cycle arrest [69]. CDDP administration is associated with several toxicities, notably nephrotoxicity and neurotoxicity [70,71]. However, it also has deleterious impact on skeletal muscle (critically reviewed in detail previously [10,72]). CDDP was originally considered a potent inducer of negative protein balance—predominantly through impacting caloric intake (i.e., food consumption), which drives protein degradation to reduce body and skeletal muscle mass [73] (Figure 2). Importantly, Sakai et al. demonstrated that CDDP can drive protein degradation independently of caloric intake (through using pair-fed controls), in part, via an Akt and forkhead box O (FoxO)-dependent signalling cascade that enhances the transcription of atrogenes MuRF-1 and Atrogin-1 [74] while synergistically activating other constituents of the UPS [75]. CDDP also promotes the accumulation of autophagosomes (an indicator of autophagy-lysosome system dysregulation) via a similar, although currently undefined, Akt/FoxO3a-dependent mechanism [34,76,77]. Furthermore, CDDP suppresses protein synthesis via a protein kinase B (Akt)-dependent mechanism, which leads to the de-phosphorylation of $p70^{S6k1}$, a downstream target of mTORC1 [78]. Thus, muscle anabolism signalling also appears to be impacted by CDDP (Figure 2). Damreuer et al. demonstrated that CDDP-mediated atrogene transcription occurs in response to trans-activation of NF-κB, specifically through the heterodimerisation of key subunit proteins, p50 and p65 [79]. Enhanced proteolysis induced by CDDP underscores skeletal muscle wasting, and this was initially thought to be the driver of functional decline [80]. However, recent findings from Conte et al. demonstrate that CDDP also dysregulates Ca^{2+} ion homeostasis, which is necessary for optimal skeletal muscle function [81]. CDDP increases the intracellular concentration of Ca^{2+}, compromises Ca^{2+} dynamics, and de-sensitises the excitability of action potentials, resulting in reduced force production [82]. CDDP-induced oxidative stress is also thought to contribute to a dysfunctional contractile apparatus, although the underlying mechanisms are presently unclear. Sirago et al. proposed that CDDP drives H_2O_2 production and oxidative stress based upon evidence of increased peroxiredoxin (PRX) sulphonylation in skeletal muscle [77,83], which is also central to CDDP's anti-cancer properties [84]. This mechanism has fascinating potential for therapeutic intervention given that PRX suppression is a key stimulant for NF-κB trans-activation [85], a critical target for CDDP-induced myopathy [9].

While CDDP is the predominate platinum-based chemotherapeutic agent experimentally evaluated for its effect on skeletal muscle health, our laboratory and others have demonstrated that analogues, carboplatin [86,87] and oxaliplatin (OXA) [88–90] can also contribute to the induction of cachectic myopathy. A complicating factor in the research surrounding platinum-based agents is the reliance on solvent, dimethyl sulphoxide (DMSO), to prepare experimental drug solutions. Using DMSO to deliver the chemotherapeutic agents CDDP and carboplatin suppresses their relative cytotoxicity in cell culture, whereas the cytotoxicity elicited by OXA is not impacted [91,92]. This highlights the complexity of interpreting the experimental data surrounding platinum-based complexes in comparison to vehicle control groups that do not disclose information regarding DMSO utilisation, an all too common feature in the accumulated literature thus far [92].

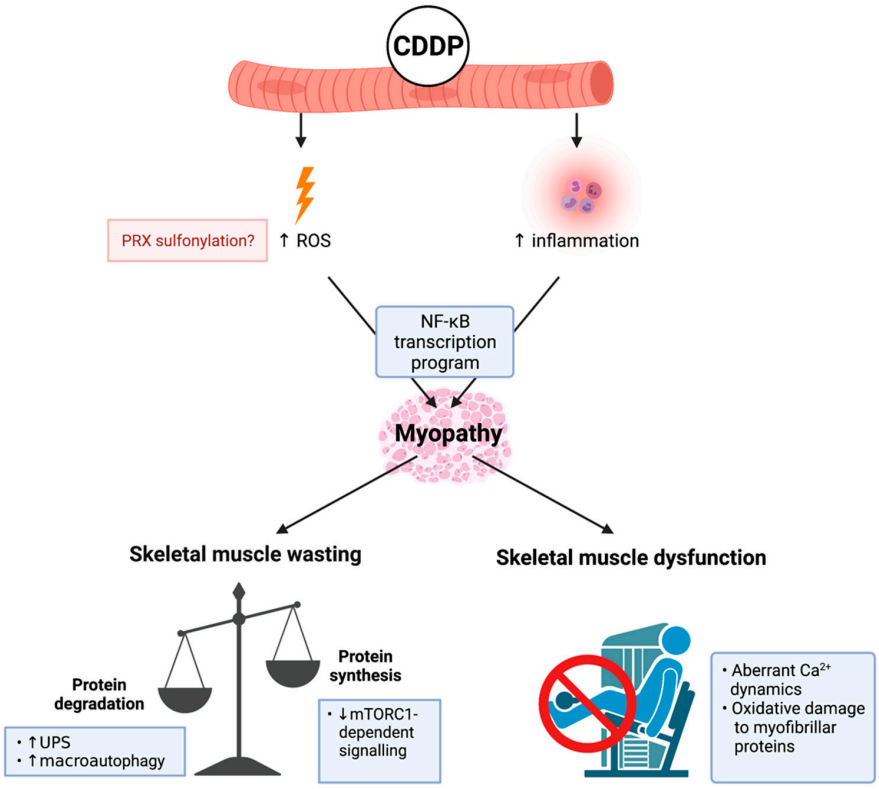

Figure 2. Known mechanisms of cisplatin (cis-diamminedichloropaltinum(II) (CDDP))-induced cachectic myopathy. CDDP promotes reactive oxygen species (ROS) production potentially through: (1) increased peroxiredoxin (PRX) sulphonylation; and (2) inflammation induced by pro-inflammatory cytokine mediated nuclear factor kappa-light-chain-enhancer of activated B cells (NF-κB) transcription program activation, which is a central mechanism of CDDP-induced cachectic myopathy. The underlying mechanism regulating CDDP-induced skeletal muscle wasting is increased protein degradation involving elevated ubiquitin-proteasomal system (UPS) activity and the promotion of macroautophagy. Additionally, there is evidence of reduced protein synthesis via mammalian target of rapamycin complex 1 (mTORC1)-dependent signalling cascades. CDDP induces skeletal muscle dysfunction through promoting aberrant calcium (Ca^{2+}) dynamics and oxidative damage to myofibrillar proteins. Created with biorender.com (accessed on 6 July 2021).

2.3. 5-Fluorouracil (5FU)

5FU is a chemotherapeutic agent from the anti-metabolite class that elicits cytotoxicity via: (1) the misincorporation of nucleotides into RNA and DNA; and (2) the inhibition of the nucleotide enzyme, thymidylate synthase. This leads to both DNA and RNA damage and cell cycle arrest [93]. 5FU is primarily utilised against colorectal cancer as a backbone constituent of multi-agent regimens. However, it can elicit debilitating side-effects independently [93], emphasised by gastrointestinal toxicities such as mucositis and enteric neuropathy [94–96]. With respect to the side-effects of 5FU on skeletal muscle, there is mixed evidence as to whether it can independently drive the loss of mass and function [97–99]. Interestingly, VanderVeen et al. demonstrated that 5FU administration impairs the homeostatic coordination of skeletal muscle repair and remodelling through reducing M1-like macrophage abundance [98]. This suggests that 5FU dysregulates monocyte recruitment and drives a shift towards a pro-fibrotic skeletal muscle microenvironment [98] (Figure 3). The Bonetto group have extensively demonstrated that the 5FU-based combination regimen, FOLFIRI [5FU, leucovorin (LV), and irinotecan (IRI)], can drive cachectic myopathy, with several mechanisms explored [35,100–103]. In skeletal muscle, FOLFIRI: (1) promotes the phosphorylation of MAPK isoforms, p38 and ERK1/2; (2) increases serum ROS levels; (3) reduces mitochondrial number and size; and (4) downregulates the ex-

pression of protein markers indicative of mitochondrial maintenance and turnover (i.e., biogenesis, fission, and fusion) [35,101,102]. Despite FOLFIRI inducing cachectic myopathy, the 5FU-based combination regimen FOLFOX [5FU, LV, and OXA] has limited impact on skeletal muscle [35]. While these data may be accounted for by methodological specifics concerning the treatment timeline and/or dosages of the FOLFOX constituents, it is an interesting observation when considered in context of findings from our laboratory. We have demonstrated that IRI (constituent of the FOLFIRI regimen) monotherapy induces cachectic myopathy [104], which is characterised by reduced expression of dystrophin, a key structural protein that connects the sarcolemma to the actin cytoskeleton and maintains cytoskeletal integrity [104]. Similarly, we recently demonstrated that 5FU monotherapy also reduces dystrophin protein expression, in addition to desmin, an intermediate filament that provides stability to sarcomeres. However, these cytoskeletal protein changes are not associated with overt cachectic myopathy or loss of function [99]. These findings highlight that: (1) 5FU may prime skeletal muscle for myopathy by reducing the abundance of key cytoskeletal structural proteins; and (2) these events (i.e., loss of dystrophin and other cytoskeletal proteins) apparently precede alterations to skeletal muscle mass or function (Figure 3). Our work suggests that cytoskeletal proteins may have potential as early biomarkers for chemotherapy-induced cachectic myopathy, although this requires further investigation to be confirmed.

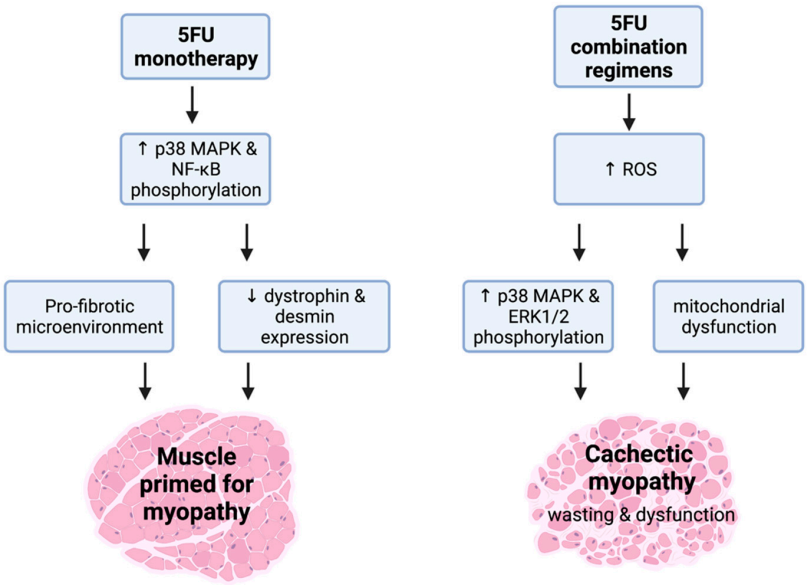

Figure 3. (5FU)-related cachectic myopathy. 5FU monotherapy promotes the phosphorylation of atrophic regulators, p38 mitogen activated protein kinase (MAPK), and nuclear factor kappa-light-chain-enhancer of activated B cells (NF-κB). These mechanistic targets are likely to be stimulated via signalling modulators including reactive oxygen species (ROS). 5FU does induce a pro-fibrotic skeletal muscle microenvironment and reduces the expression of the key cytoskeletal proteins, desmin and dystrophin, which suggests that 5FU primes muscle for cachectic myopathy. Interestingly, when additional chemotoxic insult to skeletal muscle occurs alongside 5FU such as in 5FU combination regimens, the induction of cachectic myopathy is observed. This is underscored by increased ROS production that stimulates the phosphorylation of p38 MAPK and ERK1/2 alongside mitochondrial dysfunction, leading to skeletal muscle wasting and dysfunction. Created with biorender.com (accessed on 6 July 2021).

2.4. Other Chemotherapeutic Agents

Several other chemotherapeutic agents have been investigated for their impact on skeletal muscle, albeit to a far lesser extent than DOX, CDDP, and 5FU. Distinct from platinum-based alkylating agents, chemotherapies arising from the alternative alkylating agent classes such as nitrosourea (i.e., cystemustine (CMN)) and nitrogen mustard (i.e., cyclophosphamide (CYP)) have also been investigated for their effect on skeletal

muscle [73,105–107]. Interestingly, in cancer-free mice, CMN acutely reduces body mass, and, while post-chemotherapy catch-up growth is evident, skeletal muscle mass does not completely recover [106]. However, in tumour-bearing mice, the effect of CMN manifests differently. CMN treatment (10 days) reduces skeletal muscle mass, albeit, paradoxically, concurrent with enhanced protein synthesis and reduced proteasome-dependent proteolysis at the molecular level [105,106]. These data perhaps reflect an ongoing, yet unsuccessful, attempt to recover skeletal muscle mass in response to CMN treatment. Similar to CMN, CYP administration induces an acute loss of body mass followed by compensatory catch-up growth in cancer-free mice, but skeletal muscle mass loss is only mildly impacted [107]. However, CYP reduces ambulatory capacity and skeletal muscle adenosine triphosphate (ATP) production through impairing mitochondrial function [107]. CYP may also impact skeletal muscle through inducing neutropenia (CYP is used experimentally to generate rodent models of neutropenia) [108], possibly through impacting skeletal muscle repair and remodelling efficiency. A similar effect has been reported for 5FU [98].

Gemcitabine (GCB) is a chemotherapeutic agent from the anti-metabolite class, which has often been experimentally investigated as part of a combination regimen with CDDP consistent with its clinical utility for the treatment of metastatic cancers [109–111]. Given the extensive evidence supporting that CDDP treatment induces cachectic myopathy [10,72], it is currently unclear as to what extent (if at all) GCB contributes. Current evidence demonstrates that the CDDP and GCB combination potentiates tumour-induced skeletal muscle mass loss and proteolytic activity, while GCB alone has no impact [112–114]. This does not rule out the possibility that GCB exacerbates the effects of CDDP in skeletal muscle. Another chemotherapeutic agent from the anti-metabolite class is methotrexate (MTX), which is not only utilised in cancer, but in hyper-inflammatory conditions such as rheumatoid arthritis [115]. There are no data available surrounding the effect of MTX on skeletal muscle health in cancer-based models. However, in a mouse model of diabetes, MTX was shown to elicit benefits on skeletal muscle glucose metabolism [116,117]. These findings suggest that chemotherapeutic agents from the anti-metabolite class display a modest myotoxic profile compared to other chemotherapy classes.

Mitotic inhibitors are a class of chemotherapeutic agents that have been investigated for their effect on skeletal muscle, in particular taxanes and vinca alkaloids [118]. These drugs are known for their microtubule de-stabilising properties and potent neurotoxicity [119–121]. Docetaxel (DTX) is a taxane-based chemotherapy that demonstrably reduces skeletal muscle mass. This effect is evidenced by serum markers of malnutrition and inflammation, and a pro-catabolic transcriptional program, yet skeletal muscle contractile function is not affected [122,123]. Paclitaxel (PTX) is another taxane-based agent, albeit not extensively investigated with respect to skeletal muscle. Ramos et al. highlighted the capacity of PTX to alter skeletal muscle microtubule architecture observed through α-tubulin disorganisation [118]. Additionally, alterations to microtubules by PTX are suggested to be underpinned by impaired adenosine diphosphate (ADP)-dependent bioenergetics via the binding of tubulin to the mitochondrial ADP/ATP exchanger voltage-dependent anion channel (VDAC) [118]. Ramos et al. also studied the vinca alkaloid, vinblastine (VBL), and demonstrated a similar capacity to alter tubulin architecture. However, distinct from PTX, the connection with impaired ADP bioenergetics is seemingly independent of the interaction between tubulin and VDAC [118]. Rather, the mechanism may be reflective of the lesser-known role of VBL as an inhibitor of microtubule-associated proteins, 1A/1B light chain 3B (LC3B)-II, degradation. Thus, VBL is a likely suppressor of auto-lysosomal maturation and autophagic flux [124]. Further investigation of taxanes and vinca alkaloids with regard to skeletal muscle health is warranted, given the association with microtubule perturbations and induction of dystrophic phenotypes [125].

3. Therapeutic Strategies to Mitigate Chemotherapy-Induced Cachectic s Myopathy: An Update

Currently, cachexia represents a significant unmet challenge in cancer, with no treatment approved for clinical use. This is likely due to the complexity of the syndrome,

especially at the skeletal muscle level. There are multiple contributing factors to the induction of myopathy during anti-cancer therapy. For example, muscle deconditioning due to hospitalisation-dependent factors such as prolonged periods of bed rest, reduced opportunity to undertake physical activity, and depressive mood/fatigue could contribute significantly to cachexia progression during chemotherapy administration [126]. Several investigations into therapeutic strategies to mitigate the debilitating effects of cancer cachexia are underway with multiple candidates showing promise. These include exercise and multi-target pharmaceutical/nutraceutical adjuvant interventions [127,128] (Figure 4). Herein, we summarise the current knowledge and provide insights surrounding these candidate strategies to better inform future investigations. In particular, this section will focus on therapeutic strategies that elicit protection against mitochondrial dysfunction, a key mechanistic event in the induction of cachectic myopathy [129,130]. Specifically, mitochondrial degeneration is suggested as an event preceding muscle wasting in cachexia [131], and thus is a prime therapeutic target for early intervention.

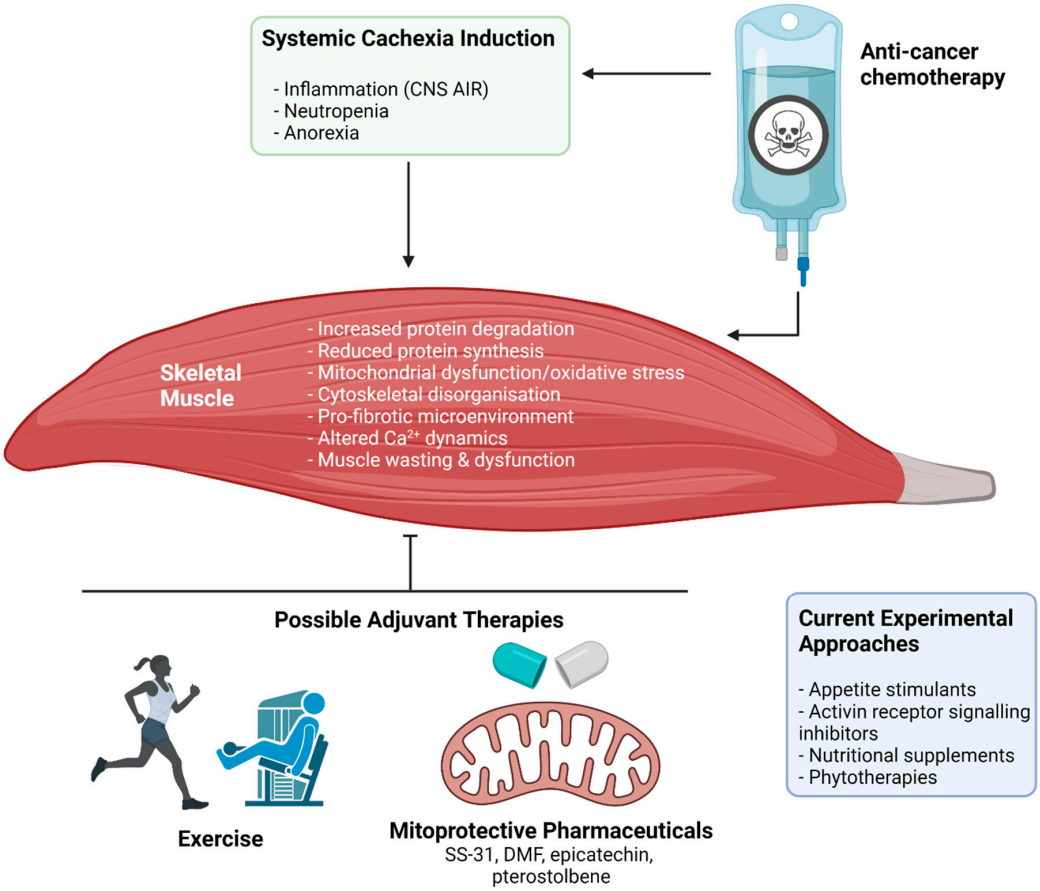

Figure 4. The impact of anti-cancer chemotherapy treatment on cachectic myopathy and possible protective therapeutic interventions. Broadly, chemotherapeutic agents used in clinical cancer treatment can both directly and indirectly target skeletal muscle through induction or amplification of systemic cachexia. The result is the initiation of a wasting and dysfunction program within skeletal muscle, involving: increased muscle protein degradation, reduced protein synthesis, mitochondrial dysfunction and oxidative stress, cytoskeletal disorganisation and reduction of key cytoskeletal proteins that stabilise the muscle membrane, pro-fibrotic signalling within the extracellular matrix, and altered calcium (Ca2+) dynamics. The result is muscle wasting and dysfunction that leaves patients weak and fatigued, which affects their capacity to undertake activities of daily living and reduces quality of life. Several potential therapeutic approaches are currently being investigated to protect against or treat these symptoms including appetite stimulants, activin receptor signalling inhibitors, nutritional supplements, and phytotherapies. Novel therapeutic strategies could include exercise and mitoprotective compounds (e.g., SS-31, BGP-15, dimethyl fumarate (DMF), epicatechin, and pterostilbene). Abbreviations: CNS AIR: central nervous system acute illness response. Created with biorender.com (accessed on 6 July 2021).

3.1. Exercise Interventions

Exercise is a non-pharmacological and cost-effective strategy that is currently being investigated for therapeutic purposes against cachexia. The therapeutic potential of exercise in the cancer setting is multi-faceted, but includes both modulation of systemic inflammation and regulatory control of the redox balance [130], two inherently related mechanisms that drive cachexia [129]. These mechanisms are also prominent drivers of chemotherapy-induced cachectic myopathy. Thus, exercise interventions could prevent the atrophy and loss of function associated with anti-cancer chemotherapy treatment. As such, exercise has been investigated in experimental models exploring its efficacy to mitigate the impact of chemotherapy (particularly DOX) on skeletal muscle health (summarised in Table 1). In general, exercise has shown modest protective efficacy against the loss of skeletal muscle mass and functionality from chemotherapy administration [132]. Smuder proposes that this is linked to the capacity of exercise to promote endogenous antioxidant expression, protein chaperoning via heat shock protein-70 (HSP-70) to mitigate proteolytic activity, and increased multi-drug resistant proteins [133]. It is important to note that the majority of studies listed in Table 1 employed exercise as a pre-conditioning strategy prior to the administration of DOX, demonstrating the capacity of exercise to prime skeletal muscle to resist DOX-induced stress [63,64,134–138]. However, the clinical compatibility of this approach is questionable since cancer treatment would need to be delayed while muscles were conditioned using exercise programs. There is also a lack of data on the efficacy of pre-treatment exercise strategies for other chemotherapeutic agents aside from DOX. Jones and Alfano highlight a paucity of clinical studies investigating the utility of exercise interventions in the pre-treatment stage [139]. Rather, exercise interventions throughout the cancer survivorship continuum have predominantly been studied during and post-chemotherapy treatment, as per the adapted Physical Exercise Across the Cancer Experience (PEACE) framework [139]. To date, only four pre-clinical studies have investigated the efficacy of exercise during chemotherapy administration. These studies investigated different chemotherapeutic agents and/or regimens as well as diverse exercise modalities [78,140–142]. This makes it difficult to form a consensus sufficient to facilitate clinical exercise prescription based upon pre-clinical data. For example, some studies employed a maximal treadmill running test to exhaustion [141,143]. This is a low-cost alternative to incorporating the use of metabolic studies that enable the quantification of peak/maximum oxygen consumption (VO_2 peak/max), which can be used to identify a relative exercise intensity [144]. Other studies have incorporated metabolic analyses enabling calculation of a relative VO_2 peak/max [144]. However, given the lack of consistency across different rodent models, a knowledge gap remains in translating exercise intensity criteria between rodents and humans [145]. Additionally, there are no known experimental studies assessing the utility of exercise in the post-treatment recovery stage.

Thus far, animal experiments investigating the utility of exercise programs to resist chemotherapy-induced cachectic myopathy have not been without their pitfalls. There are numerous confounding variables highlighted in Table 1 including the selection of rodent species, strain, age, gender, and muscle type. These are all factors that can influence the protective efficacy of exercise in the context of chemotherapy-induced myopathy [145–149]. Additionally, tissue harvest time, relative to final chemotherapy dose, is a crucial consideration since transient events versus adaptive responses can be confused when making static measurements at a fixed timepoint. It is also imperative for experimental models to evaluate the feasibility and efficacy of resistance training during chemotherapy administration, since in vivo load-induced hypertrophy has emerged as having translational potential (for review see [150]). Animal studies to date have predominately focused on endurance training. In particular, it would be of great interest to determine whether chemotherapy-treated skeletal muscle could recover from the myotrauma induced by resistance training interventions. Indeed, Huang et al. [151] demonstrates that DOX can impair the inflammatory response necessary for skeletal muscle repair and remodelling following damaged caused by eccentric-exercise. Thus, further investigation is warranted.

Experimental animal models used to investigate the efficacy of exercise interventions during the administration of chemotherapy often utilise a treatment regimen that involves the metronomic delivery of chemotherapeutic agents spread out over an extended duration. This approach, while clinically compatible, results in milder skeletal muscle effects compared to the pre-conditioning studies, which utilise a single near-maximum tolerable dosage (MTD) bolus injection of a clinically-relevant accumulated human dose [152]. However, metronomic delivery of chemotherapy is a more compatible representation of the clinical scenario. This is especially true for DOX, which is clinically administered through slow-intravenous infusion or as repeated fractional doses cyclically over several weeks, to regulate plasma concentration of the drug. As such, severe cytotoxicity is prevented while anti-cancer efficacy is maintained [153]. The utility of metronomic delivery regimens in experimental models of chemotherapy cachexia still require a balance between retaining a clinically compatible cumulative dose and maintaining survival of the animals, so that exercise training interventions can be implemented. Going forward, future studies should refer to current gold standard models published in both de Lima et al. [143] and Ballaro et al. [89], which evaluate the effect of exercise during the synergistic-induction of cachectic myopathy from both chemotherapy and cancer-related factors. If possible, a chemotherapy control group should be included alongside a cancer control group when models are being optimised. This would help inform decision making regarding choice of exercise modality and secondary targets outside of mass and function preservation (e.g., mitigating systemic inflammation or insulin resistance) [50,154,155]. Current models need to be improved to enrich the clinical interpretability of the findings, thus promoting wider translational capability.

Current clinical studies indicate that aerobic exercise training can reduce fatigue and anxiety/depressive moods to improve participation in physical activity, while resistance exercise training can improve lean mass and muscular strength [156–158]. Interestingly, there is only weak evidence that either exercise modality can preserve skeletal muscle mass or cross-sectional area (CSA) [156,159,160]. This may reflect difficulties associated with measuring muscle mass in humans [161] or the barriers associated with incorporating muscle biopsies in clinical trials such as high costs and low patient recruitment due to the invasiveness of sampling. Nevertheless, these data highlight inconsistency with data derived from chemotherapy treated, cancer-free mouse models, which demonstrate protective efficacy from exercise (see Table 1) [78,142]. Perhaps even more interesting, and consistent with the clinical data, is that exercise did not alter skeletal muscle mass or CSA in two tumour-burdened mouse models treated with chemotherapy [89,143]. Thus, tumour factors appear to be most influential in dictating whether skeletal muscle can be modulated by exercise. While mass may not necessarily be modifiable by exercise therapy, de Lima et al. importantly demonstrated that exercise training improved skeletal muscle recovery after the cessation of chemotherapy, a paradigm yet to be explored in clinical studies [143]. Considering that current exercise interventions only elicit modest protective efficacy against chemotherapy and cancer-induced cachectic myopathy at best, there is an emphasis to explore multi-modal therapeutic strategies that involve exercise prescription programs alongside pharmacological interventions for synergistic benefits. Furthermore, given that some cancer patients may have a reduced opportunity to undertake exercise training due to hospitalisation-related deconditioning, multi-targeted pharmacological and/or supplementary interventions strategies that mimic specific aspects of exercise should be identified and explored for their therapeutic efficacy.

Table 1. Experimental studies on the effect of exercise against chemotherapy-induced cachectic myopathy.

Study	Animal Information	Exercise Modality	Chemotherapy Model	Key Observations
Smuder et al., 2011 [63]	6-month-old male Sprague-Dawley rats	TR: F: 5 days; I: 30 m/min; D: 60 mins/day; T: 0° incline.	1 × IPI 20 mg/kg of DOX post-exercise. Harvest 24 h post-IPI.	TR normalised oxidative stress and damage, calpain activity and proteolysis of actin in SOL muscles.
Smuder et al., 2011 [64]	6-month-old male Sprague-Dawley rats	TR: F: 5 days; I: 30 m/min; D: 60 mins/day; T: 0° incline.	1 × IPI 20 mg/kg of DOX post-exercise. Harvest 24 h post-IPI.	TR normalised autophagy activity in SOL muscles.
Bredahl et al., 2016 [134]	Male Sprague-Dawley rats. Age not specified	1. TR with progressive overload: F: 5 days/week, for 10 weeks; I: 20 to 30 m/min; D: 20 to 60 min/day; T: incline 0 to 18°. 2. CHL: Progressive food and water elevation to stimulate voluntary bi-pedal standing or jumping [162].	1 × IPI 15 mg/kg of DOX post-exercise. Harvest 5 days post-IPI.	TR was not protective against body mass loss and exacerbated EDL muscle mass loss. RT did not alter body or skeletal muscle mass but prevented SOL contractile dysfunction.
Kavazis et al., 2014 [135]	6-month-old male Sprague-Dawley rats	TR: F: 5 days; I: 30 m/min; D: 60 mins/day; T: 0° incline.	1 × IPI 20 mg/kg of DOX post-exercise. Harvest 24 h post-IPI.	TR normalised MuRF-1 and myostatin expression.
Mackay et al., 2019 [136]	5-week-old male C57BL/6 mice	TR: F: 5 days; I: 70% of maximal speed; D: 60 mins/day; T: 0° incline.	1 × IPI 15 mg/kg of DOX post-exercise. Harvest 72 h post-IPI.	TR partially mitigated body mass loss. TR did not modulate DOX-induced iron dysregulation.
Morton et al., 2019 [137]	6-month-old female Sprague-Dawley rats	TR: F: 10 days; I: 30 m/min; D: 60 mins/day; T: 0° incline.	1 × IPI 20 mg/kg of DOX post-exercise. Harvest 48 h post-IPI.	TR normalised DIA CSA, oxidative stress and reduced mitochondrial accumulation of DOX.
Huertas et al., 2020 [138]	6-month-old female Sprague-Dawley rats	TR: F: 5 days/week, for 2 weeks; I: 30 m/min; D: 60 mins/day; T: 0° incline.	1 × IPI 20 mg/kg of DOX post-exercise. Harvest 48 h post-IPI.	TR normalised SOL dysfunction and the transcription of AChR isoforms, δ and γ.
Dickinson et al., 2017 [140]	8-week-old ovariectomised female Sprague–Dawley rats	TR with progressive overload: F: 5 days/week, for 7 weeks, starting 1-week pre-IPI and finishing 5 days post-IPI; I: 20 to 25 m/min; D: 30–40 min/day; T: 0 to 10° incline.	1 × IPI every 2 weeks, for 4 weeks of 4 mg/kg DOX. Harvested 5 days post-IPI.	Normalised REDD1 expression. No effect on body mass or SOL muscle mass.
de Lima et al., 2018 [141]	8–10-week-old male C57BL/6 mice	TR: F: 5 days/week, for 6 weeks; I: 60% of maximal speed D: 60 mins/day; T: 0° incline.	2 × IPI per week for 6 weeks of 2.5 mg/kg DOX. Harvest not described relative to final IPI.	TR did not mitigate glucose intolerance, reduced body or GSN mass or protein synthesis. However, TR normalised corticosterone levels, autophagy activity and ambulatory function.
Hojman et al., 2014 [142]	8–12-week-old female NMRI mice	VWR: VEH: 60–80 km/mouse/week; CDDP: 10–50 km/mouse/week.	1 × IPI per week of 4 mg/kg CDDP for 6 weeks. Harvest 7 days post final-IPI.	VWR partially mitigated the loss of lean and TA mass and reduced atrogene expression. Did not protect against body or fat mass loss.
Sakai et al., 2017 [78]	8–9-week-old male C57BL/6 mice	TR: F: once a day for 9 days–5 days/week pre-CDDP and 4 days/week during CDDP week; I: 15 m/min; D: 20 min/day; T: 0° incline.	1 × IPI 3 mg/kg CDDP daily for 4 days. Harvest 24 h post-IPI.	TR did not alter body mass loss, but partially normalised QD mass and CSA, and atrogene expression.

Table 1. *Cont.*

Study	Animal Information	Exercise Modality	Chemotherapy Model	Key Observations
de Lima et al., 2020 [143]	8–10-week-old male C57BL/6 mice with LLC [163]	TR: F: 5 days/week, for 2–3 weeks; I: 60% of maximal speed; D: 60 mins/day; T: 0° incline.	2 × IPI per week for 6 weeks of 2.5 mg/kg DOX. Harvest 24 h or 1-week post-IPI.	TR did not alter body mass, but enhanced GSN re-growth, normalised inflammation and atrogene expression, and enhanced tumour volume reduction.
Ballaro et al., 2019 [89]	6-week-old female Balb/c mice with c26 [164]	MWR: F: once a day, with 3 days on followed by 1 day of rest for 4 weeks; I: 11 m/min; D: 45 mins/day; T: 0° incline.	1 × IPI per week of OXA 6 mg/kg and 5FU 50 mg/kg, for 3 weeks starting at day 7 of tumour implantation. Harvest 7 days post final IPI.	MWR did not alter GSN mass, but normalised atrogene expression and mitochondrial perturbations.

Abbreviations: 5FU: 5-fluorouracil; AChR; acetylcholine receptor; c26: c26 adenocarcinoma model; CDDP: cis-diamminedichloroplatinum(II) (cisplatin); CHL: chronic hind-limb loading; CSA: cross-sectional area; DIA: diaphragm; DOX: doxorubicin; D: duration; EDL *extensor digitorum longus*; F: frequency; GSN: *gastrocnemius*; I: intensity; IPI: intraperitoneal injection; LLC: Lewis-lung carcinoma model; MWR: motorised wheel running; OXA: oxaliplatin; QD: quadriceps; REDD1: regulated in development and DNA damage response 1; SOL: *soleus*; T: type; TA: *tibialis anterior*; TR: treadmill running; VWR: voluntary wheel running.

3.2. Adjuvant Therapies

Complementary to exercise strategies, several adjuvant candidates have been evaluated for their protective potential to combat chemotherapy-induced cachectic myopathy. Drug candidates focus on different biochemical targets that are involved in diverse molecular and physiological aspects that characterise the cachectic myopathy phenotype [40]. These candidates arise from a range of different therapeutic classes including activin receptor signalling inhibitors [59,60,100,103,165], appetite stimulants [77,80,82,166–170], nutritional supplements [171–176], and phytotherapies [112,113,177–185]. Activin receptor signalling inhibitors have shown strong pre-clinical efficacy to mitigate cancer and chemotherapy-induced cachexia through preserving skeletal muscle mass and function [186]. However, there has been limited success in the clinical translation of this pharmacological target, with a Phase II trial conducted by Novartis Pharmaceuticals (NCT01433263) demonstrating that activin receptor antibody, BYM338 (Bimagrumab), improved lean mass and muscle volume, but contributed to a net loss of body mass [187].

Appetite stimulants, in particular ghrelin receptor agonists, have shown promise in the pre-clinical setting to normalise food intake and muscle mass/CSA of chemotherapy-treated mice compared to healthy counterparts [80,82,170]. These findings translated clinically as observed through the ROMANA 1 & 2 trials (NCT01387269 & NCT01387282), where anamorelin (a ghrelin receptor agonist) increased body and lean mass of advanced cancer patients. However, it was not approved for clinical use because it failed to improve grip strength—a primary endpoint of the trial [188].

Nutritional supplements including essential amino acids and fatty acids have shown the capacity to protect against cancer and chemotherapy-induced cachexia, highlighting translational potential in single supplement interventions [189]. However, nutritional supplements are only a complementary piece of the cachexia puzzle as their clinical utility is primarily dependent on the anabolic potential of the individual [190]. Additionally, nutrition-related guidelines in cancer are based mostly on expert consensus, rarely on clinical trial evidence, highlighting a greater need to investigate multi-combination nutritional supplement interventions at the clinical level [191]. Similarly, compounds from the phytotherapies class have typically not been clinically evaluated for their therapeutic efficacy to mitigate cachectic myopathy given their rare utility in Western medicine [192]. This aspect should be re-considered based on encouraging pre-clinical data—specifically, the reduction of atrogene transcription, which underscores skeletal muscle wasting and holds strong promise as a therapeutic target against cachexia [193].

An emerging therapeutic class of particular interest to our laboratory group, and others, is the utility of mitoprotective compounds to combat skeletal muscle oxidative stress. Enhanced ROS production is a common underlying mechanism associated with multiple chemotherapies [32,33] and is a key contributing factor to mitochondrial dysfunction, a tenet of cachectic myopathy [36,37]. To date, mitoprotective compounds have not been evaluated in clinical trials. However, multiple mitoprotective agents have been experimentally evaluated for their potential protective efficacy against chemotherapy-induced cachectic myopathy, which will be discussed herein.

One of the first mitoprotective agents investigated for its therapeutic efficacy alongside chemotherapy was SS-31, a cardiolipin-targeting peptide, which preserves mitochondrial cristae structure and promotes oxidative phosphorylation [194]. SS-31 was shown to attenuate DOX-induced activity of multiple proteolytic systems (e.g., UPS, apoptosis, and calpains) in various muscle types, which prevented skeletal muscle atrophy [56,68]. Further, SS-31 normalises DOX-induced ROS emission in C2C12 myotube cultures and rodent muscle, with the latter observed as an acute event [33,56]. However, Ballaro et al. demonstrated that SS-31 administration yielded a modest mitoprotection, and subsequently, limited therapeutic efficacy in a more clinically compatible model of cachectic myopathy. In this study, mice were injected with C26 colorectal adenocarcinoma cells and metronomically dosed with OXA and 5FU combination chemotherapy over five weeks [90]. These data highlight that SS-31 may be more efficacious at a preventative stage of cachexia (i.e.,

pre-cachexia) when mitochondria are less damaged [131]. Alternatively, SS-31 may elicit specific mitoprotection against the anthracycline DOX, which induces mitochondrial stress differently to platinum-based alkylating agents, albeit this would need to be confirmed in future studies of DOX utilising more clinically compatible models.

Another adjuvant mitoprotective agent is BGP-15, a hydroximic acid derivative nicotinic acid-amidoxime small molecule that can preserve skeletal muscle metabolic homeostasis and mitochondrial quality control processes [195,196]. In particular, BGP-15 has been touted as an inhibitor of poly-(ADP-ribose) polymerase-1 (PARP-1) and co-inducer of HSP-70 [197,198], which are mechanisms associated with improved mitochondrial content, function, and oxidative capacity [199,200]. Furthermore, BGP-15 has also shown pleiotropic capacity to elicit mitoprotection independent of these mechanisms [201], a likely explanation of its therapeutic potential in a range of myopathies [202–205]. Our laboratory group has evaluated the therapeutic utility of BGP-15 alongside multiple chemotherapies including OXA, IRI, and 5FU with mixed efficacy [88,99,104]. BGP-15 was protective against OXA-induced lean mass loss, while also normalising ROS generation and mitochondrial viability [88]. However, alongside IRI, BGP-15 paradoxically rescued (partially) body, lean, and skeletal muscle mass in addition to muscle contractile function, while exacerbating the IRI-induced muscle protein synthesis inhibition and reduced expression of the cytoskeletal proteins, dystrophin, and β-dystroglycan [104]. The recovery of muscle mass and function may have been due to BGP-15′s enhancement of ATP production and mitochondrial density. Indeed, the latter was also enhanced when BGP-15 was delivered alongside 5FU and was associated with improved mitochondrial fusion. Furthermore, BGP-15 suppressed the 5FU-induced phosphorylation of NF-κB and MAPK isoforms [99], two likely mechanisms involved in the induction of cachectic myopathy. Given the heterogeneity of our findings, further investigations are required with a focus on clinically compatible combination chemotherapy regimens before BGP-15 can be considered a viable therapeutic candidate to protect against cachectic myopathy.

Future studies investigating adjuvant mitoprotective candidates should consider agents that can synergistically target chemotherapy driven oxidative damage, alongside other signalling pathways involved in the induction of cachectic myopathy. One potential compound is the nuclear factor erythroid 2-related factor 2 (Nrf2) transcriptional activator, dimethyl fumarate (DMF). DMF is a methyl ester of fumaric acid purported to upregulate cytoprotective response genes, and suppress NF-κB signalling, which imparts an anti-oxidative and -inflammatory effect [206] Another Nrf2 activator with therapeutic potential in this setting could be pterostilbene [207], a dimethoxylated analogue of resveratrol, a compound with demonstrated efficacy against DOX-mediated skeletal and cardiac myopathy [208,209]. Like resveratrol, pterostilbene can prolong lifespan, mitigate oxidative stress and normalise dysregulated autophagy in experimental models [210,211]. However, pterostilbene has greater bioavailability and a longer half-life compared to resveratrol [212], suggesting greater translational potential. Finally, epicatechin is another potentially viable mitoprotective candidate, which activates Nrf2 to inhibit oxidative stress [213]. Interestingly, epicatechin has been shown to restore the expression of dystrophin and other key cytoskeletal proteins in models of myopathy such as Becker muscular dystrophy and diabetes [214,215]. This highlights the protective potential of epicatechin against the chemotherapy-induced reduction of dystrophin expression shown by our group [99,104], and in cancer-induced cachectic myopathy in which dystrophin is also reduced [216]. Importantly, the adjuvant candidates proposed are not associated with cancer growth, and thus are unlikely to impact the anti-cancer efficacy of chemotherapy treatment [206,217,218].

Other compounds have also been evaluated for their therapeutic efficacy against chemotherapy-induced cachectic myopathy, whereby mitoprotection is elicited as a secondary effect to the central mechanism. Sodium nitrate (SN) supplementation is one of these strategies. SN potentiates the nitrate/nitrite/nitric oxide (NO) pathway to increase endogenous NO production as the central mechanism [219]. Mitoprotection occurs concurrently via an alternate pathway [220]. SN is cardioprotective during DOX treatment

in mice, with the preservation of left ventricular function dependent on the mitigation of oxidative stress and mitochondrial Complex I dysfunction [221,222]. However, our evaluation of SN supplementation alongside DOX administration failed to elicit a protective effect against cachectic myopathy [223]. Interestingly, the metabolic cytoprotectant, metformin, has also been investigated alongside DOX and demonstrated no protective benefit against chemotherapy-induced cachectic myopathy. These drug candidates both promote adenosine monophosphate-activated protein kinase (AMPK) signalling to preserve cellular energy status [220,224]. Thus, they may have greater utility as a therapeutic strategy to mitigate aberrant skeletal muscle glucose uptake during chemotherapy treatment.

4. Future Directions and Conclusions

Chemotherapy is an under-appreciated contributing factor in the induction of cachectic myopathy. To date, research has predominately contextualised cancer cachexia as governed by tumour-related factors without considering the other side of the cachexia sphere—chemotherapy [9]. This is problematic with respect to the clinical compatibility of this paradigm, as the large majority of cancer patients typically receive chemotherapy as part of their treatment strategy. This highlights the need for experimental studies to reflect the synergistic insult from cancer and chemotherapy in the induction of cachectic myopathy [15]. Models that allow the exploration of both factors in combination, and, using the spectra of chemotherapeutic agents, multi-therapy regimens, and cancer sub-types, are required. Future investigations in this area also need to consider the impact of novel chemotherapeutic agents in clinical trials across all cancers. For example, the therapeutic utility of multi-kinase inhibitors is becoming increasingly prevalent [225] and they demonstrably have cachexia-inducing properties [226,227]. Additionally, drug compounds that are utilised to mitigate the side-effects of clinical chemotherapy treatment such as the well-described gastrointestinal toxicities elicited by dexamethasone [228] need to be stratified for their capacity to potentiate chemotherapy-induced cachectic myopathy [229,230].

The utility of a cachexia scoring system within investigative animal research such as the animal cachexia score (ACASCO) [231] is warranted to justify a relative cachectic burden concerning chemotherapy- and cancer-induced myopathy. This will assist with the clinical interpretation of experimental findings, and where they fit within the cachexia diagnostic continuum in human patients, which incorporates three key stages: pre-cachexia, cachexia, and refractory cachexia [14]. Specific to chemotherapy-induced cachectic myopathy, a modified scoring system should also be considered to incorporate biomarkers of oxidative stress and skeletal muscle damage, which are currently being developed for other severe skeletal myopathies that share similar features with cachectic myopathy (i.e., dystrophin loss and oxidative stress) as highlighted by Grounds et al. [232].

Despite emerging as a burgeoning sub-field of skeletal muscle wasting conditions, chemotherapy-induced myopathy is, to date, a pariah with respect to research effort and directed funding in contrast to cancer-induced myopathy [9]—comparatively, it remains on the 'dark side' of the cachexia sphere. Illuminating the mechanisms involved and the physiological repercussions as well as actively pursuing protective therapeutics will enrich clinical decision making, patient outcomes, and the quality of cancer survivorship.

Author Contributions: Conceptualisation, D.G.C., C.A.G. and E.R.; Writing—original draft preparation, D.G.C.; Writing—review and editing, E.R. and C.A.G.; Supervision, E.R. and C.A.G.; Project administration, E.R.; Funding acquisition, E.R. All authors have read and agreed to the published version of the manuscript.

Funding: This research was funded by a program establishment grant (62962602) from the Institute for Sport, Exercise, and Active Living and the Centre for Chronic Disease, Victoria University (now the Institute for Health and Sport, Victoria University).

Institutional Review Board Statement: Not applicable.

Informed Consent Statement: Not applicable.

Data Availability Statement: Not applicable.

Acknowledgments: The authors wish to thank Cara Timpani for proof-reading the manuscript.

Conflicts of Interest: E.R. is a consultant to Santhera Pharmaceuticals and Epirium Bio. The other authors declare no conflict of interest.

References

1. DeVita, V.T., Jr.; Chu, E. A history of cancer chemotherapy. *Cancer Res.* **2008**, *68*, 8643–8653. [CrossRef]
2. Reuvers, T.G.A.; Kanaar, R.; Nonnekens, J. DNA Damage-Inducing Anticancer Therapies: From Global to Precision Damage. *Cancers* **2020**, *12*, 2098. [CrossRef]
3. Hanahan, D.; Weinberg Robert, A. Hallmarks of Cancer: The Next Generation. *Cell* **2011**, *144*, 646–674. [CrossRef]
4. Chen, Y.; Jungsuwadee, P.; Vore, M.; Butterfield, D.A.; St Clair, D.K. Collateral damage in cancer chemotherapy: Oxidative stress in nontargeted tissues. *Mol. Interv.* **2007**, *7*, 147–156. [CrossRef]
5. Love, R.R.; Leventhal, H.; Easterling, D.V.; Nerenz, D.R. Side effects and emotional distress during cancer chemotherapy. *Cancer* **1989**, *63*, 604–612. [CrossRef]
6. Florescu, M.; Cinteza, M.; Vinereanu, D. Chemotherapy-induced Cardiotoxicity. *Maedica* **2013**, *8*, 59–67.
7. Giglio, P.; Gilbert, M.R. Neurologic complications of cancer and its treatment. *Curr. Oncol. Rep.* **2010**, *12*, 50–59. [CrossRef]
8. Maxwell, M.B.; Maher, K.E. Chemotherapy-induced myelosuppression. *Semin. Oncol. Nurs.* **1992**, *8*, 113–123. [CrossRef]
9. Coletti, D. Chemotherapy-induced muscle wasting: An update. *Eur. J. Transl. Myol.* **2018**, *28*, 7587. [CrossRef]
10. Conte, E.; Bresciani, E.; Rizzi, L.; Cappellari, O.; De Luca, A.; Torsello, A.; Liantonio, A. Cisplatin-Induced Skeletal Muscle Dysfunction: Mechanisms and Counteracting Therapeutic Strategies. *Int. J. Mol. Sci.* **2020**, *21*, 1242. [CrossRef]
11. Hiensch, A.E.; Bolam, K.A.; Mijwel, S.; Jeneson, J.A.L.; Huitema, A.D.R.; Kranenburg, O.; van der Wall, E.; Rundqvist, H.; Wengstrom, Y.; May, A.M. Doxorubicin-induced skeletal muscle atrophy: Elucidating the underlying molecular pathways. *Acta Physiol.* **2019**, e13400. [CrossRef]
12. Gilliam, L.A.; St Clair, D.K. Chemotherapy-induced weakness and fatigue in skeletal muscle: The role of oxidative stress. *Antioxid. Redox Signal.* **2011**, *15*, 2543–2563. [CrossRef]
13. Baracos, V.E.; Martin, L.; Korc, M.; Guttridge, D.C.; Fearon, K.C.H. Cancer-associated cachexia. *Nat. Rev. Dis. Primers* **2018**, *4*, 17105. [CrossRef]
14. Fearon, K.; Strasser, F.; Anker, S.D.; Bosaeus, I.; Bruera, E.; Fainsinger, R.L.; Jatoi, A.; Loprinzi, C.; MacDonald, N.; Mantovani, G.; et al. Definition and classification of cancer cachexia: An international consensus. *Lancet. Oncol.* **2011**, *12*, 489–495. [CrossRef]
15. Berardi, E.; Madaro, L.; Lozanoska-Ochser, B.; Adamo, S.; Thorrez, L.; Bouche, M.; Coletti, D. A Pound of Flesh: What Cachexia Is and What It Is Not. *Diagnostics* **2021**, *11*, 116. [CrossRef]
16. Caan, B.J.; Meyerhardt, J.A.; Kroenke, C.H.; Alexeeff, S.; Xiao, J.; Weltzien, E.; Feliciano, E.C.; Castillo, A.L.; Quesenberry, C.P.; Kwan, M.L.; et al. Explaining the Obesity Paradox: The Association between Body Composition and Colorectal Cancer Survival (C-SCANS Study). *Cancer Epidemiol. Biomark. Prev.* **2017**, *26*, 1008–1015. [CrossRef]
17. Martin, L.; Birdsell, L.; Macdonald, N.; Reiman, T.; Clandinin, M.T.; McCargar, L.J.; Murphy, R.; Ghosh, S.; Sawyer, M.B.; Baracos, V.E. Cancer cachexia in the age of obesity: Skeletal muscle depletion is a powerful prognostic factor, independent of body mass index. *J. Clin. Oncol.* **2013**, *31*, 1539–1547. [CrossRef]
18. Bozzetti, F. Forcing the vicious circle: Sarcopenia increases toxicity, decreases response to chemotherapy and worsens with chemotherapy. *Ann. Oncol.* **2017**, *28*, 2107–2118. [CrossRef]
19. Rausch, V.; Sala, V.; Penna, F.; Porporato, P.E.; Ghigo, A. Understanding the common mechanisms of heart and skeletal muscle wasting in cancer cachexia. *Oncogenesis* **2021**, *10*, 1. [CrossRef]
20. Scheede-Bergdahl, C.; Jagoe, R.T. After the chemotherapy: Potential mechanisms for chemotherapy-induced delayed skeletal muscle dysfunction in survivors of acute lymphoblastic leukaemia in childhood. *Front. Pharmacol.* **2013**, *4*, 49. [CrossRef]
21. Argilés, J.M.; Busquets, S.; Stemmler, B.; López-Soriano, F.J. Cancer cachexia: Understanding the molecular basis. *Nat. Rev. Cancer* **2014**, *14*, 754–762. [CrossRef]
22. Thomas, D.R. Distinguishing starvation from cachexia. *Clin. Geriatr Med.* **2002**, *18*, 883–891. [CrossRef]
23. Argilés, J.M.; López-Soriano, F.J.; Stemmler, B.; Busquets, S. Novel targeted therapies for cancer cachexia. *Biochem. J.* **2017**, *474*, 2663–2678. [CrossRef]
24. Braun, T.P.; Szumowski, M.; Levasseur, P.R.; Grossberg, A.J.; Zhu, X.; Agarwal, A.; Marks, D.L. Muscle atrophy in response to cytotoxic chemotherapy is dependent on intact glucocorticoid signaling in skeletal muscle. *PLoS ONE* **2014**, *9*, e106489. [CrossRef] [PubMed]
25. Braun, T.P.; Grossberg, A.J.; Krasnow, S.M.; Levasseur, P.R.; Szumowski, M.; Zhu, X.X.; Maxson, J.E.; Knoll, J.G.; Barnes, A.P.; Marks, D.L. Cancer- and endotoxin-induced cachexia require intact glucocorticoid signaling in skeletal muscle. *FASEB J.* **2013**, *27*, 3572–3582. [CrossRef]
26. Braun, T.P.; Zhu, X.; Szumowski, M.; Scott, G.D.; Grossberg, A.J.; Levasseur, P.R.; Graham, K.; Khan, S.; Damaraju, S.; Colmers, W.F.; et al. Central nervous system inflammation induces muscle atrophy via activation of the hypothalamic-pituitary-adrenal axis. *J. Exp. Med.* **2011**, *208*, 2449–2463. [CrossRef]

27. Pastor, F.; Dumas, K.; Barthélémy, M.-A.; Regazzetti, C.; Druelle, N.; Peraldi, P.; Cormont, M.; Tanti, J.-F.; Giorgetti-Peraldi, S. Implication of REDD1 in the activation of inflammatory pathways. *Sci. Rep.* **2017**, *7*, 7023. [CrossRef]
28. Britto, F.A.; Dumas, K.; Giorgetti-Peraldi, S.; Ollendorff, V.; Favier, F.B. Is REDD1 a metabolic double agent? Lessons from physiology and pathology. *Am. J. Physiol.-Cell Physiol.* **2020**, *319*, C807–C824. [CrossRef] [PubMed]
29. Kefaloyianni, E.; Gaitanaki, C.; Beis, I. ERK1/2 and p38-MAPK signalling pathways, through MSK1, are involved in NF-kappaB transactivation during oxidative stress in skeletal myoblasts. *Cell Signal.* **2006**, *18*, 2238–2251. [CrossRef]
30. Webster, J.M.; Kempen, L.J.A.P.; Hardy, R.S.; Langen, R.C.J. Inflammation and Skeletal Muscle Wasting During Cachexia. *Front. Physiol.* **2020**, *11*, 597675. [CrossRef]
31. Cai, D.; Frantz, J.D.; Tawa, N.E., Jr.; Melendez, P.A.; Oh, B.C.; Lidov, H.G.; Hasselgren, P.O.; Frontera, W.R.; Lee, J.; Glass, D.J.; et al. IKKbeta/NF-kappaB activation causes severe muscle wasting in mice. *Cell* **2004**, *119*, 285–298. [CrossRef]
32. Rybalka, E.; Timpani, C.A.; Cheregi, B.D.; Sorensen, J.C.; Nurgali, K.; Hayes, A. Chemotherapeutic agents induce mitochondrial superoxide production and toxicity but do not alter respiration in skeletal muscle in vitro. *Mitochondrion* **2018**, *42*, 33–49. [CrossRef]
33. Gilliam, L.A.; Moylan, J.S.; Patterson, E.W.; Smith, J.D.; Wilson, A.S.; Rabbani, Z.; Reid, M.B. Doxorubicin acts via mitochondrial ROS to stimulate catabolism in C2C12 myotubes. *Am. J. Physiol. Cell Physiol.* **2012**, *302*, C195–C202. [CrossRef] [PubMed]
34. Fanzani, A.; Zanola, A.; Rovetta, F.; Rossi, S.; Aleo, M.F. Cisplatin triggers atrophy of skeletal C2C12 myotubes via impairment of Akt signalling pathway and subsequent increment activity of proteasome and autophagy systems. *Toxicol. Appl. Pharmacol.* **2011**, *250*, 312–321. [CrossRef] [PubMed]
35. Barreto, R.; Waning, D.L.; Gao, H.; Liu, Y.; Zimmers, T.A.; Bonetto, A. Chemotherapy-related cachexia is associated with mitochondrial depletion and the activation of ERK1/2 and p38 MAPKs. *Oncotarget* **2016**, *7*, 43442–43460. [CrossRef]
36. Hyatt, H.W.; Powers, S.K. Mitochondrial Dysfunction Is a Common Denominator Linking Skeletal Muscle Wasting Due to Disease, Aging, and Prolonged Inactivity. *Antioxidants* **2021**, *10*, 588. [CrossRef] [PubMed]
37. Sorensen, J.C.; Cheregi, B.D.; Timpani, C.A.; Nurgali, K.; Hayes, A.; Rybalka, E. Mitochondria: Inadvertent targets in chemotherapy-induced skeletal muscle toxicity and wasting? *Cancer Chemother Pharm.* **2016**, *78*, 673–683. [CrossRef] [PubMed]
38. Mehl, K.A.; Davis, J.M.; Berger, F.G.; Carson, J.A. Myofiber degeneration/regeneration is induced in the cachectic ApcMin/+ mouse. *J. Appl. Physiol.* **2005**, *99*, 2379–2387. [CrossRef] [PubMed]
39. He, W.A.; Berardi, E.; Cardillo, V.M.; Acharyya, S.; Aulino, P.; Thomas-Ahner, J.; Wang, J.; Bloomston, M.; Muscarella, P.; Nau, P.; et al. NF-κB-mediated Pax7 dysregulation in the muscle microenvironment promotes cancer cachexia. *J. Clin. Investig.* **2013**, *123*, 4821–4835. [CrossRef]
40. Martin, A.; Freyssenet, D. Phenotypic features of cancer cachexia-related loss of skeletal muscle mass and function: Lessons from human and animal studies. *J. Cachexia Sarcopenia Muscle* **2021**, *12*, 252–273. [CrossRef]
41. Carvalho, C.; Santos, R.X.; Cardoso, S.; Correia, S.; Oliveira, P.J.; Santos, M.S.; Moreira, P.I. Doxorubicin: The good, the bad and the ugly effect. *Curr. Med. Chem.* **2009**, *16*, 3267–3285. [CrossRef]
42. Chatterjee, K.; Zhang, J.; Honbo, N.; Karliner, J.S. Doxorubicin cardiomyopathy. *Cardiology* **2010**, *115*, 155–162. [CrossRef] [PubMed]
43. Hayward, R.; Hydock, D.; Gibson, N.; Greufe, S.; Bredahl, E.; Parry, T. Tissue retention of doxorubicin and its effects on cardiac, smooth, and skeletal muscle function. *J. Physiol. Biochem.* **2013**, *69*, 177–187. [CrossRef] [PubMed]
44. Fabris, S.; MacLean, D.A. Skeletal Muscle an Active Compartment in the Sequestering and Metabolism of Doxorubicin Chemotherapy. *PLoS ONE* **2015**, *10*, e0139070. [CrossRef] [PubMed]
45. Fairclough, D.L.; Fetting, J.H.; Cella, D.; Wonson, W.; Moinpour, C.M. Quality of life and quality adjusted survival for breast cancer patients receiving adjuvant therapy. Eastern Cooperative Oncology Group (ECOG). *Qual. Life Res.* **1999**, *8*, 723–731. [CrossRef] [PubMed]
46. Schwartz, A.L.; Winters-Stone, K.; Gallucci, B. Exercise effects on bone mineral density in women with breast cancer receiving adjuvant chemotherapy. *Oncol. Nurs. Forum* **2007**, *34*, 627–633. [CrossRef] [PubMed]
47. van Norren, K.; van Helvoort, A.; Argiles, J.M.; van Tuijl, S.; Arts, K.; Gorselink, M.; Laviano, A.; Kegler, D.; Haagsman, H.P.; van der Beek, E.M. Direct effects of doxorubicin on skeletal muscle contribute to fatigue. *Br. J. Cancer* **2009**, *100*, 311–314. [CrossRef] [PubMed]
48. Hydock, D.S.; Lien, C.Y.; Jensen, B.T.; Schneider, C.M.; Hayward, R. Characterization of the effect of in vivo doxorubicin treatment on skeletal muscle function in the rat. *Anticancer Res.* **2011**, *31*, 2023–2028.
49. Zorzato, F.; Salviati, G.; Facchinetti, T.; Volpe, P. Doxorubicin induces calcium release from terminal cisternae of skeletal muscle. A study on isolated sarcoplasmic reticulum and chemically skinned fibers. *J. Biol. Chem.* **1985**, *260*, 7349–7355. [CrossRef]
50. Gilliam, L.A.A.; Ferreira, L.F.; Bruton, J.D.; Moylan, J.S.; Westerblad, H.; St Clair, D.K.; Reid, M.B. Doxorubicin acts through tumor necrosis factor receptor subtype 1 to cause dysfunction of murine skeletal muscle. *J. Appl. Physiol.* **2009**, *107*, 1935–1942. [CrossRef]
51. Dessouki, F.B.A.; Kukreja, R.C.; Singla, D.K. Stem Cell-Derived Exosomes Ameliorate Doxorubicin-Induced Muscle Toxicity through Counteracting Pyroptosis. *Pharmaceuticals* **2020**, *13*, 450. [CrossRef]
52. Dessouki, F.B.; Kukreja, R.C.; Singla, D.K. Doxorubicin-Induced Muscle Toxicity: A Novel Mechanism Involving Inflammation-Mediated Pyroptosis in Soleus Muscle. *FASEB J.* **2020**, *34*, 1. [CrossRef]

53. Hardin, B.J.; Campbell, K.S.; Smith, J.D.; Arbogast, S.; Smith, J.; Moylan, J.S.; Reid, M.B. TNF-α acts via TNFR1 and muscle-derived oxidants to depress myofibrillar force in murine skeletal muscle. *J. Appl. Physiol.* **2008**, *104*, 694–699. [CrossRef] [PubMed]
54. Gilliam, L.A.A.; Fisher-Wellman, K.H.; Lin, C.T.; Maples, J.M.; Cathey, B.L.; Neufer, P.D. The anticancer agent doxorubicin disrupts mitochondrial energy metabolism and redox balance in skeletal muscle. *Free Radic. Biol. Med.* **2013**, *65*, 988–996. [CrossRef] [PubMed]
55. Doerr, V.; Montalvo, R.N.; Kwon, O.S.; Talbert, E.E.; Hain, B.A.; Houston, F.E.; Smuder, A.J. Prevention of Doxorubicin-Induced Autophagy Attenuates Oxidative Stress and Skeletal Muscle Dysfunction. *Antioxidants* **2020**, *9*, 263. [CrossRef] [PubMed]
56. Min, K.; Kwon, O.S.; Smuder, A.J.; Wiggs, M.P.; Sollanek, K.J.; Christou, D.D.; Yoo, J.K.; Hwang, M.H.; Szeto, H.H.; Kavazis, A.N.; et al. Increased mitochondrial emission of reactive oxygen species and calpain activation are required for doxorubicin-induced cardiac and skeletal muscle myopathy. *J. Physiol.* **2015**, *593*, 2017–2036. [CrossRef]
57. Gilliam, L.A.; Lark, D.S.; Reese, L.R.; Torres, M.J.; Ryan, T.E.; Lin, C.T.; Cathey, B.L.; Neufer, P.D. Targeted overexpression of mitochondrial catalase protects against cancer chemotherapy-induced skeletal muscle dysfunction. *Am. J. Physiol. Endocrinol. Metab.* **2016**, *311*, E293–E301. [CrossRef]
58. Tarpey, M.D.; Amorese, A.J.; Balestrieri, N.P.; Fisher-Wellman, K.H.; Spangenburg, E.E. Doxorubicin causes lesions in the electron transport system of skeletal muscle mitochondria that are associated with a loss of contractile function. *J. Biol. Chem.* **2019**. [CrossRef] [PubMed]
59. Nissinen, T.A.; Degerman, J.; Rasanen, M.; Poikonen, A.R.; Koskinen, S.; Mervaala, E.; Pasternack, A.; Ritvos, O.; Kivela, R.; Hulmi, J.J. Systemic blockade of ACVR2B ligands prevents chemotherapy-induced muscle wasting by restoring muscle protein synthesis without affecting oxidative capacity or atrogenes. *Sci. Rep.* **2016**, *6*, 32695. [CrossRef]
60. Hulmi, J.J.; Nissinen, T.A.; Rasanen, M.; Degerman, J.; Lautaoja, J.H.; Hemanthakumar, K.A.; Backman, J.T.; Ritvos, O.; Silvennoinen, M.; Kivela, R. Prevention of chemotherapy-induced cachexia by ACVR2B ligand blocking has different effects on heart and skeletal muscle. *J. Cachexia Sarcopenia Muscle* **2018**, *9*, 417–432. [CrossRef] [PubMed]
61. Beyfuss, K.; Hood, D.A. A systematic review of p53 regulation of oxidative stress in skeletal muscle. *Redox Rep.* **2018**, *23*, 100–117. [CrossRef]
62. Supriya, R.; Tam, B.T.; Pei, X.M.; Lai, C.W.; Chan, L.W.; Yung, B.Y.; Siu, P.M. Doxorubicin Induces Inflammatory Modulation and Metabolic Dysregulation in Diabetic Skeletal Muscle. *Front. Physiol.* **2016**, *7*. [CrossRef]
63. Smuder, A.J.; Kavazis, A.N.; Min, K.; Powers, S.K. Exercise protects against doxorubicin-induced oxidative stress and proteolysis in skeletal muscle. *J. Appl. Physiol.* **2011**, *110*, 935–942. [CrossRef]
64. Smuder, A.J.; Kavazis, A.N.; Min, K.; Powers, S.K. Exercise protects against doxorubicin-induced markers of autophagy signaling in skeletal muscle. *J. Appl. Physiol.* **2011**, *111*, 1190–1198. [CrossRef]
65. Goodman, C.A. Role of mTORC1 in mechanically induced increases in translation and skeletal muscle mass. *J. Appl. Physiol.* **2019**, *127*, 581–590. [CrossRef] [PubMed]
66. D'Lugos, A.C.; Fry, C.S.; Ormsby, J.C.; Sweeney, K.R.; Brightwell, C.R.; Hale, T.M.; Gonzales, R.J.; Angadi, S.S.; Carroll, C.C.; Dickinson, J.M. Chronic doxorubicin administration impacts satellite cell and capillary abundance in a muscle-specific manner. *Physiol. Rep.* **2019**, *7*, e14052. [CrossRef] [PubMed]
67. Bohnert, K.R.; McMillan, J.D.; Kumar, A. Emerging roles of ER stress and unfolded protein response pathways in skeletal muscle health and disease. *J. Cell Physiol.* **2018**, *233*, 67–78. [CrossRef] [PubMed]
68. Montalvo, R.N.; Doerr, V.; Min, K.; Szeto, H.H.; Smuder, A.J. Doxorubicin-induced oxidative stress differentially regulates proteolytic signaling in cardiac and skeletal muscle. *Am. J. Physiol. Regul. Integr. Comp. Physiol.* **2020**, *318*, R227–R233. [CrossRef]
69. Siddik, Z.H. Cisplatin: Mode of cytotoxic action and molecular basis of resistance. *Oncogene* **2003**, *22*, 7265–7279. [CrossRef]
70. McSweeney, K.R.; Gadanec, L.K.; Qaradakhi, T.; Ali, B.A.; Zulli, A.; Apostolopoulos, V. Mechanisms of Cisplatin-Induced Acute Kidney Injury: Pathological Mechanisms, Pharmacological Interventions, and Genetic Mitigations. *Cancers* **2021**, *13*, 1572. [CrossRef]
71. Kanat, O.; Ertas, H.; Caner, B. Platinum-induced neurotoxicity: A review of possible mechanisms. *World J. Clin. Oncol.* **2017**, *8*, 329–335. [CrossRef]
72. Moreira-Pais, A.; Ferreira, R.; Gil da Costa, R. Platinum-induced muscle wasting in cancer chemotherapy: Mechanisms and potential targets for therapeutic intervention. *Life Sci.* **2018**, *208*, 1–9. [CrossRef] [PubMed]
73. Le Bricon, T.; Gugins, S.; Cynober, L.; Baracos, V.E. Negative impact of cancer chemotherapy on protein metabolism in healthy and tumor-bearing rats. *Metabolism* **1995**, *44*, 1340–1348. [CrossRef]
74. Sakai, H.; Sagara, A.; Arakawa, K.; Sugiyama, R.; Hirosaki, A.; Takase, K.; Jo, A.; Sato, K.; Chiba, Y.; Yamazaki, M.; et al. Mechanisms of cisplatin-induced muscle atrophy. *Toxicol. Appl. Pharmacol.* **2014**, *278*, 190–199. [CrossRef] [PubMed]
75. Sakai, H.; Ikeno, Y.; Tsukimura, Y.; Inomata, M.; Suzuki, Y.; Kon, R.; Ikarashi, N.; Chiba, Y.; Yamada, T.; Kamei, J. Upregulation of ubiquitinated proteins and their degradation pathway in muscle atrophy induced by cisplatin in mice. *Toxicol. Appl. Pharmacol.* **2020**, *403*, 115165. [CrossRef] [PubMed]
76. Mammucari, C.; Milan, G.; Romanello, V.; Masiero, E.; Rudolf, R.; Del Piccolo, P.; Burden, S.J.; Di Lisi, R.; Sandri, C.; Zhao, J.; et al. FoxO3 controls autophagy in skeletal muscle in vivo. *Cell Metab.* **2007**, *6*, 458–471. [CrossRef] [PubMed]
77. Sirago, G.; Conte, E.; Fracasso, F.; Cormio, A.; Fehrentz, J.A.; Martinez, J.; Musicco, C.; Camerino, G.M.; Fonzino, A.; Rizzi, L.; et al. Growth hormone secretagogues hexarelin and JMV2894 protect skeletal muscle from mitochondrial damages in a rat model of cisplatin-induced cachexia. *Sci. Rep.* **2017**, *7*, 13017. [CrossRef]

78. Sakai, H.; Kimura, M.; Isa, Y.; Yabe, S.; Maruyama, A.; Tsuruno, Y.; Kai, Y.; Sato, F.; Yumoto, T.; Chiba, Y.; et al. Effect of acute treadmill exercise on cisplatin-induced muscle atrophy in the mouse. *Pflügers Arch.-Eur. J. Physiol.* **2017**, *469*, 1495–1505. [CrossRef]
79. Damrauer, J.S.; Stadler, M.E.; Acharyya, S.; Baldwin, A.S.; Couch, M.E.; Guttridge, D.C. Chemotherapy-induced muscle wasting: Association with NF-κB and cancer cachexia. *Eur. J. Transl. Myol.* **2018**, *28*, 7590. [CrossRef]
80. Chen, J.A.; Splenser, A.; Guillory, B.; Luo, J.; Mendiratta, M.; Belinova, B.; Halder, T.; Zhang, G.; Li, Y.P.; Garcia, J.M. Ghrelin prevents tumour- and cisplatin-induced muscle wasting: Characterization of multiple mechanisms involved. *J. Cachexia Sarcopenia Muscle* **2015**, *6*, 132–143. [CrossRef]
81. Berchtold, M.W.; Brinkmeier, H.; Muntener, M. Calcium ion in skeletal muscle: Its crucial role for muscle function, plasticity, and disease. *Physiol. Rev.* **2000**, *80*, 1215–1265. [CrossRef]
82. Conte, E.; Camerino, G.M.; Mele, A.; De Bellis, M.; Pierno, S.; Rana, F.; Fonzino, A.; Caloiero, R.; Rizzi, L.; Bresciani, E.; et al. Growth hormone secretagogues prevent dysregulation of skeletal muscle calcium homeostasis in a rat model of cisplatin-induced cachexia. *J. Cachexia Sarcopenia Muscle* **2017**, *8*, 386–404. [CrossRef]
83. Wood, Z.A.; Poole, L.B.; Karplus, P.A. Peroxiredoxin evolution and the regulation of hydrogen peroxide signaling. *Science* **2003**, *300*, 650–653. [CrossRef] [PubMed]
84. Leung, A.W.Y.; Backstrom, I.; Bally, M.B. Sulfonation, an underexploited area: From skeletal development to infectious diseases and cancer. *Oncotarget* **2016**, *7*, 55811–55827. [CrossRef] [PubMed]
85. Kang, S.W.; Baines, I.C.; Rhee, S.G. Characterization of a mammalian peroxiredoxin that contains one conserved cysteine. *J. Biol. Chem.* **1998**, *273*, 6303–6311. [CrossRef] [PubMed]
86. Hain, B.A.; Jude, B.; Xu, H.; Smuin, D.M.; Fox, E.J.; Elfar, J.C.; Waning, D.L. Zoledronic Acid Improves Muscle Function in Healthy Mice Treated with Chemotherapy. *J. Bone Miner. Res.* **2020**, *35*, 368–381. [CrossRef] [PubMed]
87. Hain, B.A.; Xu, H.; Wilcox, J.R.; Mutua, D.; Waning, D.L. Chemotherapy-induced loss of bone and muscle mass in a mouse model of breast cancer bone metastases and cachexia. *JCSM Rapid Commun.* **2019**, *2*, e00075. [CrossRef]
88. Sorensen, J.C.; Petersen, A.C.; Timpani, C.A.; Campelj, D.G.; Cook, J.; Trewin, A.J.; Stojanovska, V.; Stewart, M.; Hayes, A.; Rybalka, E. BGP-15 Protects against Oxaliplatin-Induced Skeletal Myopathy and Mitochondrial Reactive Oxygen Species Production in Mice. *Front. Pharmacol.* **2017**, *8*, 137. [CrossRef]
89. Ballaro, R.; Beltra, M.; De Lucia, S.; Pin, F.; Ranjbar, K.; Hulmi, J.J.; Costelli, P.; Penna, F. Moderate exercise in mice improves cancer plus chemotherapy-induced muscle wasting and mitochondrial alterations. *FASEB J.* **2019**, *33*, 5482–5494. [CrossRef]
90. Ballarò, R.; Lopalco, P.; Audrito, V.; Beltrà, M.; Pin, F.; Angelini, R.; Costelli, P.; Corcelli, A.; Bonetto, A.; Szeto, H.H.; et al. Targeting Mitochondria by SS-31 Ameliorates the Whole Body Energy Status in Cancer- and Chemotherapy-Induced Cachexia. *Cancers* **2021**, *13*, 850. [CrossRef]
91. Yi, Y.W.; Bae, I. Effects of solvents on in vitro potencies of platinum compounds. *DNA Repair* **2011**, *10*, 1084–1085. [CrossRef] [PubMed]
92. Hall, M.D.; Telma, K.A.; Chang, K.-E.; Lee, T.D.; Madigan, J.P.; Lloyd, J.R.; Goldlust, I.S.; Hoeschele, J.D.; Gottesman, M.M. Say no to DMSO: Dimethylsulfoxide inactivates cisplatin, carboplatin, and other platinum complexes. *Cancer Res.* **2014**, *74*, 3913–3922. [CrossRef]
93. Longley, D.B.; Harkin, D.P.; Johnston, P.G. 5-fluorouracil: Mechanisms of action and clinical strategies. *Nat. Rev. Cancer* **2003**, *3*, 330–338. [CrossRef] [PubMed]
94. McQuade, R.M.; Stojanovska, V.; Donald, E.; Abalo, R.; Bornstein, J.C.; Nurgali, K. Gastrointestinal dysfunction and enteric neurotoxicity following treatment with anticancer chemotherapeutic agent 5-fluorouracil. *Neurogastroenterol. Motil.* **2016**, *28*, 1861–1875. [CrossRef] [PubMed]
95. Sougiannis, A.T.; VanderVeen, B.N.; Enos, R.T.; Velazquez, K.T.; Bader, J.E.; Carson, M.; Chatzistamou, I.; Walla, M.; Pena, M.M.; Kubinak, J.L.; et al. Impact of 5 fluorouracil chemotherapy on gut inflammation, functional parameters, and gut microbiota. *Brain Behav. Immun.* **2019**, *80*, 44–55. [CrossRef]
96. Stringer, A.M.; Gibson, R.J.; Logan, R.M.; Bowen, J.M.; Yeoh, A.S.; Hamilton, J.; Keefe, D.M. Gastrointestinal microflora and mucins may play a critical role in the development of 5-Fluorouracil-induced gastrointestinal mucositis. *Exp. Biol. Med.* **2009**, *234*, 430–441. [CrossRef]
97. Chen, H.; Xu, C.; Zhang, F.; Liu, Y.; Guo, Y.; Yao, Q. The gut microbiota attenuates muscle wasting by regulating energy metabolism in chemotherapy-induced malnutrition rats. *Cancer Chemother. Pharm.* **2020**. [CrossRef]
98. VanderVeen, B.N.; Sougiannis, A.T.; Velazquez, K.T.; Carson, J.A.; Fan, D.; Murphy, E.A. The Acute Effects of 5 Fluorouracil on Skeletal Muscle Resident and Infiltrating Immune Cells in Mice. *Front. Physiol.* **2020**, *11*, 593468. [CrossRef]
99. Campelj, D.G.; Timpani, C.A.; Cree, T.; Petersen, A.C.; Hayes, A.; Goodman, C.A.; Rybalka, E. Metronomic 5-Fluorouracil Delivery Primes Skeletal Muscle for Myopathy but Does Not Cause Cachexia. *Pharmaceuticals* **2021**, *14*, 478. [CrossRef] [PubMed]
100. Barreto, R.; Kitase, Y.; Matsumoto, T.; Pin, F.; Colston, K.C.; Couch, K.E.; O'Connell, T.M.; Couch, M.E.; Bonewald, L.F.; Bonetto, A. ACVR2B/Fc counteracts chemotherapy-induced loss of muscle and bone mass. *Sci. Rep.* **2017**, *7*, 14470. [CrossRef]
101. Barreto, R.; Mandili, G.; Witzmann, F.A.; Novelli, F.; Zimmers, T.A.; Bonetto, A. Cancer and Chemotherapy Contribute to Muscle Loss by Activating Common Signaling Pathways. *Front. Physiol.* **2016**, *7*, 472. [CrossRef] [PubMed]
102. Pin, F.; Barreto, R.; Couch, M.E.; Bonetto, A.; O'Connell, T.M. Cachexia induced by cancer and chemotherapy yield distinct perturbations to energy metabolism. *J. Cachexia Sarcopenia Muscle* **2019**, *10*, 140–154. [CrossRef]

103. O'Connell, T.M.; Pin, F.; Couch, M.E.; Bonetto, A. Treatment with Soluble Activin Receptor Type IIB Alters Metabolic Response in Chemotherapy-Induced Cachexia. *Cancers* **2019**, *11*, 1222. [CrossRef]
104. Campelj, D.G.; Timpani, C.A.; Petersen, A.C.; Hayes, A.; Goodman, C.A.; Rybalka, E. The Paradoxical Effect of PARP Inhibitor BGP-15 on Irinotecan-Induced Cachexia and Skeletal Muscle Dysfunction. *Cancers* **2020**, *12*, 3810. [CrossRef]
105. Samuels, S.E.; Knowles, A.L.; Tilignac, T.; Debiton, E.; Madelmont, J.C.; Attaix, D. Higher skeletal muscle protein synthesis and lower breakdown after chemotherapy in cachectic mice. *Am. J. Physiol. Regul. Integr. Comp. Physiol.* **2001**, *281*, R133–R139. [CrossRef] [PubMed]
106. Tilignac, T.; Temparis, S.; Combaret, L.; Taillandier, D.; Pouch, M.N.; Cervek, M.; Cardenas, D.M.; Le Bricon, T.; Debiton, E.; Samuels, S.E.; et al. Chemotherapy inhibits skeletal muscle ubiquitin-proteasome-dependent proteolysis. *Cancer Res.* **2002**, *62*, 2771–2777. [PubMed]
107. Crouch, M.L.; Knowels, G.; Stuppard, R.; Ericson, N.G.; Bielas, J.H.; Marcinek, D.J.; Syrjala, K.L. Cyclophosphamide leads to persistent deficits in physical performance and in vivo mitochondria function in a mouse model of chemotherapy late effects. *PLoS ONE* **2017**, *12*, e0181086. [CrossRef] [PubMed]
108. Judge, A.R.; Dodd, S.L. Xanthine oxidase and activated neutrophils cause oxidative damage to skeletal muscle after contractile claudication. *Am. J. Physiol. Heart Circ. Physiol.* **2004**, *286*, H252–H256. [CrossRef]
109. Lee, N.-S.; Byun, J.-H.; Bae, S.-B.; Kim, C.-K.; Lee, K.-T.; Park, S.-K.; Won, J.-H.; Hong, D.-S.; Park, H.-S. Combination of gemcitabine and cisplatin as first-line therapy in advanced non-small-cell lung cancer. *Cancer Res. Treat.* **2004**, *36*, 173–177. [CrossRef]
110. Heinemann, V. Gemcitabine plus cisplatin for the treatment of metastatic breast cancer. *Clin. Breast Cancer* **2002**, *3* (Suppl. 1), 24–29. [CrossRef] [PubMed]
111. Cohen, M.H.; Rothmann, M. Gemcitabine and cisplatin for advanced, metastatic bladder cancer. *J. Clin. Oncol.* **2001**, *19*, 1229–1231. [CrossRef]
112. Chen, M.-C.; Chen, Y.-L.; Lee, C.-F.; Hung, C.-H.; Chou, T.-C. Supplementation of Magnolol Attenuates Skeletal Muscle Atrophy in Bladder Cancer-Bearing Mice Undergoing Chemotherapy via Suppression of FoxO3 Activation and Induction of IGF-1. *PLoS ONE* **2015**, *10*, e0143594. [CrossRef] [PubMed]
113. Chen, M.-C.; Hsu, W.-L.; Hwang, P.-A.; Chen, Y.-L.; Chou, T.-C. Combined administration of fucoidan ameliorates tumor and chemotherapy-induced skeletal muscle atrophy in bladder cancer-bearing mice. *Oncotarget* **2016**, *7*, 51608–51618. [CrossRef] [PubMed]
114. Smith, R.C.; Cramer, M.S.; Mitchell, P.J.; Capen, A.; Huber, L.; Wang, R.; Myers, L.; Jones, B.E.; Eastwood, B.J.; Ballard, D.; et al. Myostatin Neutralization Results in Preservation of Muscle Mass and Strength in Preclinical Models of Tumor-Induced Muscle Wasting. *Mol. Cancer Ther.* **2015**, *14*, 1661–1670. [CrossRef]
115. Kremer, J.M.; Alarcón, G.S.; Lightfoot Jr, R.W.; Willkens, R.F.; Furst, D.E.; Williams, H.J.; Dent, P.B.; Weinblatt, M.E. Methotrexate for rheumatoid arthritis. *Arthritis Rheum. Off. J. Am. Coll. Rheumatol.* **1994**, *37*, 316–328. [CrossRef]
116. Pirkmajer, S.; Kulkarni, S.S.; Tom, R.Z.; Ross, F.A.; Hawley, S.A.; Hardie, D.G.; Zierath, J.R.; Chibalin, A.V. Methotrexate promotes glucose uptake and lipid oxidation in skeletal muscle via AMPK activation. *Diabetes* **2015**, *64*, 360–369. [CrossRef]
117. Russo, G.T.; Minutoli, L.; Bitto, A.; Altavilla, D.; Alessi, E.; Giandalia, A.; Romeo, E.L.; Stagno, M.F.; Squadrito, F.; Cucinotta, D.; et al. Methotrexate Increases Skeletal Muscle GLUT4 Expression and Improves Metabolic Control in Experimental Diabetes. *J. Nutr. Metab.* **2012**, *2012*, 132056. [CrossRef] [PubMed]
118. Ramos, S.V.; Hughes, M.C.; Perry, C.G.R. Altered skeletal muscle microtubule-mitochondrial VDAC2 binding is related to bioenergetic impairments after paclitaxel but not vinblastine chemotherapies. *Am. J. Physiol.-Cell Physiol.* **2019**, *316*, C449–C455. [CrossRef]
119. Kauffman, F.C.; Albuquerque, E.X.; Warnick, J.E.; Max, S.R. Effect of vinblastine on neural regulation of metabolism in rat skeletal muscle. *Exp. Neurol.* **1976**, *50*, 60–66. [CrossRef]
120. Chen, X.; Green, P.G.; Levine, J.D. Abnormal muscle afferent function in a model of Taxol chemotherapy-induced painful neuropathy. *J. Neurophysiol.* **2011**, *106*, 274–279. [CrossRef]
121. Bates, D.; Eastman, A. Microtubule destabilising agents: Far more than just antimitotic anticancer drugs. *Br. J. Clin. Pharmacol.* **2017**, *83*, 255–268. [CrossRef] [PubMed]
122. Chaillou, T.; McPeek, A.; Lanner, J.T. Docetaxel does not impair skeletal muscle force production in a murine model of cancer chemotherapy. *Physiol. Rep.* **2017**, *5*, e13261. [CrossRef] [PubMed]
123. Wang, H.; Li, T.L.; Hsia, S.; Su, I.L.; Chan, Y.L.; Wu, C.J. Skeletal muscle atrophy is attenuated in tumor-bearing mice under chemotherapy by treatment with fish oil and selenium. *Oncotarget* **2015**, *6*, 7758–7773. [CrossRef]
124. Ju, J.S.; Varadhachary, A.S.; Miller, S.E.; Weihl, C.C. Quantitation of "autophagic flux" in mature skeletal muscle. *Autophagy* **2010**, *6*, 929–935. [CrossRef]
125. Kerr, J.P.; Robison, P.; Shi, G.; Bogush, A.I.; Kempema, A.M.; Hexum, J.K.; Becerra, N.; Harki, D.A.; Martin, S.S.; Raiteri, R.; et al. Detyrosinated microtubules modulate mechanotransduction in heart and skeletal muscle. *Nat. Commun.* **2015**, *6*, 8526. [CrossRef] [PubMed]
126. Parry, S.M.; Puthucheary, Z.A. The impact of extended bed rest on the musculoskeletal system in the critical care environment. *Extrem. Physiol. Med.* **2015**, *4*, 16. [CrossRef] [PubMed]

127. Aversa, Z.; Costelli, P.; Muscaritoli, M. Cancer-induced muscle wasting: Latest findings in prevention and treatment. *Ther. Adv. Med Oncol.* **2017**, *9*, 369–382. [CrossRef] [PubMed]
128. Aquila, G.; Re Cecconi, A.D.; Brault, J.J.; Corli, O.; Piccirillo, R. Nutraceuticals and Exercise against Muscle Wasting during Cancer Cachexia. *Cells* **2020**, *9*, 2536. [CrossRef]
129. VanderVeen, B.N.; Fix, D.K.; Carson, J.A. Disrupted Skeletal Muscle Mitochondrial Dynamics, Mitophagy, and Biogenesis during Cancer Cachexia: A Role for Inflammation. *Oxidative Med. Cell. Longev.* **2017**, *2017*, 3292087. [CrossRef]
130. Penna, F.; Ballarò, R.; Costelli, P. The Redox Balance: A Target for Interventions Against Muscle Wasting in Cancer Cachexia? *Antioxid. Redox Signal.* **2020**, *33*, 542–558. [CrossRef]
131. Brown, J.L.; Rosa-Caldwell, M.E.; Lee, D.E.; Blackwell, T.A.; Brown, L.A.; Perry, R.A.; Haynie, W.S.; Hardee, J.P.; Carson, J.A.; Wiggs, M.P.; et al. Mitochondrial degeneration precedes the development of muscle atrophy in progression of cancer cachexia in tumour-bearing mice. *J. Cachexia Sarcopenia Muscle* **2017**, *8*, 926–938. [CrossRef] [PubMed]
132. Powers, S.K.; Duarte, J.A.; Le Nguyen, B.; Hyatt, H. Endurance exercise protects skeletal muscle against both doxorubicin-induced and inactivity-induced muscle wasting. *Pflugers Arch.* **2019**, *471*, 441–453. [CrossRef] [PubMed]
133. Smuder, A.J. Exercise stimulates beneficial adaptations to diminish doxorubicin-induced cellular toxicity. *Am. J. Physiol. Regul. Integr. Comp. Physiol.* **2019**, *317*, R662–R672. [CrossRef]
134. Bredahl, E.C.; Pfannenstiel, K.B.; Quinn, C.J.; Hayward, R.; Hydock, D.S. Effects of Exercise on Doxorubicin-Induced Skeletal Muscle Dysfunction. *Med. Sci. Sports Exerc.* **2016**, *48*, 1468–1473. [CrossRef] [PubMed]
135. Kavazis, A.N.; Smuder, A.J.; Powers, S.K. Effects of short-term endurance exercise training on acute doxorubicin-induced FoxO transcription in cardiac and skeletal muscle. *J. Appl. Physiol.* **2014**, *117*, 223–230. [CrossRef] [PubMed]
136. Mackay, A.D.; Marchant, E.D.; Munk, D.J.; Watt, R.K.; Hansen, J.M.; Thomson, D.M.; Hancock, C.R. Multitissue analysis of exercise and metformin on doxorubicin-induced iron dysregulation. *Am. J. Physiol. Endocrinol. Metab.* **2019**, *316*, E922–E930. [CrossRef]
137. Morton, A.B.; Mor Huertas, A.; Hinkley, J.M.; Ichinoseki-Sekine, N.; Christou, D.D.; Smuder, A.J. Mitochondrial accumulation of doxorubicin in cardiac and diaphragm muscle following exercise preconditioning. *Mitochondrion* **2019**, *45*, 52–62. [CrossRef]
138. Huertas, A.M.; Morton, A.B.; Hinkey, J.M.; Ichinoseki-Sekine, N.; Smuder, A.J. Modification of Neuromuscular Junction Protein Expression by Exercise and Doxorubicin. *Med. Sci. Sports Exerc.* **2020**, *52*, 1477–1484. [CrossRef]
139. Jones, L.W.; Alfano, C.M. Exercise-oncology research: Past, present, and future. *Acta Oncol.* **2013**, *52*, 195–215. [CrossRef]
140. Dickinson, J.M.; D'Lugos, A.C.; Mahmood, T.N.; Ormsby, J.C.; Salvo, L.; Dedmon, W.L.; Patel, S.H.; Katsma, M.S.; Mookadam, F.; Gonzales, R.J.; et al. Exercise Protects Skeletal Muscle during Chronic Doxorubicin Administration. *Med. Sci. Sports Exerc.* **2017**, *49*, 2394–2403. [CrossRef]
141. de Lima, E.A.; de Sousa, L.G.O.; de S Teixeira, A.A.; Marshall, A.G.; Zanchi, N.E.; Neto, J.C.R. Aerobic exercise, but not metformin, prevents reduction of muscular performance by AMPk activation in mice on doxorubicin chemotherapy. *J. Cell Physiol.* **2018**, *233*, 9652–9662. [CrossRef] [PubMed]
142. Hojman, P.; Fjelbye, J.; Zerahn, B.; Christensen, J.F.; Dethlefsen, C.; Lonkvist, C.K.; Brandt, C.; Gissel, H.; Pedersen, B.K.; Gehl, J. Voluntary exercise prevents cisplatin-induced muscle wasting during chemotherapy in mice. *PLoS ONE* **2014**, *9*, e109030. [CrossRef] [PubMed]
143. Alves de Lima, E., Jr.; Teixeira, A.A.S.; Biondo, L.A.; Diniz, T.A.; Silveira, L.S.; Coletti, D.; Busquets Rius, S.; Rosa Neto, J.C. Exercise Reduces the Resumption of Tumor Growth and Proteolytic Pathways in the Skeletal Muscle of Mice Following Chemotherapy. *Cancers* **2020**, *12*, 3466. [CrossRef] [PubMed]
144. Kemi, O.J.; Loennechen, J.P.; Wisløff, U.; Ellingsen, Ø. Intensity-controlled treadmill running in mice: Cardiac and skeletal muscle hypertrophy. *J. Appl. Physiol.* **2002**, *93*, 1301–1309. [CrossRef] [PubMed]
145. Fuller, K.N.Z.; Thyfault, J.P. Barriers in translating preclinical rodent exercise metabolism findings to human health. *J. Appl. Physiol.* **2021**, *130*, 182–192. [CrossRef]
146. Montalvo, R.N.; Doerr, V.; Nguyen, B.L.; Kelley, R.C.; Smuder, A.J. Consideration of Sex as a Biological Variable in the Development of Doxorubicin Myotoxicity and the Efficacy of Exercise as a Therapeutic Intervention. *Antioxidants* **2021**, *10*, 343. [CrossRef] [PubMed]
147. Avila, J.J.; Kim, S.K.; Massett, M.P. Differences in Exercise Capacity and Responses to Training in 24 Inbred Mouse Strains. *Front. Physiol.* **2017**, *8*, 974. [CrossRef]
148. Goh, J.; Ladiges, W. Voluntary Wheel Running in Mice. *Curr. Protoc. Mouse Biol.* **2015**, *5*, 283–290. [CrossRef] [PubMed]
149. Ikeda, S.; Kawamoto, H.; Kasaoka, K.; Hitomi, Y.; Kizaki, T.; Sankai, Y.; Ohno, H.; Haga, S.; Takemasa, T. Muscle type-specific response of PGC-1α and oxidative enzymes during voluntary wheel running in mouse skeletal muscle. *Acta Physiol.* **2006**, *188*, 217–223. [CrossRef]
150. Murach, K.A.; McCarthy, J.J.; Peterson, C.A.; Dungan, C.M. Making Mice Mighty: Recent advances in translational models of load-induced muscle hypertrophy. *J. Appl. Physiol.* **2020**, *129*, 516–521. [CrossRef]
151. Huang, S.C.; Wu, J.F.; Saovieng, S.; Chien, W.H.; Hsu, M.F.; Li, X.F.; Lee, S.D.; Huang, C.Y.; Huang, C.Y.; Kuo, C.H. Doxorubicin inhibits muscle inflammation after eccentric exercise. *J. Cachexia Sarcopenia Muscle* **2017**, *8*, 277–284. [CrossRef]
152. Yen, H.C.; Oberley, T.D.; Vichitbandha, S.; Ho, Y.S.; St Clair, D.K. The protective role of manganese superoxide dismutase against adriamycin-induced acute cardiac toxicity in transgenic mice. *J. Clin. Investig.* **1996**, *98*, 1253–1260. [CrossRef]

153. Salvatorelli, E.; Menna, P.; Minotti, G. Managing anthracycline-induced cardiotoxicity: Beginning with the end in mind. *Future Cardiol.* **2015**, *11*, 363–366. [CrossRef] [PubMed]
154. de Lima Junior, E.A.; Yamashita, A.S.; Pimentel, G.D.; De Sousa, L.G.; Santos, R.V.; Gonçalves, C.L.; Streck, E.L.; de Lira, F.S.; Rosa Neto, J.C. Doxorubicin caused severe hyperglycaemia and insulin resistance, mediated by inhibition in AMPk signalling in skeletal muscle. *J. Cachexia Sarcopenia Muscle* **2016**, *7*, 615–625. [CrossRef]
155. Hardee, J.P.; Counts, B.R.; Carson, J.A. Understanding the Role of Exercise in Cancer Cachexia Therapy. *Am. J. Lifestyle Med.* **2017**, *13*, 46–60. [CrossRef]
156. Campbell, K.L.; Winters-Stone, K.M.; Wiskemann, J.; May, A.M.; Schwartz, A.L.; Courneya, K.S.; Zucker, D.S.; Matthews, C.E.; Ligibel, J.A.; Gerber, L.H.; et al. Exercise Guidelines for Cancer Survivors: Consensus Statement from International Multidisciplinary Roundtable. *Med. Sci. Sports Exerc.* **2019**, *51*, 2375–2390. [CrossRef]
157. Battaglini, C.; Bottaro, M.; Dennehy, C.; Rae, L.; Shields, E.; Kirk, D.; Hackney, A.C. The effects of an individualized exercise intervention on body composition in breast cancer patients undergoing treatment. *Sao Paulo Med J.* **2007**, *125*, 22–28. [CrossRef]
158. Courneya, K.S.; Segal, R.J.; Mackey, J.R.; Gelmon, K.; Reid, R.D.; Friedenreich, C.M.; Ladha, A.B.; Proulx, C.; Vallance, J.K.; Lane, K.; et al. Effects of aerobic and resistance exercise in breast cancer patients receiving adjuvant chemotherapy: A multicenter randomized controlled trial. *J. Clin. Oncol.* **2007**, *25*, 4396–4404. [CrossRef]
159. Mijwel, S.; Cardinale, D.A.; Norrbom, J.; Chapman, M.; Ivarsson, N.; Wengström, Y.; Sundberg, C.J.; Rundqvist, H. Exercise training during chemotherapy preserves skeletal muscle fiber area, capillarization, and mitochondrial content in patients with breast cancer. *FASEB J.* **2018**, *32*, 5495–5505. [CrossRef] [PubMed]
160. Lønbro, S.; Farup, J.; Bentsen, S.; Voss, T.; Rittig, N.; Wang, J.; Ørskov, M.; Højris, I.; Mikkelsen, U.R. Lean body mass, muscle fibre size and muscle function in cancer patients during chemotherapy and 10 weeks exercise. *JCSM Clin. Rep.* **2017**, *2*, 1–15. [CrossRef]
161. Buckinx, F.; Landi, F.; Cesari, M.; Fielding, R.A.; Visser, M.; Engelke, K.; Maggi, S.; Dennison, E.; Al-Daghri, N.M.; Allepaerts, S.; et al. Pitfalls in the measurement of muscle mass: A need for a reference standard. *J. Cachexia Sarcopenia Muscle* **2018**, *9*, 269–278. [CrossRef]
162. Yao, W.; Jee, W.S.; Chen, J.L.; Li, C.Y.; Frost, H.M. A novel method to 'exercise' rats: Making rats rise to erect bipedal stance for feeding-raised cage model. *J. Musculoskelet Neuronal Interact* **2001**, *1*, 241–247.
163. Puppa, M.J.; Gao, S.; Narsale, A.A.; Carson, J.A. Skeletal muscle glycoprotein 130's role in Lewis lung carcinoma-induced cachexia. *FASEB J.* **2014**, *28*, 998–1009. [CrossRef]
164. Aulino, P.; Berardi, E.; Cardillo, V.M.; Rizzuto, E.; Perniconi, B.; Ramina, C.; Padula, F.; Spugnini, E.P.; Baldi, A.; Faiola, F.; et al. Molecular, cellular and physiological characterization of the cancer cachexia-inducing C26 colon carcinoma in mouse. *BMC Cancer* **2010**, *10*, 363. [CrossRef]
165. Hatakeyama, S.; Summermatter, S.; Jourdain, M.; Melly, S.; Minetti, G.C.; Lach-Trifilieff, E. ActRII blockade protects mice from cancer cachexia and prolongs survival in the presence of anti-cancer treatments. *Skelet. Muscle* **2016**, *6*, 26. [CrossRef] [PubMed]
166. Garcia, J.M.; Scherer, T.; Chen, J.A.; Guillory, B.; Nassif, A.; Papusha, V.; Smiechowska, J.; Asnicar, M.; Buettner, C.; Smith, R.G. Inhibition of cisplatin-induced lipid catabolism and weight loss by ghrelin in male mice. *Endocrinology* **2013**, *154*, 3118–3129. [CrossRef] [PubMed]
167. Yu, A.P.; Pei, X.M.; Sin, T.K.; Yip, S.P.; Yung, B.Y.; Chan, L.W.; Wong, C.S.; Siu, P.M. Acylated and unacylated ghrelin inhibit doxorubicin-induced apoptosis in skeletal muscle. *Acta Physiol.* **2014**, *211*, 201–213. [CrossRef]
168. Bresciani, E.; Rizzi, L.; Molteni, L.; Ravelli, M.; Liantonio, A.; Ben Haj Salah, K.; Fehrentz, J.A.; Martinez, J.; Omeljaniuk, R.J.; Biagini, G.; et al. JMV2894, a novel growth hormone secretagogue, accelerates body mass recovery in an experimental model of cachexia. *Endocrine* **2017**, *58*, 106–114. [CrossRef]
169. Brierley, D.I.; Harman, J.R.; Giallourou, N.; Leishman, E.; Roashan, A.E.; Mellows, B.A.D.; Bradshaw, H.B.; Swann, J.R.; Patel, K.; Whalley, B.J.; et al. Chemotherapy-induced cachexia dysregulates hypothalamic and systemic lipoamines and is attenuated by cannabigerol. *J. Cachexia Sarcopenia Muscle* **2019**, *10*, 844–859. [CrossRef] [PubMed]
170. Miyake, M.; Hori, S.; Itami, Y.; Oda, Y.; Owari, T.; Fujii, T.; Ohnishi, S.; Morizawa, Y.; Gotoh, D.; Nakai, Y.; et al. Supplementary Oral Anamorelin Mitigates Anorexia and Skeletal Muscle Atrophy Induced by Gemcitabine Plus Cisplatin Systemic Chemotherapy in a Mouse Model. *Cancers* **2020**, *12*, 1942. [CrossRef]
171. Wu, Y.-Q.; Dang, R.-L.; Tang, M.-M.; Cai, H.-L.; Li, H.-D.; Liao, D.-H.; He, X.; Cao, L.-J.; Xue, Y.; Jiang, P. Long Chain Omega-3 Polyunsaturated Fatty Acid Supplementation Alleviates Doxorubicin-Induced Depressive-Like Behaviors and Neurotoxicity in Rats: Involvement of Oxidative Stress and Neuroinflammation. *Nutrients* **2016**, *8*, 243. [CrossRef]
172. Almasud, A.A.; Giles, K.H.; Miklavcic, J.J.; Martins, K.J.B.; Baracos, V.E.; Putman, C.T.; Guan, L.L.; Mazurak, V.C. Fish oil mitigates myosteatosis and improves chemotherapy efficacy in a preclinical model of colon cancer. *PLoS ONE* **2017**, *12*, e0183576. [CrossRef]
173. Wu, C.T.; Liao, J.M.; Ko, J.L.; Lee, Y.L.; Chang, H.Y.; Wu, C.H.; Ou, C.C. D-Methionine Ameliorates Cisplatin-Induced Muscle Atrophy via Inhibition of Muscle Degradation Pathway. *Integr. Cancer Ther.* **2019**, *18*. [CrossRef] [PubMed]
174. Torok, Z.A.; Busekrus, R.B.; Hydock, D.S. Effects of Creatine Supplementation on Muscle Fatigue in Rats Receiving Doxorubicin Treatment. *Nutr. Cancer* **2020**, *72*, 252–259. [CrossRef] [PubMed]
175. Stacchiotti, A.; Rovetta, F.; Ferroni, M.; Corsetti, G.; Lavazza, A.; Sberveglieri, G.; Aleo, M.F. Taurine rescues cisplatin-induced muscle atrophy in vitro: A morphological study. *Oxid. Med. Cell Longev.* **2014**, *2014*, 840951. [CrossRef] [PubMed]

176. Bredahl, E.C.; Busekrus, R.B.; Hydock, D.S. The combined effect of creatine and resistance training on doxorubicin-induced muscle dysfunction. *Nutr. Cancer* **2020**, *72*, 939–947. [CrossRef] [PubMed]
177. Lobina, C.; Carai, M.A.; Loi, B.; Gessa, G.L.; Riva, A.; Cabri, W.; Petrangolini, G.; Morazzoni, P.; Colombo, G. Protective effect of Panax ginseng in cisplatin-induced cachexia in rats. *Future Oncol.* **2014**, *10*, 1203–1214. [CrossRef]
178. Wang, H.; Chan, Y.-L.; Li, T.-L.; Wu, C.-J. Improving cachectic symptoms and immune strength of tumour-bearing mice in chemotherapy by a combination of *Scutellaria baicalensis* and Qing-Shu-Yi-Qi-Tang. *Eur. J. Cancer* **2012**, *48*, 1074–1084. [CrossRef] [PubMed]
179. Chen, M.C.; Hsu, W.L.; Chou, T.C. Anti-cachectic effect of Antrodia cinnamomea extract in lung tumor-bearing mice under chemotherapy. *Oncotarget* **2018**, *9*, 19584–19596. [CrossRef]
180. Chen, J.M.; Yang, T.T.; Cheng, T.S.; Hsiao, T.F.; Chang, P.M.; Leu, J.Y.; Wang, F.S.; Hsu, S.L.; Huang, C.F.; Lai, J.M. Modified Sijunzi decoction can alleviate cisplatin-induced toxicity and prolong the survival time of cachectic mice by recovering muscle atrophy. *J. Ethnopharmacol.* **2019**, *233*, 47–55. [CrossRef]
181. Huang, T.H.; Wu, T.H.; Guo, Y.H.; Li, T.L.; Chan, Y.L.; Wu, C.J. The concurrent treatment of Scutellaria baicalensis Georgi enhances the therapeutic efficacy of cisplatin but also attenuates chemotherapy-induced cachexia and acute kidney injury. *J. Ethnopharmacol.* **2019**, *243*, 112075. [CrossRef]
182. Lee, C.; Jeong, H.; Lee, H.; Hong, M.; Park, S.Y.; Bae, H. Magnolol Attenuates Cisplatin-Induced Muscle Wasting by M2c Macrophage Activation. *Front. Immunol.* **2020**, *11*, 77. [CrossRef]
183. Zhang, H.; Chi, M.; Chen, L.; Sun, X.; Wan, L.; Yang, Q.; Guo, C. Linalool Prevents Cisplatin Induced Muscle Atrophy by Regulating IGF-1/Akt/FoxO Pathway. *Front. Pharmacol.* **2020**, *11*, 598166. [CrossRef]
184. Hong, M.; Han, I.H.; Choi, I.; Cha, N.; Kim, W.; Kim, S.K.; Bae, H. Magnoliae Cortex Alleviates Muscle Wasting by Modulating M2 Macrophages in a Cisplatin-Induced Sarcopenia Mouse Model. *Int. J. Mol. Sci.* **2021**, *22*, 3188. [CrossRef] [PubMed]
185. Abulizi, A.; Hu, L.; Ma, A.; Shao, F.-y.; Zhu, H.-z.; Lin, S.-m.; Shao, G.-y.; Xu, Y.; Ran, J.-h.; Li, J.; et al. Ganoderic acid alleviates chemotherapy-induced fatigue in mice bearing colon tumor. *Acta Pharmacol. Sin.* **2021**. [CrossRef] [PubMed]
186. Hulmi, J.J.; Nissinen, T.A.; Penna, F.; Bonetto, A. Targeting the Activin Receptor Signaling to Counteract the Multi-Systemic Complications of Cancer and Its Treatments. *Cells* **2021**, *10*, 516. [CrossRef] [PubMed]
187. Marceca, G.P.; Londhe, P.; Calore, F. Management of Cancer Cachexia: Attempting to Develop New Pharmacological Agents for New Effective Therapeutic Options. *Front. Oncol.* **2020**, *10*. [CrossRef] [PubMed]
188. Temel, J.S.; Abernethy, A.P.; Currow, D.C.; Friend, J.; Duus, E.M.; Yan, Y.; Fearon, K.C. Anamorelin in patients with non-small-cell lung cancer and cachexia (ROMANA 1 and ROMANA 2): Results from two randomised, double-blind, phase 3 trials. *Lancet. Oncol.* **2016**, *17*, 519–531. [CrossRef]
189. van de Worp, W.R.P.H.; Schols, A.M.W.J.; Theys, J.; van Helvoort, A.; Langen, R.C.J. Nutritional Interventions in Cancer Cachexia: Evidence and Perspectives From Experimental Models. *Front. Nutr.* **2020**, *7*. [CrossRef] [PubMed]
190. Prado, C.M.; Purcell, S.A.; Laviano, A. Nutrition interventions to treat low muscle mass in cancer. *J. Cachexia Sarcopenia Muscle* **2020**, *11*, 366–380. [CrossRef]
191. Prado, C.M.; Anker, S.D.; Coats, A.J.S.; Laviano, A.; von Haehling, S. Nutrition in the spotlight in cachexia, sarcopenia and muscle: Avoiding the wildfire. *J. Cachexia Sarcopenia Muscle* **2021**, *12*, 3–8. [CrossRef] [PubMed]
192. Kuchta, K.; Cameron, S. Phytotherapy for Cachexia: Where Do We Stand? *Front. Pharmacol.* **2020**, *11*. [CrossRef] [PubMed]
193. Bowen, T.S.; Adams, V.; Werner, S.; Fischer, T.; Vinke, P.; Brogger, M.N.; Mangner, N.; Linke, A.; Sehr, P.; Lewis, J.; et al. Small-molecule inhibition of MuRF1 attenuates skeletal muscle atrophy and dysfunction in cardiac cachexia. *J. Cachexia Sarcopenia Muscle* **2017**, *8*, 939–953. [CrossRef] [PubMed]
194. Szeto, H.H. First-in-class cardiolipin-protective compound as a therapeutic agent to restore mitochondrial bioenergetics. *Br. J. Pharmacol.* **2014**, *171*, 2029–2050. [CrossRef] [PubMed]
195. Horvath, O.; Ordog, K.; Bruszt, K.; Kalman, N.; Kovacs, D.; Radnai, B.; Gallyas, F.; Toth, K.; Halmosi, R.; Deres, L. Modulation of Mitochondrial Quality Control Processes by BGP-15 in Oxidative Stress Scenarios: From Cell Culture to Heart Failure. *Oxidative Med. Cell. Longev.* **2021**, *2021*, 6643871. [CrossRef] [PubMed]
196. Pető, Á.; Kósa, D.; Fehér, P.; Ujhelyi, Z.; Sinka, D.; Vecsernyés, M.; Szilvássy, Z.; Juhász, B.; Csanádi, Z.; Vígh, L.; et al. Pharmacological Overview of the BGP-15 Chemical Agent as a New Drug Candidate for the Treatment of Symptoms of Metabolic Syndrome. *Molecules* **2020**, *25*, 429. [CrossRef]
197. Literati-Nagy, B.; Peterfai, E.; Kulcsar, E.; Literati-Nagy, Z.; Buday, B.; Tory, K.; Mandl, J.; Sumegi, B.; Fleming, A.; Roth, J.; et al. Beneficial effect of the insulin sensitizer (HSP inducer) BGP-15 on olanzapine-induced metabolic disorders. *Brain Res. Bull.* **2010**, *83*, 340–344. [CrossRef] [PubMed]
198. Racz, I.; Tory, K.; Gallyas, F., Jr.; Berente, Z.; Osz, E.; Jaszlits, L.; Bernath, S.; Sumegi, B.; Rabloczky, G.; Literati-Nagy, P. BGP-15-a novel poly(ADP-ribose) polymerase inhibitor-protects against nephrotoxicity of cisplatin without compromising its antitumor activity. *Biochem. Pharmacol.* **2002**, *63*, 1099–1111. [CrossRef]
199. Henstridge, D.C.; Bruce, C.R.; Drew, B.G.; Tory, K.; Kolonics, A.; Estevez, E.; Chung, J.; Watson, N.; Gardner, T.; Lee-Young, R.S.; et al. Activating HSP72 in rodent skeletal muscle increases mitochondrial number and oxidative capacity and decreases insulin resistance. *Diabetes* **2014**, *63*, 1881–1894. [CrossRef]
200. Bai, P.; Canto, C.; Oudart, H.; Brunyanszki, A.; Cen, Y.; Thomas, C.; Yamamoto, H.; Huber, A.; Kiss, B.; Houtkooper, R.H.; et al. PARP-1 inhibition increases mitochondrial metabolism through SIRT1 activation. *Cell Metab.* **2011**, *13*, 461–468. [CrossRef]

201. Sapra, G.; Tham, Y.K.; Cemerlang, N.; Matsumoto, A.; Kiriazis, H.; Bernardo, B.C.; Henstridge, D.C.; Ooi, J.Y.; Pretorius, L.; Boey, E.J.; et al. The small-molecule BGP-15 protects against heart failure and atrial fibrillation in mice. *Nat. Commun.* **2014**, *5*, 5705. [CrossRef]
202. Salah, H.; Li, M.; Cacciani, N.; Gastaldello, S.; Ogilvie, H.; Akkad, H.; Namuduri, A.V.; Morbidoni, V.; Artemenko, K.A.; Balogh, G.; et al. The chaperone co-inducer BGP-15 alleviates ventilation-induced diaphragm dysfunction. *Sci. Transl. Med.* **2016**, *8*, 350ra103. [CrossRef] [PubMed]
203. Gehrig, S.M.; van der Poel, C.; Sayer, T.A.; Schertzer, J.D.; Henstridge, D.C.; Church, J.E.; Lamon, S.; Russell, A.P.; Davies, K.E.; Febbraio, M.A.; et al. Hsp72 preserves muscle function and slows progression of severe muscular dystrophy. *Nature* **2012**, *484*, 394–398. [CrossRef] [PubMed]
204. Literati-Nagy, B.; Kulcsar, E.; Literati-Nagy, Z.; Buday, B.; Peterfai, E.; Horvath, T.; Tory, K.; Kolonics, A.; Fleming, A.; Mandl, J.; et al. Improvement of insulin sensitivity by a novel drug, BGP-15, in insulin-resistant patients: A proof of concept randomized double-blind clinical trial. *Horm. Metab. Res.* **2009**, *41*, 374–380. [CrossRef] [PubMed]
205. Chung, J.; Nguyen, A.K.; Henstridge, D.C.; Holmes, A.G.; Chan, M.H.; Mesa, J.L.; Lancaster, G.I.; Southgate, R.J.; Bruce, C.R.; Duffy, S.J.; et al. HSP72 protects against obesity-induced insulin resistance. *Proc. Natl. Acad. Sci. USA* **2008**, *105*, 1739–1744. [CrossRef]
206. Kourakis, S.; Timpani, C.A.; de Haan, J.B.; Gueven, N.; Fischer, D.; Rybalka, E. Dimethyl Fumarate and Its Esters: A Drug with Broad Clinical Utility? *Pharmaceuticals* **2020**, *13*, 306. [CrossRef]
207. Bhakkiyalakshmi, E.; Dineshkumar, K.; Karthik, S.; Sireesh, D.; Hopper, W.; Paulmurugan, R.; Ramkumar, K.M. Pterostilbene-mediated Nrf2 activation: Mechanistic insights on Keap1:Nrf2 interface. *Bioorganic Med. Chem.* **2016**, *24*, 3378–3386. [CrossRef]
208. Sin, T.K.; Tam, B.T.; Yu, A.P.; Yip, S.P.; Yung, B.Y.; Chan, L.W.; Wong, C.S.; Rudd, J.A.; Siu, P.M. Acute Treatment of Resveratrol Alleviates Doxorubicin-Induced Myotoxicity in Aged Skeletal Muscle Through SIRT1-Dependent Mechanisms. *J. Gerontol. Ser. A Biomed. Sci. Med Sci.* **2016**, *71*, 730–739. [CrossRef]
209. Dolinsky, V.W.; Rogan, K.J.; Sung, M.M.; Zordoky, B.N.; Haykowsky, M.J.; Young, M.E.; Jones, L.W.; Dyck, J.R.B. Both aerobic exercise and resveratrol supplementation attenuate doxorubicin-induced cardiac injury in mice. *Am. J. Physiol.-Endocrinol. Metab.* **2013**, *305*, E243–E253. [CrossRef]
210. Cheng, Y.; Di, S.; Fan, C.; Cai, L.; Gao, C.; Jiang, P.; Hu, W.; Ma, Z.; Jiang, S.; Dong, Y.; et al. SIRT1 activation by pterostilbene attenuates the skeletal muscle oxidative stress injury and mitochondrial dysfunction induced by ischemia reperfusion injury. *Apoptosis* **2016**, *21*, 905–916. [CrossRef]
211. Zhang, L.; Cui, L.; Zhou, G.; Jing, H.; Guo, Y.; Sun, W. Pterostilbene, a natural small-molecular compound, promotes cytoprotective macroautophagy in vascular endothelial cells. *J. Nutr. Biochem.* **2013**, *24*, 903–911. [CrossRef]
212. Riche, D.M.; McEwen, C.L.; Riche, K.D.; Sherman, J.J.; Wofford, M.R.; Deschamp, D.; Griswold, M. Analysis of safety from a human clinical trial with pterostilbene. *J. Toxicol.* **2013**, *2013*, 463595. [CrossRef]
213. Lan, X.; Han, X.; Li, Q.; Wang, J. (-)-Epicatechin, a Natural Flavonoid Compound, Protects Astrocytes Against Hemoglobin Toxicity via Nrf2 and AP-1 Signaling Pathways. *Mol. Neurobiol.* **2017**, *54*, 7898–7907. [CrossRef]
214. Taub, P.R.; Ramirez-Sanchez, I.; Ciaraldi, T.P.; Gonzalez-Basurto, S.; Coral-Vazquez, R.; Perkins, G.; Hogan, M.; Maisel, A.S.; Henry, R.R.; Ceballos, G.; et al. Perturbations in skeletal muscle sarcomere structure in patients with heart failure and type 2 diabetes: Restorative effects of (-)-epicatechin-rich cocoa. *Clin. Sci.* **2013**, *125*, 383–389. [CrossRef]
215. McDonald, C.M.; Ramirez-Sanchez, I.; Oskarsson, B.; Joyce, N.; Aguilar, C.; Nicorici, A.; Dayan, J.; Goude, E.; Abresch, R.T.; Villarreal, F.; et al. (-)-Epicatechin induces mitochondrial biogenesis and markers of muscle regeneration in adults with Becker muscular dystrophy. *Muscle Nerve* **2021**, *63*, 239–249. [CrossRef]
216. Acharyya, S.; Butchbach, M.E.; Sahenk, Z.; Wang, H.; Saji, M.; Carathers, M.; Ringel, M.D.; Skipworth, R.J.; Fearon, K.C.; Hollingsworth, M.A.; et al. Dystrophin glycoprotein complex dysfunction: A regulatory link between muscular dystrophy and cancer cachexia. *Cancer Cell* **2005**, *8*, 421–432. [CrossRef] [PubMed]
217. Mena, S.; Rodriguez, M.L.; Ponsoda, X.; Estrela, J.M.; Jaattela, M.; Ortega, A.L. Pterostilbene-induced tumor cytotoxicity: A lysosomal membrane permeabilization-dependent mechanism. *PLoS ONE* **2012**, *7*, e44524. [CrossRef] [PubMed]
218. Suraweera, T.L.; Rupasinghe, H.P.V.; Dellaire, G.; Xu, Z. Regulation of Nrf2/ARE Pathway by Dietary Flavonoids: A Friend or Foe for Cancer Management? *Antioxidants* **2020**, *9*, 973. [CrossRef]
219. Jansson, E.A.; Huang, L.; Malkey, R.; Govoni, M.; Nihlén, C.; Olsson, A.; Stensdotter, M.; Petersson, J.; Holm, L.; Weitzberg, E.; et al. A mammalian functional nitrate reductase that regulates nitrite and nitric oxide homeostasis. *Nat. Chem. Biol.* **2008**, *4*, 411–417. [CrossRef] [PubMed]
220. Lundberg, J.O.; Carlström, M.; Weitzberg, E. Metabolic Effects of Dietary Nitrate in Health and Disease. *Cell Metab.* **2018**, *28*, 9–22. [CrossRef]
221. Xi, L.; Zhu, S.G.; Hobbs, D.C.; Kukreja, R.C. Identification of protein targets underlying dietary nitrate-induced protection against doxorubicin cardiotoxicity. *J. Cell Mol. Med.* **2011**, *15*, 2512–2524. [CrossRef]
222. Zhu, S.G.; Kukreja, R.C.; Das, A.; Chen, Q.; Lesnefsky, E.J.; Xi, L. Dietary nitrate supplementation protects against Doxorubicin-induced cardiomyopathy by improving mitochondrial function. *J. Am. Coll Cardiol.* **2011**, *57*, 2181–2189. [CrossRef]
223. Campelj, D.G.; Debruin, D.A.; Timpani, C.A.; Hayes, A.; Goodman, C.A.; Rybalka, E. Sodium nitrate co-supplementation does not exacerbate low dose metronomic doxorubicin-induced cachexia in healthy mice. *Sci. Rep.* **2020**, *10*, 15044. [CrossRef]

224. Vial, G.; Detaille, D.; Guigas, B. Role of Mitochondria in the Mechanism(s) of Action of Metformin. *Front. Endocrinol.* **2019**, *10*. [CrossRef] [PubMed]
225. Kannaiyan, R.; Mahadevan, D. A comprehensive review of protein kinase inhibitors for cancer therapy. *Expert Rev. Anticancer Ther.* **2018**, *18*, 1249–1270. [CrossRef]
226. Huot, J.R.; Essex, A.L.; Gutierrez, M.; Barreto, R.; Wang, M.; Waning, D.L.; Plotkin, L.I.; Bonetto, A. Chronic Treatment with Multi-Kinase Inhibitors Causes Differential Toxicities on Skeletal and Cardiac Muscles. *Cancers* **2019**, *11*, 571. [CrossRef]
227. Toledo, M.; Penna, F.; Oliva, F.; Luque, M.; Betancourt, A.; Marmonti, E.; López-Soriano, F.J.; Argilés, J.M.; Busquets, S. A multifactorial anti-cachectic approach for cancer cachexia in a rat model undergoing chemotherapy. *J. Cachexia Sarcopenia Muscle* **2016**, *7*, 48–59. [CrossRef] [PubMed]
228. Cassileth, P.A.; Lusk, E.J.; Torri, S.; DiNubile, N.; Gerson, S.L. Antiemetic efficacy of dexamethasone therapy in patients receiving cancer chemotherapy. *Arch. Intern. Med.* **1983**, *143*, 1347–1349. [CrossRef] [PubMed]
229. Gouspillou, G.; Scheede-Bergdahl, C.; Spendiff, S.; Vuda, M.; Meehan, B.; Mlynarski, H.; Archer-Lahlou, E.; Sgarioto, N.; Purves-Smith, F.M.; Konokhova, Y.; et al. Anthracycline-containing chemotherapy causes long-term impairment of mitochondrial respiration and increased reactive oxygen species release in skeletal muscle. *Sci. Rep.* **2015**, *5*, 8717. [CrossRef]
230. Sakai, H.; Kimura, M.; Tsukimura, Y.; Yabe, S.; Isa, Y.; Kai, Y.; Sato, F.; Kon, R.; Ikarashi, N.; Narita, M.; et al. Dexamethasone exacerbates cisplatin-induced muscle atrophy. *Clin. Exp. Pharmacol. Physiol.* **2019**, *46*, 19–28. [CrossRef] [PubMed]
231. Betancourt, A.; Busquets, S.; Ponce, M.; Toledo, M.; Guàrdia-Olmos, J.; Peró-Cebollero, M.; López-Soriano, F.J.; Argilés, J.M. The animal cachexia score (ACASCO). *Anim. Model. Exp. Med.* **2019**, *2*, 201–209. [CrossRef] [PubMed]
232. Grounds, M.D.; Terrill, J.R.; Al-Mshhdani, B.A.; Duong, M.N.; Radley-Crabb, H.G.; Arthur, P.G. Biomarkers for Duchenne muscular dystrophy: Myonecrosis, inflammation and oxidative stress. *Dis. Models Mech.* **2020**, *13*, dmm043638. [CrossRef] [PubMed]

Chapter 2

Sodium nitrate co-supplementation does not exacerbate low dose metronomic doxorubicin-induced cachexia in healthy mice

Campelj DG, Debruin DA, Timpani CA, Hayes A, Goodman CA, Rybalka E. Sodium nitrate co-supplementation does not exacerbate low dose metronomic doxorubicin-induced cachexia in healthy mice. Sci Rep. 2020 Sep 24;10(1):15044. doi: 10.1038/s41598-020-71974-z. PMID: 32973229; PMCID: PMC7518269.

Preface

Doxorubicin (DOX), a particularly toxic anthracycline, has been well studied regarding its effects on skeletal muscle [1]. In fact, most of the known mechanisms of chemotherapy-induced muscle wasting and dysfunction, have been elucidated in experimental studies using DOX [1]. In our first study, we selected DOX for this reason. But rather than deliver DOX through a single bolus maximum tolerated dose as has been commonly used in other studies [2-10], we delivered it using a low-dose, metronomic regimen, to align with the clinical use of DOX in anti-cancer treatment. Ours is the first study to investigate the impact of low-dose metronomic DOX administration on cachexia and skeletal muscle parameters.

With respect to a therapeutic adjuvant, we chose to examine sodium nitrate (SN) supplementation. SN has been shown to protect cardiac muscle against DOX toxicity [11, 12] and we were interested to understand whether it could afford the same protection to skeletal muscle. In fact, some published research from our laboratory group, which examined the capacity for SN supplementation to attenuate the progression of severe muscle wasting disease, Duchenne muscular dystrophy (DMD), showed that SN exacerbates myopathy [13]. This finding was unexpected to us at the time, and we linked these negative effects to the heightened oxidative stress evident in dystrophic muscles [13, 14]. Since DOX induces mitochondrial dysfunction and oxidative stress [4, 15, 16], we wanted to confirm that SN wouldn't exacerbate cachexia since it was being touted by Xi et al, for its capacity as a therapeutic adjuvant that could be rapidly implemented in the clinic to protect the heart against DOX toxicity [11].

The aims of this study were to quantitate the impact of low-dose metronomic DOX treatment on skeletal muscle and to evaluate whether SN could protect muscle against DOX. We hypothesized that: (1) the metronomic DOX treatment regimen would induces cachexia and skeletal muscle wasting and dysfunction; and (2) that SN would exacerbate DOX-induced skeletal myopathy as it did in our previous studies using dystrophic *mdx* mice.

VICTORIA UNIVERSITY

THE NEW WAY TO DO UNI

OFFICE FOR RESEARCH TRAINING, QUALITY AND INTEGRITY

DECLARATION OF CO-AUTHORSHIP AND CO-CONTRIBUTION: PAPERS INCORPORATED IN THESIS

This declaration is to be completed for each conjointly authored publication and placed at the beginning of the thesis chapter in which the publication appears.

1. PUBLICATION DETAILS (to be completed by the candidate)

Title of Paper/Journal/Book: Sodium Nitrate co-supplementation does not exacerbate low dose metronomic doxorubicin-induced cachexia in healthy mice

Surname: Campelj

First name: Dean

Institute: Institute for Health and Sport

Candidate's Contribution (%): 70

Status:

Accepted and in press: ☐ Date:

Published: ☑ Date: 24/09/2020

2. CANDIDATE DECLARATION

I declare that the publication above meets the requirements to be included in the thesis as outlined in the HDR Policy and related Procedures – policy.vu.edu.au.

Dean Campelj Digitally signed by Dean Campelj Date: 2021.05.21 12:06:21 +10'00'

Signature **Date**

3. CO-AUTHOR(S) DECLARATION

In the case of the above publication, the following authors contributed to the work as follows:

The undersigned certify that:

1. They meet criteria for authorship in that they have participated in the conception, execution or interpretation of at least that part of the publication in their field of expertise;
2. They take public responsibility for their part of the publication, except for the responsible author who accepts overall responsibility for the publication;

3. There are no other authors of the publication according to these criteria;

4. Potential conflicts of interest have been disclosed to a) granting bodies, b) the editor or publisher of journals or other publications, and c) the head of the responsible academic unit; and

5. The original data will be held for at least five years from the date indicated below and is stored at the following **location(s)**:

Victoria University R Drive

Name(s) of Co-Author(s)	Contribution (%)	Nature of Contribution	Signature	Date
Danielle A Debruin	3	Cardiomyopathy analyses	[redacted]	18/05/21
Cara A Timpani	5	Citrate synthase analyses; manuscript review and editing		18/05/21
Alan Hayes	2	Methodological resources, manuscript review and editing		18/05/21
Craig A Goodman	10	Methodological resources, supervision, manuscript review and editing		18/05/21
Emma Rybalka	10	Conception, funding, methodological resources, manuscript review and editing		18/05/21

Updated: September 2019

SCIENTIFIC REPORTS
natureresearch

Check for updates

OPEN

Sodium nitrate co-supplementation does not exacerbate low dose metronomic doxorubicin-induced cachexia in healthy mice

Dean G. Campelj[1,2], Danielle A. Debruin[1,2], Cara A. Timpani[1,2], Alan Hayes[1,2,3], Craig A. Goodman[2,4] & Emma Rybalka[1,2]✉

The purpose of this study was to determine whether (1) sodium nitrate (SN) treatment progressed or alleviated doxorubicin (DOX)-induced cachexia and muscle wasting; and (2) if a more-clinically relevant low-dose metronomic (LDM) DOX treatment regimen compared to the high dosage bolus commonly used in animal research, was sufficient to induce cachexia in mice. Six-week old male Balb/C mice (n = 16) were treated with three intraperitoneal injections of either vehicle (0.9% NaCl; VEH) or DOX (4 mg/kg) over one week. To test the hypothesis that sodium nitrate treatment could protect against DOX-induced symptomology, a group of mice (n = 8) were treated with 1 mM $NaNO_3$ in drinking water during DOX (4 mg/kg) treatment (DOX + SN). Body composition indices were assessed using echoMRI scanning, whilst physical and metabolic activity were assessed via indirect calorimetry, before and after the treatment regimen. Skeletal and cardiac muscles were excised to investigate histological and molecular parameters. LDM DOX treatment induced cachexia with significant impacts on both body and lean mass, and fatigue/malaise (i.e. it reduced voluntary wheel running and energy expenditure) that was associated with oxidative/nitrostative stress sufficient to induce the molecular cytotoxic stress regulator, nuclear factor erythroid-2-related factor 2 (NRF-2). SN co-treatment afforded no therapeutic potential, nor did it promote the wasting of lean tissue. Our data re-affirm a cardioprotective effect for SN against DOX-induced collagen deposition. In our mouse model, SN protected against LDM DOX-induced cardiac fibrosis but had no effect on cachexia at the conclusion of the regimen.

Anthracyclines are a class of chemotherapeutic agents that are currently utilized as treatments for multiple cancers due to their potent anti-cancer efficacy[1]. One of the most common anthracyclines in clinical use is doxorubicin (DOX), which inhibits topoisomerase-II, leading to DNA damage and cell cycle arrest[2]. DOX also promotes toxicity through the reduction of its quinone moiety to an unstable semiquinone, during its metabolism by NADH dehydrogenase/Complex I of the mitochondrial ETC. In this setting, it hijacks homeostatic redox cycling to induce formation of superoxide (O_{2-}) anion radicals and subsequently increases production of reactive oxygen species (ROS) leading to oxidative damage[3]. Despite the robust anti-cancer effectivity of DOX, its staunch cytotoxic profile promotes non-specific, off-target effects in healthy tissue (in particular cardiac and skeletal muscle; for extensive reviews see[4,5], respectively) limiting its clinical utility and increasing the risk of morbidity and mortality[6]. As such, there is warranted clinical interest in preserving cardiac and skeletal muscle health during DOX administration, and a variety of adjunct therapeutics have been purported to attenuate the negative side-effects of DOX on these tissues.

Of clinical interest, a potential therapeutic strategy to protect against DOX-induced cardiotoxicity is sodium nitrate (SN) co-supplementation. SN acts by augmenting the nitrate/nitrite/nitric oxide (NO) pathway via a

[1]Institute for Health and Sport, Victoria University, Melbourne, VIC, Australia. [2]Australian Institute for Musculoskeletal Science (AIMSS), Victoria University, St Albans, Victoria, Australia. [3]Department of Medicine - Western Health, Melbourne Medical School, The University of Melbourne, Melbourne, VIC, Australia. [4]Centre for Muscle Research (CMR), Department of Physiology, The University of Melbourne, Parkville, VIC, Australia. ✉email: emma.rybalka@vu.edu.au

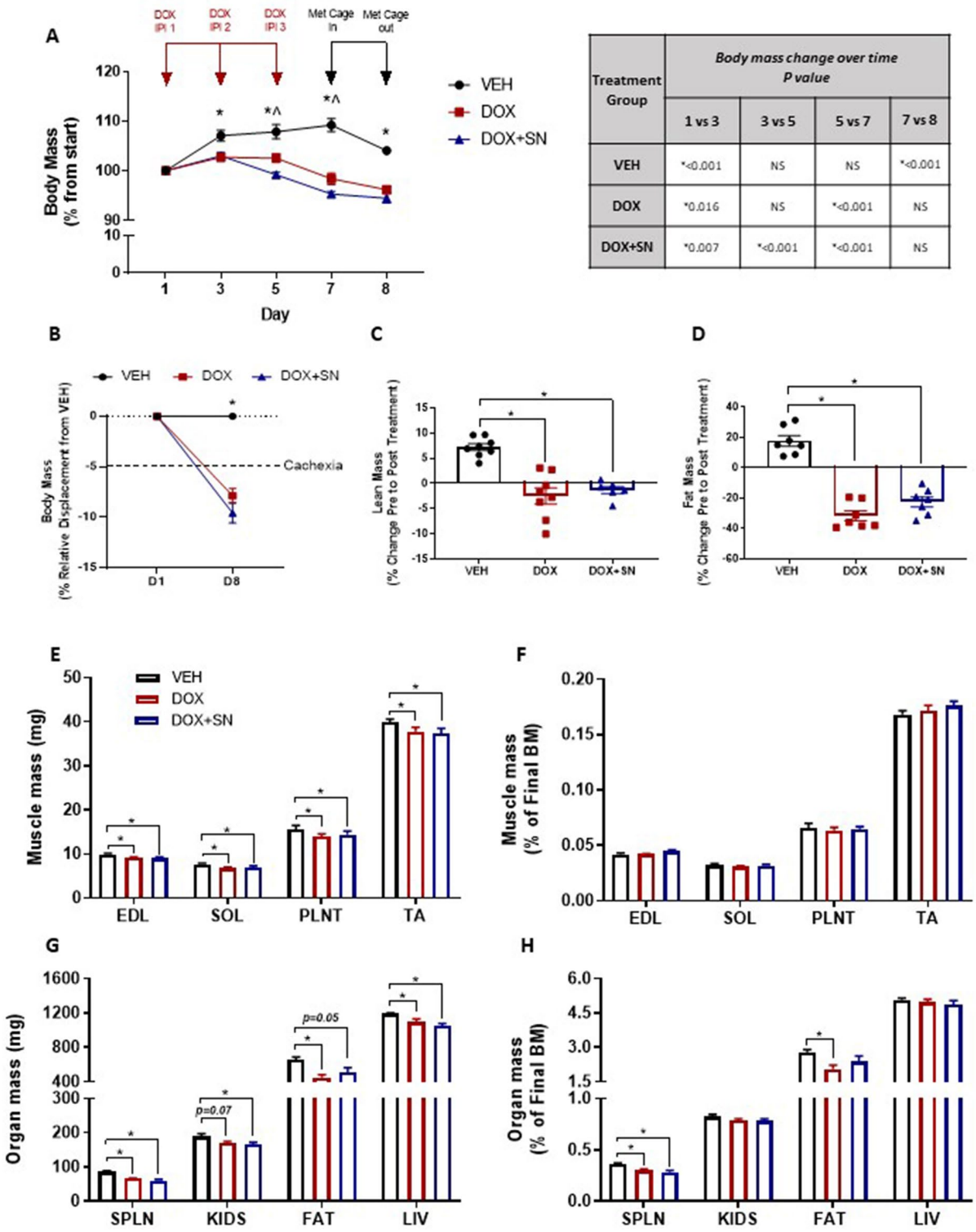

Treatment Group	*Body mass change over time P value*			
	1 vs 3	3 vs 5	5 vs 7	7 vs 8
VEH	*<0.001	NS	NS	*<0.001
DOX	*0.016	NS	*<0.001	NS
DOX+SN	*0.007	*<0.001	*<0.001	NS

◂**Figure 1.** The effect of LDM DOX administration and SN co-supplementation on body mass and composition indices, muscle and organ mass. (**A**) Body mass was measured throughout the experimental timeline and repeated measures analysis performed. A 5% increase in body mass was observed between day 1 and 3 in the VEH mice (*$p < 0.05$), which was inhibited by DOX such that by day 3, both DOX and DOX + SN mice had a lower body mass compared to VEH (*$p < 0.05$). Body mass was stable from day 3 to 7 in VEH mice, but declined steadily with DOX treatment from day 5 (*$p < 0.05$) and DOX + SN treatment from day 3 (*$p < 0.05$). As such the body mass of DOX and DOX + SN mice was lower compared to VEH at day 5 and 7 (*$p < 0.05$). Weight loss during this period was actually exacerbated by SN supplementation (^$p < 0.05$ DOX + SN versus DOX). Body mass declined during the 24 h metabolic cage stay between day 7 and 8 in VEH mice (*$p < 0.05$) due to participation in voluntary wheel running. Exercise-induced weight loss was not observed in DOX and DOX + SN mice (since they did not run as far as VEH mice) albeit body mass was still lower for these groups compared to VEH mice (*$p < 0.05$). (**B**) As defined by a > 5% reduction in body mass displacement relative to the VEH, LDM DOX and DOX + SN treatment induced cachexia (*^$p < 0.05$). Mirroring body mass changes, both (**C**) lean and (**D**) fat mass was significantly lower in DOX and DOX + SN mice compared to VEH mice (*$p < 0.05$). (**E**) The mass of extensor digitorum longus (EDL), soleus (SOL), plantaris (PLNT) and tibialis anterior (TA) muscles was significantly reduced by DOX administered alone and in the DOX + SN treatment compared to VEH mice (*$p < 0.05$). However, when (**F**) muscle mass was corrected for final body mass (BM), there was no treatment effect observed. Like muscles, organ mass was either lower, or trended to be lower following DOX treatment either alone or in the DOX + SN treatment for each of (**G**) spleen (SPLN; *$p < 0.05$ for DOX and DOX + SN compared to VEH), kidneys (KIDS; $p = 0.07$ DOX versus VEH and *$p < 0.05$ DOX + SN versus VEH), fat (epididymal and subcutaneous; FAT; *$p < 0.05$ for DOX versus VEH and $p = 0.05$ for DOX + SN versus VEH) and liver (LIV; *$p < 0.05$ for DOX and DOX + SN versus VEH). (**H**) When corrected for final BM, DOX treatment showed specific targeting of both SPLN (*$p < 0.05$ for both DOX and DOX + SN versus VEH) and FAT (*$p < 0.05$ for DOX versus VEH) which was independent of overall body mass reduction . $n = 7–8$ per group.

nitric oxide synthase (NOS)-independent mechanism, to increase NO production[7,8]. Importantly, this strategy has been shown to have therapeutic cardioprotective effects in other pre-clinical models of cardiomyopathy[9–14]. Pertinent to DOX-induced cardiomyopathy, two foundational studies have been conducted exploring the cardioprotective potential of SN co-supplementation. Data has demonstrated benefits to left ventricular function secondary to promoting anti-oxidant activity, and reducing oxidative stress via the inhibition of lipid peroxidation and amelioration of mitochondrial Complex I dysfunction[15,16]. Despite the strong cardioprotective efficacy of SN co-supplementation against DOX-induced cardiotoxicity, it is currently unclear as to whether SN co-supplementation elicits protective effects against the skeletal muscle toxicity induced by DOX.

DOX-induced skeletal muscle toxicity is widely accepted to be a consequence of its metabolism at Complex I of the mitochondrial ETC, resulting in mitochondrial dysfunction secondary to the enhancement of oxidative stress. As a consequence, DOX treatment is associated with skeletal muscle atrophy/wasting, as well as functional deficits[17–25] as characterized by reduced force production and increased susceptibility to skeletal muscle fatigue in pre-clinical animal models[26–29]. These data are consistent with clinical descriptions of exercise intolerance, a lesser capacity for activities of daily living and reduced quality of life in patients following chemotherapy treatment[30–32]. The functional benefits of SN co-supplementation on the skeletal muscular system in both rodents and humans is well documented, whereby enhanced NO bioavailability augments functional adaptations that lower the oxidative cost of exercise, subsequently improving fatigue resistance and exercise tolerance[33–35]. However, in skeletal myopathic conditions, SN co-supplementation has equivocally been shown to enhance myopathy[36,37]. In a pro-oxidant setting, akin to that induced by DOX administration, enhancing the bioavailability of NO alongside superfluous superoxide anions driven by DOX metabolism leads to peroxynitrite formation and the exacerbation of nitrostative stress[38].Thus, an aim of this study was to determine whether SN co-supplementation could afford the same therapeutic benefit as that observed previously against DOX-induced cardiotoxicity, or whether SN co-supplementation would exacerbate myopathy as per our previous study in the *mdx* mouse model of Duchenne Muscular Dystrophy[37].

A second aim of this study was to investigate the effects of low-dose, metronomic (LDM) DOX administration on skeletal and cardiac muscle. A current problem with pre-clinical research using rodent models to investigate DOX-induced toxicity surrounds the administration of a single maximum tolerable dose (MTD) injection of DOX to induce a severe scenario of toxicity and mortality[39]. This largely misrepresents the clinical scenario, in which DOX is administered repeatedly at a fractional dosage over a set time-course, to give a cumulative dose equivalent to the MTD. Recently, there has been interest in the LDM administration of chemotherapeutic agents to reduce systemic toxicity, whilst maintaining the anti-cancer efficacy of treatment[40,41]. Remarkably, there is few data derived from animal studies using LDM DOX administration to investigate potential therapeutic adjuncts against DOX-induced side-effects. As such, the clinical applicability of experimental adjuvants is largely unknown. In this study we utilized a murine model of LDM administration of DOX in an attempt to reduce the severe toxicity profile associated with the MTD model, whilst still being able to make insights into DOX-induced cardiac and skeletal muscle toxicity. Furthermore, utilizing a LDM model of DOX administration allows for a more translatable screening of potential therapeutic strategies to protect against the negative side-effects elicited to cardiac and skeletal muscle from DOX.

Results

Assessment of body composition indices, muscle and organ mass. We found that LDM DOX administration induced growth inhibition initially (i.e. from day 1–5), which progressively led to a loss of body mass from day 5 to 7 ($p < 0.05$ DOX and DOX + SN different from VEH; Fig. 1A & Supp Fig. 1) that was exacerbated by SN supplementation ($p < 0.05$ DOX + SN from DOX; Fig. 1A and Supp Fig. 1). Whereas VEH mice lost body mass during the 24 h spent (i.e. from day 7 to 8) in the metabolic cages with access to running wheels, DOX and DOX + SN treated mice did not (Fig. 1A). By the experimental endpoint at day 8, DOX-treated mice were cachetic ($p < 0.05$; Fig. 1B), but cachexia was neither exacerbated nor alleviated by SN treatment (i.e. DOX and DOX + SN mice were comparable in the degree of body weight displacement from VEH mice; Fig. 1B). Unsurprisingly, DOX-induced cachexia was mirrored in body composition indices measured via PRE- and POST-treatment echoMRI scans. DOX administration induced significant lean and fat mass loss which could not be rescued by SN co-supplementation ($p < 0.05$; Fig. 1C, D & Supp Fig. 1). Interestingly, while this wasting phenotype was characterised by both the loss of raw skeletal muscle mass ($p < 0.01$; Fig. 1E) and organ mass ($p < 0.0001$; Fig. 1G), skeletal muscle mass (Fig. 1F) was not a specific target of DOX like some organs were (Fig. 1H) with spleen and fat mass being the only tissues to waste disproportionately to body mass ($p < 0.05$; Fig. 1H). There was no significant effect of SN co-supplementation on any measure of muscle or organ mass relative to DOX treatment alone (Fig. 1E–H). Our data highlight that LDM DOX administration induces a wasting phenotype that broadly impacts the skeletal muscles, adipose tissue and organs, but which specifically wastes the spleen and adipose tissue, which is neither rescued nor exacerbated by SN co-supplementation.

Assessment of ambulatory and metabolic activity via indirect calorimetry. DOX treatment has been previously shown to induce exercise intolerance in cancer patients[30], while dietary nitrate supplementation is a potentiator of exercise performance in healthy humans[42]. Thus, in this study, we assessed the effects of LDM DOX and DOX + SN treatment on voluntary physical and metabolic activity over a 24 h period in mice. There was a strong trend for LDM DOX treatment to reduce wheel running activity between the PRE and POST periods compared to VEH (p = 0.08; Fig. 2A,B) and this effect was significant in the DOX + SN group ($p < 0.05$; Fig. 2A,B). The reduction in voluntary wheel running activity was concomitant with reduced energy expenditure in the PRE to POST treatment periods ($p < 0.05$; Fig. 2A,C), which was interesting because the PRE-treatment energy expenditure of this particular cohort of mice was significantly higher than that of the VEH and DOX + SN groups ($p < 0.05$ for both; Fig. 2A). The DOX-induced reduction in energy expenditure was associated with reduced wheel-running activity ($p < 0.05$; Fig. 2B) rather than changes to metabolism, as reflected by the RQ (Fig. 2D), and thus, is likely comparable to mental and physical fatigue reported by human patients during chemotherapy treatment[43] rather than true physiological fatigue. SN co-supplementation had no effect on the DOX-induced changes in energy expenditure (Fig. 2A), but it did elevate the RQ compared to VEH (p,0.05; Fig. 2D) and there was a trend toward the same effect compared to DOX treatment alone (p = 0.09; Fig. 2D), suggestive of increased dependency on glucose as a substrate during activity.

Assessment of cardiac muscle mass and histology. Cardiotoxicity is a well-established side-effect of DOX treatment and severity is dose-dependent[44]. In our study, LDM DOX administration had no effect on heart mass (Fig. 3A,B), while SN co-supplementation reduced raw heart mass ($p < 0.05$, Fig. 3A), albeit this was not significant when normalised to body mass (Fig. 3B). We investigated histological changes induced by chemotherapy, with LDM DOX administration increasing the total diameter of the heart ($p < 0.05$; Fig. 3C). Interestingly, there were no significant effects elicited from LDM DOX administration on morphological cardiac muscle indices (Fig. 3D). LDM DOX administration did, however, increase collagen deposition in cardiac tissue (Fig. 3E), suggestive of early-stage myocardial fibrosis that would likely reduce the contractility of the heart[45,46]. SN has demonstrable therapeutic benefit in mitigating DOX-induced cardiotoxicity in mice when supplemented prior to, and following, the administration of a single MTD bolus of DOX[15]. In our study, DOX + SN treatment actually enhanced the DOX-induced reduction in heart mass (Fig. 3A), however, this appeared to be related to the larger body mass reduction observed with DOX + SN versus DOX-treatment alone since this effect was abolished when heart mass was normalised to body weight (Fig. 3B). We did observe a strong trend for DOX + SN treatment to mitigate the enlarged total heart diameter induced by DOX-treatment (p = 0.08; Fig. 3C), and this is likely related to the beneficial effect that SN co-supplementation had on collagen deposition through the cardiac tissue, in which collagen content was reduced compared to both DOX and VEH mice ($p < 0.05$; Fig. 3E). Interestingly, SN co-supplementation increased LV wall thickness compared to both VEH and DOX treatment ($p < 0.05$; Fig. 3D), however it significantly reduced the LV and RV lumen diameter ($p < 0.05$ DOX + SN versus VEH and DOX; Fig. 3D). Overall, our data suggest that SN co-supplementation has protective effects against a mild pro-collagenic driven cardiofibrosis induced by LDM DOX treatment, which may be related to the smaller heart size.

Assessment of skeletal muscle histology. Neither DOX administration, nor SN co-supplementation, had a significant effect on the fibre CSA or skeletal muscle architecture of the TA when stained with H&E (Fig. 4A & B). Furthermore, there was no change in fat deposition, measured via ORO staining (Fig. 4C), nor mitochondrial abundance/activity, as indicated by SDH staining (Fig. 4D) from DOX administration or SN co-supplementation. To determine whether there were differential effects of DOX with and without SN co-supplementation on oxidative versus glycolytic fibres, we conducted CSA analysis on distinct populations of these fibre types based upon SDH staining intensity. There was no effect of DOX on the CSA of either oxidative or glycolytic fibres (Fig. 4E). DOX + SN treatment significantly reduced the CSA of glycolytic fibres ($p < 0.05$ DOX + SN versus VEH; $p = 0.07$ DOX + SN versus DOX; Fig. 4E) but had no effect on oxidative fibres, suggestive of nitrate-mediated fibre type transformation from IIb to IIa type.

A

Pre-Treatment				Shapiro-Wilk Normality Test	*P* value		
	VEH (A)	DOX (B)	DOX+SN (C)	Pass (Y/N)	A vs B	A vs C	B vs C
Wheel activity (m)	2297.9 ± 369.9	3435.9 ± 548.8	2566.8 ± 256.0	Y	0.286	0.930	0.498
Cage activity (m)	137.3 ± 9.0	108.9 ± 14.9	120.3 ± 7.4	Y	0.473	0.792	0.867
Total Energy Expenditure (kcal)	9.3 ± 0.1	10.6 ± 0.3*	9.5 ± 0.4^	Y	0.003*	0.802	0.017^
Average RQ (VCO_2/VO_2)	0.86 ± 0.01	0.87 ± 0.01	0.83 ± 0.01#^	Y	0.898	0.081#	0.035*
Post-Treatment				**Shapiro-Wilk Normality Test**	***P* value**		
	VEH (A)	DOX (B)	DOX+SN (C)	Pass (Y/N)	A vs B	A vs C	B vs C
Wheel activity (m)	4452.0 ± 860.5	3411.8 ± 368.3	1895.1 ± 770.0*	Y	0.400	0.008*	0.172
Cage activity (m)	104.1 ± 18.7	83.4 ± 12.8	99.6 ± 12.2	N	0.467	0.577	0.869
Total Energy Expenditure (kcal)	10.5 ± 0.3	8.9 ± 0.1*	8.4 ± 0.2*	Y	<0.001*	<0.001*	0.655
Average RQ (VCO_2/VO_2)	0.87 ± 0.01	0.90 ± 0.01#	0.91 ± 0.01#	Y	0.069#	0.052#	0.977

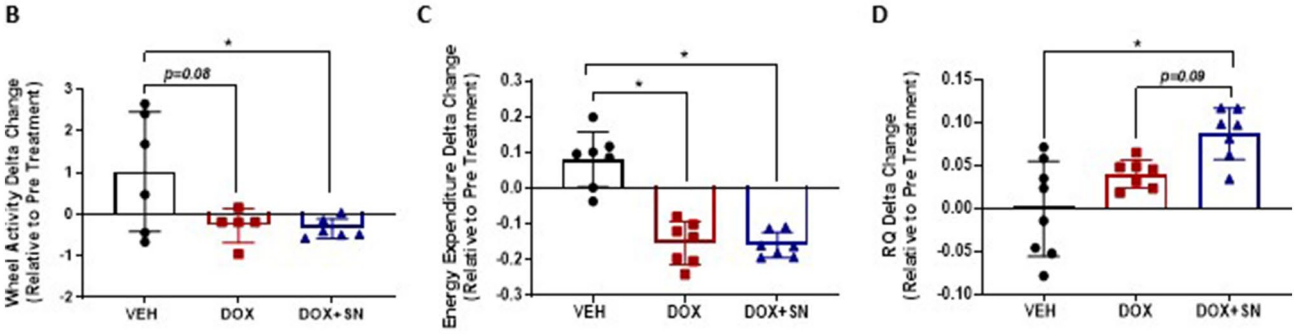

Figure 2. The effect of LDM DOX administration and SN co-supplementation on ambulatory and metabolic activity. (**A**) Data are displayed for ambulatory (wheel and cage meters) and metabolic activity (energy expenditure and respiratory quotient (RQ) parameters over 24 h in each of the PRE and POST treatment periods. (**B**) There was a strong trend for DOX to increase wheel running activity and a significant effect of DOX + SN treatment on wheel running activity in the PRE to POST treatment periods, (**C**) This was mirrored by significant reductions in energy expenditure between the PRE and POST treatment periods for both DOX and DOX + SN (*^$p < 0.05$). (**D**) While there was no effect of DOX on the respiratory quotient (RQ), DOX + SN significantly increased the RQ in favour of glucose as an energy substrate compared to VEH (*$p < 0.05$) and there was a strong trend for the same effect compared to DOX treatment alone ($p = 0.09$); $n = 5–7$ per group.

Assessment of molecular redox signalling pathways in skeletal muscle. Metabolised by Complex I of the mitochondrial ETC, DOX is a well-known inducer of superoxide production as a by-product of its metabolism[4,5,13]. Similarly, we have previously demonstrated that in a pro-oxidant environment, SN co-supplementation has a damaging effect on skeletal muscle secondary to a higher peroxynitrite production[37]. Thus, we next investigated whether oxidative or nitrostative stress played a role in the DOX-induced reduction in energy expenditure. Interestingly, there was no effect of LDM DOX administration on 4-hydroxy-2-nonenal (4-HNE; Fig. 5A,J), a marker of lipid peroxidation. However, there was a significant increase in nitrotyrosine ($p < 0.05$;

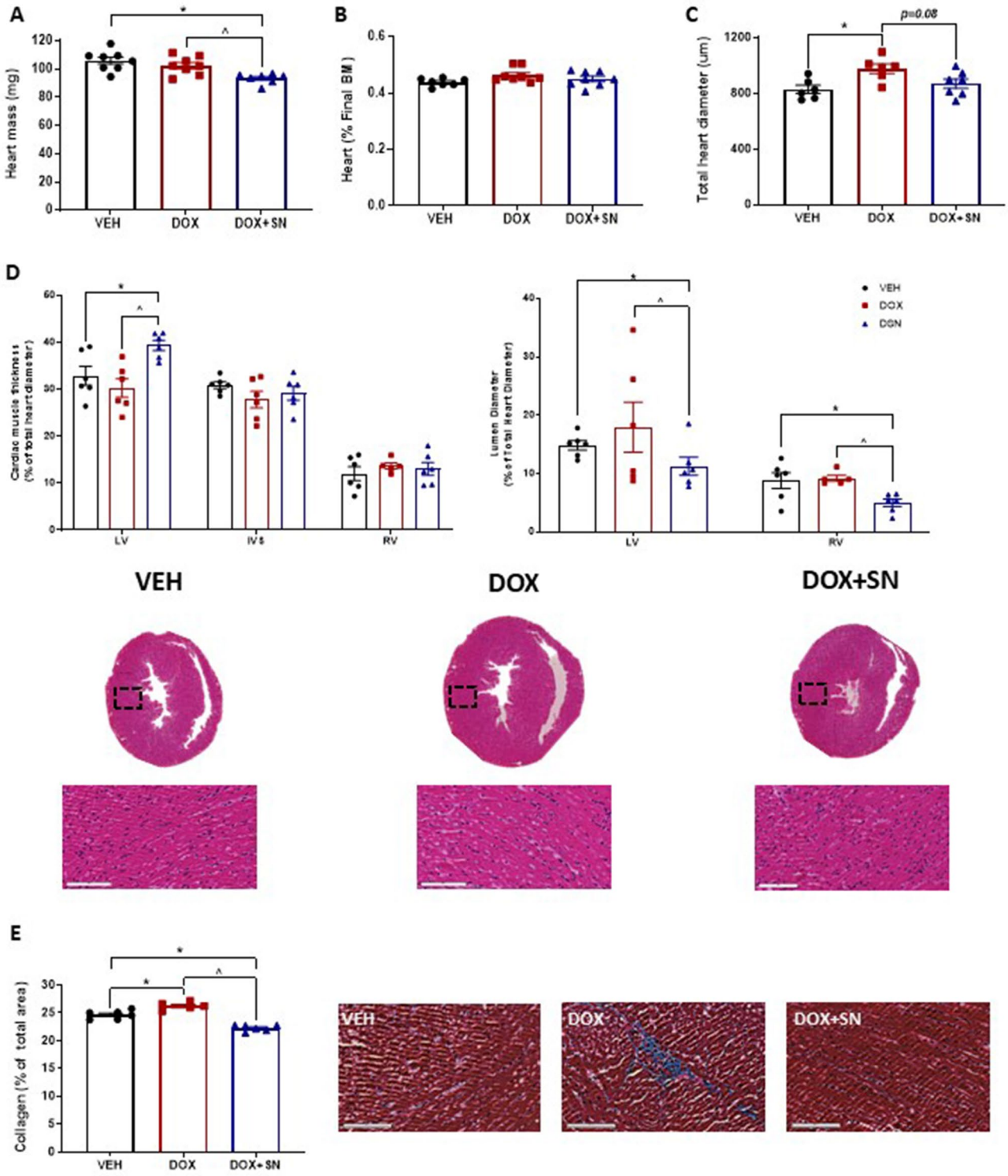
A
Heart mass (mg)
VEH
DOX
DOX+SN
B
Heart (% Final BM)
C
Total heart diameter (um)
p=0.08
D
Cardiac muscle thickness (% of total heart diameter)
LV
IVS
RV
Lumen Diameter (% of Total Heart Diameter)
VEH
DOX
DOX+SN
E
Collagen (% of total area)

◂**Figure 3.** The effect of LDM DOX administration and SN co-supplementation on cardiac muscle histology. (**A**) Heart mass was weighed immediately post-harvest, with DOX + SN treatment reducing heart mass compared to VEH (*$p < 0.05$) and DOX (^$p < 0.05$) mice. (**B**) When expressed as a percentage of the final body mass (BM), there were no significant differences in heart mass between groups. Gross morphological cardiac muscle indices were evaluated from H&E stained sections, measured in triplicate and normalised to (**C**) total heart diameter, which was increased in DOX mice (*$p < 0.05$) compared to VEH. However, DOX + SN treatment had a tendency (p = 0.08) to correct this DOX-induced change back to VEH control levels. (**D**) Next, we made morphological measurements of the cardiac muscle and ventricular lumen components of the lower hear (expressed as a percentage of total heart diameter). DOX + SN treatment increased the wall thickness of left ventricle (LV) compared to VEH (*$p < 0.05$) and DOX (^$p < 0.05$) mice, however, the intraventricular septum (IVS) and right ventricular (RV) wall thickness were unchanged from treatments. DOX + SN treatment also reduced the diameter of the LV and RV lumen (*$p < 0.05$ DOX + SN versus VEH and ^$p < 0.05$ DOX + SN versus DOX). (**E**) Representative images of the H&E sections displayed. (**F**) Heart sections were also stained using Masson's trichrome to evaluate the relative percentage of collagen/fibrotic connective tissue. DOX-treated mice had a greater relative percentage of collagen (*$p < 0.05$) compared to VEH, while DOX + SN mice corrected this phenomenon by reducing the relative percentage of collagen compared to VEH (*$p < 0.05$) and DOX(^$p < 0.05$). $n = 6–7$.

Fig. 5B,J), a marker of excessive peroxynitrite ($ONOO^-$) production. Surprisingly, SN co-supplementation did not augment the DOX-induced increase in nitrotyrosine expression ($p < 0.05$; Fig. 5B,J). LDM DOX administration also significantly increased the expression of the redox status sensor, nuclear factor erythroid-2-related factor 2 (NRF-2; $p < 0.05$; Fig. 5C,J), and this was unchanged by SN co-supplementation. Since NRF-2 is the master regulator of the anti-oxidant response to cellular stress[47], we wanted to investigate changes to regulators or downstream targets of NRF-2. The protein expression of the negative regulator of NRF-2, Keap-1 (Fig. 5D,J), nor the serine 349 residue on p62 (Fig. 5E,J), which plays a role in balancing the NRF-2 and Keap-1 interaction, did not alter in response to LDM DOX administration. Interestingly, we were able to demonstrate that LDM DOX administration significantly upregulated DJ-1 protein expression, which is a positive regulator of NRF-2 activation through enhancing NRF-2 stability and reducing ubiquitination and Keap-1 dependent degradation[48,49], but not when co-supplemented with SN ($p < 0.05$; Fig. 5F,J). The protein expression of anti-oxidant enzymes that are transcriptional targets of NRF-2, being NAD(P)H dehydrogenase quinone-1 (NQO-1), superoxide dismutase-1 (SOD-1) and heme oxygenase-1 (HO-1) (Fig. 5G-J), were not altered by LDM DOX administration nor SN co-supplementation.

Assessment of molecular mitochondrial content signalling in skeletal muscle. In light of the observation that administration of the LDM DOX regimen increased NRF-2 protein expression in skeletal muscle of mice with and without SN co-supplementation, and NRF-2 can modulate mitochondrial function and maintenance, we wanted to investigate whether molecular markers of mitochondrial content and remodelling were also affected. While we saw a trend for DOX to increase citrate synthase (CS) activity ($p = 0.097$; Fig. 6A), the gold standard marker of mitochondrial content[50] , there was no change to the protein expression of Complex I, II, IV and V from treatment groups (Fig. 6B, F) suggesting unchanged mitochondrial content. However, there was a strong trend for LDM DOX administration ($p = 0.07$; Fig. 6B) to reduce Complex III protein expression, whilst DOX + SN treatment did significantly reduce Complex III protein expression ($p < 0.05$; Fig. 6B, F). To assess damage to the mitochondrial pool, we also probed for cytochrome C (Cyt-c), which was significantly increased by both LDM DOX and DOX + SN treatment ($p < 0.05$, Fig. 6C, F). Following on from this finding we wanted to investigate if there were any effects on molecular markers of mitochondrial remodelling and stress, hence we probed for a member of the PGC-1 family (PGC-1β) and activation (phosphorylation) of adenosine monophosphate-activated protein kinase (AMPK). PGC-1β was significantly increased from LDM DOX administration ($p < 0.05$, Fig. 6D,F) but was normalised to VEH control levels by SN co-supplementation ($p < 0.05$, Fig. 6D,F). AMPK activation was unaffected by DOX treatment but was significantly increased by SN supplementation ($p < 0.05$; Fig. 6E,F).

Discussion

The major findings in this study are that the LDM DOX chemotherapy regimen is sufficient to reduce body, lean and fat mass (i.e. induce cachexia) and cause malaise, as exhibited by reduced energy expenditure and wheel running activity. This study also supports the two main studies in the literature advocating the efficacy of SN co-supplementation as a therapeutic strategy to mitigate DOX-induced cardiofibrosis[15,16]. SN co-supplementation protected against a LDM DOX-induced collagen deposition within the heart, whilst not exacerbating the reduction in end-point body composition indices and muscle/organ mass. SN co-supplementation did not produce a beneficial effect, nor was it detrimental at the skeletal muscle level and it was unable to attenuate DOX-induced cachexia.

In this study, we were able to induce a progressive form of chemotherapy–induced cachexia with LDM DOX administration, as defined by the > 5% reduction in end-point body mass which was driven by reductions in both lean and fat mass[51] and was unaffected by SN co-supplementation. The wasting of lean tissue by LDM DOX administration was predominately driven by visceral organ (spleen, liver, kidney) mass loss, with no impact on hindlimb skeletal muscle mass relative to body weight, albeit hindlimb muscle mass was reduced by DOX commensurate with the loss of body mass. We saw no evidence of muscle fibre atrophy (i.e. fibre CSA) of TA muscles. While this finding was unexpected, we postulate that skeletal muscle toxicity (similar to cardiac muscle toxicity)

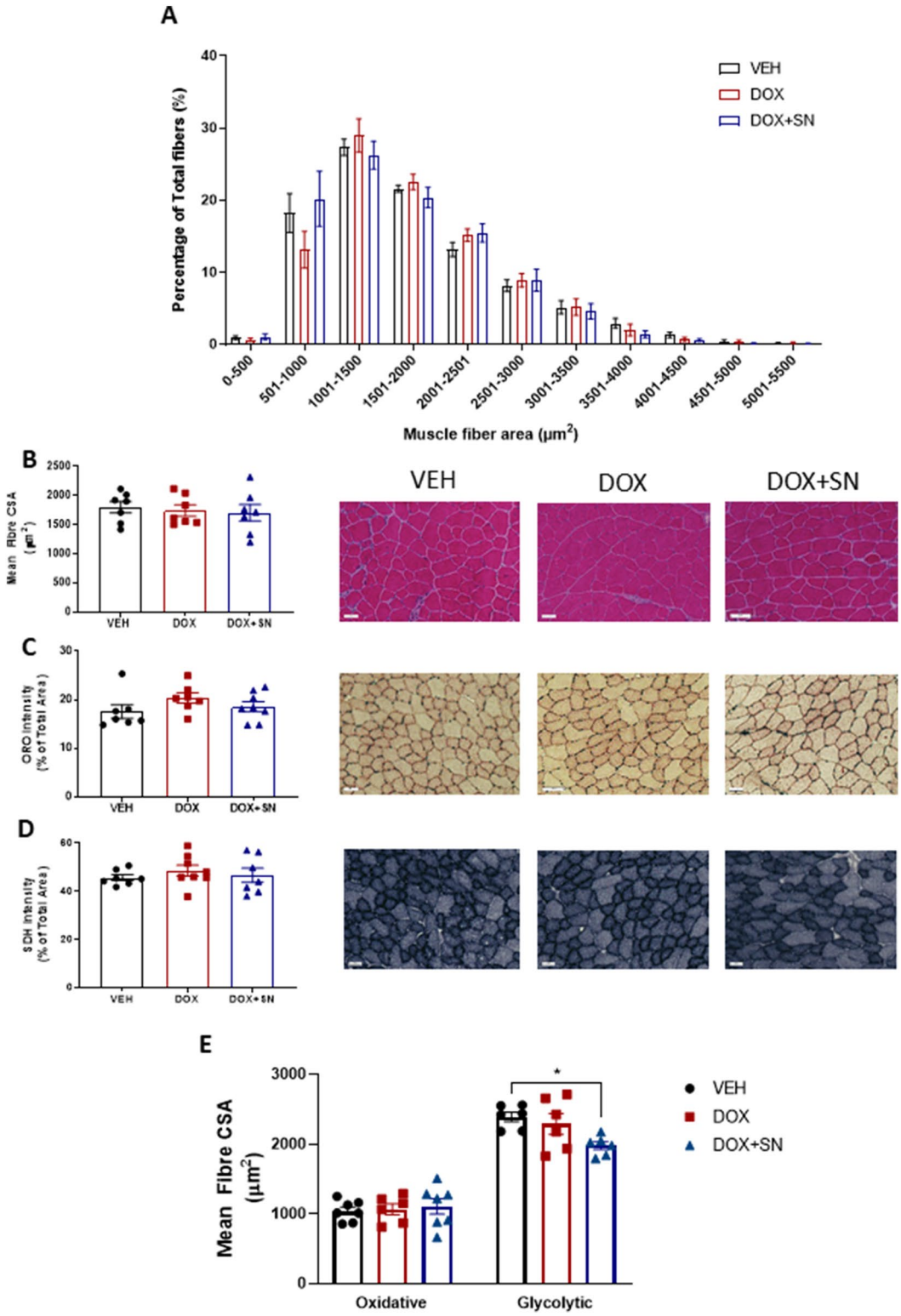

Figure 4. The effect of LDM DOX administration and SN co-supplementation on skeletal muscle histology. Tibialis anterior (TA) muscles were cryosectioned and underwent H&E staining to assess skeletal muscle architecture and fibre cross-sectional area (CSA). (**A**) The relative distribution of fibre size normalized as a percentage of total fibres; and (**B**) mean muscle fibre cross sectional area (CSA); demonstrated no significant differences between groups. Skeletal muscle cross sections also underwent (**C**) Oil Red O (ORO) staining to evaluate lipid content; and (**D**) Succinate Dehydrogenase (SDH) staining to evaluate mitochondrial content. There were no significant effects of treatments on these indices. (**E**) To assess whether fibre types were affected differently by either DOX alone of with SN supplementation, SDH-stained sections were used to determine the CSA of isolated oxidative and glycolytic fibre populations. There was no effect of DOX treatment on the CSA of either oxidative or glycolytic fibres, however, DOX + SN treatment decreased the mean CSA of glycolytic fibres (*$p < 0.05$) $n = 6–8$.

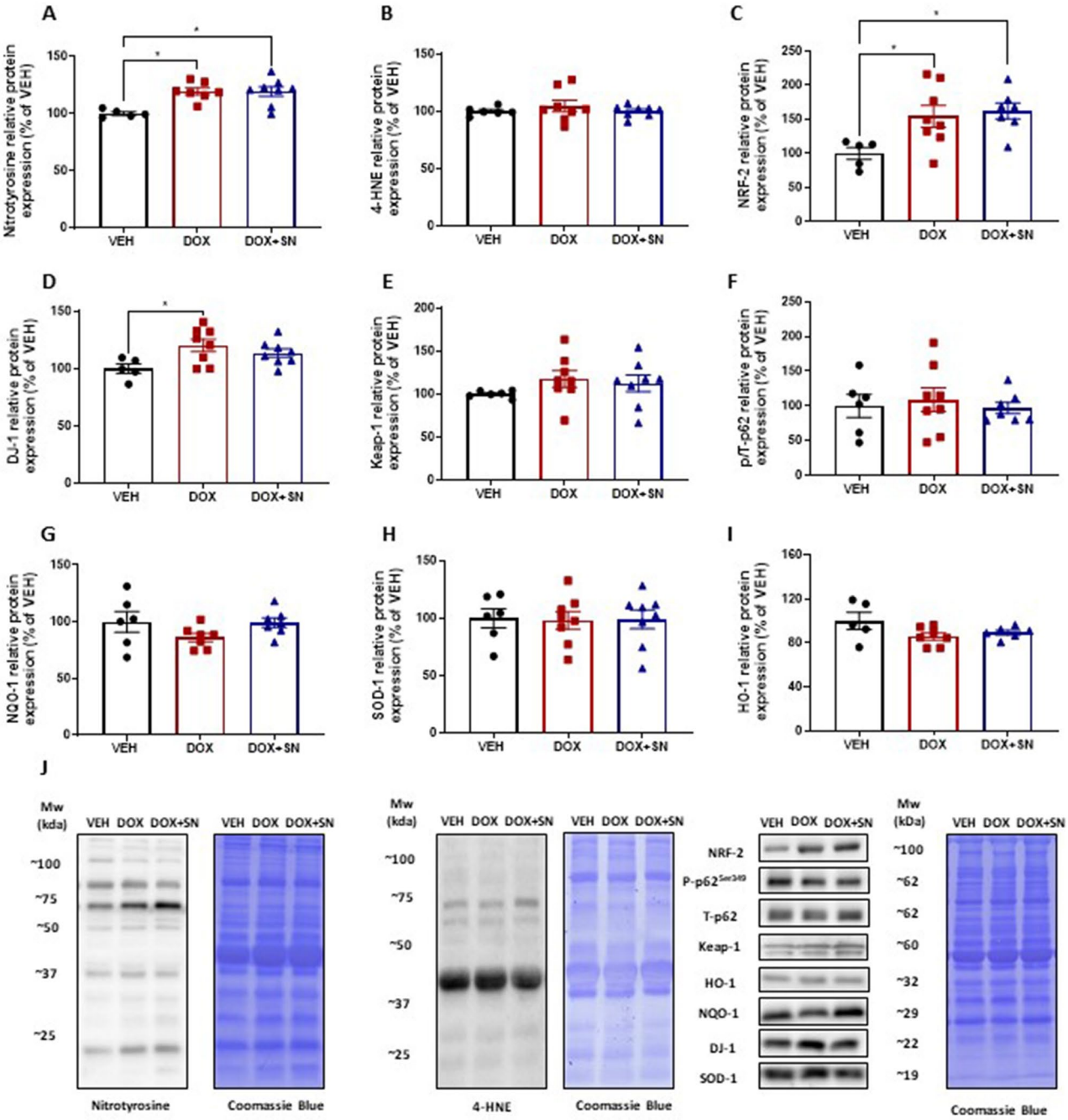

Figure 5. The effect of LDM DOX administration and SN co-supplementation on molecular markers of oxidative stress and the anti-oxidant response in skeletal muscle. Western blotting experiments were undertaken utilizing soleus muscle homogenate. When probing for molecular markers of oxidative stress, there was no significant change in (**A**) 4-HNE protein expression, a marker of lipid peroxidation, between treatment groups, but there was a significant increase in (**B**) nitrotyrosine protein expression, a marker of excessive peroxynitrite ($ONOO^-$) production in DOX and DOX + SN treated mice (*$p < 0.05$) compared to VEH. There was also a significant increase in (**C**) NRF-2 protein expression, the master regulator of the anti-oxidant response to cellular stress, in DOX and DOX + SN treated mice (*$p < 0.05$) compared to VEH. (**D**) DJ-1 protein expression was probed for as a positive regulator of NRF-2 activation, which was interestingly, shown to increase in DOX mice (*$p < 0.05$) compared to VEH, whilst there was no significant change in DOX + SN treated mice. Negative regulators of NRF-2, i.e. (**E**) Keap-1, (**F**) phosphorylated $p62^{ser349}$ and total p62 (depicted as a ratio of the total), were not significantly changed from treatment. Downstream targets of the anti-oxidant response, i.e. (**G**) NQO-1, (**H**) SOD-1 and (**I**) HO-1 did not significantly change from treatment. (**J**) Representative images of the antibodies are displayed alongside a representative image of Coomassie Blue used to normalize to total protein content. $n = 5–8$.

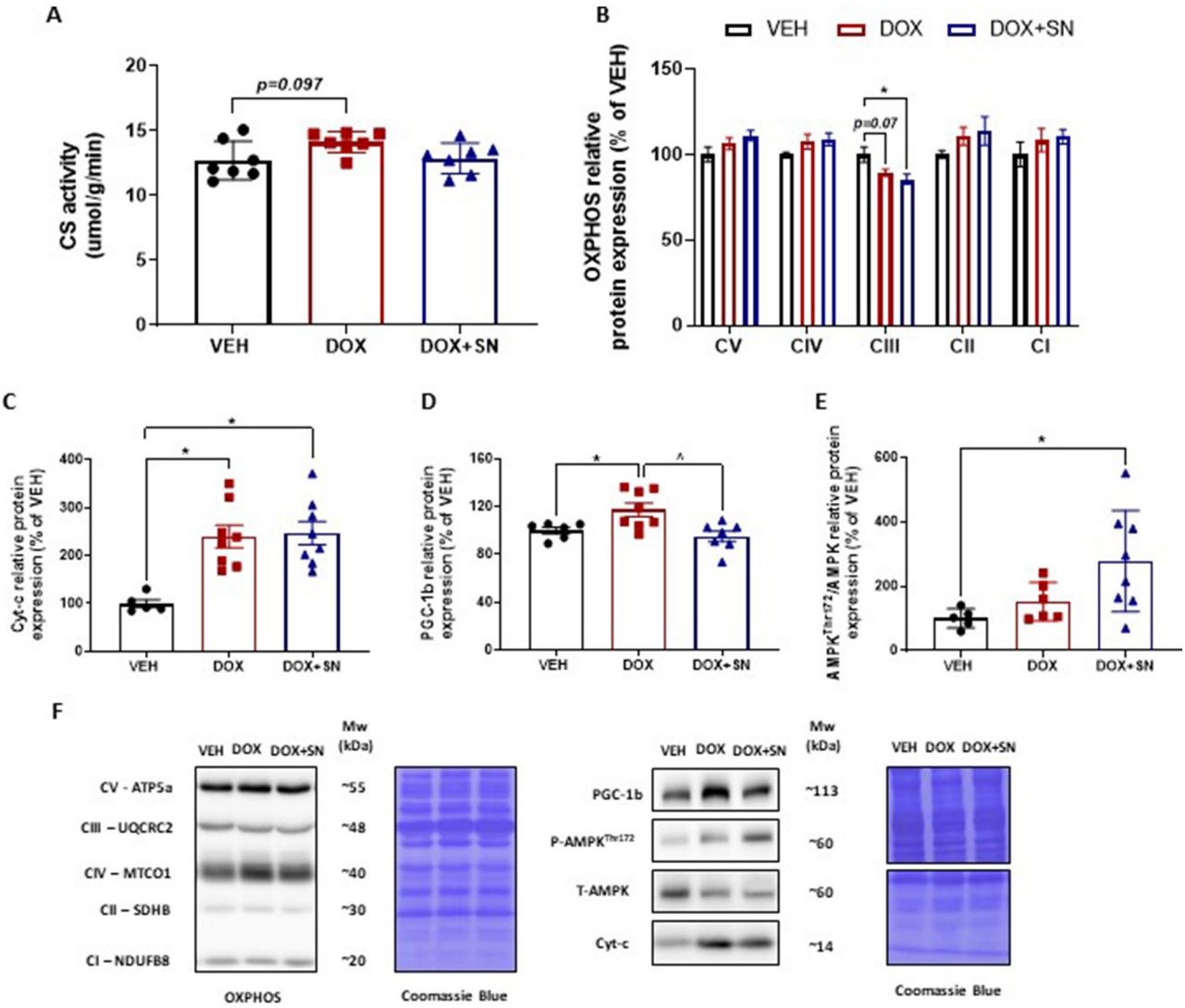

Figure 6. The effect of LDM DOX administration and SN co-supplementation on molecular markers of mitochondrial content in skeletal muscle. Western blotting experiments were undertaken utilizing soleus muscle homogenate. (**A**) CS activity was assessed as a gold standard marker of mitochondrial content. There was a trend towards increased CS activity induced by DOX (p = 0.07) but no effect of DOX + SN. Molecular indicators of mitochondrial complex protein content were probed for using the (**B**) OXPHOS cocktail, with no significant change in the protein expression of Complex V (CV)—ATP5A, Complex IV (CIV)—MTCO1, Complex II (CII)—SDHB and Complex I (CI)—NDUFB8 from treatment groups. However, the protein expression of Complex III (CIII)—UQCRC2 displayed a trend to be reduced in DOX mice ($p = 0.07$) compared to VEH, but was significantly reduced in DOX + SN treated mice (*$p < 0.05$) compared to VEH. Additionally, (**C**) Cytochrome-c (Cyt-c) protein expression, a marker of mitochondrial content, was significantly increased in both DOX and DOX + SN mice (*$p < 0.05$) compared to VEH. To assess mitochondrial remodelling, we also probed for a member of the PGC-1 family, i.e. (**D**) PGC-1β, which was shown to be significantly increased in DOX treated mice (*$p < 0.05$), but was normalised in DOX + SN mice compared to DOX (^$p < 0.05$) and VEH (p > 0.05). As a marker of metabolic stress, we also probed for (**E**) phosphorylated (i.e. activated) compared to total adenosine monophosphate activated protein kinase (AMPK) and showed no effect of DOX treatment alone, but a marked increase with DOX + SN treatment compared to VEH ($p < 0.05$). (**F**) Representative images of the antibodies are displayed alongside a representative image of Coomassie Blue used to normalize to total protein content. $n = 5–8$.

is dose dependent[44] since other studies that utilized a higher cumulative dose of DOX (i.e. 20–30 mg/kg) have demonstrated significant skeletal muscle wasting[17–20]. Despite the lack of evidence for skeletal muscle wasting/atrophy in this model, it is still of interest that our model of LDM DOX administration (12 mg/kg; total cumulative dose over 7 days) can have a substantial acute effect on body and lean (visceral) mass i.e. an ~ 9% reduction compared to VEH control. This is comparative to a study by Nissinen et al. which utilized a cumulative dose of 24 mg/kg over 4 weeks and demonstrated similar body and lean mass loss, although evidence of skeletal muscle

mass loss was also observed[18] suggesting that skeletal muscle wasting induced from DOX administration is both a time and dose dependent event. Supporting this statement is a recent study by Tarpey et al.[29], which utilized a single MTD injection of DOX (20 mg/kg) with mice culled 72-h post-injection, to demonstrate a significant reduction in body mass but no change in the mass or CSA of hindlimb skeletal muscle. Thus, the LDM DOX regimen utilised in this study represents a more clinically-relevant rodent model of DOX-induced cachexia in being able to induce similar body composition changes, without the severe systemic toxicity associated with the single MTD injection model[39]. Further improvement to the LDM DOX administration model could involve increasing the cumulative dose while administering DOX over both a longer duration, and for multiple LDM cycles, to enhance the potential for the effective pre-clinical screening of therapeutics to mitigate the side-effects of chronic DOX-induced toxicity.

The regimen of LDM DOX administration used in our study allowed the observation of an acute mild pro-collagenic cardiomyopathy involving early changes to the overall heart diameter, but with no change to crude heart mass. SN co-supplementation elicited a protective effect by preventing the induction of myocardial fibrosis. The increase in fibrotic tissue prevalence in the heart is a consistent hallmark of DOX-induced cardiotoxicity[52–56], and our data demonstrate this precedes DOX-induced myocardial toxicity. Surprisingly, SN co-supplementation increased left ventricular wall thickness compared to both the VEH and DOX control group. We postulate that this finding is relative to enhanced left ventricular performance, which has previously been demonstrated by Zhu et al., where SN supplemented prior to, and following, the administration of a single MTD bolus of DOX, improved left-ventricular ejection fraction and fractional shortening through improved Ca^{2+} cycling and contractility[15]. Interestingly, SN co-supplementation reduced total heart diameter, heart mass and the left and right ventricular lumen diameter relative to the DOX control group, which we hypothesise is part of the potential protective effect of SN co-supplementation during LDM DOX administration. In this regard, maintaining a smaller, but more efficient heart may be beneficial for resisting the cardiac fibrosis induced by DOX treatment. Indeed, smaller stature humans and animals are thought to be more resistant to cardiovascular disease than their taller/larger counterparts[57].

Fatigue and malaise represents a complex interplay between central nervous system drive, mental state and physiological function, and with chemotherapy treatment, is further complicated by nausea and a general feeling of unwell alongside altered gut function, which impacts macro and micro nutrient intake and uptake[58–60]. Chemotherapy administration induces chronic and debilitating fatigue, and this manifests physiologically in the skeletal muscular system as contractile and mitochondrial dysfunction (reviewed by us previously[25]). Thus, "fatigue" in the context of the present study likely represents the inability to generate both the mental and cellular energy to perform normal skeletal muscle function rather than true physiological fatigue, whereby normal skeletal muscle function cannot be durably maintained despite maximal effort. In this study, LDM DOX administration reduced voluntary wheel activity and energy expenditure in a synergistic manner, which was not alleviated by SN co-supplementation. DOX has previously been shown to impair skeletal muscle function and wheel running performance in mice, and this has been associated with mitochondrial dysfunction resulting from changes to the redox status of skeletal muscle[17,20,29,61,62]. In our study, DOX-induced "fatigue" was associated with a molecular marker of increased nitrosative stress (i.e. abundance of proteins with nitrosylated tyrosines), an indicator of increased peroxynitrite ($ONOO^-$) levels. Excess peroxynitrite production can lead to impaired mitochondrial energy metabolism via inhibition of glycolysis and depletion of ATP pools[63]. Interestingly, SN co-supplementation did not further exacerbate the DOX-induced increase in nitrotyrosine expression, which was surprising given that we have previously demonstrated an escalation of muscle damage when SN was supplemented to an already pro-oxidant environment in the dystrophic *mdx* mouse model of Duchenne Muscular Dystrophy[37]. The postulated divergence in efficacy of SN co-supplementation between this study and our previous work in the *mdx* mouse is two-fold; with the first being acute versus chronic co-supplementation (i.e. 1 versus 8 weeks in this versus our *mdx* study) which may be protective rather than promotive of oxidative/nitrosative stress. The second factor is that the dynamics of the pro-oxidant environment may be influential. Dystrophic muscle is in a chronic state of oxidative stress, thus superfluous nitrate promoted excess peroxynitrite formation which exceeded the antioxidant buffering capacity, subsequently escalating myopathy. In contrast, LDM DOX administration which was metronomic and of reasonably short duration allowed for redox balancing in between doses in this study.

Surprisingly, the LDM regimen of DOX administration utilized in this study did not induce the expected increase in lipid peroxidation (a marker of oxidative stress), as indicated by 4-HNE protein expression. There have been mixed results in the literature to this effect, with Smuder et al. displaying a striking increase in 4-HNE protein expression when mice were culled 24 h post a single 20 mg/kg injection of DOX[23], whereas Gouspillou et al. were unable to show changes to 4-HNE protein expression when mice were treated with a cumulative dose of DOX, i.e. 40 mg/kg over 12 weeks[20]. Collectively, these data in conjunction with ours suggest that LDM DOX delivery induces hormesis through NRF-2 to protect the muscle from oxidative stress, and that DJ-1, which has antioxidant properties[48,49], is central to the hormetic response at the low DOX dose given in our study. In contrast, cytotoxic insults (i.e. single bolus MTD DOX treatment) overwhelms endogenous cytoprotective mechanisms to induce Phase II antioxidant enzymes such as SOD[23].

We have previously demonstrated that DOX induces mitochondrial toxicity and reduces the mitochondrial pool in cultured myoblasts and myotubes[64]. In this study, we assessed the mitochondrial content by probing CS activity and mitochondrial ETC complex density in SOL and SDH content in TA, mitochondrial toxicity by probing Cyt-c, as well as the mitochondrial remodelling marker, PGC1β. We saw no change from either LDM DOX administration, nor SN co-supplementation, in the mitochondrial content of slow type I SOL muscle or the SDH content of whole fast type II TA cross-sections. However, both Cyt-c and PGC1β were elevated by DOX treatment highlighting the onset of mitochondrial toxicity and turnover as shown previously following the administration of various chemotherapeutic agents to human breast cancer cell lines[65]. Sanchez-Alcazar et al. have shown that increased expression of Cyt-c within the mitochondria and induction of PGC1-mediated mitochondrial

biogenesis is an early cytoprotective response to anticancer agents, preceding Cyt-C release into the cytoplasm and the induction of apoptosis[65]. LDM DOX administration appears sufficient to induce mitochondrial toxicity but also turnover to preserve skeletal muscle mass.

Surprisingly, and in contrast to the expression profile of all other mitochondrial ETC complex subunits, we observed a reduction in the protein expression of Complex III following DOX treatment (with and without SN). The reduction in the Complex III subunit, UQCRC2, was an unexpected finding, as previous studies have shown that after a single MTD injection of DOX neither the protein expression of UQCRC2 in permeabilized myofibers[62], nor the native protein content of Complex III in isolated mitochondria from skeletal muscle, is altered[29]. However, we postulate that the reduction in UQCRC2 content from LDM administration and SN co-supplementation could be a molecular marker of the exercise intolerance shown by DOX-treated mice in our activity/calorimetry studies. Others have shown increased UQCRC2 expression in the skeletal muscle of young mice exposed to cages with voluntary running wheels[66] and that Complex III activity is reduced in sedentary mice compared to mice that have undergone treadmill running-based exercise training[67]. Interestingly, humans with mutations on the cytochrome b subunit of the Complex III assembly, display exercise intolerance and have a reduced protein expression of the UQCRC2 subunit in skeletal muscle[68–71].

NO signalling in skeletal muscle is strongly associated with glucose uptake and utilisation during contraction[72] which may be beneficial in circumstances such as during DOX administration, where mitochondrial dysfunction, damage, toxicity and ROS production escalate and energy production capacity is compromised. We have previously demonstrated that nitrate supplementation can augment contraction-induced glucose uptake in healthy type II skeletal muscles, but rather has a suppressive effect on glucose uptake in the pro-oxidative environment of dystrophic *mdx* type II skeletal muscles[37]. While we have not undertaken glucose uptake or contraction studies here, the activation (phosphorylation) of AMPK in DOX + SN treated SOL along with the higher RQ derived from calorimetry studies during voluntary wheel running activity, suggest a greater dependency on glucose metabolism following SN supplementation. Consistent with the known effects of nitrate supplementation on muscle fibre type switching from fast glycolytic (i.e. type IIb) to fast oxidative glycolytic (type IIa) phenotype[73], we have also demonstrated a reduction in the CSA of glycolytic fibres. These adaptations could be of benefit to skeletal muscles long term, particularly in mitigating the contractile dysfunction and higher fatiguability reported by others in mice[17,27] and humans[74] following chemotherapy administration.

There were several limitations of our research worthy of mention. Firstly, our study examined the effects of LDM DOX administration on skeletal and cardiac muscle in an attempt to generate more clinically-relevant data than traditional single bolus MTD DOX administration which is typically given in animal studies to elicit skeletal muscle wasting and cardiotoxicity: in hindsight, our study would have benefited greatly from including a MTD group treated both with and without SN to contrast the DOX delivery regimens and the efficacy of SN against them. Secondly, our choice of limb muscles with different fibre-type profiles makes it difficult to compare and contrast our histological data (derived from the predominantly fast type II fibre TA muscle) with our molecular data (derived from the predominantly slow type I SOL muscle). TA is a common choice for histological analyses in mouse hind limb muscle because it is of sufficient size to rigorously generate fibre size distributions (i.e. to count enough (> 250) fibres). We chose SOL for our molecular studies since these centred around mitochondrial and oxidation markers which are more pronounced in slow oxidative muscle—we have undertaken CSA analyses on oxidative (slow type I) and glycolytic (fast type II) fibre populations and demonstrated no differential effects of DOX on specific fibre types though. Thirdly, we used mice aged ~ 6w of age which is prior to complete sexual maturation at 8w of age. Therefore, the effects observed on body, lean and fat mass indices may be different at this age when mice are still growing, versus in mature adult or aging mice when growth has ceased.

In conclusion, we demonstrate that the LDM DOX chemotherapy regimen is sufficient to induce cachexia (lean and fat mass wasting inclusive) and fatigue as characterised by reduced participation in voluntary exercise, which appears to be underlined by oxidative/nitrostative stress. Interestingly, the administration of LDM DOX induced mild oxidative stress in skeletal muscle, which subsequently evoked a NRF-2 driven anti-oxidant response through DJ-1. SN co-supplementation afforded no protective therapeutic potential alongside the administration of LDM DOX, but nor did it promote the wasting of lean tissue. Importantly, we have evidence of a SN co-supplementation driven cardioprotective effect against DOX-induced collagen deposition, however, the therapeutic efficacy of SN as an adjunct during DOX administration still requires further examination.

Methods

Animals. *Experimental design and treatments.* Six-week old male Balb/c mice were acquired from the Animal Resource Centre (ARC, Western Australia) and were randomly allocated to treatment groups (n = 8) upon arrival. Mice were housed on a 12-h light/dark cycle with ad libitum access to food i.e. standard mice chow and water supply throughout the experiments. Mice were administered with either VEH (0.9% NaCl) or DOX (4 mg/kg in 0.9% NaCl; Sigma Aldrich, Australia) via intraperitoneal injection 3 times over a 7 day period (i.e. on day 1, 3 and 5; for a cumulative dose of 12 mg/kg) which is the equivalent to a low cumulative clinical dose[5,75], thus depicting a model of LDM DOX administration. SN was co-supplemented in drinking water (85 mg/L^{-1} (1 mM) (Sigma Aldrich, Australia)) throughout the duration of the LDM DOX regimen in a third group of animals (DOX + SN group). This dose of SN is equivalent to that used previously by us and others, demonstrating efficacy to transiently increase plasma and skeletal muscle nitrate levels[37,76]. Animals were weighed prior to the commencement of treatment (PRE), on each day of treatment and at the experimental endpoint. Food and water consumption were monitored throughout the duration of the treatment protocol.

Body composition analyses. Echo Magnetic Resonance Imaging (echoMRI) was utilized to assess the effect of DOX and DOX + SN on body composition. Live mice were placed into an echoMRI body composition

analyzer (EMR-150, Echo Medical Systems, USA) on day 1 (PRE) and day 8 (POST) of the treatment protocol. Total lean and fat mass were quantified via triplicate scans spaced 30 s apart. Data are the delta change in the mean of triplicate scans between the PRE and POST testing periods.

Indirect calorimetry & activity monitoring. To evaluate the impact of DOX and DOX + DOX + SN on the physical and associated metabolic activity of mice, animals were individually housed for 24 h in Promethion Metabolic cages (Sable Systems, LV, USA) on day 0–1 (PRE) and day 7–8 (POST). Cages allowed free access to food, water and a running wheel. Real-time voluntary activity and whole-body metabolic activity was monitored throughout both 24-h periods, with the key variables of wheel running, ambulatory activity (pedestrian meters), energy expenditure and the respiratory quotient (VCO_2/VO_2) analysed as described by us previously[77]. Data presented are the total for a circadian cycle (i.e. of the diurnal phase recorded from 7am-7 pm and the nocturnal phase recorded from 7 pm-7am) in the PRE and POST periods, or the delta change between the PRE and POST periods..

Surgery. At the conclusion of treatment (POST) live analyses, non-recovery surgery was performed on animals. Mice were deeply anaesthetised via isoflurane inhalation (5% induction and 2–3% maintenance) and non-survival surgery was performed. Tissues of interest were surgically excised, weighed and snap-frozen for post-hoc analyses in the following order: (1) SOL muscle was taken for western blotting experiments; and (2) TA muscle and heart were taken for histological assessment. Additional tissues of interest harvested were skeletal muscles *extensor digitorum longus* (EDL) and *plantaris* (PLNT), alongside epididymal and subcutaneous fat, spleen, kidney and liver, which were also weighed prior to being snap-frozen.

Histological analyses. *Skeletal muscle histology.* All histological protocols were performed as described by us previously[37,78]. To determine whether LDM DOX had atrophic effects on skeletal muscle and subsequently, whether DOX + SN either exacerbated or rescued any such atrophy, we next assessed the hindlimb muscle, TA histologically. TA muscles were cryopreserved in optimal cutting temperature compound (Sakura Finetek) using liquid nitrogen-cooled isopentane. TA's were sectioned (10 µm, -20 °C, Leica CM1950) and mounted. Three histological stains were employed to assess various histopathological features. Haematoxylin & Eosin (H&E) was utilised to evaluate muscle fibre size and architecture. Oil Red O (ORO) staining evaluated lipid content within the whole muscle. Succinate dehydrogenase (SDH) staining was utilized to assess the SDH activity, which is indicative of a more oxidative phenotype and subsequently a marker of both mitochondrial density and fibre-type transformation. For H&E, ORO and SDH, slides were imaged on a Zeiss Axio Imager Z2 microscope (Carl Zeiss MicroImaging GmbH, Germany) at 20 × magnification, respectively. All images were analysed using ImageJ software (NIH, USA).

To evaluate fibre type-specific effects of DOX and DOX + SN treatment, glycolytic and oxidative areas of the TA were identified in SDH stained sections and at least 250 fibres were counted for each fibre type (i.e. a total of at least 500 fibres per section) in each of those areas. The CSA of these fibres was determined as described by us previously[37,78].

Cardiac muscle histology. The cardiotoxic effects of DOX are well established, and previous research suggests a therapeutic effect for SN in this regard. Thus, in this study, we also sought to investigate the impact of our treatments on the heart. Whole hearts were snap-frozen before being transferred to a 10% neutral buffered formalin for 48 h for fixation. Once fixed, serial sections were cut at 10 µm diagonally at the mid-ventricle. H&E staining was performed to assess gross changes in cardiac muscle, with morphological indices measured including left and right ventricular diameter and thickness as well as interventricular septum thickness[79]. Masson's Trichrome staining was performed to assess collagen/fibrotic connective tissue content. All sections were imaged at × 20 using a Zeiss Axio Imager Z2 microscope (Carl Zeiss MicroImaging GmbH, Germany). Masson's trichrome stained sections were quantified using a colour histogram and calculated as a percentage of the total heart cross sectional area.

Western blot analyses. All western blotting protocols were performed as previously described by us[78,80]. Since both DOX and SN are notorious producers of ROS[64,81], we next investigated the effect of DOX and DOX + SN treatment on molecular markers of oxidative stress related damage, downstream anti-oxidant response targets and mitochondrial content and remodelling/biogenesis. Western blot experiments were performed from frozen SOL homogenates. SOL muscles were homogenized for 20-30 s in ice-cold Western Immunoprecipitation Kinase (WIK) buffer (40mMTris, pH 7.5; 1 mM EDTA; 5 mM EGTA; 0.5% TritonX-100; 25 mM β-glycerophosphate; 25 mM NaF; 1 mM Na_3VO_4; 10 µg/ml leupeptin; and 1 mM PMSF). Homogenate was centrifuged at 3,500 rpm for 5 min at 4 °C, before the pellet was resuspended and the whole muscle homogenate was used for further analysis. Protein concentrations were determined using a sample assay kit (Bio-Rad Laboratories, Hercules, CA, USA), to ensure equal loading on the gels. Samples were prepared with equivalent amounts of protein (20–40 µg) in Laemmli buffer, heated for 5 min at 95 °C, and subjected to electrophoretic separation on 7.5% or 12% SDS-acrylamide gels. The only exception to this was when probing for the Total OXPHOS cocktail antibody samples were heated for 5 min at 40 °C, as per supplier recommendations. Following electrophoretic separation, proteins were transferred to a polyvinylidene fluoride (PVDF) membrane, blocked with 5% not-fat milk powder in Tris-buffered saline containing 0.1% Tween 20 (TBST) for 1 h followed by an overnight incubation at 4 °C with primary antibody dissolved in TBST containing either 1% BSA or 3% non-fat milk powder. The following antibodies were used: anti-4-HNE (1:1,000; #ab46545, Abcam), Total OXPHOS cocktail (1:1,000; #ab110413, Abcam), anti-PGC-1β (1:500; #ab176328, Abcam), anti $AMPK^{Thr172}$ (1:1,000, #2535,

CST, anti-AMPK (1:1,000, #2603, CST), Cyt-c (1:2000; #11940, CST), anti-DJ-1 (1:1,000; #5933, CST), anti-Keap-1 (1:1,000; # 8047, CST), anti-NQO-1 (1:1,000; #62,262, CST), anti-NRF-2 (1:1,000; #12721, CST), anti-p62^{Ser349} (1:1,000; #95697, CST), anti-p62 (1:1,000; #5114, CST), anti-HO-1 (1:1,000; #ADI-SPA-894, Enzo Life sciences), anti-SOD-1 (1:2000; #ADI-SOD-101, Enzo Life Sciences) and anti-nitrotyrosine (1:1,000; #06–284, Millipore). After overnight incubation, the membranes were washed 3 separate times for 10 min each in TBST and then probed with a peroxidase-conjugated secondary antibody (1:5,000; anti-rabbit IgG, Vector Laboratories or 1:20,000; anti-mouse IgG, Vector Laboratories) for 1 h at room temperature. Following another set of 3 separate washes for 10 min in TBST, the blots were developed with a DARQ CCD camera mounted to a Fusion FX imaging system (Vilber Lourmat, Eberhardzell, Germany) using ECL Prime reagent (Amersham, Piscataway, NJ, USA). Once the images were captured, the membranes were stained with Coomassie Blue to verify equal loading of total protein in all lanes. Densitometric measurements were carried out using FusionCAPTAdvance software (Vilber Lourmat).

Citrate synthase activity. CS activity was assessed as a marker of mitochondrial content on SOL homogenates prepared for WB analyses and as described by us previously[37,78]. Homogenates were added to reagent cocktail containing (100 mM TRIS buffer, 1 mM DTNB and 3 mM Acetyl CoA) and oxaloacetate (10 mM) was used to initiate the reaction in a plate-based spectrophotometer at 412 nm (25 °C for 5 m). CS activity was calculated using the extinction coefficient of 13.6[82].

Statistics. Data is presented as mean ± standard error of the mean, unless stated otherwise. Data sets were tested for normality using a Shapiro–Wilk test. For normal data, a one-way ANOVA with Tukey's post-Hoc test was used to detect treatment differences for all data except for muscle and organ mass and cardiac muscle morphology data where a two-way ANOVA was used with treatment and muscle/organ type/cardiac morphology as factors. Where interactions were detected, one-way ANOVA was used for multiple comparisons. Repeated measures ANOVA's were used to assess time-dependent effects on body weight and body composition and voluntary activity/calorimetry changes between the PRE and POST periods. An α-value of 0.05 was considered significant. Data was analysed using Graphpad prism (GraphPad Software, San Diego, CA 92,108, USA).

Ethical approval. All experimental procedures were approved by the Victoria University Animal Ethics Committee (AEETH15/006) and conformed to the Australian Code of Practice for the Care and Use of Animals for Scientific Purposes.

Received: 19 April 2020; Accepted: 17 August 2020
Published online: 14 September 2020

References

1. Carvalho, C. *et al.* Doxorubicin: the good, the bad and the ugly effect. *Curr. Med. Chem.* **16**(25), 3267–3285 (2009).
2. Thorn, C. F. *et al.* Doxorubicin pathways: pharmacodynamics and adverse effects. *Pharmacog. Genom.* **21**(7), 440–446 (2011).
3. McGowan, J. V. *et al.* Anthracycline chemotherapy and cardiotoxicity. *Cardiovasc. Drugs Ther.* **31**(1), 63–75 (2017).
4. Octavia, Y. *et al.* Doxorubicin-induced cardiomyopathy: from molecular mechanisms to therapeutic strategies. *J. Mol. Cell Cardiol.* **52**(6), 1213–1225 (2012).
5. Hiensch, A.E., Bolam, K.A., Mijwel, S., Jeneson, J.A.L., Huitema, A.D.R., & Kranenburg, O., et al. Doxorubicin-induced skeletal muscle atrophy: Elucidating the underlying molecular pathways. *Acta Physiol* (Oxf). 2019:e13400.
6. Chen, Y., Jungsuwadee, P., Vore, M., Butterfield, D. A. & St Clair, D. K. Collateral damage in cancer chemotherapy: oxidative stress in nontargeted tissues. *Mol. Interventions* **7**(3), 147–156 (2007).
7. Nyakayiru, J. *et al.* Sodium nitrate ingestion increases skeletal muscle nitrate content in humans. *J. Appl. Physiol.* **123**(3), 637–44 (2017).
8. Jansson, E. A. *et al.* A mammalian functional nitrate reductase that regulates nitrite and nitric oxide homeostasis. *Nat. Chem. Biol.* **4**(7), 411–417 (2008).
9. Bhaswant, M., Brown, L., McAinch, A.J., Mathai, M.L. Beetroot and sodium nitrate ameliorate cardiometabolic changes in diet-induced obese hypertensive rats. Mol. Nutr. Food Res. 2017;61(12).
10. Webb, A. *et al.* Reduction of nitrite to nitric oxide during ischemia protects against myocardial ischemia-reperfusion damage. *Proc. Natl. Acad. Sci. USA.* **101**(37), 13683–13688 (2004).
11. Rammos, C. *et al.* Impact of dietary nitrate on age-related diastolic dysfunction. *Eur. J. Heart Fail.* **18**(6), 599–610 (2016).
12. Apostoli, G. L., Solomon, A., Smallwood, M. J., Winyard, P. G. & Emerson, M. Role of inorganic nitrate and nitrite in driving nitric oxide-cGMP-mediated inhibition of platelet aggregation in vitro and in vivo. *JTH* **12**(11), 1880–1889 (2014).
13. Kina-Tanada, M. *et al.* Long-term dietary nitrite and nitrate deficiency causes the metabolic syndrome, endothelial dysfunction and cardiovascular death in mice. *Diabetologia* **60**(6), 1138–1151 (2017).
14. Hendgen-Cotta, U. B. *et al.* Dietary nitrate supplementation improves revascularization in chronic ischemia. *Circulation* **126**(16), 1983–1992 (2012).
15. Zhu, S. G. *et al.* Dietary nitrate supplementation protects against Doxorubicin-induced cardiomyopathy by improving mitochondrial function. *J. Am. Coll. Cardiol.* **57**(21), 2181–2189 (2011).
16. Xi, L., Zhu, S. G., Hobbs, D. C. & Kukreja, R. C. Identification of protein targets underlying dietary nitrate-induced protection against doxorubicin cardiotoxicity. *J. Cell Mol. Med.* **15**(11), 2512–2524 (2011).
17. de Lima, E. A. *et al.* Aerobic exercise, but not metformin, prevents reduction of muscular performance by AMPk activation in mice on doxorubicin chemotherapy. *J. Cell Physiol.* **233**(12), 9652–62 (2018).
18. Nissinen, T. A. *et al.* Systemic blockade of ACVR2B ligands prevents chemotherapy-induced muscle wasting by restoring muscle protein synthesis without affecting oxidative capacity or atrogenes. *Sci. Rep.* **6**, 32695 (2016).
19. Min, K. *et al.* Increased mitochondrial emission of reactive oxygen species and calpain activation are required for doxorubicin-induced cardiac and skeletal muscle myopathy. *J. Physiol.* **593**(8), 2017–2036 (2015).

20. Gouspillou, G. *et al.* Anthracycline-containing chemotherapy causes long-term impairment of mitochondrial respiration and increased reactive oxygen species release in skeletal muscle. *Sci. Rep.* **5**, 8717 (2015).
21. Sin, T. K. *et al.* Acute treatment of resveratrol alleviates doxorubicin-induced myotoxicity in aged skeletal muscle through SIRT1-dependent mechanisms. *J. Gerontol. A Biol. Sci. Med. Sci.* **71**(6), 730–739 (2016).
22. Gilliam, L. A. *et al.* Doxorubicin acts via mitochondrial ROS to stimulate catabolism in C2C12 myotubes. *Am. J. Physiol. Cell Physiol.* **302**(1), C195-202 (2012).
23. Smuder, A. J., Kavazis, A. N., Min, K. & Powers, S. K. Exercise protects against doxorubicin-induced oxidative stress and proteolysis in skeletal muscle. *J. Appl. Physiol.* **110**(4), 935–42 (2011).
24. Hulmi, J. J. *et al.* Prevention of chemotherapy-induced cachexia by ACVR2B ligand blocking has different effects on heart and skeletal muscle. *J. Cachexia Sarcopenia Muscle.* **9**(2), 417–432 (2018).
25. Sorensen, J. C. *et al.* Mitochondria: Inadvertent targets in chemotherapy-induced skeletal muscle toxicity and wasting?. *Cancer Chemother. Pharmacol.* **78**(4), 673–683 (2016).
26. Hydock, D. S., Lien, C. Y., Jensen, B. T., Schneider, C. M. & Hayward, R. Characterization of the effect of in vivo doxorubicin treatment on skeletal muscle function in the rat. *Anticancer Res.* **31**(6), 2023–2028 (2011).
27. Bredahl, E. C. & Hydock, D. S. Creatine supplementation and doxorubicin-induced skeletal muscle dysfunction: an ex vivo investigation. *Nutr. Cancer.* **69**(4), 607–615 (2017).
28. van Norren, K. *et al.* Direct effects of doxorubicin on skeletal muscle contribute to fatigue. *Br. J. Cancer.* **100**(2), 311–314 (2009).
29. Tarpey, M. D., Amorese, A. J., Balestrieri, N. P., Fisher-Wellman, K. H. & Spangenburg, E. E. Doxorubicin causes lesions in the electron transport system of skeletal muscle mitochondria that are associated with a loss of contractile function. *J. Biol. Chem.* **294**(51), 19709–19722 (2019).
30. Beaudry, R. I. *et al.* Determinants of exercise intolerance in breast cancer patients prior to anthracycline chemotherapy. *Physiol. Rep.* **7**(1), e13971 (2019).
31. Reding, K.W., Brubaker, P., D'Agostino, R., Kitzman, D.W., Nicklas, B., Langford, D., et al. Increased skeletal intermuscular fat is associated with reduced exercise capacity in cancer survivors: a cross-sectional study. *Cardio-Oncol.* **5**(1) (2019).
32. Jones, L. W., Eves, N. D., Haykowsky, M., Freedland, S. J. & Mackey, J. R. Exercise intolerance in cancer and the role of exercise therapy to reverse dysfunction. *Lancet Oncol.* **10**(6), 598–605 (2009).
33. Bailey, S. J. *et al.* Dietary nitrate supplementation enhances muscle contractile efficiency during knee-extensor exercise in humans. *J. Appl. Physiol.* **109**(1), 135–48 (2010).
34. Hernandez, A. *et al.* Dietary nitrate increases tetanic [Ca2+]i and contractile force in mouse fast-twitch muscle. *J. Physiol.* **590**(15), 3575–3583 (2012).
35. Larsen, F. J. *et al.* Dietary inorganic nitrate improves mitochondrial efficiency in humans. *Cell Metab.* **13**(2), 149–159 (2011).
36. Jarosz, J., White, C. & Grow, W. A. Sodium nitrate decreases agrin-induced acetylcholine receptor clustering. *BMC Pharmacol. Toxicol.* **17**(1), 20 (2016).
37. Timpani, C. A. *et al.* Attempting to compensate for reduced neuronal nitric oxide synthase protein with nitrate supplementation cannot overcome metabolic dysfunction but rather has detrimental effects in dystrophin-deficient mdx muscle. *Neurotherapeut. J. Am. Soc. Exp. NeuroTherapeut.* **14**(2), 429–446 (2017).
38. Akolkar, G., Bagchi, A. K., Ayyappan, P., Jassal, D. S. & Singal, P. K. Doxorubicin-induced nitrosative stress is mitigated by vitamin C via the modulation of nitric oxide synthases. *Am. J. Physiol. Cell Physiol.* **312**(4), C418–C427 (2017).
39. Wang, L. *et al.* Protection against doxorubicin-induced myocardial dysfunction in mice by cardiac-specific expression of carboxyl terminus of hsp70-interacting protein. *Sci. Rep.* **6**, 28399 (2016).
40. Kerbel, R. S. & Shaked, Y. The potential clinical promise of "multimodality" metronomic chemotherapy revealed by preclinical studies of metastatic disease. *Cancer Lett.* **400**, 293–304 (2017).
41. Mainetti, L. E. *et al.* Therapeutic efficacy of metronomic chemotherapy with cyclophosphamide and doxorubicin on murine mammary adenocarcinomas. *Ann. Oncol.* **24**(9), 2310–2316 (2013).
42. Porcelli, S. *et al.* Effects of a short-term high-nitrate diet on exercise performance. *Nutrients.* **8**(9), 534 (2016).
43. Marques-Aleixo, I. *et al.* The beneficial role of exercise in mitigating doxorubicin-induced Mitochondrionopathy. *Biochim. Biophys. Acta Rev. Cancer.* **1869**(2), 189–199 (2018).
44. Zhou, S., Starkov, A., Froberg, M. K., Leino, R. L. & Wallace, K. B. Cumulative and irreversible cardiac mitochondrial dysfunction induced by doxorubicin. *Cancer Res.* **61**(2), 771–777 (2001).
45. Farhad H, Staziaki PV, Addison D, Coelho-Filho OR, Shah RV, Mitchell RN, et al. Characterization of the changes in cardiac structure and function in mice treated with anthracyclines using serial cardiac magnetic resonance imaging. *Circ. Cardiovasc. Imaging*. 9(12) (2016)
46. Yu, Y., Yin, G., Bao, S. & Guo, Z. Kinetic alterations of collagen and elastic fibres and their association with cardiac function in acute myocardial infarction. *Mol. Med. Rep.* **17**(3), 3519–3526 (2018).
47. Nguyen, T., Sherratt, P. J., Nioi, P., Yang, C. S. & Pickett, C. B. Nrf2 controls constitutive and inducible expression of ARE-driven genes through a dynamic pathway involving nucleocytoplasmic shuttling by Keap1. *J. Biol. Chem.* **280**(37), 32485–32492 (2005).
48. Clements, C. M., McNally, R. S., Conti, B. J., Mak, T. W. & Ting, J. P. DJ-1, a cancer- and Parkinson's disease-associated protein, stabilizes the antioxidant transcriptional master regulator Nrf2. *Proc. Natl. Acad Sci. USA.* **103**(41), 15091–15096 (2006).
49. Hayes, J. D. & Dinkova-Kostova, A. T. The Nrf2 regulatory network provides an interface between redox and intermediary metabolism. *Trends Biochem. Sci.* **39**(4), 199–218 (2014).
50. Larsen, S. *et al.* Biomarkers of mitochondrial content in skeletal muscle of healthy young human subjects. *J. Physiol.* **590**(14), 3349–3360 (2012).
51. Fearon, K. *et al.* Definition and classification of cancer cachexia: an international consensus. *Lancet Oncol.* **12**(5), 489–495 (2011).
52. Zheng, D. *et al.* Calpain-2 promotes MKP-1 expression protecting cardiomyocytes in both in vitro and in vivo mouse models of doxorubicin-induced cardiotoxicity. *Arch Toxicol.* **93**(4), 1051–1065 (2019).
53. Wang, Y. *et al.* GCN2 deficiency ameliorates doxorubicin-induced cardiotoxicity by decreasing cardiomyocyte apoptosis and myocardial oxidative stress. *Redox Biol.* **17**, 25–34 (2018).
54. Hallajian, F. *et al.* Evaluation of the effect of resveratrol and doxorubicin on (99m)Tc-MIBI uptake in breast cancer cell xenografts in mice. *Cancer Biother. Radiopharm.* **33**(9), 403–410 (2018).
55. Lue, Y. *et al.* Humanin analog enhances the protective effect of dexrazoxane against doxorubicin-induced cardiotoxicity. *Am. J. Physiol. Heart Circul. Physiol.* **315**(3), H634–H643 (2018).
56. Pillai, V. B. *et al.* Honokiol, an activator of Sirtuin-3 (SIRT3) preserves mitochondria and protects the heart from doxorubicin-induced cardiomyopathy in mice. *Oncotarget.* **8**(21), 34082–34098 (2017).
57. Samaras, T. T. Shorter height is related to lower cardiovascular disease risk - a narrative review. *Indian Heart J.* **65**(1), 66–71 (2013).
58. McQuade, R. M. *et al.* Oxaliplatin-induced enteric neuronal loss and intestinal dysfunction is prevented by co-treatment with BGP-15. *Br. J. Pharmacol.* **175**(4), 656–677 (2018).
59. McQuade, R. M. *et al.* Co-treatment with BGP-15 exacerbates 5-fluorouracil-induced gastrointestinal dysfunction. *Front. Neurosci.* **13**, 449 (2019).
60. McQuade, R. M. *et al.* Irinotecan-induced gastrointestinal dysfunction is associated with enteric neuropathy, but increased numbers of cholinergic myenteric neurons. *Front. Physiol.* **8**, 391 (2017).

61. Gilliam, L. A. & St Clair, D. K. Chemotherapy-induced weakness and fatigue in skeletal muscle: the role of oxidative stress. *Antioxid. Redox Signal.* **15**(9), 2543–2563 (2011).
62. Gilliam, L. A. A. *et al.* The anticancer agent doxorubicin disrupts mitochondrial energy metabolism and redox balance in skeletal muscle. *Free Radical Biol. Med.* **65**, 988–996 (2013).
63. Fogli, S., Nieri, P. & Breschi, M. C. The role of nitric oxide in anthracycline toxicity and prospects for pharmacologic prevention of cardiac damage. *Faseb j.* **18**(6), 664–675 (2004).
64. Rybalka, E. *et al.* Chemotherapeutic agents induce mitochondrial superoxide production and toxicity but do not alter respiration in skeletal muscle in vitro. *Mitochondrion* **42**, 33–49 (2018).
65. Sánchez-Alcázar, J. A., Khodjakov, A. & Schneider, E. Anticancer drugs induce increased mitochondrial cytochrome c expression that precedes cell death. *Cancer Res.* **61**(3), 1038–1044 (2001).
66. Crilly, M. J., Tryon, L. D., Erlich, A. T. & Hood, D. A. The role of Nrf2 in skeletal muscle contractile and mitochondrial function. *J. Appl. Physiol.* **121**(3), 730–40 (2016).
67. Song, M. *et al.* Trimetazidine restores the positive adaptation to exercise training by mitigating statin-induced skeletal muscle injury. *J. Cachexia Sarcopenia Muscle.* **9**(1), 106–118 (2018).
68. Bouzidi, M. F. *et al.* Decreased expression of ubiquinol-cytochrome c reductase subunits in patients exhibiting mitochondrial myopathy with progressive exercise intolerance. *NMD.* **3**(5–6), 599–604 (1993).
69. Dumoulin, R. *et al.* A novel gly290asp mitochondrial cytochromebmutation linked to a complex III deficiency in progressive exercise intolerance. *Mol. Cell. Probes* **10**(5), 389–391 (1996).
70. Andreu, A. L. *et al.* Exercise intolerance due to mutations in the cytochrome b gene of mitochondrial DNA. *N. Engl. J. Med.* **341**(14), 1037–1044 (1999).
71. Tucker, E. J. *et al.* Mutations in the UQCC1-interacting protein, UQCC2, cause human complex III deficiency associated with perturbed cytochrome b protein expression. *PLoS Genet.* **9**(12), e1004034 (2013).
72. Merry, T. L., Steinberg, G. R., Lynch, G. S. & McConell, G. K. Skeletal muscle glucose uptake during contraction is regulated by nitric oxide and ROS independently of AMPK. *Am. J. Physiol. Endocrinol. Metab.* **298**(3), E577–E585 (2010).
73. Roberts, L. D. *et al.* Inorganic nitrate mimics exercise-stimulated muscular fiber-type switching and myokine and γ-aminobutyric acid release. *Diabetes* **66**(3), 674–688 (2017).
74. Richardson, A. & Ream, E. The experience of fatigue and other symptoms in patients receiving chemotherapy. *Eur. J. Cancer Care.* **5**, 24–30 (1996).
75. Nair, A. B. & Jacob, S. A simple practice guide for dose conversion between animals and human. *J. Basic Clin. Pharm.* **7**(2), 27–31 (2016).
76. Carlstrom, M. *et al.* Dietary inorganic nitrate reverses features of metabolic syndrome in endothelial nitric oxide synthase-deficient mice. *Proc. Natl. Acad. Sci. USA.* **107**(41), 17716–17720 (2010).
77. Sorensen, J. C. *et al.* BGP-15 Protects against oxaliplatin-induced skeletal myopathy and mitochondrial reactive oxygen species production in mice. *Front. Pharmacol.* **8**, 137 (2017).
78. Timpani, C. A. *et al.* Adenylosuccinic acid therapy ameliorates murine Duchenne Muscular Dystrophy. *Sci. Rep.* **10**(1), 1125 (2020).
79. Bar, C. *et al.* Telomerase expression confers cardioprotection in the adult mouse heart after acute myocardial infarction. *Nat. Commun.* **5**, 5863 (2014).
80. Goodman, C. A. *et al.* Novel insights into the regulation of skeletal muscle protein synthesis as revealed by a new nonradioactive in vivo technique. *FASEB J.* **25**(3), 1028–1039 (2011).
81. Monaco, C. M. F. *et al.* Sodium nitrate supplementation alters mitochondrial H2O2 emission but does not improve mitochondrial oxidative metabolism in the heart of healthy rats. *Am. J. Physiol. Regul. Integr. Comp. Physiol.* **315**(2), R191–R204 (2018).
82. Srere PA. [1] Citrate synthase: [EC 4.1.3.7. Citrate oxaloacetate-lyase (CoA-acetylating)]. Methods in Enzymology. 13: Academic Press; 1969. p. 3–11.

Acknowledgements
The authors wish to acknowledge students Ben Butcher and James Sorensen whom contributed to preliminary data acquisition in the early stages of this project.

Author contributions
D.C. performed animal treatments, animal surgeries, body composition analyses, metabolic cage activity analyses, western blotting experiments and manuscript preparation, whilst contributing to the histological analysis; D.D. contributed to the histological analyses and preparation of figures; C.T. performed citrate synthase analyses and contributed to the data interpretation and manuscript preparation; A.H. funded the research and contributed to manuscript preparation; C.G. contributed to the data interpretation and manuscript preparation; E.R. designed, funded the research and contributed to data interpretation and manuscript preparation.

Funding
This study was funded by former Institute of Sport, Exercise and Active Living, and Centre for Chronic Disease, program grants (both Victoria University).

Competing interests
E.R. is a scientific consultant to Santhera Pharmaceuticals. The other authors have no conflict of interest.

Additional information
Supplementary information is available for this paper at https://doi.org/10.1038/s41598-020-71974-z.

Correspondence and requests for materials should be addressed to E.R.

Reprints and permissions information is available at www.nature.com/reprints.

Publisher's note Springer Nature remains neutral with regard to jurisdictional claims in published maps and institutional affiliations.

Chapter 3

The paradoxical effect of PARP inhibitor BGP-15 on irinotecan-induced cachexia and skeletal muscle dysfunction

Campelj DG, Timpani CA, Petersen AC, Hayes A, Goodman CA, Rybalka E. The Paradoxical Effect of PARP Inhibitor BGP-15 on Irinotecan-Induced Cachexia and Skeletal Muscle Dysfunction. Cancers (Basel). 2020 Dec 17;12(12):3810. doi: 10.3390/cancers12123810. PMID: 33348673; PMCID: PMC7766767.

Preface

In this study, we transitioned away from DOX to evaluate other chemotherapeutic agents for their capacity to induce cachexia. Given that cachexia is highly prevalent in solid-tumor cancers of the gastrointestinal system, such as colorectal cancer (CRC) [17], we were interested in the chemotherapies utilized in this setting. Two of the most common chemotherapy regimens administered in CRC are FOLFIRI and FOLFOX [18]. The FOLFIRI regimen comprises the concomitant delivery of irinotecan (IRI), 5-fluorouracil (5FU) and leucovorin (LEU), while the FOLFOX comprises oxaliplatin (OXA), 5FU and LEU. Subsequently, we were interested in evaluating these agents for their capacity to induce cachexia with a focus on perturbations to skeletal muscle homeostasis. This project arose out of mutual-interest between our skeletal muscle focused laboratory and a collaborating laboratory group interested in chemotherapy-induced toxicities to the gastrointestinal tract (for publications see - [19-23]). As such, we were interested in evaluating the impact of these chemotherapy drugs on cachexia and skeletal muscle. Initial data from our laboratory highlighted that OXA induces skeletal myopathy, but does not alter body mass [24]. Further, findings from Barreto *et al.* demonstrated that the FOLFIRI is a more potent induced of cachexia compared to FOLFOX [25], thus we hypothesises that IRI might be a significant driver of muscle cachexia.

Given we observed no therapeutic potential of SN supplementation when administered alongside DOX to mitigate muscle cachexia, we chose not to continue these investigations in this Chapter 3. Instead, we chose to investigate the therapeutic potential of mitoprotective compound, BGP-15 [26]. BGP-15 is marketed as a heat shock protein-70 (HSP-70) co-inducer and poly (ADP-ribose) polymerase-1 (PARP-1) inhibitor [27, 28], that is protective in a range of myopathic conditions [29-31]. Additionally, we have previously shown that the combination of BGP-15 alongside OXA is protective against chemotherapy-induced skeletal myopathy [24]. Subsequently, we aimed to evaluate the adjuvant therapeutic potential of BGP-15 in combination

with IRI. We hypothesized that IRI would cause cachexia involving skeletal muscle wasting and dysfunction, and that BGP-15 could therapeutically protect skeletal muscle from the insult of IRI.

VICTORIA UNIVERSITY

THE NEW WAY TO DO UNI

OFFICE FOR RESEARCH TRAINING, QUALITY AND INTEGRITY

DECLARATION OF CO-AUTHORSHIP AND CO-CONTRIBUTION: PAPERS INCORPORATED IN THESIS

This declaration is to be completed for each conjointly authored publication and placed at the beginning of the thesis chapter in which the publication appears.

1. PUBLICATION DETAILS (to be completed by the candidate)

Title of Paper/Journal/Book: The paradoxical effect of PARP inhibitor BGP-15 on irinotecan-induced cachexia and skeletal muscle dysfunction

Surname: Campelj

First name: Dean

Institute: Institute for Health and Sport

Candidate's Contribution (%): 70

Status:

Accepted and in press: ☐ Date:

Published: ☑ Date: 17/12/2020

2. CANDIDATE DECLARATION

I declare that the publication above meets the requirements to be included in the thesis as outlined in the HDR Policy and related Procedures – policy.vu.edu.au.

Dean Campelj Digitally signed by Dean Campelj Date: 2021.05.21 12:09:05 +10'00'

Signature **Date**

3. CO-AUTHOR(S) DECLARATION

In the case of the above publication, the following authors contributed to the work as follows:

The undersigned certify that:

1. They meet criteria for authorship in that they have participated in the conception, execution or interpretation of at least that part of the publication in their field of expertise;
2. They take public responsibility for their part of the publication, except for the responsible author who accepts overall responsibility for the publication;

3. There are no other authors of the publication according to these criteria;

4. Potential conflicts of interest have been disclosed to a) granting bodies, b) the editor or publisher of journals or other publications, and c) the head of the responsible academic unit; and

5. The original data will be held for at least five years from the date indicated below and is stored at the following **location(s)**:

Victoria University R Drive

Name(s) of Co-Author(s)	Contribution (%)	Nature of Contribution	Signature	Date
Cara A Timpani	5	Histological analyses, citrate synthase analyses	[redacted]	18/05/21
Aaron C Petersen	2.5	Conception, provision of BGP-15, manuscript review and editing		18/05/21
Alan Hayes	2.5	Methodological resources, manuscript review and editing		18/05/21
Craig A Goodman	10	Conception, supervision, methodological resources, manuscript review and editing		18/05/21
Emma Rybalka	10	Conception, supervision, methodological resources, manuscript review and editing		18/05/21

Updated: September 2019

cancers

MDPI

Article

The Paradoxical Effect of PARP Inhibitor BGP-15 on Irinotecan-Induced Cachexia and Skeletal Muscle Dysfunction

Dean G. Campelj [1,2], Cara A. Timpani [1,2], Aaron C. Petersen [1,2], Alan Hayes [1,2,3], Craig A. Goodman [2,4,*] and Emma Rybalka [1,2,*]

1 Institute for Health and Sport (IHeS), Victoria University, Melbourne, VIC 8001, Australia; dean.campelj@live.vu.edu.au (D.G.C.); cara.timpani@vu.edu.au (C.A.T.); aaron.petersen@vu.edu.au (A.C.P.); alan.hayes@vu.edu.au (A.H.)
2 Australian Institute for Musculoskeletal Science, Victoria University, St Albans, VIC 3021, Australia
3 Department of Medicine–Western Health, Melbourne Medical School, The University of Melbourne, Melbourne, VIC 3021, Australia
4 Centre for Muscle Research (CMR), Department of Physiology, The University of Melbourne, Parkville, VIC 3010, Australia
* Correspondence: craig.goodman@unimelb.edu.au (C.A.G.); emma.rybalka@vu.edu.au (E.R.); Tel.: +61-3-839-58226 (E.R.)

Received: 27 November 2020; Accepted: 14 December 2020; Published: 17 December 2020

Simple Summary: Both cancer and the chemotherapy used to treat it are drivers of cachexia, a life-threatening body-wasting condition which complicates cancer treatment. Poly-(ADP-ribose) polymerase (PARP) inhibitors are currently being investigated as a treatment against cancer. Here, we present paradoxical evidence that they might also be useful for mitigating the skeletal muscle specific side-effects of anti-cancer chemotherapy or exacerbate them. BGP-15 is a small molecule PARP inhibitor which protected against irinotecan (IRI)-induced cachexia and loss of skeletal muscle mass and dysfunction in our study. However, peculiarly, BGP-15 adjuvant therapy reduced protein synthesis rates and the expression of key cytoskeletal proteins associated with the dystrophin-associated protein complex and increased matrix metalloproteinase activity, while it increased the propensity for fast-twitch muscles to tear during fatiguing contraction. Our data suggest that both IRI and BGP-15 cause structural remodeling involving proteins associated with the contractile apparatus, cytoskeleton and/or the extracellular matrix which may be only transient and ultimately beneficial or may paradoxically onset a muscular dystrophy phenotype and be detrimental if more permanent.

Abstract: Chemotherapy-induced muscle wasting and dysfunction is a contributing factor to cachexia alongside cancer and increases the risk of morbidity and mortality. Here, we investigate the effects of the chemotherapeutic agent irinotecan (IRI) on skeletal muscle mass and function and whether BGP-15 (a poly-(ADP-ribose) polymerase-1 (PARP-1) inhibitor and heat shock protein co-inducer) adjuvant therapy could protect against IRI-induced skeletal myopathy. Healthy 6-week-old male Balb/C mice (n = 24; 8/group) were treated with six intraperitoneal injections of either vehicle, IRI (30 mg/kg) or BGP-15 adjuvant therapy (IRI+BGP; 15 mg/kg) over two weeks. IRI reduced lean and tibialis anterior mass, which were attenuated by IRI+BGP treatment. Remarkably, IRI reduced muscle protein synthesis, while IRI+BGP reduced protein synthesis further. These changes occurred in the absence of a change in crude markers of mammalian/mechanistic target of rapamycin (mTOR) Complex 1 (mTORC1) signaling and protein degradation. Interestingly, the cytoskeletal protein dystrophin was reduced in both IRI- and IRI+BGP-treated mice, while IRI+BGP treatment also decreased β-dystroglycan, suggesting significant remodeling of the cytoskeleton. IRI reduced absolute force production of the soleus and extensor digitorum longus (EDL) muscles, while IRI+BGP rescued absolute force production of the soleus and strongly trended to rescue force output of the

EDL (p = 0.06), which was associated with improvements in mass. During the fatiguing stimulation, IRI+BGP-treated EDL muscles were somewhat susceptible to rupture at the musculotendinous junction, likely due to BGP-15's capacity to maintain the rate of force development within a weakened environment characterized by significant structural remodeling. Our paradoxical data highlight that BGP-15 has some therapeutic advantage by attenuating IRI-induced skeletal myopathy; however, its effects on the remodeling of the cytoskeleton and extracellular matrix, which appear to make fast-twitch muscles more prone to tearing during contraction, could suggest the induction of muscular dystrophy and, thus, require further characterization.

Keywords: anti-cancer treatments; chemotherapy; PARP-1 inhibitor; BGP-15; skeletal muscle; cachexia; muscle wasting; myopathy; dystrophin; mechanotransduction

1. Introduction

Cachexia is a chronic and often fatal consequence of cancer and the chemotherapeutic agents used to treat it. It is a complex wasting syndrome defined as a >5% loss of body mass, which features lean tissue wasting with or without a loss of fat mass [1], as well as prominent skeletal myopathy that manifests as both wasting and dysfunction [2–4]. Historically, cancer-related cachexia was considered a tumor-induced phenomenon; however, mounting evidence suggests that chemotherapy drugs plays a prominent role in the progression of cachexia independent of the tumor [5–8]. Several chemotherapeutic agents from different drug classes (and with different mechanisms of action) elicit skeletal muscle toxicity [9], which, at the molecular level, involves disruption of proteostasis in favor of protein degradation and mitochondrial dysfunction through which oxidative stress/damage is escalated [10–12]. Despite these data, most chemotherapeutic agents in clinical utility have not been evaluated for their potential to induce skeletal myopathy. As such, muscle wasting as a side-effect of anti-cancer chemotherapy treatment is a largely overlooked factor, despite contributing to dose-limiting toxicities and poorer survival outcomes [13].

Irinotecan (IRI) is a chemotherapeutic agent commonly utilized as part of anti-cancer treatment regimens against colorectal, pancreatic and small-cell lung cancer [14–16]. As a potent topoisomerase I inhibitor [17], IRI treatment causes severe gastrointestinal toxicity, neutropenia and asthenia [18]. Recently, skeletal muscle wasting has also emerged as a major off-target event and is a key prognostic indicator of mortality in IRI-treated cancer patients [19,20]. Recent studies have established that the FOLFIRI (Folinic acid.leucovorin, fluorouracil and IRI regimen), in which IRI is a staple (in addition to toleucovorin and 5-fluorouracil), induces skeletal muscle wasting and dysfunction in otherwise healthy mice [11]. Although it has never been evaluated independently, IRI likely drives this myopathy, since treatment with the FOLFOX (Folinic acid/leucovorin), fluorouracil and oxaliplatin) regimen, which includes leucovorin and 5-fluorouracil but substitutes IRI for oxaliplatin, had no effect on skeletal muscle [11]. Multi-omics analysis of FOLFIRI-treated mouse muscles [21,22] and in vitro cell culture studies with IRI [23] implicate mitochondrial dysfunction, characterized by the downregulation of proteins associated with mitochondrial dynamics and oxidative phosphorylation and reduced adenosine triphosphate (ATP) synthesis, glucose metabolism and mitochondrial viability in this myopathy. However, the molecular events occurring up- and/or downstream of the mitochondria that result in muscle wasting and dysfunction are currently unknown. Therefore, in this study, our first aim was to characterize the effect of IRI treatment on the skeletal muscular system in vivo and investigate the underlying molecular mechanisms.

Currently, there is no approved treatment against cachexia, despite many adjuvant therapeutics having been clinically evaluated (reviewed recently in [24]) Targeting the mitochondria could be therapeutically advantageous in this regard since they appear implicit in IRI-induced skeletal myopathy. One potential therapeutic candidate is the small molecule BGP-15, a hydroximic acid

derivative nicotinic acid-amidoxime [25], which has demonstrated therapeutic potential in treating skeletal myopathy associated with Duchenne Muscular Dystrophy [26,27], ventilation-induced diaphragm dysfunction [28–31], sarcopenia [32], diabetes [33–35] and oxaliplatin treatment [36]. BGP-15 inhibits poly-(ADP-ribose) polymerase-1 (PARP-1) [37], a repressor of mitochondrial function [38,39], and co-induces heat shock protein-70 (HSP-70) [40,41], which increases mitochondrial content, function and oxidative capacity [42]. HSP-70 activation also plays a role in the maintenance of skeletal muscle mass, in part, by regulating proteostasis [43]. Key to the success of any adjuvant administered to protect against the side-effects of chemotherapy is that tumor growth is not accentuated—in a pre-clinical cancer model, BGP-15 did not affect tumor growth [44], nor did it impact the anti-cancer efficacy of cisplatin [37]. Collectively, these data highlight that BGP-15 may be useful as an adjuvant candidate during anti-cancer chemotherapy to mitigate cachectic skeletal myopathy. Thus, our secondary aim was to evaluate the protective efficacy of BGP-15 adjuvant therapy against IRI-induced skeletal myopathy and investigate the underlying mechanisms through which BGP-15 functions in the chemotoxic environment.

In this study, we conclude that anti-cancer IRI treatment causes significant cachexia featuring muscle atrophy and dysfunction in mice, which could be attenuated with BGP-15 adjuvant therapy. For the first time, we show that IRI causes cytoskeletal changes involving the loss of dystrophin protein expression which negatively impact skeletal muscle mass and function. BGP-15 adjuvant therapy causes further remodeling as well as pro-mitochondrial activity but makes fast-twitch muscles more prone to tearing during fatiguing contraction. It is difficult to ascertain from our data whether BGP-15 adjuvant therapy is beneficial in the long term or whether it induces a type of muscular dystrophy and is therefore deleterious. The potential negative impact of BGP-15 on the skeletal muscular system when teamed with chemotherapeutic agents should be considered in the broader context of using PARP inhibitors as staples in anti-cancer therapy.

2. Results

2.1. Irinotecan (IRI) Induces Cachexia Which Is Mitigated by BGP-15

In order to determine the capacity for IRI and IRI+BGP treatment to induce and mitigate cachexia, respectively, body mass and composition, as well as skeletal muscle mass indices, were assessed. IRI-treated mice lost ~5% of their body mass over the course of the treatment period, which was partially mitigated by IRI+BGP treatment ($p < 0.05$; Figure 1A). When expressed relative to the vehicle (VEH) group, which gained ~5% of their initial body mass over the treatment period, IRI treatment caused marked cachexia with a ~10% displacement from normal/expected body mass ($p < 0.05$; Figure 1B). Combined IRI+BGP treatment attenuated body mass displacement to <5% (pre-cachexia) ($p < 0.05$ compared to IRI; Figure 1B). Unsurprisingly, lean mass data mirrored body mass data, with IRI treatment inducing a ~5% loss of lean mass compared to VEH, which was also partially mitigated by IRI+BGP treatment but still significantly lower than VEH control lean mass ($p < 0.05$; Figure 1C). There was, however, no protective effect from IRI+BGP treatment on fat mass, with both IRI and IRI+BGP treatment inducing a ~20% reduction in fat mass compared to VEH ($p < 0.05$; Figure 1D). These reductions in body composition indices were not due to differences found in food consumption between treatment groups ($p > 0.05$; Figure 1E).

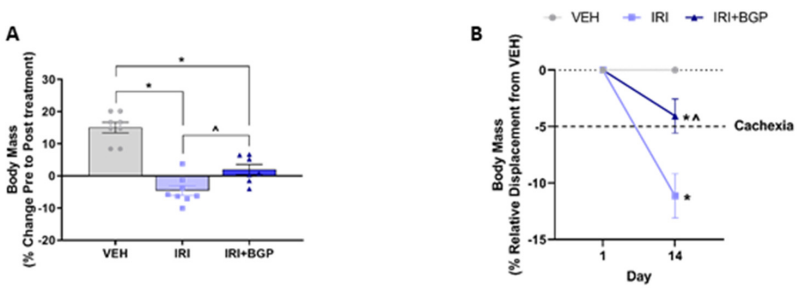

Figure 1. *Cont.*

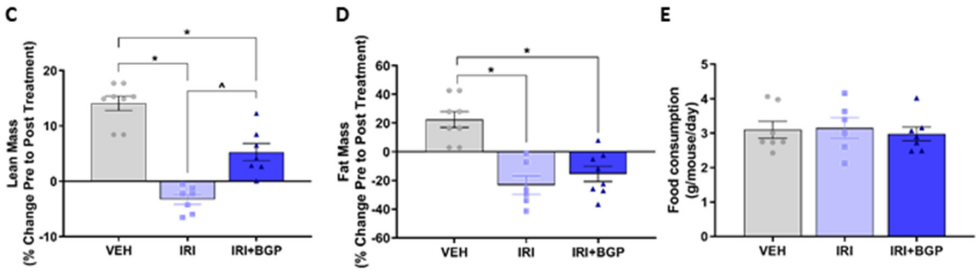

Figure 1. The effect of irinotecan (IRI) and IRI with BGP-15 (IRI+BGP) treatment on body composition indices and food consumption. Body composition parameters were measured pre- and post-treatment with body mass presented as (**A**) percentage change from Pre to Post treatment and (**B**) relative displacement percentage compared to vehicle (VEH) from Pre to Post treatment. (**C**) Lean and (**D**) fat mass are presented as a percentage change from Pre to Post treatment. (**E**) Food consumption was monitored throughout the treatment period. * = $p < 0.05$ compared to VEH; ˆ = $p < 0.05$ compared to IRI; $n = 7$–8.

2.2. IRI Treatment Causes Muscular Atrophy Which Is Normalized by BGP-15

To explore whether the IRI-induced loss of lean mass was emulated in skeletal muscle, we sought to determine whether IRI and IRI+BGP treatment could influence crude mass of a selection of hindlimb muscles or the cross-sectional area (CSA) of tibialis anterior (TA) fibers. There were no significant differences in raw mass or the muscle to body mass ratios between treatment groups for extensor digitorum longus (EDL), soleus (SOL) or heart muscles ($p > 0.05$; Figure 2A). However, both TA raw mass and the TA to body mass ratio were significantly reduced following IRI treatment ($p < 0.05$), which was protected against by IRI+BGP treatment ($p < 0.05$; Figure 2A). Histological fiber size profiling demonstrated a left shift in the CSA frequency distribution induced by IRI treatment, which was normalized to VEH control levels by IRI+BGP treatment (Figure 2B). Furthermore, mean fiber CSA and the pooled fiber size distribution were also significantly reduced following IRI treatment compared to VEH ($p < 0.05$; Figure 2C–E) and IRI+BGP treatment partially rescued both of these measures ($p < 0.05$; Figure 2C–E). There was no evidence of muscle damage elicited by IRI treatment by way of centronucleated fibers and immune cell infiltrate (Figure 2E).

A

	Muscle Mass (mg)			Muscle/Body Mass Ratio (mg/g)		
	VEH	IRI	IRI+BGP	VEH	IRI	IRI+BGP
EDL	9.30 ± 1.94	9.10 ± 1.18	9.36 ± 1.27	0.41 ± 0.09	0.38 ± 0.04	0.43 ± 0.06
SOL	8.80 ± 1.11	7.57 ± 1.08	7.97 ± 2.05	0.38 ± 0.04	0.33 ± 0.05	0.37 ± 0.09
TA	40.38 ± 1.75	34.50 ± 2.64*	39.59 ± 2.37^	1.76 ± 0.08	1.51 ± 0.11*	1.82 ± 0.10^
Heart	105.45 ± 4.75	101.66 ± 3.71	103.11 ± 1.73	4.59 ± 0.25	4.45 ± 0.23	4.71 ± 0.07

Figure 2. *Cont.*

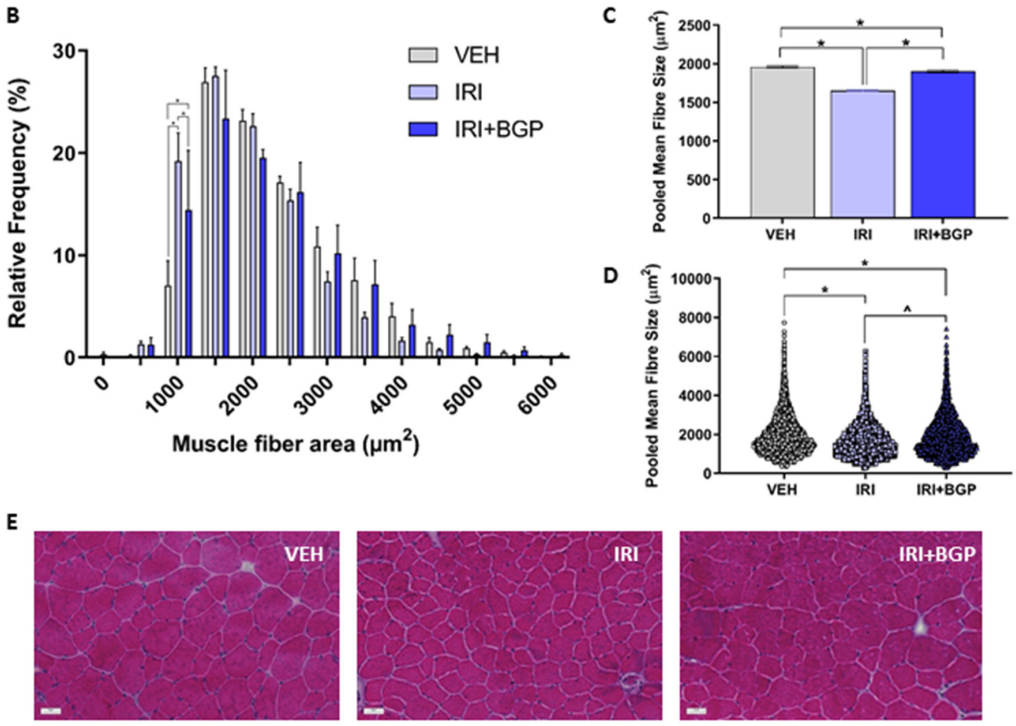

Figure 2. The effect of irinotecan (IRI) and IRI with BGP-15 (IRI+BGP) treatment on muscle mass and fiber size. (**A**) Skeletal muscle masses of extensor digitorum longus (EDL), soleus (SOL), tibialis anterior (TA) and heart were measured post-mortem and are presented as both raw mass and as a muscle mass to body mass ratio. TA cross-sections were hematoxylin and eosin (H&E)-stained to assess the skeletal muscle histological fiber size with data presented as (**B**) muscle fiber cross-sectional area (CSA) percentage relative frequency distribution, (**C**) the mean group pooled muscle fiber CSA (of all fibers counted) and (**D**) the group pooled fiber size distribution. (**E**) Representative images of H&E-stained TA cross-sections show no evidence of muscle damage (e.g., centronucleated fibers and immune cell infiltrate). Scale bar = 50 μm; * = $p < 0.05$ compared to VEH, ^ = $p < 0.05$ compared to IRI; n = 6–8 for muscle weights; n = 4–6 for histology.

2.3. IRI Reduces Protein Synthesis which Is Exacerbated by BGP-15

To investigate changes to molecular signaling of protein turnover as a potential mechanism for IRI-induced muscle fiber atrophy, we initially assessed skeletal muscle protein synthesis signaling via the in vivo surface sensing of translation (SUnSET) method [45], which measures the rate of puromycin-labelled peptide production as an indicator of overall protein synthesis rates. IRI treatment reduced protein synthesis compared to VEH, and surprisingly, IRI+BGP treatment further reduced protein synthesis ($p < 0.05$; Figure 3A,J). These decreases in protein synthesis were independent of a change in the phosphorylation of eIF2a, a highly characterized inhibitor of protein synthesis [46] ($p > 0.05$; Figure 3B,J). Given its prominent role regulating skeletal muscle protein synthesis [47], we next probed for markers involved in the activation of mammalian/mechanistic target of rapamycin (mTOR) Complex 1 (mTORC1) signaling and mTORC1's downstream targets. Interestingly, we demonstrated no significant differences between treatment groups in Akt^{Thr308}, $p70s6k1^{Thr389}$ or $4E\text{-}BP1^{Thr37/46}$ phosphorylation ($p > 0.05$; Figure 3C–E,J), although there was a trend for IRI+BGP treatment to increase p70s6k1 signaling relative to IRI ($p = 0.08$; Figure 3D,J). There was, however, a reduction in Akt^{Ser473} phosphorylation with both IRI and IRI+BGP treatments ($p < 0.05$; Figure 3F,J), a site targeted by mTORC2 (mTOR Complex 2) signaling [48]. On the alternative side of protein turnover, we saw no significant effect between treatment groups in crude static molecular markers of protein degradation, i.e., total ubiquitinated proteins, Atrogin-1 or muscle RING-finger protein-1

(MuRF-1) ($p > 0.05$; Figure 3G–J). Full-length Western blots, densitometry data and total protein data are provided in Figures S1, S2 and S4 and Table S1.

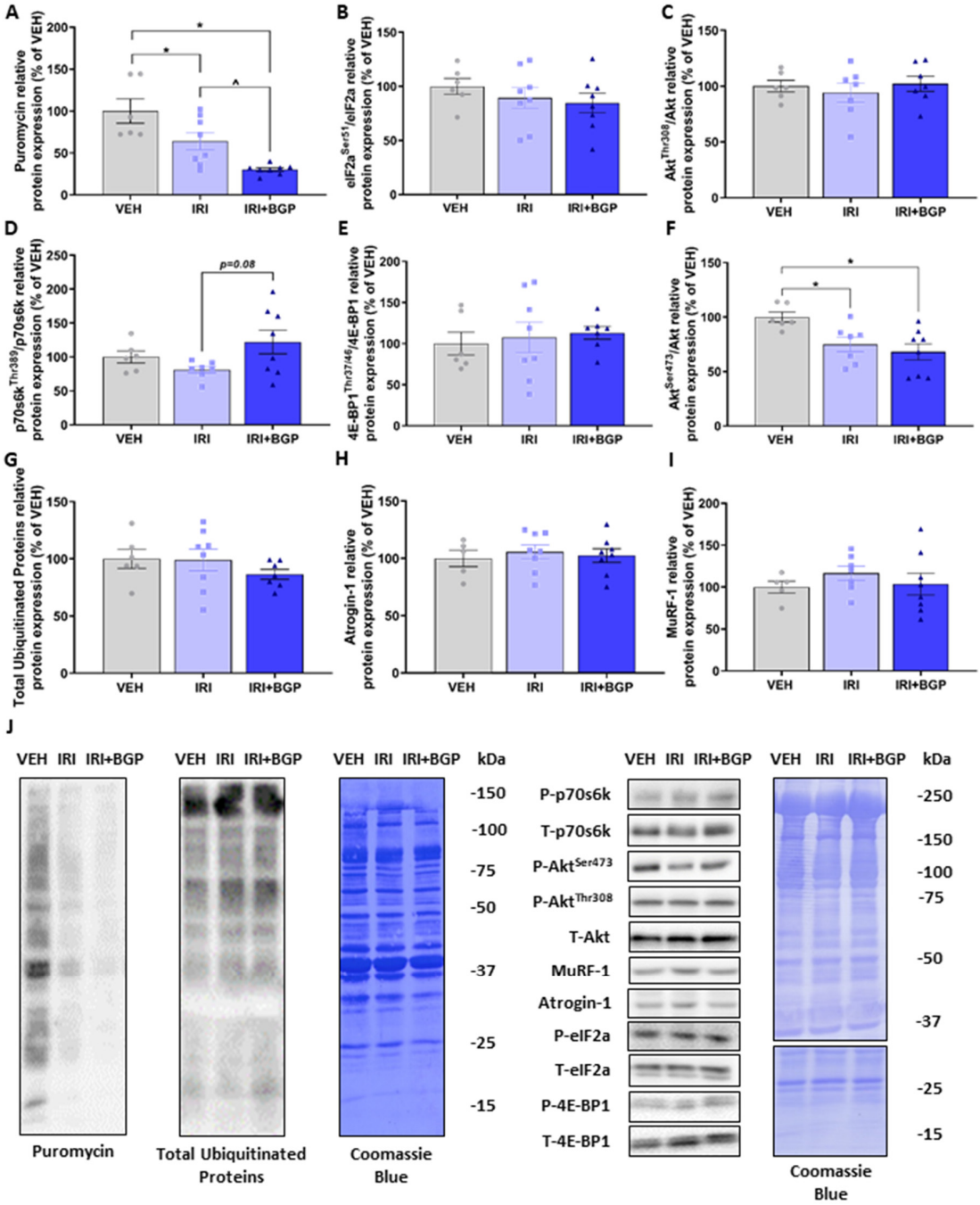

Figure 3. The effect of irinotecan (IRI) and IRI with BGP-15 (IRI+BGP) treatment on protein synthesis and degradation signaling. Western blotting experiments were undertaken on tibialis anterior (TA) homogenate—data are expressed as a relative percentage of the vehicle (VEH) control group. Samples were probed for (**A**) puromycin as a marker of protein synthesis via the surface sensing of translation (SUnSET) method, (**B**) eIF2a^{Ser51} relative to total eIF2a, (**C**) Akt^{Thr308} relative to total Akt, (**D**) p70s6k^{Thr389} relative to total p70s6k, (**E**) 4E-BP1$^{Thr37/46}$ relative to total 4E-BP1, (**F**) Akt^{Ser473} relative to total Akt, (**G**) Ubiquitin, (H) Atrogin-1 and (**I**) MuRF-1. (**J**) Western blot representative images are displayed alongside a Coomassie Blue representative image, which was used as the protein loading control. * = $p < 0.05$ compared to VEH, ˆ = $p < 0.05$ compared to IRI; n = 5–8.

2.4. Assessment of Molecular Markers of Sarcolemmal Membrane Integrity

Since IRI+BGP enhanced the IRI-induced reduction in protein synthesis rate without affecting crude markers of protein degradation, we wanted to investigate whether this might be a consequence of perturbed mechanotransduction through exploring skeletal muscle structural protein expression. Utilizing homogenized TA muscles which are from the same hindlimb anterior compartment and have similar fiber type distributions (i.e., predominately fast-twitch, glycolytic type II fibers) as EDL muscles, we initially probed for laminin, which links the extracellular matrix (ECM) to the sarcolemmal membrane. There was no significant effect on the protein expression of laminin between treatment groups ($p > 0.05$; Figure 4A,M); however, when we assessed the protein expression of dystrophin, a key structural protein that connects the sarcolemmal membrane to the actin cytoskeleton, IRI treatment was found to induce a significant reduction, which was not mitigated by IRI+BGP treatment ($p < 0.05$; Figure 4B,M). We then probed other key structural proteins located on the sarcolemmal membrane and demonstrated that IRI+BGP treatment significantly reduced the protein expression of β-dystroglycan relative to VEH- and IRI-treated mice ($p < 0.05$; Figure 4C,M), but there were no significant changes from treatment to the protein expression of sarcoglycan isoforms α and δ ($p > 0.05$; Figure 4D,E,M). There was no significant effect between treatment groups on the protein expression of the intermediate filament desmin ($p > 0.05$; Figure 4F,M), a key structural protein that connects the sarcomere to the subsarcolemmal cytoskeleton. Full-length Western blots, densitometry data and total protein data are provided in Figures S2 and S4 and Table S1.

It has previously been shown in non-muscle cells that BGP-15 can induce remodeling of plasma membrane lipid rafts, in part, by a Ras-related C3 botulinum toxin substrate 1 (Rac1) GTPase-dependent mechanism [49]. Furthermore, Rac1 signaling has been shown to mediate matrix metalloproteinases' (MMPs) activity in multiple cell types [50–53], which are a group of proteolytic enzymes that can degrade key structural components of the contractile apparatus assembly and the ECM, such as troponin and collagen, respectively, to facilitate remodeling [54–56]. As such, we wanted to assess whether BGP-15 improved muscle mass and function through MMP-9 and MMP-2 activity-dependent structural remodeling. Consistent with our HSP-70 protein expression data, there was no significant effect of IRI or IRI+BGP treatment on Rac1 ($p > 0.05$; Figure 4G,M) or MMP-9 and MMP-2 protein expression ($p > 0.05$; Figure 4H,I,M) when probing TA homogenate. However, when we evaluated MMP-9 and MMP-2 activity in EDL homogenate (EDL muscles have a similar fiber type composition to TA muscles) via gelatin zymography, we found a strong trend for IRI+BGP treatment to increase MMP-9 activity relative to VEH ($p = 0.08$; Figure 4J,N) whilst also significantly reducing MMP-2 activity compared to VEH and IRI treatments ($p < 0.05$; Figure 4K,N). We also identified that IRI+BGP treatment shifted homeostatic MMP activity through increasing the MMP-9 to MMP-2 (MMP-9/MMP-2) activity ratio compared to VEH and IRI treatments ($p < 0.05$ and $p = 0.06$, respectively; Figure 4L,N), an event likely driven by contractile apparatus/cytoskeletal/ECM remodeling [55–57]. Full-length Western blots, densitometry data and total protein data are provided in Figures S2 and S4 and Table S1.

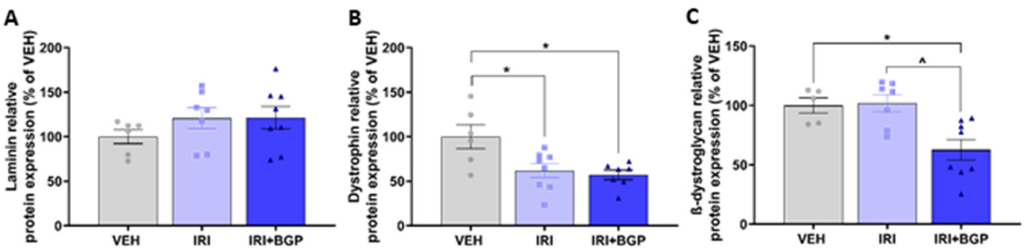

Figure 4. *Cont.*

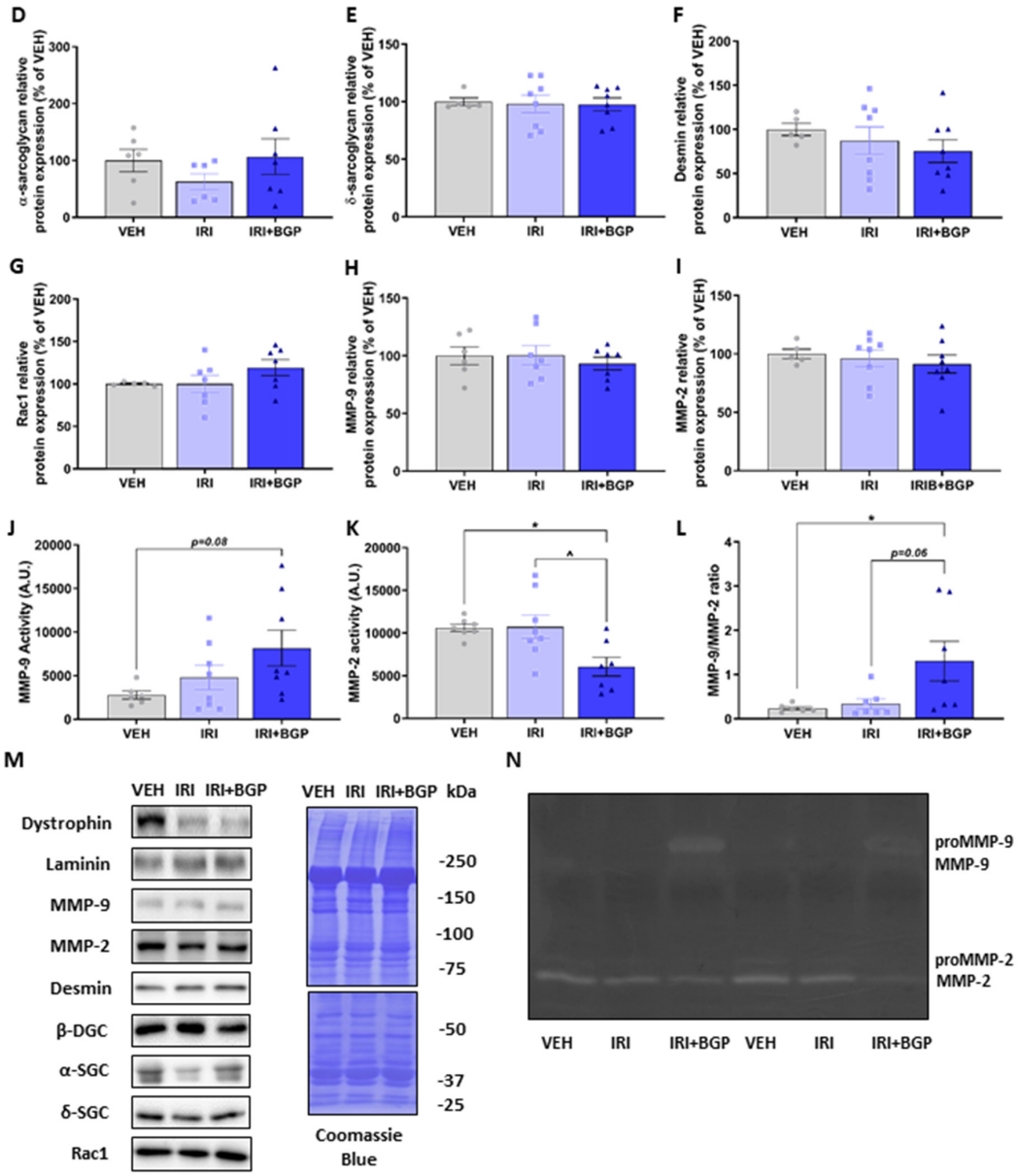

Figure 4. The effect of irinotecan (IRI) and IRI with BGP-15 (IRI+BGP) treatments on molecular markers of sarcolemmal integrity and extracellular matrix (ECM) remodeling. Western blotting experiments were undertaken in tibialis anterior (TA) muscle, with samples probed for (**A**) Laminin, (**B**) Dystrophin, (**C**) β-dystroglycan (β-DGC), (**D**) α-sarcoglycan (α-SGC), (**E**) δ-sarcoglycan (δ-SGC), (**F**) Desmin, (**G**) Rac1 and matrix metalloproteinase (MMP) isoforms (**H**) MMP-9 and (**I**) MMP-2. Gelatin zymography experiments were conducted using extensor digitorum longus (EDL) muscle homogenate (same anterior hindlimb muscle compartment as the TA) to assess the activity of (**J**) MMP-9 and (**K**) MMP-2. (**L**) The ratio of MMP-9 to MMP-2 was utilized to indicate the shift of gelatinolytic MMP activity. Western blotting data are expressed as a relative percentage of the vehicle (VEH) control group and (**M**) representative images are displayed alongside the Coomassie Blue representative image, which was used as the protein loading control. (**N**) Representative image of zymography data is displayed. * = $p < 0.05$ compared to VEH; ˆ = $p < 0.05$ compared to IRI; n = 5–8.

2.5. Assessment of Skeletal Muscle Contractile Function

We examined the contractile function of the predominately slow-twitch SOL and the predominately fast-twitch EDL muscles. We found no significant differences between treatment groups in the

force–frequency relationships of either SOL or EDL muscles ($p > 0.05$; Figure 5A,B); however, we demonstrated that the absolute force production of SOL and EDL muscles was significantly reduced by IRI treatment ($p < 0.05$; Figure 5C,D). IRI+BGP treatment was protective against IRI-induced skeletal muscle dysfunction with absolute force normalization in the SOL muscle ($p < 0.05$; Figure 5C) and a strong trend toward improved absolute force production of the EDL muscle ($p = 0.06$; Figure 5D) relative to IRI-treated animals. When we accounted for the physiological CSA, there was no significant effect on specific force production of the SOL compared to VEH ($p > 0.05$; Figure 5E), but IRI treatment did reduce specific force production of the EDL ($p < 0.05$; Figure 5F). Interestingly, there was a trend for IRI+BGP treatment to improve the specific force production of the SOL relative to both IRI and VEH groups ($p = 0.09$; Figure 5E); however, IRI+BGP exhibited no ameliorative effect on the IRI-induced reduction in specific force production of the EDL ($p > 0.05$; Figure 5F). Mirroring the absolute force data, we demonstrated a reduction in the twitch force (Pt) and the rate of force development (df/dt) for EDL ($p < 0.05$; Figure 5G) and SOL ($p < 0.05$ and $p = 0.08$, respectively; Figure 5G) from IRI treatment, which was mitigated by IRI+BGP treatment, normalizing twitch force to VEH control levels ($p < 0.05$; Figure 5G). We then assessed two factors involved in calcium (Ca^{2+}) handling (i.e., time to peak tension (TTP) and half relaxation time ($\frac{1}{2}$RT)), which may play a role in the underlying mechanism of IRI-induced dysfunction; however, there was no significant effect of IRI or IRI+BGP treatment on these measures ($p > 0.05$; Figure 5G). We also assessed fatigue susceptibility in SOL and EDL muscles by conducting a fatiguing stimulation protocol that induces a progressive reduction in force output of ~65–75% (Figure 5H,I). There was no significant effect of IRI or IRI+BGP treatment on the fatigability of SOL muscles ($p > 0.05$; Figure 5H), nor of IRI treatment on EDL muscles ($p > 0.05$; Figure 5I). However, it was observed that IRI+BGP-treated EDL muscles had an increased susceptibility to rupture at the musculotendinous junction during the fatigue protocol, with 50% ($n = 3/6$) tearing during the initial 3–4 stimulated contractions and the remaining 50% ($n = 3/6$) tearing but continuing to be partially responsive to stimuli (Figure 5I). Despite these ex vivo functional observations, there was no significant effect of IRI or IRI+BGP-15 on voluntary exercise, with wheel distance ($p > 0.05$; Figure 5J) and speed ($p < 0.05$; Figure 5K) unaffected by treatment over a 24-h assessment period. There was, however, a strong trend for IRI to reduce overall cage activity, which was not mitigated by IRI+BGP-15 treatment ($p = 0.07$ for IRI and $p = 0.05$ for IR+BGP-15 versus VEH; Figure 5L).

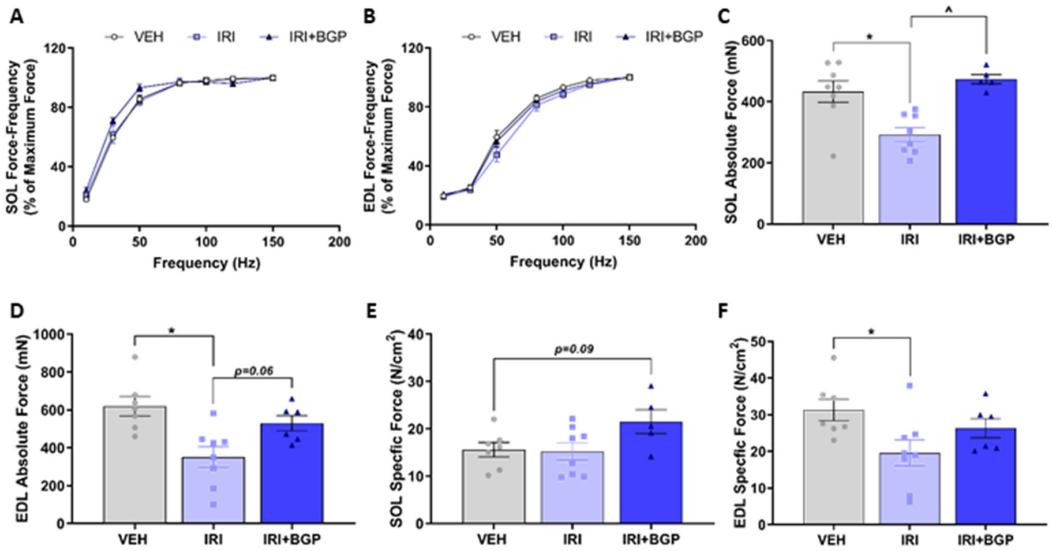

Figure 5. *Cont.*

G

	SOL			EDL		
	VEH	IRI	IRI+BGP	VEH	IRI	IRI+BGP
Pt (mN)	17.03± 2.33	9.89 ± 1.23*	20.2 ± 1.75^	31.78 ± 3.95	17.41 ± 2.94*	32.07 ± 2.49^
TTP (msecs)	27.12 ± 0.47	27.83 ± 1.35	28.1 ± 0.62	20.38 ± 0.54	19.21 ± 0.55	19.25 ± 0.61
½ RT (msecs)	48.71 ± 1.25	60.5 ± 4.99	58.13 ± 5.33	32.68 ± 3.02	27.08 ± 1.49	33.67 ± 2.02
df/dt (mN/msecs)	0.61 ± 0.08	0.37 ± 0.06 #	0.65± 0.09^	1.58 ± 0.20	0.91 ± 0.15*	1.68± 0.09^

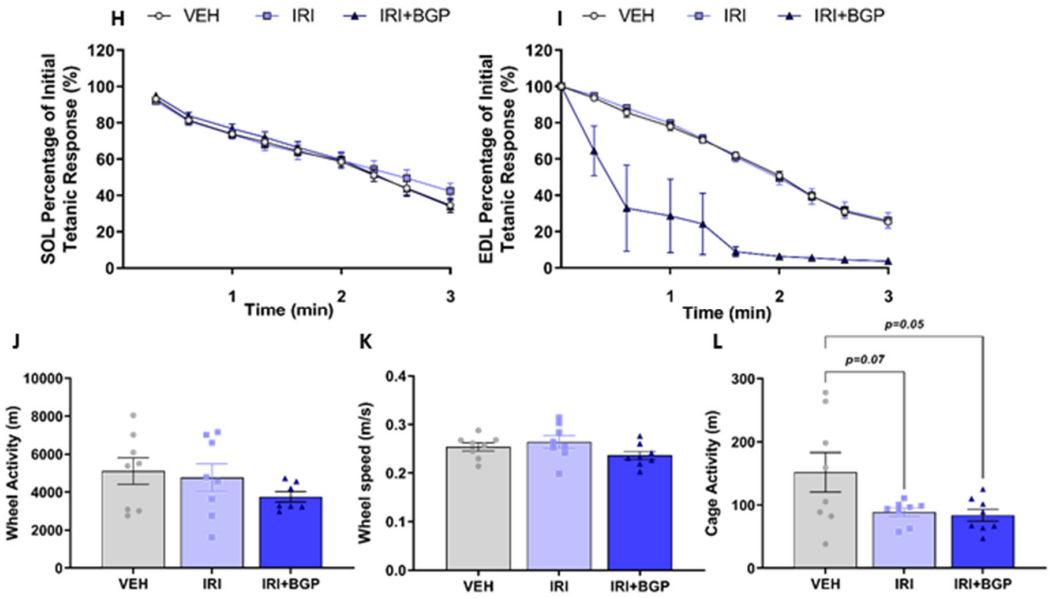

Figure 5. The effect of irinotecan (IRI) and IRI with BGP-15 (IRI+BGP) treatment on skeletal muscle function. Soleus (SOL) and extensor digitorum longus (EDL) muscles underwent ex vivo assessment of contractile function, with (**A**,**B**) force–frequency relationships and (**C**,**D**) absolute and (**E**,**F**) specific force production determined. (**G**) Single twitch properties, i.e., Pt = single twitch force, TTP = time to peak, $\frac{1}{2}$ RT = half relaxation time and df/dt = rate of force production, were also evaluated for SOL and EDL muscles. Additionally, (**H**) SOL and (**I**) EDL muscles underwent fatigue protocols (sequential supramaximal tetanic stimulations) to assess fatigue susceptibility. To correlate ex vivo function data with overall physical activity, mice were housed in Promethion metabolic cages containing running wheels for 24 h prior to endpoint muscle collection. Voluntary wheel running (**J**) distance and (**K**) speed were assessed in addition to (**L**) cage activity over these 24 h. * = $p < 0.05$ compare to VEH; # $p = 0.08$ compared to VEH, ^ = $p < 0.05$ compared to IRI; n = 5–8.

2.6. Assessment of Skeletal Muscle Metabolic Phenotype

Since we have previously demonstrated that IRI treatment can reduce skeletal muscle mitochondrial viability in vitro [58], we undertook mitochondrial profiling on muscles derived from IRI- and IRI+BGP-treated mice to determine whether similar effects could be observed. Initially, we assessed citrate synthase (CS) activity in TA homogenate as a marker of mitochondrial density. While there was no significant effect of IRI treatment, IRI+BGP treatment significantly increased CS activity compared to the VEH control group ($p < 0.05$; Figure 6A). Additionally, we conducted mitochondrial metabolic phenotyping experiments in isolated flexor digitorum brevis (FDB) muscle using extracellular flux technology to determine the relative contribution of oxidative and glycolytic metabolism. There was no effect of IRI treatment on the resting basal respiration compared to VEH ($p > 0.05$); however, IRI+BGP treatment significantly increased basal respiration compared to VEH and IRI groups ($p < 0.05$; Figure 6B). Similarly, ATP production rate was significantly increased by IRI+BGP treatment compared to the VEH and IRI groups ($p < 0.05$; Figure 6C); however, there was no significant

effect of any treatment group on the coupling efficiency ($p > 0.05$; Figure 6D). Interestingly, IRI treatment increased spare respiratory capacity relative to VEH ($p < 0.05$; Figure 6E), although IRI+BGP treatment had no effect on this mitochondrial functional parameter ($p > 0.05$; Figure 6E). We also demonstrated no impact of either IRI or IRI+BGP treatment on glycolytic metabolism as there was no significant effect of treatment on basal extracellular acidification rate (ECAR) or ECAR metabolic potential, which is indicative of the maximal ECAR capacity ($p > 0.05$; Figure 6F,G, respectively).

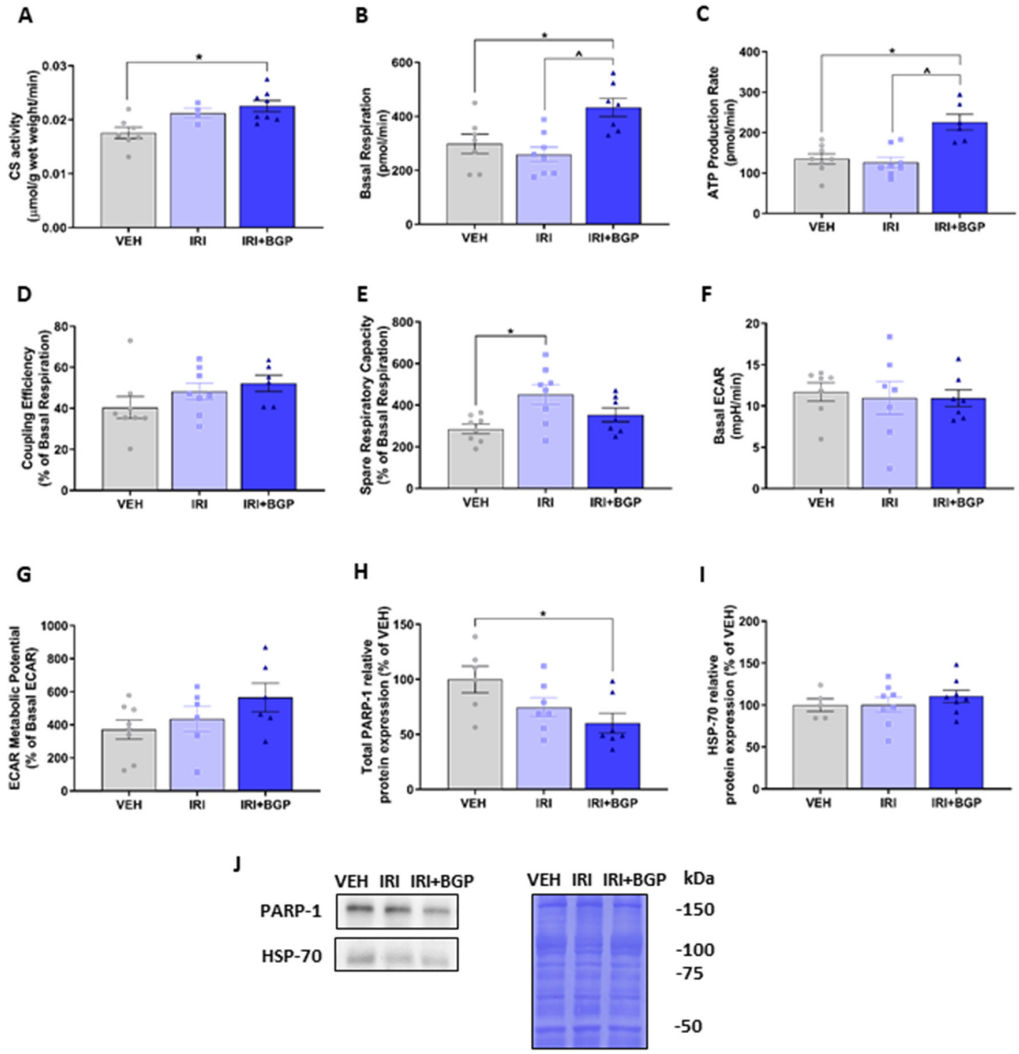

Figure 6. The effect of irinotecan (IRI) and IRI with BGP-15 (IRI+BGP) treatment on skeletal muscle mitochondrial metabolic phenotyping. (**A**) Tibialis anterior (TA) homogenate was analyzed for citrate synthase (CS) activity as a marker of mitochondrial density. Isolated flexor digitorum brevis (FDB) fibers were utilized for mitochondrial metabolic analyses with oxidative respiration indices, i.e., (**B**) basal respiration, (**C**) adenosine triphosphate (ATP) production rate, (**D**) coupling efficiency, (**E**) spare respiratory capacity, as well as glycolytic respiration indices, i.e., (**F**) basal extracellular acidification rate (ECAR) and (**G**) ECAR metabolic potential, measured. Furthermore, Western blotting experiments were undertaken and TA homogenate was probed for (**H**) total poly-(ADP-ribose) polymerase-1 (PARP-1) and (**I**) heat shock protein-70 (HSP-70)—these data are expressed as a relative percentage of the vehicle (VEH) control group. (**J**) Western blot representative images are displayed alongside a Coomassie Blue representative image, which was used as the protein loading control. * = $p < 0.05$ compare to VEH; ˆ = $p < 0.05$ compared to IRI; n = 4–8 for CS activity and n = 5–8 for metabolic phenotyping and Western blotting.

To examine whether the mechanisms underlying the enhanced mitochondrial function from IRI+BGP treatment adhered to the previously confirmed targets of BGP-15 (i.e., HSP-70 co-induction and PARP-1 inhibition) [26,37], we next undertook Western blotting in TA homogenates. We showed that IRI+BGP treatment reduced total PARP-1 protein expression ($p < 0.05$; Figure 6H,J) but did not alter HSP-70 protein expression ($p > 0.05$; Figure 6I,J). IRI treatment alone did not significantly affect either target ($p > 0.05$; Figure 6H–J). Full-length Western blots, densitometry data and total protein data are provided in Figures S3 and S4 and Table S1.

2.7. Assessment of Redox Balance and Mitochondrial Content Signaling Pathways in Skeletal Muscle

Since skeletal muscle dysfunction caused by chemotherapeutic agents has previously been associated with oxidative stress potentiated through increased reactive oxygen species (ROS) production [59], we wanted to investigate molecular markers of redox balance and mitochondrial content in skeletal muscle. There was no effect of IRI or IRI+BGP treatment on the protein expression of 4-Hydroxynoneal (4-HNE), a marker of lipid peroxidation, which is a key hallmark of oxidative stress [60] ($p > 0.05$; Figure 7A,L); nuclear factor erythroid 2 (NFE2)-related factor 2 (Nrf-2), the master transcriptional regulator of the anti-oxidant response to cellular stress ($p > 0.05$; Figure 7B,L); or the downstream antioxidant targets of Nrf-2, hemeoxygenase-1 (HO-1) and superoxide dismutase-1 (SOD1) ($p > 0.05$; Figure 7C,D,L). Similarly, there was no significant difference in the protein expression of the negative regulator of Nrf-2, Kelch-like ECH-associated protein 1 (Keap-1), from IRI or IRI+BGP treatment ($p > 0.05$; Figure 7E,L). Interestingly, the protein expression of DJ-1, a highly conserved protein that can positively regulate Nrf-2 activity [61], was significantly increased by IRI+BGP treatment compared to VEH ($p < 0.05$; Figure 7F,L), whilst there was a modest trend for IRI treatment to increase DJ-1 protein expression relative to VEH ($p = 0.09$; Figure 7F,L).These data were further supported by normal expression of mitogen-activated protein kinase (MAPK) signaling, i.e., p38, ERK 1/2 and JNK ($p > 0.05$; Figure 7G–I,L), which is sensitive to acute increases in oxidative stress [62], between treatment groups. However, there was a modest trend for IRI+BGP treatment to increase p38 phosphorylation relative to VEH ($p = 0.09$; Figure 7G,L). Additionally, there were no significant differences between treatment groups in the protein expression of molecular markers of mitochondrial remodeling (i.e., cytochrome c (Cyt-c); $p > 0.05$; Figure 7J,L) and content (i.e., commonly probed protein subunits of the mitochondrial Complexes I–V; $p > 0.05$; Figure 7K,L). Full-length Western blots, densitometry data and total protein data are provided in Figures S1, S3 and S4 and Table S1.

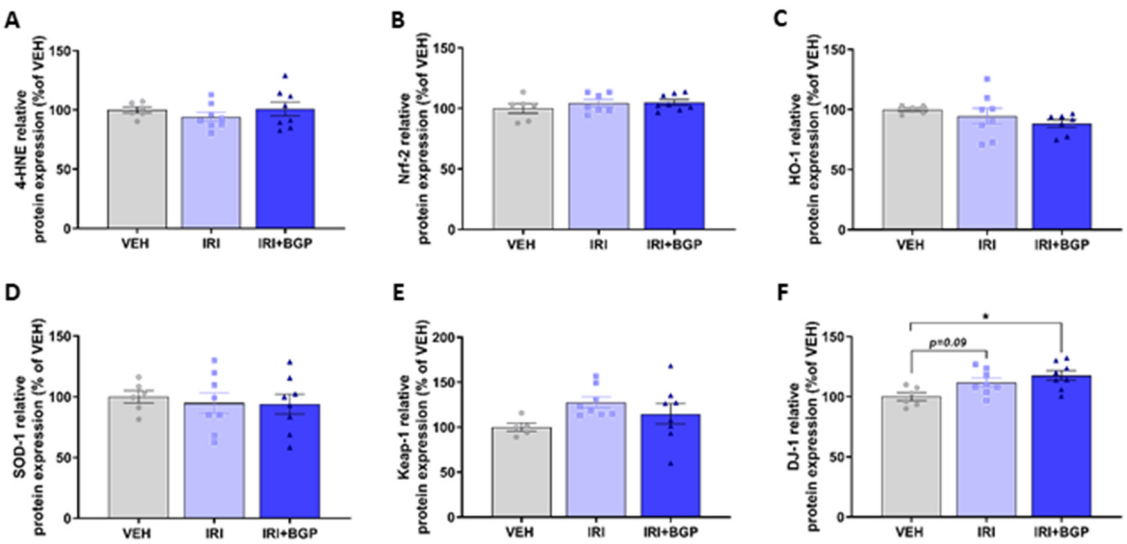

Figure 7. *Cont.*

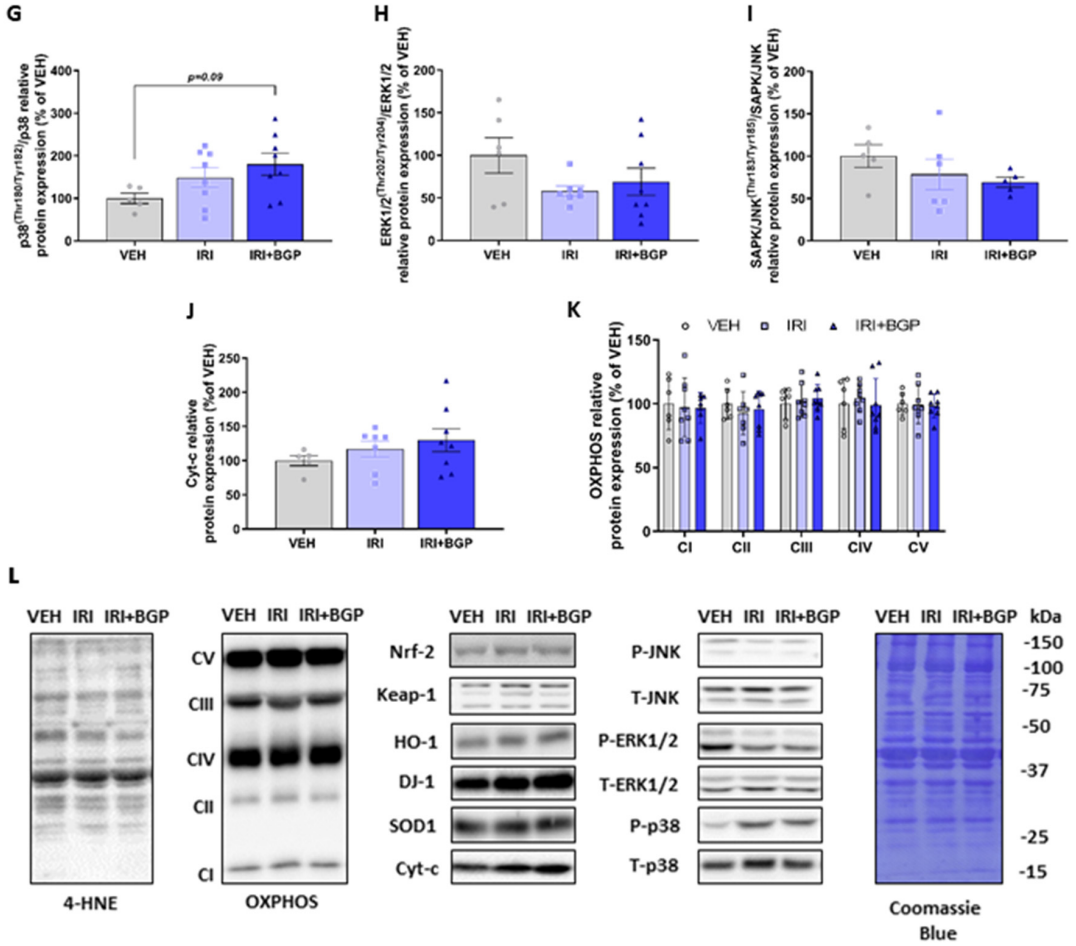

Figure 7. The effect of irinotecan (IRI) and IRI with BGP-15 (IRI+BGP) treatment on oxidative and mitochondrial stress signaling pathways. Western blotting experiments were undertaken and tibialis anterior (TA) homogenate was probed for oxidative stress signaling markers; (**A**) 4-Hydroxynoneal (4-HNE), (**B**) nuclear factor erythroid 2 (NFE2)-related factor 2 (Nrf-2), (**C**) hemeoxygenase-1 (HO-1), (**D**) superoxide dismutase-1 (SOD1), (**E**) Kelch-like ECH-associated protein 1 (Keap-1), (**F**) protein deglycase (DJ-1), and mitogen-activated protein kinases (MAPKs)—which are sensitive to oxidative stress—(**G**) p38 (Thr^{180}/Tyr^{182}) relative to total p38, (**H**) extracellular signal-regulated protein kinase (ERK1/2; $Thr^{202}/Tyr^{204)}$ relative to total ERK1/2 and (**I**) c-Jun N-terminal kinase (JNK;Thr^{183}/Tyr^{185}) relative to total JNK are displayed. Additionally, mitochondrial stress and content markers (**J**) Cyt-c and (**K**) the OXPHOS cocktail, i.e., Complex V (CV) subunit ATP5A, Complex IV (CIV) subunit MTCO1, Complex III (CIII) subunit UQCRC, Complex II (CII) subunit SDHB and Complex I (CI) subunit NDUFB8, were probed for. These data are expressed as a relative percentage of the vehicle (VEH) control group. (**L**) Western blot representative images are displayed alongside a Coomassie Blue representative image, which was used as the protein loading control. * = $p < 0.05$ compare to VEH; $n = 5–8$.

3. Discussion

This is the first study to examine the effect of IRI treatment and BGP-15 adjuvant therapy on skeletal muscle mass and function. Our novel findings show that BGP-15 adjuvant therapy mitigates the IRI-induced wasting phenotype, which is underscored by a protective maintenance of skeletal muscle mass and fiber size. Fascinatingly, we observed a paradoxical finding where BGP-15 adjuvant therapy exacerbated the IRI-induced reduction in protein synthesis independent of mTORC1 signaling but ameliorated the IRI-induced skeletal muscle dysfunction, whilst also potentiating oxidative metabolism, apparently through suppression of PARP-1. While we showed indications of cytoskeletal and/or ECM

remodeling (through changes to the dystrophin-associated protein complex (DAPC) and the MMP-9 to MMP-2 ratio) driven by both IRI and the addition of BGP-15, it is difficult to conclude whether these changes are short-lived and ultimately beneficial or whether they detrimentally progress a muscular dystrophy-like phenotype. Indeed, IRI+BGP-15 muscles were more prone to tearing due to the shear stress associated with ex vivo fatiguing contraction, although there was no evidence of histopathology.

3.1. Skeletal Muscle Mass versus Protein Synthesis: The Paradoxical Effect of BGP-15 Adjuvant Therapy

We have demonstrated in this study that IRI induced a cachectic phenotype characterized by skeletal muscle wasting, i.e., diminished crude TA mass and fiber CSA, mirroring previous data where IRI administered as part of the FOLFIRI chemotherapy combination regimen contributed to the induction of cachexia [11,63]. One of the underlying mechanisms of skeletal muscle mass loss in the cachectic phenotype has been proposed to be impaired protein synthesis rates, which was first demonstrated by Emery et al. [64] in cachectic cancer patients. More recently, in the absence of cancer, chemotherapeutic agents such as doxorubicin have been shown to reduce skeletal muscle protein synthesis rates independent of key mTORC1 and eIF2a regulatory signaling [65,66]. Consistent with these data, we found that IRI-induced muscle wasting was independent of reduced protein synthesis through mTORC1 inhibition. This suggests that IRI treatment alone, or in a combination regimen, can significantly impact skeletal muscle mass, placing IRI amongst doxorubicin and cisplatin as chemotherapeutic agents with skeletal muscle toxicity profiles [9]. Surprisingly, however, we found that BGP-15 adjuvant therapy further reduced basal protein synthesis rates. One question that arises from these data is: how did BGP-15 adjuvant therapy attenuate crude muscle and fiber wasting/atrophy when protein synthesis was even lower than with IRI treatment alone? While this question remains herein unanswered, if muscle mass is broadly determined by the balance between protein synthesis and degradation rates, our data suggest that BGP-15 adjuvant therapy likely decreased the rate of protein degradation to an even larger extent than the reduction in protein synthesis, leading to a net increase in protein accretion. BGP-15 has previously been shown to co-induce HSP-70 [26,29,67], and we postulate that the activation of HSP-70 may be a key factor in regulating (i.e., lowering) protein degradation [43]. For example, the overexpression of HSP-70 has been shown to partially mitigate the hindlimb unloading-induced escalation of proteolytic activity [68]. Unfortunately, we were unable to detect the co-induction of HSP-70 by BGP-15 adjuvant therapy. In a C2C12 muscle cell culture, we have observed that HSP-70 expression is significantly elevated at 30 min following treatment with 1mM BGP-15 (administered with chemotherapeutic agent, 5-fluorouracil), reaching a peak at 1 h and subsiding by 2 h (D. Campelj [69]). Our observations are consistent with others describing BGP-15-mediated HSP-70 induction < 24 h after treatment [26,29,67]. Thus, HSP-70 induction by BGP-15 is acute. transient and, therefore, undetectable in our study as we harvested muscles 3 days post the final treatment. A recent study by Salah et al. [28] illustrated that a 10-day treatment course of daily, high-dose (40 mg/kg) BGP-15 could rescue a range of proteolytic post-translational modifications induced by ventilation-induced diaphragm dysfunction. In contrast, our data show no effect of BGP-15 adjuvant therapy on crude static markers of protein degradation (i.e., the protein expression of atrogin-1, MuRF1 and total ubiquitinated proteins) at the end of the treatment period. However, we cannot rule out decreased proteasomal and/or lysosomal activity, despite no change in the steady state levels of these markers, or that changes in the markers may have occurred at an earlier time point. Clearly, more studies are now required to explore this fascinating phenomenon further.

3.2. The Relationship between Protein Synthesis and Cytoskeletal Re-Modelling: A Potential Role for Mechanotransduction?

Another question that arises from our data is: what was/were the mTORC1-independent mechanism(s) responsible for the IRI- and BGP-15-mediated reduction in basal protein synthesis rates? With regards to IRI treatment, one potential answer may lie in the suppression of Akt phosphorylation at the Ser^{473} residue. Akt^{Ser473} phosphorylation is indicative of mTORC2 activity [48]; mTORC2 has

recently emerged as a regulator of plasma membrane homeostasis [70], and specific to skeletal muscle, sarcolemmal integrity is considered to be sensitive to Akt^{Ser473} phosphorylation [71]. Furthermore, mTORC2 activity has recently been implicated in mechanical overload-induced increases in protein synthesis and muscle growth (for a review, see [72]). Considering these two points, we postulate that the reduction in protein synthesis induced by IRI treatment and exacerbated by BGP-15 adjuvant therapy may be reflective of compromised mechanotransduction underlined by reduced Akt^{Ser473} phosphorylation and compromised cytoskeletal stability, although the timing of the cascade of events is unknown. Indeed, we demonstrated a decrease in dystrophin expression from IRI treatment (both alone and in combination with BGP-15) alongside a decrease in β-dystroglycan from BGP-15 adjuvant therapy, imitating the step-like reduction observed in protein synthesis rates. Altered expression of cytoskeletal structural proteins in skeletal muscle of chemotherapy-treated mice has previously been demonstrated via transcriptomic [73] and proteomic [22] screening; however, follow-up analysis has not been conducted. Since it has long been speculated that skeletal muscle protein synthesis regulation is tension-dependent [74], better understanding of the underlying mechanistic control of the mechanotransduction signaling pathways that influence tension is of significant interest [72,75–80]. Importantly, our data are the first to identify the DAPC in the complex interplay between mTORC2 signaling, mechanotransduction and protein synthesis.

3.3. The Functional Consequence of Cytoskeletal Remodeling by IRI Treatment and BGP-15 Adjuvant Therapy

In this study, we demonstrate that IRI administration reduces skeletal muscle force production in a muscle/fiber-type-independent manner, which is consistent with the dysfunction induced from other chemotherapeutic agents [11,81,82]. A contributing factor to IRI-induced skeletal muscle dysfunction may be the reduction in dystrophin protein expression, a key member of the DAPC, which acts as an anchoring protein supporting the stability of sarcomeric and sarcolemmal proteins. Swiderski et al. [83] highlight several amino acid residues in the cysteine-rich and C-terminus domains of the dystrophin protein that are susceptible to post-translational modifications, including phosphorylation by multiple kinases, such as Ca^{2+}/calmodulin-dependent kinase, which can impact skeletal muscle function [84]. Indeed, the loss of dystrophin has been associated with dysregulated Ca^{2+} signaling [85], which has also been observed as a key perturbation underlying cisplatin- and doxorubicin-induced skeletal muscle dysfunction [86,87]. Thus, it would be of interest in future investigations to determine the post-translational modifications to the dystrophin protein when challenged by multiple chemotherapeutic agents, including IRI. Since BGP-15 adjuvant therapy preserved skeletal muscle contractile function, which has previously been shown in other myopathic models [27,31,32,67], the reduction in both dystrophin and β-dystroglycan expression appears not to have the same impact on muscle function as it does in muscular dystrophy models. That being said, an interesting finding of our study was that IRI+BGP-15-treated EDL muscles had an increased susceptibility to tear from the shear stress of repeated contractions during our ex vivo fatigue protocol. This may be due, in part, to the increased force production and the combined reduction in dystrophin and β-dystroglycan expression in the IRI+BGP-15-treated muscles compared to the IRI-only-treated muscles. Indeed, protein constituents of the DAPC, such as dystrophin and β-dystroglycan, play an integral role in preserving skeletal muscle stiffness and elasticity [88], assisting in the maintenance of cytoskeletal integrity during muscle contraction [89]. In addition, we demonstrated that BGP-15 adjuvant therapy increased the MMP-9/MMP-2 activity ratio, which is proposed to play a role in remodeling of the ECM and cytoskeletal structural and contractile proteins in skeletal [56] and cardiac muscle [55]. While the order of remodeling events cannot be ascertained from our data, these events combined might account for proneness to musculotendinous rupture in IRI+BGP-15-treated muscles, Future studies are required to elucidate the muscle- and ECM-specific remodeling that is induced by IRI and BGP-15.

3.4. BGP-15 Adjuvant Therapy Potentiates Skeletal Muscle Oxidative Metabolism through PARP-1 Inhibition

In this study, BGP-15 adjuvant therapy enhanced skeletal muscle oxidative metabolism, highlighted by the increase in basal oxygen consumption rate, ATP production and CS activity. The pro-oxidative metabolic effect of BGP-15 adjuvant therapy appears to be driven via the inhibition of PARP-1 and perhaps even as a latent effect of the transient co-induction of HSP-70 [26,29,67] in response to IRI treatment. PARP-1 inhibition exerts cellular protection in environments with excess PARP-1 activity, which is considered to promote destabilization of the mitochondrial membranes, leading to the impairment of mitochondrial function [90]. While we saw no evidence of increased PARP-1 or reduced mitochondrial function elicited by IRI treatment, PARP-1 inhibition by BGP-15 still inferred pro-mitochondrial activity. This could be due to the timepoint at which we harvested tissue (i.e., 3 days post final IRI injection), which may have preceded the acute mitochondrial perturbations elicited by IRI, as previously published by us in C2C12 myoblasts and myotubes [58]. Furthermore, the FOLFIRI regimen, of which IRI is a constituent, has been previously shown to induce acute skeletal muscle mitochondrial perturbations, highlighted by impaired mitochondrial biogenesis and enhanced pro-oxidant signaling [11]. This suggests that the metronomic delivery of IRI potentially instigates mitohormesis in skeletal muscle, where, initially, there is an acute metabolic challenge exerted upon mitochondria from IRI administration; however, with repeat insults from IRI, mitochondria adapt and become more adept at handling the prolonged metabolic challenge [91]. In this scenario, PARP-1 inhibition would transiently enhance the mitochondrial adaptations to the metabolic challenges by protecting against nicotinamide adenine dinucleotide (NAD) depletion and, through the promotion of DJ-1, aiding metabolic re-programming [92]. This hypothesis is based on the assumption that these mitohormetic protective adaptations include increasing PARP activity, for example, PARylation, which is activated during mitochondrial DNA repair and integrity maintenance [93] at the expense of depleting NAD and impairing mitochondrial function.

3.5. Limitations

There were some limitations to our research that are worthy of mention. In the first instance, we conducted our study using 6-week-old mice and treated them over 2 weeks, up to 8 weeks of age. Mice are considered sexually mature at 8 weeks of age; hence, we treated our mice during the pubertal developmental period but measured the impact of treatment at sexual maturity. Cachexia is well documented in pediatric cancer patients and involves both tumor- and chemotherapy-mediated pathogenesis [94]. Notably, however, pediatric cancer cachexia differs from adult cachexia in that it predominantly manifests as stunted growth [95] which, along with significant skeletal muscle dysfunction, can persist throughout the lifespan [96]. While the cachexia observed in our IRI-treated mice may have included an element of growth repression, we also observed loss of body, lean and fat mass from the pre- to post-treatment period, which is consistent with the accepted definition of cachexia [1]. Secondly, our experimental design lacked a BGP-15-only cohort. This would not have been so problematic had BGP-15 not induced further inhibition of protein synthesis or expression of the cytoskeletal mechanotransduction proteins, dystrophin and β-dystroglycan on top of that already elicited by IRI. That being said, we postulate that these effects of BGP-15 are specific to its activity in an IRI-induced cellular stress environment since induction of HSP-72 and repression of PARP-1 have been previously associated with enhanced protein synthesis and skeletal muscle accretion [97].

4. Materials and Methods

4.1. Animals

4.1.1. Ethical Approval

All experimental procedures were approved by the Victoria University Animal Ethics Committee (AEETH15/006) and conformed to the Australian Code of Practice for the Care and Use of Animals for Scientific Purposes.

4.1.2. Experimental Design and Treatments

Male Balb/c mice were acquired from the Animal Resource Centre (ARC, Western Australia) and randomly allocated to treatment groups (n = 8) upon arrival. Mice were housed on a 12-h light/dark cycle with ad libitum access to food (i.e., standard mice chow) and water supply throughout the experiments. Mice were administered either vehicle (VEH; 0.1% dimethyl sulfoxide (DMSO) in sterile water), irinotecan (IRI; 30 mg/kg (Sigma Aldrich, Sydney, Australia) dissolved in 0.1% DMSO) or BGP-15 adjuvant therapy with IRI (IRI+BGP; 15 mg/kg (BGP-15 donated by N-gene Research Laboratories, New York, NY, USA) dissolved in 0.1% DMSO). Treatments were administered via intraperitoneal injection six times over a fifteen-day period (i.e., on days 1, 3 5, 8, 10 and 12). The cumulative dose of IRI administered is equivalent to the 180 mg/m^2 cumulative dose utilized in standard clinical regimens [98], as previously described by us [99], while the dose of BGP-15 is equivalent to that previously used by our group to protect against chemotherapy-induced skeletal myopathy [36]. Animals were weighed prior to the commencement of treatment (PRE) on each day of treatment and at the experimental endpoint. Food and water consumption were monitored throughout the duration of the treatment protocol.

4.2. Body Composition

Echo magnetic resonance imaging (echoMRI) was utilized to assess the effect of IRI treatment and BGP-15 adjuvant therapy on body composition indices of lean and fat mass. Live mice were placed into an echoMRI body composition analyzer (EMR-150, Echo Medical Systems, Houston, TX, USA) on day 1 (Pre) and day 15 (Post) of the treatment protocol, as previously described [8]. Lean and fat mass was quantified via triplicate scans spaced 30 s apart and reported as the mean of these triplicate scans.

4.3. Physical Activity Assessment

To evaluate the impact of IRI treatment and BGP-15 adjuvant therapy on the physical activity of mice, animals were individually housed for 24 h immediately prior to treatment commencement and the experimental endpoint in Promethion Metabolic cages (Sable Systems, Las Vegas, NV, USA). Cages allowed free access to food, water and a running wheel. Real-time voluntary activity associated with wheel running and general cage-based ambulatory activity was evaluated as described by us previously [8,36]. Data presented pertain to the total 24-h post-treatment period.

4.4. Surgery

At the conclusion of the treatment regimen and following the final echoMRI scan, mice were deeply anesthetized via isoflurane inhalation and administered an intraperitoneal injection of 0.040 μmol/g puromycin (Millipore, Sydney, Australia) dissolved in 100 μL of 0.9% saline to measure protein synthesis [45]. Thereafter, non-recovery surgery was performed. Muscles of interest were surgically excised for ex vivo analysis in the following order: (1) left and right flexor digitorum brevis (FDB) muscles for the measurement of mitochondrial functional parameters; (2) right extensor digitorum longus (EDL) and soleus (SOL) muscles for the assessment of contractile properties. Following this, at exactly 30 min after the injection of puromycin: (3) right tibialis anterior (TA) muscles were harvested and immediately snap-frozen for Western blotting experiments; and (4) the left TA was weighed and

prepared for histological assessment prior to snap-freezing. The remaining tissues were then harvested (i.e., the left EDL and SOL and the heart), weighed and snap-frozen.

4.5. Ex Vivo Skeletal Muscle Contractile Function

Ex vivo evaluation of skeletal muscle contractile properties was performed as previously described by us [100–102], using the predominantly fast-twitch fiber EDL and the predominately slow-twitch fiber SOL muscles. These muscles were exposed and loops were tied at both tendons with 4.0 surgical silk thread before being dissected from the hindlimb and placed into individual organ baths of a Myodynamics Muscle Strip Myograph System (DMT-Asia Pacific, Bella Vista, Australia). Each organ bath was filled with Krebs solution (NaCl 118 mM, $MgSO_4{\cdot}7H_2O$ 1 mM, KCl 4.75 mM, Na_2HPO 1 mM, $CaCl_2$ 2.5 mM, $NaHCO_3$ 24 mM and glucose 11 mM; pH 7.4) infused with carbogen (5% CO_2 in O_2) and maintained at a temperature of 30 °C. The proximal end of the muscle was tied to the force transducer, while the distal end was tied to a micromanipulator, with stimulating electrodes flanking the muscle belly. Data were collected and analyzed using LabChart Pro version 8.0 software (ADInstruments, Bella Vista, Australia). Initially, the optimal length (L_o) of each muscle was established through the delivery of sequential twitch contractions, whilst incrementally stretching each muscle, until the point where the greatest force that was produced by the muscle was found and the length of the muscle at this point was measured with calipers. Once L_o was determined, a force–frequency protocol was performed utilizing supramaximal square wave 0.2-ms pulses at an incremental range of frequencies (i.e., 10, 20, 30, 40, 50, 60 80, 100, 120 and 150 Hz), with a 3-min rest period in between each stimulation to prevent fatigue. The training duration of pulses was 350 and 500 ms for the EDL and SOL muscles, respectively, due to their differing muscle fiber characteristics. The muscles were then stimulated with three single-twitch contractions for the analysis of basic contractile properties, i.e., peak twitch force (Pt), time to peak (TTP), half relaxation time ($\frac{1}{2}$ RT) and maximum rate of force development (df/dt). To investigate fatigue susceptibility, muscles next underwent a three-minute fatigue protocol, where EDL muscles were tetanically stimulated as above at 100 Hz, while SOL muscles were tetanically stimulated every two seconds at 80 Hz to elicit a comparable level of fatigue. Absolute force (P_o) was considered as the force produced from the first tetanic response stimulated during the fatigue protocol. Specific force (sP_o) was assessed as a normalized force relative to the physiological cross-sectional area (CSA) which takes into consideration three key variables of force production (i.e., muscle mass, optimal length and muscle density (~1.06 mg mm^{-3})), and was calculated using the equation $sP_o = P_o \times$ (muscle mass/1.06 $\times L_o \times$ fiber length:muscle length ratio), as previously described [103].

4.6. Mitochondrial Respiratory Phenotyping

4.6.1. Flexor Digitorum Brevis Muscle Fiber Isolation

In order to conduct mitochondrial metabolic profiling, FDB muscles were harvested from both feet and fibers were isolated using a protocol established by Schuh et al. [104], as performed by us previously [36,102,105]. FDB muscles were incubated in 1 mL of pre-warmed dissociation medium (Dulbecco's modified Eagle medium (DMEM), Gibco 10566016; 2% FBS, Bovogen Biologicals; 4 mg/mL collagenase A, Roche 10103586001; 50 µg/mL gentamycin, Sigma Aldrich, Sydney, Australia, G1397) for 1 h and 45 min (37 °C, 5% CO_2). Following this dissociation period, FDB bundles were placed into ~1.5 mL of incubation medium (DMEM, high glucose, GlutaMAX™ supplement, Gibco/Thermo Fisher Scientific, Scoresby, Australia 10566016; 2% FBS, Bovogen Biologicals; 50 µg/mL gentamycin, Sigma Aldrich G1397) and triturated with pipette tips of decreasing bore size to yield single fibers.

4.6.2. Seahorse Microplate Preparation

To facilitate fiber adherence to Seahorse XF24 cell culture V7 microplates (Seahorse Bioscience, Mulgrave., Australia), wells were coated with 5 µL of extracellular matrix (Sigma Aldrich, Sydney,

AustraliaE1270) diluted in DMEM (1:1). Then, 75 µL of isolated FDB fibers was aliquoted into coated wells and confluency was determined using light microscopy. A minimum of ~60% confluency, i.e., the estimated percentage of the well bottom covered by isolated FDB fibers, was deemed optimal. If a well did not meet this requirement, an additional 50 µL aliquot of fibers was dispensed into wells.

4.6.3. Mitochondrial Metabolic Profiling Using the XF24 Extracellular Flux Analyzer

Mitochondrial metabolic profiling was performed using extracellular flux analysis (Seahorse Bioscience/Agilent, Mulgrave, Australia) as described by us previously [105]. Basal, phosphorylating, maximal and non-mitochondrial respiration was measured initially through the sequential addition of 2 µg/mL oligomycin, 400 nm carbonyl cyanide-p-trifluoromethoxyphenylhydrazone (FCCP) with 10 mM sodium pyruvate, and 1 µM antimycin A, respectively. The extracellular acidification rate (ECAR) was concomitantly measured as an indicator of anaerobic glycolysis.

4.7. Skeletal Muscle Histology

All histological experiments were completed as previously described by us [36,105]. To determine whether IRI had atrophic effects on skeletal muscle and, subsequently, whether BGP-15 adjuvant therapy could rescue any atrophy, we histologically assessed TA muscles which were cryopreserved in optimal cutting temperature compound (Sakura Finetek, Maumee, OH, USA). TAs were sectioned (10 µm, −20°C, Leica CM1950, Leica Biosystems, Mount Waverley, Australia) and mounted onto glass slides and then stained with hematoxylin and eosin (H&E) to evaluate muscle fiber size through CSA. All slides were imaged on a Zeiss Axio Imager Z2 microscope (Carl Zeiss MicroImaging GmbH, Oberkochen, Germany) at 20× magnification and analyzed as described previously [36,105] using ImageJ software (NIH, Bethesda, MD, USA).

4.8. Western Blot Analyses

Western blotting was utilized to explore the effect of IRI treatment and BGP-15 adjuvant therapy on molecular signaling pathways surrounding protein synthesis and degradation, cell stress and membrane structure. All Western blotting protocols were completed as previously described by us [45,105]. Frozen TA muscles were homogenized using an Omni Tissue Homogenizer (TH220, Omni International, Kennesaw, GA, USA) for 20 s in ice-cold Western immunoprecipitation kinase (WIK) buffer (40 mM Tris, pH 7.5; 1 mM ethylenediaminetetraacetic acid (EDTA); 5 mM etheylen glycol-bis(β-aminoethyl ether)-N, N, N′, N′-tetraacetic acid (EGTA); 0.5% TritonX-100; 25 mM β-glycerophosphate; 25 mM NaF; 1 mM Na3VO4; 10 g/mL leupeptin; and 1 mM phenylmethylsulfonyl fluoride (PMSF). Muscle homogenate was centrifuged at 3500 rpm for 5 min at 4 °C, before the pellet was resuspended and the muscle homogenate was frozen for further analysis. Protein concentrations were determined using a sample assay kit (Bio-Rad Laboratories, Hercules, CA, USA) to ensure equal loading on the gels. Samples were prepared with equivalent amounts of protein in either 2× sodium dodecyl sulfate (SDS) sample buffer (20% (v/v) glycerol; 100 mM Tris-Base, pH 6.8; 4% (w/v) SDS; 0.017% (w/v) bromophenol blue; 0.25 M dithiothreitol (DTT)) or 4× Laemmli buffer (Bio-Rad Laboratories, Hercules, CA, USA) reduced in 50 mM DTT, heated for 5 min at 95 °C and subjected to electrophoretic separation on 7.5–12% SDS-acrylamide gels. Antibodies that required exceptions to this protocol include Total oxidative phosphorylation (OXPHOS) cocktail (1:1000; ab110413; Abcam, Cambridge, UK), where samples were heated for 5 min at 40 °C, and anti-α-sarcoglycan (1:200; IVD3(1)A9; Developmental Studies Hybridoma Bank (DSHB)), which was probed in samples under non-denaturing and non-reducing conditions, as per supplier recommendations. Following electrophoretic separation, proteins were transferred to a polyvinylidene fluoride membrane, blocked with 5% not-fat milk powder in Tris-buffered saline containing 0.1% Tween 20 (TBST) for 1 h followed by an overnight incubation at 4 °C with primary antibody dissolved in TBST containing either 1% BSA or 3% non-fat milk powder. The following primary antibodies were used: anti-phospho 4E-BP1$^{(Thr37/46)}$ (1:1000; #2855; Cell Signalling Technology (CST, Danvers, MA, USA)), anti-4E-BP1 (1:1000; #9452; CST), anti-4-HNE (1:1000; ab46545; Abcam,

Cambridge, UK), anti-phospho Akt^{Ser473} (1:2000; #4060; CST), anti-phospho Akt^{Thr308} (1:2000; #13038; CST), anti-Akt (1:1000; #4691; CST), anti-Atrogin-1 (1:1000; AP2041; ECM Biosciences, Versailles, KY, USA), anti-β-Dystroglycan (1:500; MANDAG2 (7D11); DSHB), anti-Cytochrome C (1:2000; #11940, CST), anti-δ-Sarcoglycan (1:1000; ab137101; Abcam), anti-Desmin (1:1000; #5332; CST), anti-DJ-1 (1:1000; #5933; 1:1000), anti-Dystrophin (1:200; ab15277; Abcam), anti-phospho eIF2a^{Ser51} (1:1000; #3398; CST), anti-eIF2a (1:1000; #5324; CST), anti-phospho ERK1/2$^{(Thr202/Tyr204)}$ (1:1000; #9101; CST), anti-ERK1/2 (1:1000; #9102; CST), anti-HO-1 (1:1000; ADI-SPA-896; Enzo Life Sciences, Farmigdale, NY, USA), anti-HSP-70 (1:1000; ADI-SPA-812; Enzo Life Sciences), anti-phospho JNK$^{(Thr183/Tyr185)}$ (1:1000; #4668; CST), anti-JNK (1:1000; #9252; CST), anti-Keap-1 (1:1000; #8047; CST), anti-Laminin (1:2000; L9393; Sigma-Aldrich, Sydney, Australia), anti-MMP-2 (1:1000; ab92536; Abcam), anti-MMP-9 (1:300; AF909; R&D Systems), anti-MuRF-1 (1:200; AF5366; R&D Systems, Minneapolis, MN, USA); anti-NRF-2 (1:1000; #12721, CST), anti-phospho p38$^{(Thr180/Tyr182)}$ (1:1000; #4511; CST), anti-p38 (1:1000; #9212; CST), anti-phospho p70s6k$^{(Thr389)}$ (1:1000; #9234; CST), anti-p70s6k (1:1000; #2708; CST), anti-PARP-1 (1:1000; 9542, CST), anti-Puromycin (1:5000; MABE343; Merck Millipore, Bayswater, Australia), anti-Rac1 (1:500; #05-389; Merck Millipore), anti-SOD1 (1:3000; ADI-SOD-101; Enzo Life Sciences) and anti-Ubiquitin (1:3000; sc8017; Santa Cruz, Dalla, TX, USA). After overnight incubation, membranes were washed 3 separate times for 10 min each in TBST and then probed with a horseradish peroxidase-conjugated secondary antibody (1:5,000; anti-rabbit IgG, 1:5,000; anti-goat IgG or 1:20,000; anti-mouse IgG, Vector Laboratories, Burlingame, CA, USA) in 5% not-fat milk powder in TBST for 1 h at room temperature. Membranes that were probed with anti-Puromycin were incubated in anti-mouse IgG Fc 2a-specific horseradish peroxidase-conjugated secondary antibody (1:50,000; Jackson ImmunoResearch Laboratories Inc., West Grove, PA, USA), as previously described [45]. Following another set of 3 separate 10-min washes in TBST, the blots were developed with a DARQ CCD camera mounted to a Fusion FX imaging system (Vilber Lourmat, Eberhardzell, Germany) using ECL Prime reagent (Amersham, Piscataway, NJ, USA). Once images were captured, the membranes were stained with Coomassie Blue and then normalized to total protein. Densitometric measurements were carried out using FusionCAPTAdvance software (Vilber Lourmat, Eberhardzell, Germany).

4.9. Citrate Synthase Activity

Citrate Synthase (CS) activity was measured as a marker of mitochondrial density and/or anaplerosis. Homogenized TA muscles in WIK buffer (as described above) were added to the reagent cocktail (100 mM Tris Buffer, 1 mM 5,5′-Dithiobis(2-nitrobenzoic acid) (DTNB) and 3 mM Acetyl CoA), and to initiate the reaction, oxaloacetate (10 mM) was added just prior to measuring CS activity spectrophotometrically (412 nm, 25 °C, 5 min). CS activity was calculated using the extinction coefficient of 13.6 [106] and expressed relative to muscle wet weight.

4.10. Zymography Analyses for Gelatinase Activity

Zymography was performed via gelatin-infused SDS-PAGE to detect the gelatinolytic activity of matrix metalloproteinases (MMPs), specifically the isoforms MMP-2 and MMP-9, based on a previously established protocol [56]. EDL muscles were placed in ice-cold zymography homogenization buffer (50 mM Tris-HCl; 150 mM NaCl; 10 mM $CaCl_2$; pH 7.5) and were homogenized using the Omni Tissue Homogenizer (TH220, Omni International, Kennesaw, GA, USA) for 3 sets at medium speed for 8 s. Muscle homogenate was centrifuged at 3500 rpm for 5 min at 4 °C, before the pellet was resuspended and the muscle homogenate frozen for further analysis. Protein concentrations were determined using an RC DC sample assay kit (Bio-Rad Laboratories, Hercules, CA, USA) to ensure equal loading on the gels. Samples were then prepared in 4X SDS sample buffer (400 mM Tris-HCl, pH 6.8; 4% (w/v) SDS; 20% glycerol (v/v); 0.005% (w/v) bromophenol blue) under non-reducing, non-denaturing conditions, with 100 μg of protein loaded onto 0.75-mm thick 7.5% SDS-acrylamide gels that were co-polymerized with 1% (w/v) gelatin (Sigma, Sydney, Australia). After gel electrophoresis was completed, gels were washed twice for 40 min in denaturing buffer (2.5% (v/v) Triton-X; 50 mM Tris-HCl; 5 mM $CaCl_2$; pH 7.6)

to remove SDS. After this, gels were washed twice for 15 min in renaturing buffer (50 mM Tris-HCl; 5 mM $CaCl_2$; pH 7.6) before being incubated overnight (~18 h) at 37 °C in developing buffer (50 mM Tris-HCl; 150 mM NaCl; 10 mM $CaCl_2$; 1 μM $ZnCL_2$; 0.02% (w/v) NaN_3; pH 7.5). The gels were then stained for 3 h in Coomassie Blue solution (0.05% (w/v) Coomassie Brilliant Blue; 30% (v/v) methanol; 10% (v/v) acetic acid) before being incubated for 3 h in de-stain solution (30% (v/v) methanol; 10% (v/v) acetic acid), allowing the visualization of the digestion of gelatin (i.e., gelatinase activity) against the dark blue background. Gels were imaged using an Epson Perfection V700 Photo Scanner (Epson, Sydney, Australia). Samples were run in duplicate on separate gels, with images semi-quantitatively analyzed using Image J software (NIH, Bethesda, MD, USA), according to a previously established method [107], with the mean area density reported.

4.11. Statistics

Data are presented as mean ± standard error of the mean (SEM). Data were analyzed using GraphPad prism v8 (GraphPad Software, San Diego, CA, USA). A one-way ANOVA with Tukey's post-hoc test was utilized to detect treatment differences for parametric data, while Dunn's multiple comparison test was utilized to analyze non-parametric data, with an α-value of 0.05 considered significant. A two-way repeated measures ANOVA was used to detect differences between treatment and stimulation frequency/time for force–frequency relationships and fatigue susceptibility studies, with Tukey's post-hoc test utilized for multiple comparisons.

5. Conclusions

This study shows, for the first time, that, independent of cancer, IRI treatment diminishes body mass indices, underlined by reduced skeletal muscle mass and, subsequently, contractile function, which were mitigated by the PARP inhibitor BGP-15. The protective effect of BGP-15 adjuvant therapy occurred alongside a paradoxical reduction in protein synthesis rates, likely underlined by aberrant proteostasis; however, this needs to be confirmed. Additionally, IRI treatment and BGP-15 reduced mTORC2 signaling and caused changes to the expression of cytoskeletal mechanotransduction proteins associated with the DAPC in a step-like manner that mirrored the reduction in protein synthesis rates. These data highlight remodeling of the contractile apparatus, cytoskeleton and/or ECM that is induced by IRI and even more so by IRI+BGP-15. It is difficult to conclude from our data whether BGP-15, when teamed with IRI treatment, is beneficial for the skeletal muscular system or not, since on the one hand, BGP-15 mitigated many of the cachectic side-effects of IRI treatment, but on the other hand, it made fast-twitch muscles more prone to tearing, despite rescuing function. Time-course studies should be undertaken to determine whether the down regulation of DAPC constituent proteins evoked by both IRI and IRI+BGP-15 induces a muscular dystrophy-like phenotype in the long term. This aspect should be of significant clinical consideration before instigating the mainstream use of PARP inhibitors in anti-cancer treatment and when prescribing IRI-based chemotherapy regimens to patients, since the maintenance of body and, particularly, skeletal muscle mass improves patient survival and long-term outcomes during cancer treatment.

Supplementary Materials: The following are available online at http://www.mdpi.com/2072-6694/12/12/3810/s1, Figure S1: Full-length Western blot images relating to whole membrane related proteins, Figure S2: Full-length Western blot images relating to the data presented in Figures 3 and 4, Figure S3: Full-length Western blot images relating to the data presented in Figures 6 and 7, Figure S4: Protein expression of antibodies that were probed for levels of phosphorylated and total protein, Table S1: Densitometry summary data from representative Western blot images.

Author Contributions: Conceptualization, E.R. and A.C.P.; methodology, D.G.C., C.A.T., A.H., C.A.G. and E.R.; validation, D.G.C. and C.A.T.; formal analysis, D.G.C. and C.A.T.; investigation, D.G.C. and C.A.T.; resources, A.H., C.A.G. and E.R.; data curation, D.G.C., C.A.T., C.A.G. and E.R.; writing—original draft preparation, D.G.C., C.A.G. and E.R.; writing—review and editing, D.G.C., C.A.T., A.C.P., A.H., C.A.G. and E.R.; supervision, E.R. and C.A.G.; project administration, E.R.; funding acquisition, E.R., A.H. and A.C.P. All authors have read and agreed to the published version of the manuscript.

Funding: This research was funded by program establishment grants from the Institute for Sport, Exercise and Active Living and the Centre for Chronic Disease, Victoria University (now the Institute for Health and Sport, Victoria University).

Acknowledgments: The authors wish to acknowledge the research assistant Nancy Pompeani and the students Ben Butcher and James Sorensen who contributed to preliminary data acquisition in the early stages of this project. We would like to thank N-Gene Research Laboratories (New York, NY, USA) for kindly donating BGP-15. We would also like to acknowledge the Developmental Studies Hybridoma Bank (DSHB) for the use of the β-dystroglycan (MANDAG2(7D11)) and α-sarcoglycan (IVD3(1)A9) antibodies developed by Morris, G.E. (Wolfson Centre for Inherited Neuromuscular Disease, RJAH Orthopaedic Hospital, Oswestry, UK) and Campbell, K.P. (University of Iowa), respectively, which were obtained from the DSHB, created by the National Institute of Child Health and Human Development (NICHD) of the NIH and maintained at The University of Iowa, Department of Biology, Iowa City, IA 52242. We would also like to thank John Price (Victoria University, Victoria, Australia) for in-kind donation of Rac1 antibody.

Conflicts of Interest: E.R. is a consultant to Santhera Pharmaceuticals. The authors declare no conflict of interest.

References

1. Fearon, K.; Strasser, F.; Anker, S.D.; Bosaeus, I.; Bruera, E.; Fainsinger, R.L.; Jatoi, A.; Loprinzi, C.; MacDonald, N.; Mantovani, G.; et al. Definition and classification of cancer cachexia: An international consensus. *Lancet Oncol.* **2011**, *12*, 489–495. [CrossRef]
2. Kalantar-Zadeh, K.; Rhee, C.; Sim, J.J.; Stenvinkel, P.; Anker, S.D.; Kovesdy, C.P. Why cachexia kills: Examining the causality of poor outcomes in wasting conditions. *J. Cachexia Sarcopenia Muscle* **2013**, *4*, 89–94. [CrossRef] [PubMed]
3. Martin, L.; Birdsell, L.; Macdonald, N.; Reiman, T.; Clandinin, M.T.; McCargar, L.J.; Murphy, R.; Ghosh, S.; Sawyer, M.B.; Baracos, V.E. Cancer cachexia in the age of obesity: Skeletal muscle depletion is a powerful prognostic factor, independent of body mass index. *J. Clin. Oncol.* **2013**, *31*, 1539–1547. [CrossRef] [PubMed]
4. Jang, M.K.; Park, C.; Hong, S.; Li, H.; Rhee, E.; Doorenbos, A.Z. Skeletal Muscle Mass Change During Chemotherapy: A Systematic Review and Meta-analysis. *Anticancer Res.* **2020**, *40*, 2409–2418. [CrossRef] [PubMed]
5. Da Rocha, I.M.G.; Marcadenti, A.; de Medeiros, G.O.C.; Bezerra, R.A.; Rego, J.F.M.; Gonzalez, M.C.; Fayh, A.P.T. Is cachexia associated with chemotherapy toxicities in gastrointestinal cancer patients? A prospective study. *J. Cachexia Sarcopenia Muscle* **2019**, *10*, 445–454. [CrossRef] [PubMed]
6. Damrauer, J.S.; Stadler, M.E.; Acharyya, S.; Baldwin, A.S.; Couch, M.E.; Guttridge, D.C. Chemotherapy-induced muscle wasting: Association with NF-κB and cancer cachexia. *Eur. J. Transl. Myol.* **2018**, *28*, 7590. [CrossRef] [PubMed]
7. Sorensen, J.C.; Cheregi, B.D.; Timpani, C.A.; Nurgali, K.; Hayes, A.; Rybalka, E. Mitochondria: Inadvertent targets in chemotherapy-induced skeletal muscle toxicity and wasting? *Cancer Chemother. Pharmacol.* **2016**, *78*, 673–683. [CrossRef]
8. Campelj, D.G.; Debruin, D.A.; Timpani, C.A.; Hayes, A.; Goodman, C.A.; Rybalka, E. Sodium nitrate co-supplementation does not exacerbate low dose metronomic doxorubicin-induced cachexia in healthy mice. *Sci. Rep.* **2020**, *10*, 15044. [CrossRef]
9. Coletti, D. Chemotherapy-induced muscle wasting: An update. *Eur. J. Transl. Myol.* **2018**, *28*, 7587. [CrossRef]
10. Hiensch, A.E.; Bolam, K.A.; Mijwel, S.; Jeneson, J.A.L.; Huitema, A.D.R.; Kranenburg, O.; van der Wall, E.; Rundqvist, H.; Wengstrom, Y.; May, A.M. Doxorubicin-induced skeletal muscle atrophy: Elucidating the underlying molecular pathways. *Acta Physiol.* **2019**, e13400. [CrossRef]
11. Barreto, R.; Waning, D.L.; Gao, H.; Liu, Y.; Zimmers, T.A.; Bonetto, A. Chemotherapy-related cachexia is associated with mitochondrial depletion and the activation of ERK1/2 and p38 MAPKs. *Oncotarget* **2016**, *7*, 43442–43460. [CrossRef] [PubMed]
12. Moreira-Pais, A.; Ferreira, R.; Gil da Costa, R. Platinum-induced muscle wasting in cancer chemotherapy: Mechanisms and potential targets for therapeutic intervention. *Life Sci.* **2018**, *208*, 1–9. [CrossRef] [PubMed]
13. Kurk, S.; Peeters, P.; Stellato, R.; Dorresteijn, B.; de Jong, P.; Jourdan, M.; Creemers, G.J.; Erdkamp, F.; de Jongh, F.; Kint, P.; et al. Skeletal muscle mass loss and dose-limiting toxicities in metastatic colorectal cancer patients. *J. Cachexia Sarcopenia Muscle* **2019**, *10*, 803–813. [CrossRef] [PubMed]

14. Ohe, Y.; Ohashi, Y.; Kubota, K.; Tamura, T.; Nakagawa, K.; Negoro, S.; Nishiwaki, Y.; Saijo, N.; Ariyoshi, Y.; Fukuoka, M. Randomized phase III study of cisplatin plus irinotecan versus carboplatin plus paclitaxel, cisplatin plus gemcitabine, and cisplatin plus vinorelbine for advanced non-small-cell lung cancer: Four-Arm Cooperative Study in Japan. *Ann. Oncol.* **2007**, *18*, 317–323. [CrossRef] [PubMed]
15. Falcone, A.; Ricci, S.; Brunetti, I.; Pfanner, E.; Allegrini, G.; Barbara, C.; Crinò, L.; Benedetti, G.; Evangelista, W.; Fanchini, L. Phase III trial of infusional fluorouracil, leucovorin, oxaliplatin, and irinotecan (FOLFOXIRI) compared with infusional fluorouracil, leucovorin, and irinotecan (FOLFIRI) as first-line treatment for metastatic colorectal cancer: The Gruppo Oncologico Nord Ovest. *J. Clin. Oncol.* **2007**, *25*, 1670–1676.
16. Conroy, T.; Desseigne, F.; Ychou, M.; Bouché, O.; Guimbaud, R.; Bécouarn, Y.; Adenis, A.; Raoul, J.-L.; Gourgou-Bourgade, S.; de la Fouchardière, C. FOLFIRINOX versus gemcitabine for metastatic pancreatic cancer. *N. Engl. J. Med.* **2011**, *364*, 1817–1825. [CrossRef]
17. Mathijssen, R.H.; Verweij, J.; Loos, W.J.; de Bruijn, P.; Nooter, K.; Sparreboom, A. Irinotecan pharmacokinetics-pharmacodynamics: The clinical relevance of prolonged exposure to SN-38. *Br. J. Cancer* **2002**, *87*, 144–150. [CrossRef]
18. De Man, F.M.; Goey, A.K.L.; van Schaik, R.H.N.; Mathijssen, R.H.J.; Bins, S. Individualization of Irinotecan Treatment: A Review of Pharmacokinetics, Pharmacodynamics, and Pharmacogenetics. *Clin. Pharm.* **2018**, *57*, 1229–1254. [CrossRef]
19. Kurita, Y.; Kobayashi, N.; Tokuhisa, M.; Goto, A.; Kubota, K.; Endo, I.; Nakajima, A.; Ichikawa, Y. Sarcopenia is a reliable prognostic factor in patients with advanced pancreatic cancer receiving FOLFIRINOX chemotherapy. *Pancreatology* **2019**, *19*, 127–135. [CrossRef]
20. Barret, M.; Antoun, S.; Dalban, C.; Malka, D.; Mansourbakht, T.; Zaanan, A.; Latko, E.; Taieb, J. Sarcopenia is linked to treatment toxicity in patients with metastatic colorectal cancer. *Nutr. Cancer* **2014**, *66*, 583–589. [CrossRef]
21. Vashi, P.G.; Gorsuch, K.; Wan, L.; Hill, D.; Block, C.; Gupta, D. Sarcopenia supersedes subjective global assessment as a predictor of survival in colorectal cancer. *PLoS ONE* **2019**, *14*, e0218761. [CrossRef] [PubMed]
22. Pin, F.; Barreto, R.; Couch, M.E.; Bonetto, A.; O'Connell, T.M. Cachexia induced by cancer and chemotherapy yield distinct perturbations to energy metabolism. *J. Cachexia Sarcopenia Muscle* **2019**, *10*, 140–154. [CrossRef] [PubMed]
23. Barreto, R.; Mandili, G.; Witzmann, F.A.; Novelli, F.; Zimmers, T.A.; Bonetto, A. Cancer and Chemotherapy Contribute to Muscle Loss by Activating Common Signaling Pathways. *Front. Physiol.* **2016**, *7*, 472. [CrossRef] [PubMed]
24. Cheregi, B.; Timpani, C.; Nurgali, K.; Hayes, A.; Rybalka, E. Chemotherapy-induced mitochondrial respiratory dysfunction, oxidant production and death in healthy skeletal muscle C2C12 myoblast and myotube models. *Neuromuscul. Disord.* **2015**, *25*, S202. [CrossRef]
25. Pető, Á.; Kósa, D.; Fehér, P.; Ujhelyi, Z.; Sinka, D.; Vecsernyés, M.; Szilvássy, Z.; Juhász, B.; Csanádi, Z.; Vígh, L.; et al. Pharmacological Overview of the BGP-15 Chemical Agent as a New Drug Candidate for the Treatment of Symptoms of Metabolic Syndrome. *Molecules* **2020**, *25*, 429. [CrossRef]
26. Kennedy, T.L.; Swiderski, K.; Murphy, K.T.; Gehrig, S.M.; Curl, C.L.; Chandramouli, C.; Febbraio, M.A.; Delbridge, L.M.; Koopman, R.; Lynch, G.S. BGP-15 Improves Aspects of the Dystrophic Pathology in mdx and dko Mice with Differing Efficacies in Heart and Skeletal Muscle. *Am. J. Pathol.* **2016**, *186*, 3246–3260. [CrossRef]
27. Gehrig, S.M.; van der Poel, C.; Sayer, T.A.; Schertzer, J.D.; Henstridge, D.C.; Church, J.E.; Lamon, S.; Russell, A.P.; Davies, K.E.; Febbraio, M.A.; et al. Hsp72 preserves muscle function and slows progression of severe muscular dystrophy. *Nature* **2012**, *484*, 394–398. [CrossRef]
28. Salah, H.; Li, M.; Cacciani, N.; Gastaldello, S.; Ogilvie, H.; Akkad, H.; Namuduri, A.V.; Morbidoni, V.; Artemenko, K.A.; Balogh, G.; et al. The chaperone co-inducer BGP-15 alleviates ventilation-induced diaphragm dysfunction. *Sci. Transl. Med.* **2016**, *8*, 350ra103. [CrossRef]
29. Smuder, A.J.; Morton, A.B.; Hall, S.E.; Wiggs, M.P.; Ahn, B.; Wawrzyniak, N.R.; Sollanek, K.J.; Min, K.; Kwon, O.S.; Nelson, W.B.; et al. Effects of exercise preconditioning and HSP72 on diaphragm muscle function during mechanical ventilation. *J. Cachexia Sarcopenia Muscle* **2019**, *10*, 767–781. [CrossRef]
30. Ogilvie, H.; Cacciani, N.; Akkad, H.; Larsson, L. Targeting Heat Shock Proteins Mitigates Ventilator Induced Diaphragm Muscle Dysfunction in an Age-Dependent Manner. *Front. Physiol.* **2016**, *7*, 417. [CrossRef]

31. Cacciani, N.; Salah, H.; Li, M.; Akkad, H.; Backeus, A.; Hedstrom, Y.; Jena, B.P.; Bergquist, J.; Larsson, L. Chaperone co-inducer BGP-15 mitigates early contractile dysfunction of the soleus muscle in a rat ICU model. *Acta Physiol.* **2020**, *229*, e13425. [CrossRef] [PubMed]
32. Nascimento, T.L.; Mestril, R.; Miyabara, E.H. Overexpression of HSP70 attenuates sarcopenia by suppressing the expression of miR-133b. *JCSM Rapid Commun.* **2020**. [CrossRef]
33. Literati-Nagy, B.; Kulcsar, E.; Literati-Nagy, Z.; Buday, B.; Peterfai, E.; Horvath, T.; Tory, K.; Kolonics, A.; Fleming, A.; Mandl, J.; et al. Improvement of insulin sensitivity by a novel drug, BGP-15, in insulin-resistant patients: A proof of concept randomized double-blind clinical trial. *Horm. Metab. Res.* **2009**, *41*, 374–380. [CrossRef] [PubMed]
34. Literati-Nagy, B.; Tory, K.; Peitl, B.; Bajza, A.; Koranyi, L.; Literati-Nagy, Z.; Hooper, P.L.; Vigh, L.; Szilvassy, Z. Improvement of insulin sensitivity by a novel drug candidate, BGP-15, in different animal studies. *Metab. Syndr. Relat. Disord.* **2014**, *12*, 125–131. [CrossRef]
35. Chung, J.; Nguyen, A.K.; Henstridge, D.C.; Holmes, A.G.; Chan, M.H.; Mesa, J.L.; Lancaster, G.I.; Southgate, R.J.; Bruce, C.R.; Duffy, S.J.; et al. HSP72 protects against obesity-induced insulin resistance. *Proc. Natl. Acad. Sci. USA* **2008**, *105*, 1739–1744. [CrossRef]
36. Sorensen, J.C.; Petersen, A.C.; Timpani, C.A.; Campelj, D.G.; Cook, J.; Trewin, A.J.; Stojanovska, V.; Stewart, M.; Hayes, A.; Rybalka, E. BGP-15 Protects against Oxaliplatin-Induced Skeletal Myopathy and Mitochondrial Reactive Oxygen Species Production in Mice. *Front. Pharmacol.* **2017**, *8*, 137.
37. Racz, I.; Tory, K.; Gallyas, F., Jr.; Berente, Z.; Osz, E.; Jaszlits, L.; Bernath, S.; Sumegi, B.; Rabloczky, G.; Literati-Nagy, P. BGP-15—A novel poly(ADP-ribose) polymerase inhibitor—Protects against nephrotoxicity of cisplatin without compromising its antitumor activity. *Biochem. Pharmacol.* **2002**, *63*, 1099–1111. [CrossRef]
38. Mohamed, J.S.; Wilson, J.C.; Myers, M.J.; Sisson, K.J.; Alway, S.E. Dysregulation of SIRT-1 in aging mice increases skeletal muscle fatigue by a PARP-1-dependent mechanism. *Aging* **2014**, *6*, 820–834. [CrossRef]
39. Bai, P.; Canto, C.; Oudart, H.; Brunyanszki, A.; Cen, Y.; Thomas, C.; Yamamoto, H.; Huber, A.; Kiss, B.; Houtkooper, R.H.; et al. PARP-1 inhibition increases mitochondrial metabolism through SIRT1 activation. *Cell Metab.* **2011**, *13*, 461–468. [CrossRef]
40. Literati-Nagy, Z.; Tory, K.; Literati-Nagy, B.; Kolonics, A.; Torok, Z.; Gombos, I.; Balogh, G.; Vigh, L., Jr.; Horvath, I.; Mandl, J.; et al. The HSP co-inducer BGP-15 can prevent the metabolic side effects of the atypical antipsychotics. *Cell Stress Chaperones* **2012**, *17*, 517–521. [CrossRef]
41. Budzyński, M.A.; Crul, T.; Himanen, S.V.; Toth, N.; Otvos, F.; Sistonen, L.; Vigh, L. Chaperone co-inducer BGP-15 inhibits histone deacetylases and enhances the heat shock response through increased chromatin accessibility. *Cell Stress Chaperones* **2017**, *22*, 717–728. [CrossRef] [PubMed]
42. Henstridge, D.C.; Bruce, C.R.; Drew, B.G.; Tory, K.; Kolonics, A.; Estevez, E.; Chung, J.; Watson, N.; Gardner, T.; Lee-Young, R.S.; et al. Activating HSP72 in rodent skeletal muscle increases mitochondrial number and oxidative capacity and decreases insulin resistance. *Diabetes* **2014**, *63*, 1881–1894. [CrossRef] [PubMed]
43. Fernández-Fernández, M.R.; Valpuesta, J.M. Hsp70 chaperone: A master player in protein homeostasis. *F1000Research* **2018**, *7*. [CrossRef] [PubMed]
44. Kardon, T.; Nagy, G.; Csala, M.; Kiss, A.; Schaff, Z.; Nagy, P.L.; Wunderlich, L.; Banhegyi, G.; Mandl, J. Influence of BGP-15, a nicotinic amidoxime derivative, on the vascularization and growth of murine hepatoma xenografts. *Anticancer Res.* **2006**, *26*, 1023–1028. [PubMed]
45. Goodman, C.A.; Mabrey, D.M.; Frey, J.W.; Miu, M.H.; Schmidt, E.K.; Pierre, P.; Hornberger, T.A. Novel insights into the regulation of skeletal muscle protein synthesis as revealed by a new nonradioactive in vivo technique. *FASEB J.* **2011**, *25*, 1028–1039. [CrossRef]
46. Gordon, B.S.; Kelleher, A.R.; Kimball, S.R. Regulation of muscle protein synthesis and the effects of catabolic states. *Int. J. Biochem. Cell Biol.* **2013**, *45*, 2147–2157. [CrossRef]
47. Goodman, C.A. Role of mTORC1 in mechanically induced increases in translation and skeletal muscle mass. *J. Appl Physiol* **2019**, *127*, 581–590. [CrossRef]
48. Sarbassov, D.D.; Guertin, D.A.; Ali, S.M.; Sabatini, D.M. Phosphorylation and regulation of Akt/PKB by the rictor-mTOR complex. *Science* **2005**, *307*, 1098–1101. [CrossRef]
49. Gombos, I.; Crul, T.; Piotto, S.; Gungor, B.; Torok, Z.; Balogh, G.; Peter, M.; Slotte, J.P.; Campana, F.; Pilbat, A.M.; et al. Membrane-lipid therapy in operation: The HSP co-inducer BGP-15 activates stress signal transduction pathways by remodeling plasma membrane rafts. *PLoS ONE* **2011**, *6*, e28818. [CrossRef]

50. Murthy, S.; Ryan, A.; He, C.; Mallampalli, R.K.; Carter, A.B. Rac1-mediated mitochondrial H_2O_2 generation regulates MMP-9 gene expression in macrophages via inhibition of SP-1 and AP-1. *J. Biol. Chem.* **2010**, *285*, 25062–25073. [CrossRef]
51. Zhuge, Y.; Xu, J. Rac1 mediates type I collagen-dependent MMP-2 activation. role in cell invasion across collagen barrier. *J. Biol. Chem.* **2001**, *276*, 16248–16256. [CrossRef] [PubMed]
52. Lin, Y.C.; Chen, L.H.; Varadharajan, T.; Tsai, M.J.; Chia, Y.C.; Yuan, T.C.; Sung, P.J.; Weng, C.F. Resveratrol inhibits glucose-induced migration of vascular smooth muscle cells mediated by focal adhesion kinase. *Mol. Nutr. Food Res.* **2014**, *58*, 1389–1401. [CrossRef] [PubMed]
53. Meng, D.; Lv, D.D.; Fang, J. Insulin-like growth factor-I induces reactive oxygen species production and cell migration through Nox_4 and Rac_1 in vascular smooth muscle cells. *Cardiovasc. Res.* **2008**, *80*, 299–308. [CrossRef] [PubMed]
54. Csapo, R.; Gumpenberger, M.; Wessner, B. Skeletal Muscle Extracellular Matrix—What Do We Know About Its Composition, Regulation, and Physiological Roles? A Narrative Review. *Front. Physiol.* **2020**, *11*. [CrossRef] [PubMed]
55. Wang, W.; Schulze, C.J.; Suarez-Pinzon, W.L.; Dyck, J.R.; Sawicki, G.; Schulz, R. Intracellular action of matrix metalloproteinase-2 accounts for acute myocardial ischemia and reperfusion injury. *Circulation* **2002**, *106*, 1543–1549. [CrossRef] [PubMed]
56. Ren, X.; Lamb, G.D.; Murphy, R.M. Distribution and activation of matrix metalloproteinase-2 in skeletal muscle fibers. *Am. J. Physiol. Cell Physiol.* **2019**, *317*, C613–C625. [CrossRef]
57. Zimowska, M.; Brzoska, E.; Swierczynska, M.; Streminska, W.; Moraczewski, J. Distinct patterns of MMP-9 and MMP-2 activity in slow and fast twitch skeletal muscle regeneration in vivo. *Int. J. Dev. Biol.* **2008**, *52*, 307–314. [CrossRef]
58. Rybalka, E.; Timpani, C.A.; Cheregi, B.D.; Sorensen, J.C.; Nurgali, K.; Hayes, A. Chemotherapeutic agents induce mitochondrial superoxide production and toxicity but do not alter respiration in skeletal muscle in vitro. *Mitochondrion* **2018**, *42*, 33–49. [CrossRef]
59. Gilliam, L.A.; St Clair, D.K. Chemotherapy-induced weakness and fatigue in skeletal muscle: The role of oxidative stress. *Antioxid Redox Signal.* **2011**, *15*, 2543–2563. [CrossRef]
60. Deavall, D.G.; Martin, E.A.; Horner, J.M.; Roberts, R. Drug-induced oxidative stress and toxicity. *J. Toxicol.* **2012**, *2012*, 645460. [CrossRef]
61. Clements, C.M.; McNally, R.S.; Conti, B.J.; Mak, T.W.; Ting, J.P. DJ-1, a cancer- and Parkinson's disease-associated protein, stabilizes the antioxidant transcriptional master regulator Nrf2. *Proc. Natl. Acad. Sci. USA* **2006**, *103*, 15091–15096. [CrossRef] [PubMed]
62. Kefaloyianni, E.; Gaitanaki, C.; Beis, I. ERK1/2 and p38-MAPK signalling pathways, through MSK1, are involved in NF-kappaB transactivation during oxidative stress in skeletal myoblasts. *Cell Signal.* **2006**, *18*, 2238–2251. [CrossRef] [PubMed]
63. Barreto, R.; Kitase, Y.; Matsumoto, T.; Pin, F.; Colston, K.C.; Couch, K.E.; O'Connell, T.M.; Couch, M.E.; Bonewald, L.F.; Bonetto, A. ACVR2B/Fc counteracts chemotherapy-induced loss of muscle and bone mass. *Sci. Rep.* **2017**, *7*, 14470. [CrossRef] [PubMed]
64. Emery, P.W.; Edwards, R.H.; Rennie, M.J.; Souhami, R.L.; Halliday, D. Protein synthesis in muscle measured in vivo in cachectic patients with cancer. *Br. Med. J. Clin. Res. Ed.* **1984**, *289*, 584–586. [CrossRef] [PubMed]
65. De Lima, E.A.; de Sousa, L.G.O.; de S Teixeira, A.A.; Marshall, A.G.; Zanchi, N.E.; Neto, J.C.R. Aerobic exercise, but not metformin, prevents reduction of muscular performance by AMPk activation in mice on doxorubicin chemotherapy. *J. Cell Physiol.* **2018**, *233*, 9652–9662. [CrossRef] [PubMed]
66. Nissinen, T.A.; Degerman, J.; Rasanen, M.; Poikonen, A.R.; Koskinen, S.; Mervaala, E.; Pasternack, A.; Ritvos, O.; Kivelä, R.; Hulmi, J.J. Systemic blockade of ACVR2B ligands prevents chemotherapy-induced muscle wasting by restoring muscle protein synthesis without affecting oxidative capacity or atrogenes. *Sci. Rep.* **2016**, *6*, 32695. [CrossRef]
67. Nascimento, T.L.; Silva, M.T.; Miyabara, E.H. BGP-15 improves contractile function of regenerating soleus muscle. *J. Muscle Res. Cell Motil.* **2018**, *39*, 25–34. [CrossRef]
68. Senf, S.M.; Dodd, S.L.; McClung, J.M.; Judge, A.R. Hsp70 overexpression inhibits NF-kappaB and Foxo3a transcriptional activities and prevents skeletal muscle atrophy. *FASEB J. Off. Publ. Fed. Am. Soc. Exp. Biol.* **2008**, *22*, 3836–3845. [CrossRef]

69. Campelj, D.G.; Cree, T.M.; Goodman, C.A.; Rybalka, E. The timecourse of HSP70 induction by BGP-15 in C2C12 myotubes. Victoria University, Melbourne, VIC 8001, Australia. Personal observation, 2020.
70. Riggi, M.; Kusmider, B.; Loewith, R. The flipside of the TOR coin—TORC2 and plasma membrane homeostasis at a glance. *J. Cell Sci.* **2020**, *133*. [CrossRef]
71. Kim, M.H.; Kay, D.I.; Rudra, R.T.; Chen, B.M.; Hsu, N.; Izumiya, Y.; Martinez, L.; Spencer, M.J.; Walsh, K.; Grinnell, A.D.; et al. Myogenic Akt signaling attenuates muscular degeneration, promotes myofiber regeneration and improves muscle function in dystrophin-deficient mdx mice. *Hum. Mol. Genet.* **2011**, *20*, 1324–1338. [CrossRef]
72. Ogasawara, R.; Jensen, T.E.; Goodman, C.A.; Hornberger, T.A. Resistance Exercise-Induced Hypertrophy: A Potential Role for Rapamycin-Insensitive mTOR. *Exercise Sport Sci. Rev.* **2019**. [CrossRef] [PubMed]
73. Hulmi, J.J.; Nissinen, T.A.; Rasanen, M.; Degerman, J.; Lautaoja, J.H.; Hemanthakumar, K.A.; Backman, J.T.; Ritvos, O.; Silvennoinen, M.; Kivelä, R. Prevention of chemotherapy-induced cachexia by ACVR2B ligand blocking has different effects on heart and skeletal muscle. *J. Cachexia Sarcopenia Muscle* **2018**, *9*, 417–432. [CrossRef] [PubMed]
74. Goldberg, A.L.; Etlinger, J.D.; Goldspink, D.F.; Jablecki, C. Mechanism of work-induced hypertrophy of skeletal muscle. *Med. Sci. Sports* **1975**, *7*, 185–198. [PubMed]
75. Hornberger, T.A.; Esser, K.A. Mechanotransduction and the regulation of protein synthesis in skeletal muscle. *Proc. Nutr. Soc.* **2004**, *63*, 331–335. [CrossRef] [PubMed]
76. Goodman, C.A. The Role of mTORC1 in Regulating Protein Synthesis and Skeletal Muscle Mass in Response to Various Mechanical Stimuli. *Rev. Physiol. Biochem. Pharmacol.* **2014**, *166*, 43–95. [CrossRef]
77. Wackerhage, H.; Schoenfeld, B.J.; Hamilton, D.L.; Lehti, M.; Hulmi, J.J. Stimuli and sensors that initiate skeletal muscle hypertrophy following resistance exercise. *J. Appl. Physiol.* **2019**. [CrossRef]
78. Fischer, M.; Rikeit, P.; Knaus, P.; Coirault, C. YAP-Mediated Mechanotransduction in Skeletal Muscle. *Front. Physiol.* **2016**, *7*. [CrossRef]
79. Kirby, T.J. Mechanosensitive pathways controlling translation regulatory processes in skeletal muscle and implications for adaptation. *J. Appl. Physiol. (1985)* **2019**, *127*, 608–618. [CrossRef]
80. Olsen, L.A.; Nicoll, J.X.; Fry, A.C. The skeletal muscle fiber: A mechanically sensitive cell. *Eur. J. Appl. Physiol.* **2019**, *119*, 333–349. [CrossRef]
81. Van Norren, K.; van Helvoort, A.; Argiles, J.M.; van Tuijl, S.; Arts, K.; Gorselink, M.; Laviano, A.; Kegler, D.; Haagsman, H.P.; van der Beek, E.M. Direct effects of doxorubicin on skeletal muscle contribute to fatigue. *Br. J. Cancer* **2009**, *100*, 311–314. [CrossRef]
82. Conte, E.; Bresciani, E.; Rizzi, L.; Cappellari, O.; De Luca, A.; Torsello, A.; Liantonio, A. Cisplatin-Induced Skeletal Muscle Dysfunction: Mechanisms and Counteracting Therapeutic Strategies. *Int. J. Mol. Sci.* **2020**, *21*, 1242. [CrossRef]
83. Swiderski, K.; Shaffer, S.A.; Gallis, B.; Odom, G.L.; Arnett, A.L.; Scott Edgar, J.; Baum, D.M.; Chee, A.; Naim, T.; Gregorevic, P.; et al. Phosphorylation within the cysteine-rich region of dystrophin enhances its association with β-dystroglycan and identifies a potential novel therapeutic target for skeletal muscle wasting. *Hum. Mol. Genet.* **2014**, *23*, 6697–6711. [CrossRef] [PubMed]
84. Eilers, W.; Jaspers, R.T.; de Haan, A.; Ferrié, C.; Valdivieso, P.; Flück, M. CaMKII content affects contractile, but not mitochondrial, characteristics in regenerating skeletal muscle. *BMC Physiol.* **2014**, *14*, 7. [CrossRef]
85. Allen, D.G.; Whitehead, N.P.; Froehner, S.C. Absence of Dystrophin Disrupts Skeletal Muscle Signaling: Roles of Ca^{2+}, Reactive Oxygen Species, and Nitric Oxide in the Development of Muscular Dystrophy. *Physiol. Rev.* **2016**, *96*, 253–305. [CrossRef]
86. Conte, E.; Camerino, G.M.; Mele, A.; De Bellis, M.; Pierno, S.; Rana, F.; Fonzino, A.; Caloiero, R.; Rizzi, L.; Bresciani, E. Growth hormone secretagogues prevent dysregulation of skeletal muscle calcium homeostasis in a rat model of cisplatin-induced cachexia. *J. Cachexia Sarcopenia Muscle* **2017**, *8*, 386–404.
87. Guigni, B.A.; Fix, D.K.; Bivona, J.J., 3rd; Palmer, B.M.; Carson, J.A.; Toth, M.J. Electrical stimulation prevents doxorubicin-induced atrophy and mitochondrial loss in cultured myotubes. *Am. J. Physiol. Cell Physiol.* **2019**, *317*, C1213–C1228. [CrossRef]
88. Sanarica, F.; Mantuano, P.; Conte, E.; Cozzoli, A.; Capogrosso, R.F.; Giustino, A.; Cutrignelli, A.; Cappellari, O.; Rolland, J.F.; De Bellis, M.; et al. Proof-of-concept validation of the mechanism of action of Src tyrosine kinase inhibitors in dystrophic mdx mouse muscle: In vivo and in vitro studies. *Pharmacol. Res.* **2019**, *145*, 104260. [CrossRef]

89. Petrof, B.J.; Shrager, J.B.; Stedman, H.H.; Kelly, A.M.; Sweeney, H.L. Dystrophin protects the sarcolemma from stresses developed during muscle contraction. *Proc. Natl. Acad. Sci. USA* **1993**, *90*, 3710–3714. [CrossRef]
90. Gallyas, F., Jr.; Sumegi, B. Mitochondrial Protection by PARP Inhibition. *Int. J. Mol. Sci* **2020**, *21*, 2767. [CrossRef]
91. Valera-Alberni, M.; Canto, C. Mitochondrial stress management: A dynamic journey. *Cell Stress* **2018**, *2*, 253–274. [CrossRef]
92. Shi, S.Y.; Lu, S.Y.; Sivasubramaniyam, T.; Revelo, X.S.; Cai, E.P.; Luk, C.T.; Schroer, S.A.; Patel, P.; Kim, R.H.; Bombardier, E.; et al. DJ-1 links muscle ROS production with metabolic reprogramming and systemic energy homeostasis in mice. *Nat. Commun.* **2015**, *6*, 7415. [CrossRef] [PubMed]
93. Brunyanszki, A.; Szczesny, B.; Virag, L.; Szabo, C. Mitochondrial poly(ADP-ribose) polymerase: The Wizard of Oz at work. *Free Radic. Biol. Med.* **2016**, *100*, 257–270. [CrossRef] [PubMed]
94. Couluris, M.; Mayer, J.L.R.; Freyer, D.R.; Sandler, E.; Xu, P.; Krischer, J.P. The effect of cyproheptadine hydrochloride (periactin) and megestrol acetate (megace) on weight in children with cancer/treatment-related cachexia. *J. Pediatr. Hematol. Oncol.* **2008**, *30*, 791–797. [CrossRef] [PubMed]
95. Aoyagi, T.; Terracina, K.P.; Raza, A.; Matsubara, H.; Takabe, K. Cancer cachexia, mechanism and treatment. *World J. Gastrointest Oncol.* **2015**, *7*, 17–29. [CrossRef] [PubMed]
96. Boland, A.M.; Gibson, T.M.; Lu, L.; Kaste, S.C.; DeLany, J.P.; Partin, R.E.; Lanctot, J.Q.; Howell, C.R.; Nelson, H.H.; Chemaitilly, W.; et al. Dietary Protein Intake and Lean Muscle Mass in Survivors of Childhood Acute Lymphoblastic Leukemia: Report From the St. Jude Lifetime Cohort Study. *Phys. Ther.* **2016**, *96*, 1029–1038. [CrossRef] [PubMed]
97. Chacon-Cabrera, A.; Mateu-Jimenez, M.; Langohr, K.; Fermoselle, C.; García-Arumí, E.; Andreu, A.L.; Yelamos, J.; Barreiro, E. Role of PARP activity in lung cancer-induced cachexia: Effects on muscle oxidative stress, proteolysis, anabolic markers, and phenotype. *J. Cell Physiol.* **2017**, *232*, 3744–3761. [CrossRef]
98. Kohne, C.H.; Hofheinz, R.; Mineur, L.; Letocha, H.; Greil, R.; Thaler, J.; Fernebro, E.; Gamelin, E.; Decosta, L.; Karthaus, M. First-line panitumumab plus irinotecan/5-fluorouracil/leucovorin treatment in patients with metastatic colorectal cancer. *J. Cancer Res. Clin. Oncol.* **2012**, *138*, 65–72. [CrossRef]
99. McQuade, R.M.; Stojanovska, V.; Donald, E.L.; Rahman, A.A.; Campelj, D.G.; Abalo, R.; Rybalka, E.; Bornstein, J.C.; Nurgali, K. Irinotecan-Induced Gastrointestinal Dysfunction Is Associated with Enteric Neuropathy, but Increased Numbers of Cholinergic Myenteric Neurons. *Front. Physiol.* **2017**, *8*, 391. [CrossRef]
100. Debruin, D.A.; Timpani, C.A.; Lalunio, H.; Rybalka, E.; Goodman, C.A.; Hayes, A. Exercise may ameliorate the detrimental side effects of high vitamin D supplementation on muscle function in mice. *J. Bone Miner. Res.* **2020**, *35*, 1092–1106. [CrossRef]
101. Hayes, A.; Williams, D.A. Long-term clenbuterol administration alters the isometric contractile properties of skeletal muscle from normal and dystrophin-deficient mdx mice. *Clin. Exp. Pharmacol. Physiol.* **1994**, *21*, 757–765. [CrossRef]
102. Timpani, C.A.; Trewin, A.J.; Stojanovska, V.; Robinson, A.; Goodman, C.A.; Nurgali, K.; Betik, A.C.; Stepto, N.; Hayes, A.; McConell, G.K.; et al. Attempting to Compensate for Reduced Neuronal Nitric Oxide Synthase Protein with Nitrate Supplementation Cannot Overcome Metabolic Dysfunction but Rather Has Detrimental Effects in Dystrophin-Deficient mdx Muscle. *Neurother. J. Am. Soc. Exp. Neurother.* **2017**, *14*, 429–446. [CrossRef] [PubMed]
103. Brooks, S.V.; Faulkner, J.A. Contractile properties of skeletal muscles from young, adult and aged mice. *J. Physiol.* **1988**, *404*, 71–82. [CrossRef] [PubMed]
104. Schuh, R.A.; Jackson, K.C.; Khairallah, R.J.; Ward, C.W.; Spangenburg, E.E. Measuring mitochondrial respiration in intact single muscle fibers. *Am. J. Physiol. Regul. Integr. Comp. Physiol.* **2012**, *302*, R712–R719. [CrossRef] [PubMed]
105. Timpani, C.A.; Goodman, C.A.; Stathis, C.G.; White, J.D.; Mamchaoui, K.; Butler-Browne, G.; Gueven, N.; Hayes, A.; Rybalka, E. Adenylosuccinic acid therapy ameliorates murine Duchenne Muscular Dystrophy. *Sci. Rep.* **2020**, *10*, 1125. [CrossRef]
106. Srere, P. [1] Citrate synthase:[EC 4.1. 3.7. Citrate oxaloacetate-lyase (CoA-acetylating)]. *Methods Enzymol.* **1969**, *13*, 3–11.

107. Hu, X.; Beeton, C. Detection of functional matrix metalloproteinases by zymography. *J. Vis. Exp.* **2010**. [CrossRef]

Chapter 4

Metronomic 5-fluorouracil delivery primes skeletal muscle for myopathy but does not cause cachexia

Campelj DG, Timpani CA, Cree T, Petersen AC, Hayes A, Goodman CA, Rybalka E. Metronomic 5-Fluorouracil Delivery Primes Skeletal Muscle for Myopathy but Does Not Cause Cachexia. Pharmaceuticals. 2021; 14(5):478. doi: 10.3390/ph14050478.

Preface

This study was an extension of the key concepts described in Chapter 3. In this study we replaced chemotherapeutic agent IRI, with 5FU, the backbone of both the FOLFIRI and FOLFOX regimens, and assessed its capacity to drive cachexia induction as a mono-therapy, independent of its utility in multi-agent regimens. We also combined mitoprotective agent BGP-15 with 5FU, as it demonstrated modest therapeutic efficacy to protect against chemotherapeutic-induced skeletal myopathy in our previous investigations [24, 32]. The aim of this study was to evaluate the protective potential of BGP-15 in combination with 5FU treatment We hypothesized that 5FU would induce muscle cachexia and that BGP-15 could protect against these effects.

VICTORIA UNIVERSITY

THE NEW WAY TO DO UNI

OFFICE FOR RESEARCH TRAINING, QUALITY AND INTEGRITY

DECLARATION OF CO-AUTHORSHIP AND CO-CONTRIBUTION: PAPERS INCORPORATED IN THESIS

This declaration is to be completed for each conjointly authored publication and placed at the beginning of the thesis chapter in which the publication appears.

1. PUBLICATION DETAILS (to be completed by the candidate)

Title of Paper/Journal/Book: Metronomic 5-fluorouracil delivery primes skeletal muscle for myopathy but does not cause cachexia

Surname: Campelj

First name: Dean

Institute: Institute for Sustainable Industries and Livea

Candidate's Contribution (%): 70

Status:

Accepted and in press: ☐ Date:

Published: ☑ Date: 18/05/21

2. CANDIDATE DECLARATION

I declare that the publication above meets the requirements to be included in the thesis as outlined in the HDR Policy and related Procedures – policy.vu.edu.au.

Dean Campelj Digitally signed by Dean Campelj Date: 2021.05.21 12:11:12 +10'00'

Signature **Date**

3. CO-AUTHOR(S) DECLARATION

In the case of the above publication, the following authors contributed to the work as follows:

The undersigned certify that:

1. They meet criteria for authorship in that they have participated in the conception, execution or interpretation of at least that part of the publication in their field of expertise;
2. They take public responsibility for their part of the publication, except for the responsible author who accepts overall responsibility for the publication;

3. There are no other authors of the publication according to these criteria;

4. Potential conflicts of interest have been disclosed to a) granting bodies, b) the editor or publisher of journals or other publications, and c) the head of the responsible academic unit; and

5. The original data will be held for at least five years from the date indicated below and is stored at the following **location(s)**:

Victoria University R Drive

Name(s) of Co-Author(s)	Contribution (%)	Nature of Contribution	Signature	Date
Cara A Timpani	5	Histological analyses, citrate synthase analyses, manuscript review and editing	[redacted]	18/05/21
Tabitha Cree	5	Cell culture experiments	[redacted]	18/05/21
Aaron C Petersen	1	Conception, provision of BGP-15, manuscript revision	[redacted]	18/05/21
Alan Hayes	1	Methodological resources, manuscript revision	[redacted]	18/05/21
Craig A Goodman	9	Conception, supervision, methodological resources, manuscript review and editing	[redacted]	18/05/21
Emma Rybalka	9	Conception, funding, supervision,resources,manuscript review and editing	[redacted]	18/05/21

Updated: September 2019

pharmaceuticals

MDPI

Article

Metronomic 5-Fluorouracil Delivery Primes Skeletal Muscle for Myopathy but Does Not Cause Cachexia

Dean G. Campelj [1,2], Cara A. Timpani [1,2,3], Tabitha Cree [1,2], Aaron C. Petersen [1,2], Alan Hayes [1,2,3], Craig A. Goodman [2,4,*] and Emma Rybalka [1,2,3,*]

1 Institute for Health and Sport, Victoria University, Melbourne, VIC 8001, Australia; dean.campelj@live.vu.edu.au (D.G.C.); cara.timpani@vu.edu.au (C.A.T.); tabitha.cree@live.vu.edu.au (T.C.); aaron.petersen@vu.edu.au (A.C.P.); alan.hayes@vu.edu.au (A.H.)
2 Australian Institute for Musculoskeletal Science (AIMSS), Inherited and Acquired Myopathy Program, Victoria University, St Albans, VIC 3021, Australia
3 Department of Medicine-Western Health, Melbourne Medical School, The University of Melbourne, Melbourne, VIC 3021, Australia
4 Centre for Muscle Research (CMR), Department of Physiology, The University of Melbourne, Parkville, VIC 3010, Australia
* Correspondence: craig.goodman@unimelb.edu.au (C.A.G.); emma.rybalka@vu.edu.au (E.R.)

Abstract: Skeletal myopathy encompasses both atrophy and dysfunction and is a prominent event in cancer and chemotherapy-induced cachexia. Here, we investigate the effects of a chemotherapeutic agent, 5-fluorouracil (5FU), on skeletal muscle mass and function, and whether small-molecule therapeutic candidate, BGP-15, could be protective against the chemotoxic challenge exerted by 5FU. Additionally, we explore the molecular signature of 5FU treatment. Male Balb/c mice received metronomic tri-weekly intraperitoneal delivery of 5FU (23 mg/kg), with and without BGP-15 (15 mg/kg), 6 times in total over a 15 day treatment period. We demonstrated that neither 5FU, nor 5FU combined with BGP-15, affected body composition indices, skeletal muscle mass or function. Adjuvant BGP-15 treatment did, however, prevent the 5FU-induced phosphorylation of p38 MAPK and p65 NF-κB subunit, signalling pathways involved in cell stress and inflammatory signalling, respectively. This as associated with mitoprotection. 5FU reduced the expression of the key cytoskeletal proteins, desmin and dystrophin, which was not prevented by BGP-15. Combined, these data show that metronomic delivery of 5FU does not elicit physiological consequences to skeletal muscle mass and function but is implicit in priming skeletal muscle with a molecular signature for myopathy. BGP-15 has modest protective efficacy against the molecular changes induced by 5FU.

Keywords: chemotherapy; cachexia; 5-fluorouracil; skeletal muscle; p38; NF-κB; dystrophin; desmin

Citation: Campelj, D.G.; Timpani, C.A.; Cree, T.; Petersen, A.C.; Hayes, A.; Goodman, C.A.; Rybalka, E. Metronomic 5-Fluorouracil Delivery Primes Skeletal Muscle for Myopathy but Does Not Cause Cachexia. *Pharmaceuticals* **2021**, *14*, 478. https://doi.org/10.3390/ph14050478

Academic Editor: Dinender K. Singla

Received: 31 March 2021
Accepted: 12 May 2021
Published: 17 May 2021

1. Introduction

Colorectal cancer (CRC) is a significant contributor to worldwide morbidity and mortality, with approximately 1.9 million new CRC cases and 900,000 CRC-related deaths reported in 2020 (GLOBOCAN 2020) [1]. The underlying causes of CRC progression and mortality are multi-faceted and still being discovered. A key risk factor that complicates responsivity to anti-cancer treatment, and, therefore survivability, is the metabolic wasting syndrome, cachexia, which is prevalent in ~45% of CRC patients [2]. Cachexia is characterised by the ongoing loss of skeletal muscle mass, with or without loss of fat mass, where patients are non-responsive to nutritional intervention and manifest progressive functional impairment [3]. Clinically, skeletal muscle atrophy and poor recovery from the loss of skeletal muscle mass have been established as two prominent prognostic factors of mortality in cachectic cancer patients [4]. Recently, anti-cancer treatment, i.e., chemotherapy, has surfaced as a key contributor to the progression of cachexia, with emerging literature suggesting that chemotherapy can induce skeletal muscle mass loss and dysfunction (skeletal myopathy) [5,6] with lifelong impact [7].

Chemotherapy is a mainstay of advanced CRC treatment strategies and is used complementarily to surgical tumour resection or in advanced staging due to metastasis or resistance to radiotherapy. The anti-metabolite, 5-fluorouracil (5FU), is primarily utilized in the treatment of advanced CRC as a backbone constituent of multi-agent regimens, such as FOLFIRI [5FU, leucovorin (LV) and irinotecan (IRI)] and FOLFOX [5FU, LV and oxaliplatin (OXA)] (for extensive review, see [8]). 5FU administration can elicit significant side-effects including, but not limited to, cardiotoxicity, gastrointestinal toxicity, neurotoxicity and pancytopenia [9], with lean mass suggested to be an independent determinant of dose-limiting toxicity from 5FU-based regimens [10]. Barreto et al. have demonstrated that the 5FU-based FOLFIRI regimen induces a cachectic phenotype in cancer-free mice, underscored by the loss of body and lean mass, and skeletal myopathy [11]. This was in contrast with the FOLFOX regimen, which did not induce any of these effects [11]. These data suggest that IRI is more impactful on the musculoskeletal system than OXA, and to this effect, we have recently demonstrated that IRI causes acute cachexia, lean tissue wasting and skeletal muscle dysfunction [12]. However, whether 5FU also induces cachectic wasting and skeletal myopathy, independent from the other constituents in the FOLFIRI regimen, is unclear [13,14]. Such information is of clinical importance so that the risk of cachexia during administration of FOLFIRI and other 5FU-based regimens can be predicted and clinically managed.

Chemotherapy-induced skeletal muscle wasting is underlined by compromised proteostasis in favour of protein degradation [6]. It is characterised by a molecular signature of myopathy involving the activation of the stress-inducible mitogen-activated protein kinases (MAPK), p38 and ERK1/2 [11], and key transcription factor for inflammatory genes, nuclear factor-κB (NF-κB) [15]. Since MAPK phosphorylation can interact with NF-κB phosphorylation during oxidative stress [16], it is suggested that there is a link between these two target pathways, leading to the induction of a pro-catabolic environment [17,18]. Specifically, 5FU is a potent activator of p38 MAPK signalling in vitro [19], and in vivo evidence from the 5FU-based FOLFIRI regimen supports the same—increased phosphorylation of p38 MAPK associated with enhanced oxidative stress and reduced mitochondrial quality control signalling [11]. These data are consistent with findings from our laboratory, where 5FU potentiated mitochondrial superoxide production and reduced mitochondrial viability in C2C12 skeletal muscle cells [20]. The FOLFIRI regimen also reduces mitochondrial content, which is associated with abnormalities in muscle morphology at the level of the sarcomere [11,21]. This was of interest to our group since we have recently shown that the chemotherapeutic agent, IRI, compromised cytoskeletal stability through reducing dystrophin protein expression [12]. While the mechanism underlying the effect of chemotherapy on skeletal muscle cytoskeletal composition is still undefined, it may be an event related to chemotherapy-induced NF-κB activation [15], suggesting that NF-κB activity plays a role in the decay of structural integrity of muscles [22]. Therefore, in this study, our first aim was to characterise the effect of 5FU treatment on skeletal muscle mass and function, and to investigate the underlying molecular mechanisms with emphasis on the potential connection between p38 MAPK and NF-κB signalling, mitochondrial dynamics and structural cytoskeletal proteins.

There is estimated to be 3.15 million new CRC cases worldwide in 2040 [1], highlighting the growing burden of cancer and the current need for novel therapeutic strategies to support current anti-cancer treatments and promote survivability. BGP-15 is a nicotinic amidoxime derivate and small-molecule therapeutic candidate which acts as a cytoprotectant through the inhibition of poly (ADP) ribose polymerase -1 (PARP-1) and co-induction of heat shock protein-70 (HSP-70) [23,24]. BGP-15-mediated PARP-1 inhibition and HSP-70 co-induction are associated with improved mitochondrial content, function and oxidative capacity [25,26]. However, BGP-15 has also been shown to elicit mitoprotection independent of these targets, highlighting its pleiotropic efficacy [27]. Consequently, BGP-15 has promise in the treatment of a range of skeletal myopathies, including diabetes, Duchenne Muscular Dystrophy and ventilation-induced diaphragm dysfunction (for extensive review

see [28]). We have evaluated the adjuvant therapeutic potential of BGP-15 to protect against the induction of skeletal myopathy from chemotherapeutic agents IRI and OXA [12,29], with mixed efficacy. However, since 5FU is a potent activator of p38 MAPK, and BGP-15 has been shown to inhibit pan-MAPK activity [30], the potential for BGP-15 to be more efficacious when administered with 5FU is substantial. Thus, our secondary aim was to evaluate the protective efficacy of BGP-15 adjuvant therapy against 5FU-induced skeletal myopathy and investigate the underlying mechanisms through which BGP-15 functions as a p38 MAPK inhibitor in a chemotoxic environment.

2. Results

2.1. Assessment of Body Composition Indices, Skeletal Muscle Mass and Function

To explore the potential contribution of 5FU treatment on the induction of cachexia and efficacy of 5FU+BGP treatment, we examined a suite of body composition and skeletal muscle size indices. Interestingly, 5FU did not inhibit growth nor reduce body, lean or fat mass, and subsequently, 5FU+BGP also did not affect these parameters (Figure 1A–C; Table S1). Consistent with body composition data, raw skeletal muscle mass and skeletal muscle mass to body mass ratios for EDL, SOL and TA muscles were not significantly different between treatment groups (Figure 1D), although, 5FU+BGP displayed a trend to increase the TA to body mass ratio compared to 5FU treatment ($p = 0.07$, Figure 1D). Organ mass also remained unchanged between treatment groups (Table S1). We then undertook muscle fibre size analysis in TA cross-sections, with no significant differences found between treatment groups for the relative frequency percentage of muscle fibre cross-sectional areas (CSA) (Figure 1E,G) nor the mean fibre CSA (Figure 1F,G). Next, we assessed the ex vivo contractile function of EDL and SOL muscles. Neither 5FU, nor 5FU+BGP treatment affected skeletal muscle functional parameters of EDL or SOL, with no change observed in force–frequency relationships (Figure 2A), force production characteristics, i.e., P_t, P_o, P_t/P_o and sP_o (Figure 2B).

2.2. Assessment of Cytoskeletal Structural Protein Expression

Previously, we have shown an association between skeletal muscle dysfunction and reduced expression of proteins associated with the dystrophin-associated protein complex (DAPC) induced by IRI treatment [12]. Thus, we investigated these parameters in the context of this study. 5FU treatment induced a reduction in the abundance of the cytoskeleton proteins, desmin and dystrophin ($p < 0.05$, Figure 3A,B), and 5FU+BGP treatment did not protect against these changes. There was no impact of 5FU, nor 5FU+BGP, treatment on the protein expression of additional cytoskeletal structural proteins laminin, β-dystroglycan, δ-sarcoglycan, dystrobrevin, syntrophin and talin (Figure 3A,B). Next, we explored the effect of 5FU and 5FU+BGP treatment on Akt^{Ser473} phosphorylation, an established target of Mechanistic Target of Rapamycin Complex 2 (mTORC2) [31]. mTORC2 activity has been shown to be involved in the regulation of plasma membrane homeostasis and cytoskeletal organization [32]. Thus, we were interested in mTORC2 activity in the context of the reduced expression of desmin and dystrophin—the phosphorylation of Akt^{Ser473} is indicative of mTORC2 activation. We showed that 5FU treatment reduced the phosphorylation of Akt^{Ser473} compared to VEH ($p < 0.05$, Figure 3C,E), while 5FU+BGP-15 treatment did not alter the 5FU-induced changes to Akt^{Ser473} signalling (Figure 3C).

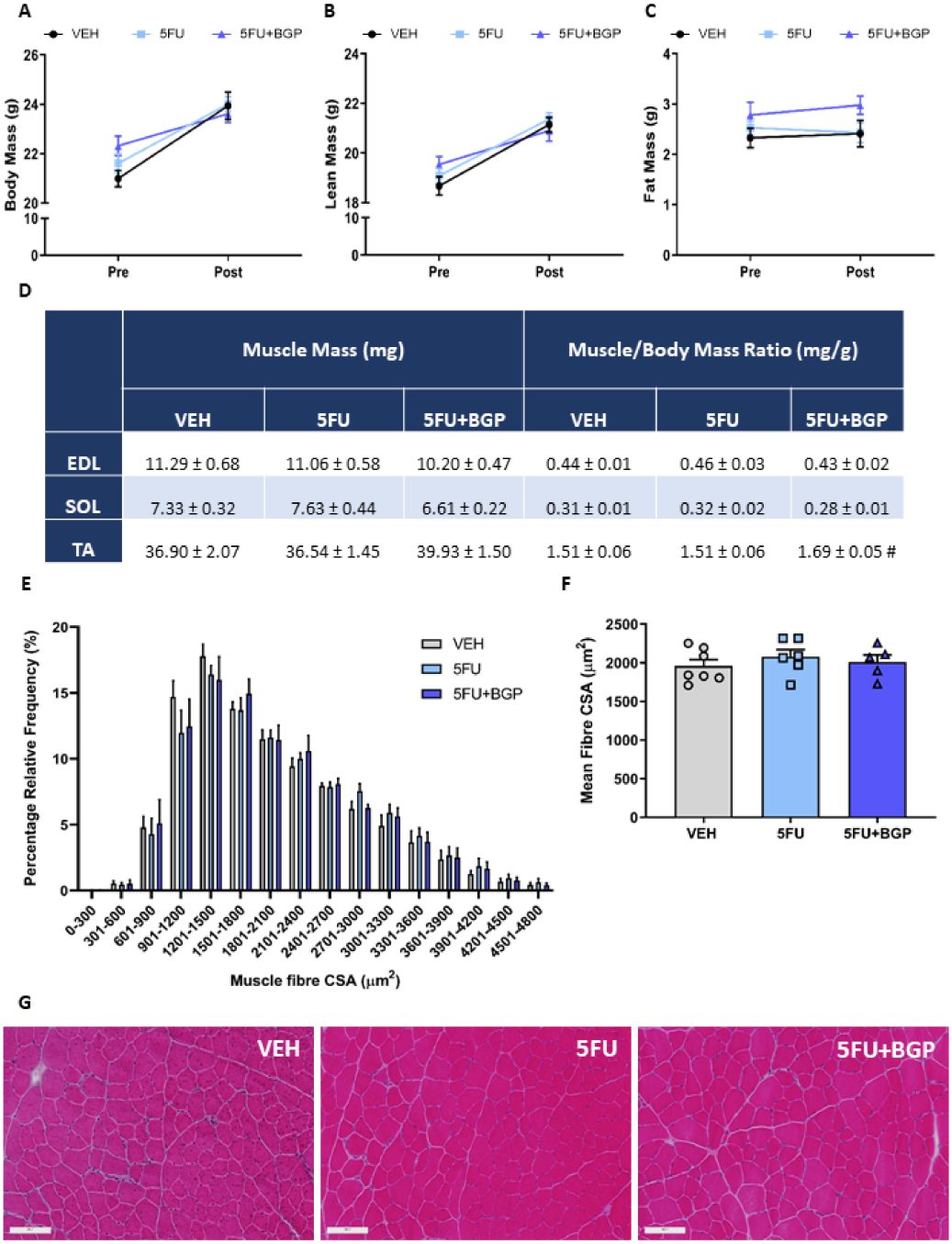

	Muscle Mass (mg)			Muscle/Body Mass Ratio (mg/g)		
	VEH	5FU	5FU+BGP	VEH	5FU	5FU+BGP
EDL	11.29 ± 0.68	11.06 ± 0.58	10.20 ± 0.47	0.44 ± 0.01	0.46 ± 0.03	0.43 ± 0.02
SOL	7.33 ± 0.32	7.63 ± 0.44	6.61 ± 0.22	0.31 ± 0.01	0.32 ± 0.02	0.28 ± 0.01
TA	36.90 ± 2.07	36.54 ± 1.45	39.93 ± 1.50	1.51 ± 0.06	1.51 ± 0.06	1.69 ± 0.05 #

Figure 1. The effect of 5-fluorouracil (5FU) and 5FU with BGP-15 (5FU+BGP) treatment on body composition and muscle size indices. Body composition parameters were measured and presented as pre- and post-treatment data points for (**A**) body, (**B**) lean and (**C**) fat mass. (**D**) Hindlimb skeletal muscles extensor digitorum longus (EDL), soleus (SOL), and tibialis anterior (TA) were weighed post-treatment and data presented as raw mass and muscle to body mass ratios (# $p = 0.07$; compared to 5FU). TA cross-sections were H&E-stained and underwent histological fibre size analysis with data presented as (**E**) percentage relative frequency distribution of the muscle fibre cross-sectional area (CSA) and (**F**) mean muscle fibre CSA. (**G**) Representative images of H&E-stained TA cross-sections are displayed. Scale bar = 100 μm. $n = 7$–8 for body composition indices; $n = 4$–8 for muscle weights; $n = 5$–7 for histology. Data are mean ± SEM.

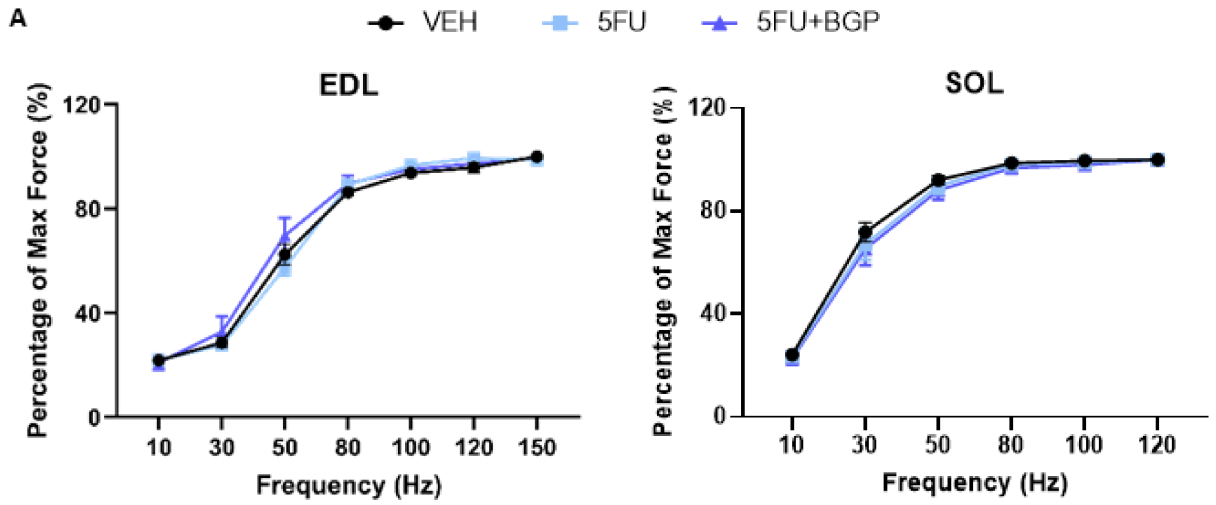

B

	EDL			SOL		
	VEH	5FU	5FU+BGP	VEH	5FU	5FU+BGP
P_t (mN)	109.2 ± 5.2	106.2 ± 9.6	100.1 ± 16.6	61.8 ± 5.6	60.7 ± 5.4	51.1 ± 7.3
P_o (mN)	530.4 ± 22.9	533.7 ± 23.1	505.7 ± 52.1	281.8 ± 13.0	300.3 ± 16.7	250.6 ± 30.6
P_t/P_o	0.256 ± 0.013	0.249 ± 0.013	0.249 ± 0.022	0.252 ± 0.009	0.251 ± 0.014	0.220 ± 0.012
pCSA (cm^2)	0.021 ± 0.001	0.020 ± 0.001	0.022 ± 0.001	0.014 ± 0.001	0.013 ± 0.001	0.011 ± 0.001
sP_o (mN)	24.40 ± 1.03	24.86 ± 1.54	23.18 ± 3.14	22.10 ± 0.34	23.36± 1.28	21.26 ± 4.95

Figure 2. The effect of 5-fluorouracil (5FU) and 5FU with BGP-15 (5FU+BGP) treatment on skeletal muscle contractile function. Extensor digitorum longus (EDL) and soleus (SOL) muscles underwent ex vivo assessment of contractile functional properties, with (**A**) force–frequency relationships and (**B**) force production characteristics analyzed, including; Peak twitch force (P_t), Absolute tetanic force production (P_o), twitch to tetanus ratio (P_t/P_o), physiological cross-sectional area (pCSA) and Specific force production (sP_o). *n* = 4–8 for ex vivo contractile function. Data are mean ± SEM.

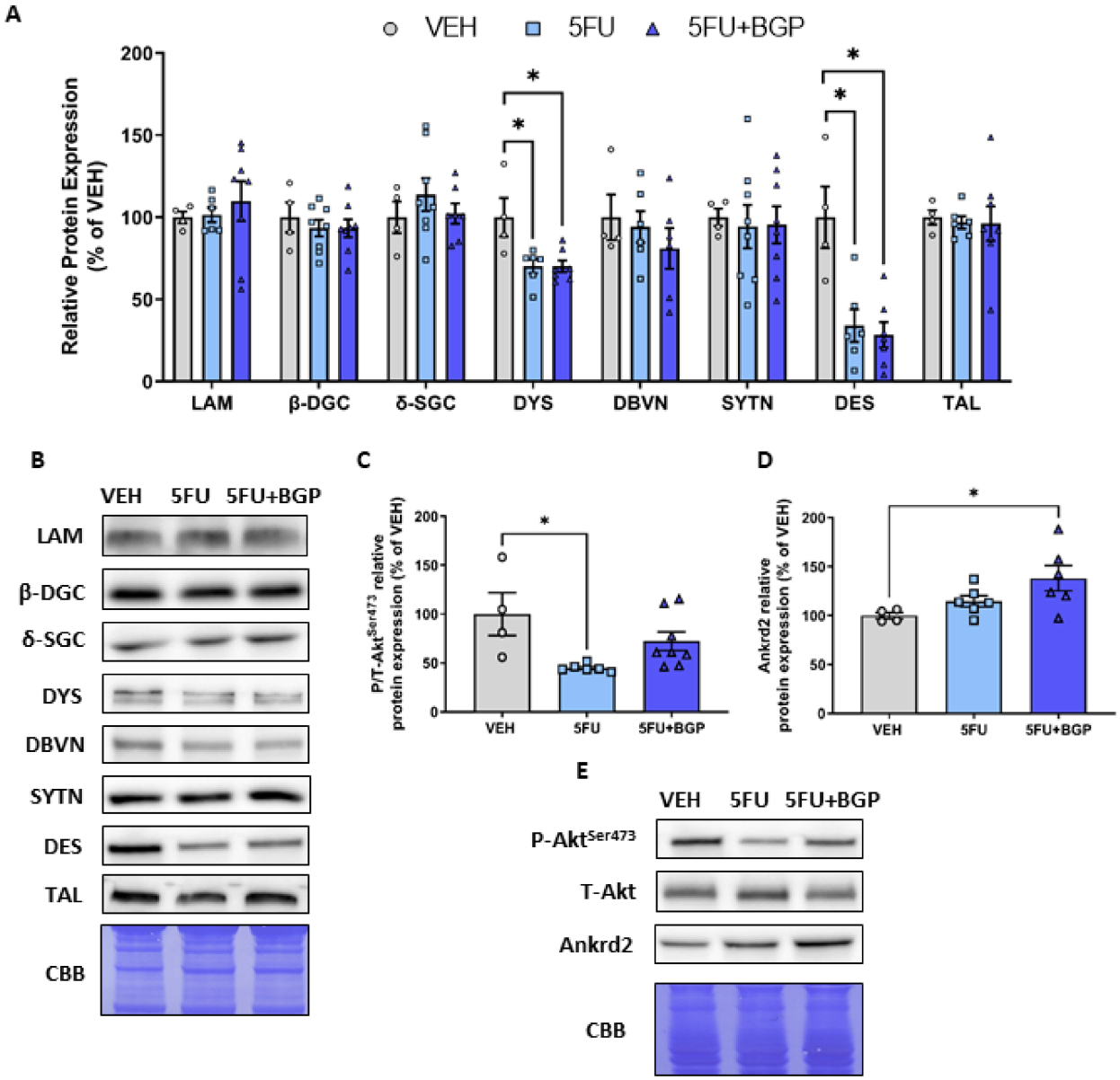

Figure 3. The effect of 5-fluorouracil (5FU) and 5FU with BGP-15 (5FU+BGP) treatment on expression of cytoskeletal structural proteins. Western blotting experiments were undertaken in tibialis anterior (TA) muscle homogenate, with samples probed for (**A**,**B**) cytoskeletal structural proteins including; laminin (LAM), β-dystroglycan (β-DGC), δ-sarcoglycan (δ-SGC), dystrophin (DYS), dystrobrevin (DBVN), syntrophin (SYTN), desmin (DES) and talin (TAL). (**C**) Phosphorylated (Ser473) and total Akt were probed for as an indicator of mammalian target of rapamycin Complex 2 (mTORC2) activity. (**D**) Ankrd2 was probed for as a marker of mechano-sensitvit. (**E**) Representative images for phosphorylated Akt^{Ser473}, total Akt and Ankrd2 displayed. Protein expression was normalised to total protein derived from Coomassie Brilliant Blue (CBB) staining and presented relative to vehicle (VEH) control group. * = $p < 0.05$; $n = 4$ for VEH and $n = 6$–8 for 5FU and 5FU+BGP groups for Western blotting. Data are mean ± SEM.

Given our evidence that 5FU reduced desmin and dystrophin expression and Akt^{Ser473} phosphorylation, we investigated potential changes to the mechano-sensitive protein, ankyrin repeat domain protein 2 (Ankrd2), a member of Muscle Ankyrin Repeat Domain (MARP) family of titin filament-based stress response proteins [33]. Ankrd2 could be a target of chemotherapy within skeletal muscle since it is responsive to oxidative stress, a key mechanism of chemotherapy-induced muscle wasting. We demonstrated that 5FU treatment did not affect Ankrd2 protein expression (Figure 3D,E). However, 5FU+BGP treatment increased Ankrd2 expression relative to VEH ($p < 0.05$, Figure 3D,E). These data

suggest that BGP-15 may be promoting a futile adaptive stress response that enhances mechano-sensitivity, despite the perturbed cytoskeletal environment. Full-length blots are provided in Figure S1 and densitometry summary data are provided in Table S2.

2.3. Assessment of Skeletal Muscle Stress Signalling

Since 5FU has been shown to potently activate p38-MAPK signalling [19], we wanted to assess the effect of 5FU and 5FU+BGP treatment on p38-MAPK and other molecular markers of skeletal muscle stress signalling. Consistent with the literature, 5FU treatment increased the phosphorylation of p38; ($p < 0.05$, Figure 4A,E). However, the phosphorylation of other MAPK family members, ERK1/2 or JNK, were not affected (Figure 4B,C,E). Importantly, 5FU+BGP-15 treatment completely mitigated the 5FU-induced increase in p38 phosphorylation ($p < 0.05$, Figure 4A,E). Furthermore, and consistent with BGP-15′s reported role as a suppressor of MAPK activity [28], 5FU+BGP-15 reduced basal levels of ERK1/2 and JNK phosphorylation relative to 5FU treatment ($p < 0.05$, Figure 4B,C,E). 5FU also increased the phosphorylation of the p65 subunit of NF-κB, a transcriptional mediator of pro-inflammatory genes [34], and this was inhibited by co-treatment with BGP+15 ($p < 0.05$, Figure 4D,E). Full-length blots are provided in Figure S2 and densitometry summary data are provided in Table S2.

2.4. Assessment of Skeletal Muscle Oxidative Capacity and Mitochondrial Dynamics

Next, we examined skeletal muscle oxidative capacity and markers of mitochondrial dynamics, as previously we have shown in vitro that 5FU reduces mitochondrial viability in C2C12 myoblast and myotubes [20]. Further, BGP-15 adjunct therapy alongside the anti-cancer agent, IRI, increased mitochondrial density and oxidative metabolism [12]. Interestingly, skeletal muscle oxidative capacity, as measured histologically via SDH staining, was not affected by 5FU and 5FU+BGP treatment (Figure 5A–C). 5FU treatment did not affect mitochondrial content as measured by CS activity (Figure 5D), although 5FU+BGP-15 treatment enhanced CS activity compared to VEH ($p < 0.05$, Figure 5D). We thought this may occur through the proposed mechanistic targets of BGP-15, i.e., HSP-70 co-induction or PARP-1 inhibition [23,24], which augment mitoprotection [25,26]. However, we demonstrated that there was no change to the protein expression of HSP-70 or PARP-1 from 5FU or 5FU+BGP treatment (Figure 5E,F,H). Next, we evaluated molecular markers of mitochondrial dynamics, including mitochondrial biogenesis, i.e., mitochondrial transcription factor A (TFAM) and peroxisome proliferator-activated receptor-gamma coactivator-1 (PGC-1) isoforms α and β, and mitochondrial fusion, i.e., optic atrophy 1 (OPA1), and fission, i.e., dynamin-related protein 1 (DRP1). There were no changes to TFAM, PGC-1α, PGC-1β and DRP-1 from 5FU or 5FU+BGP treatment (Figure 5G,H), but there was a significant increase in OPA-1 protein expression from 5FU+BGP treatment compared to VEH, with no change pertaining to 5FU treatment (Figure 5G,H). This suggests that the increase in mitochondrial content with 5FU+BGP may, in part, be a result of enhanced mitochondrial fusion, a reported pleiotropic effect of BGP-15 [35]. Full-length blots are provided in Figure S2.

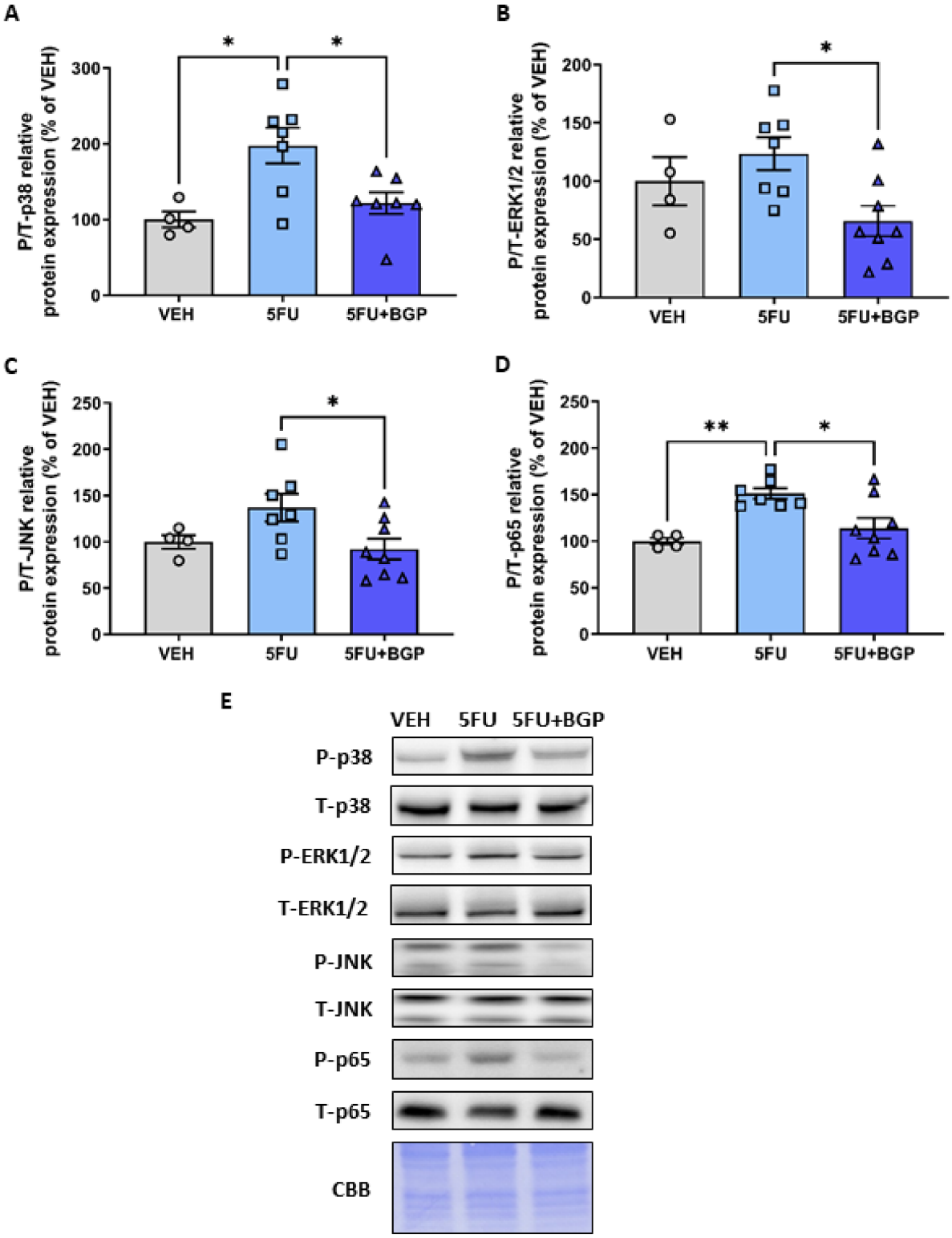

Figure 4. The effect of 5-fluorouracil (5FU) and 5FU with BGP-15 (5FU+BGP) treatment on molecular markers of cellular stress. Western blotting experiments were undertaken on tibialis anterior muscle homogenate. Samples were probed for (**A**) phosphorylated (Thr180/Tyr182) and total p38, (**B**) phosphorylated (Thr202/Tyr204) and total ERK1/2, (**C**) phosphorylated (Thr183/Tyr185) and total JNK, (**D**) phosphorylated (Ser536) and total NF-κB subunit protein p65. Data are presented as phosphorylated to total protein ratios and normalised to total protein derived from Coomassie Brilliant Blue (CBB) staining and expressed as a relative percentage of the vehicle (VEH) control grou (**E**) Western blotting and CBB representative images are displayed. * = $p < 0.05$; $n = 4$ for VEH and $n = 6$–8 for 5FU and 5FU+BGP groups. Data are mean ± SEM. ** = $p < 0.01$.

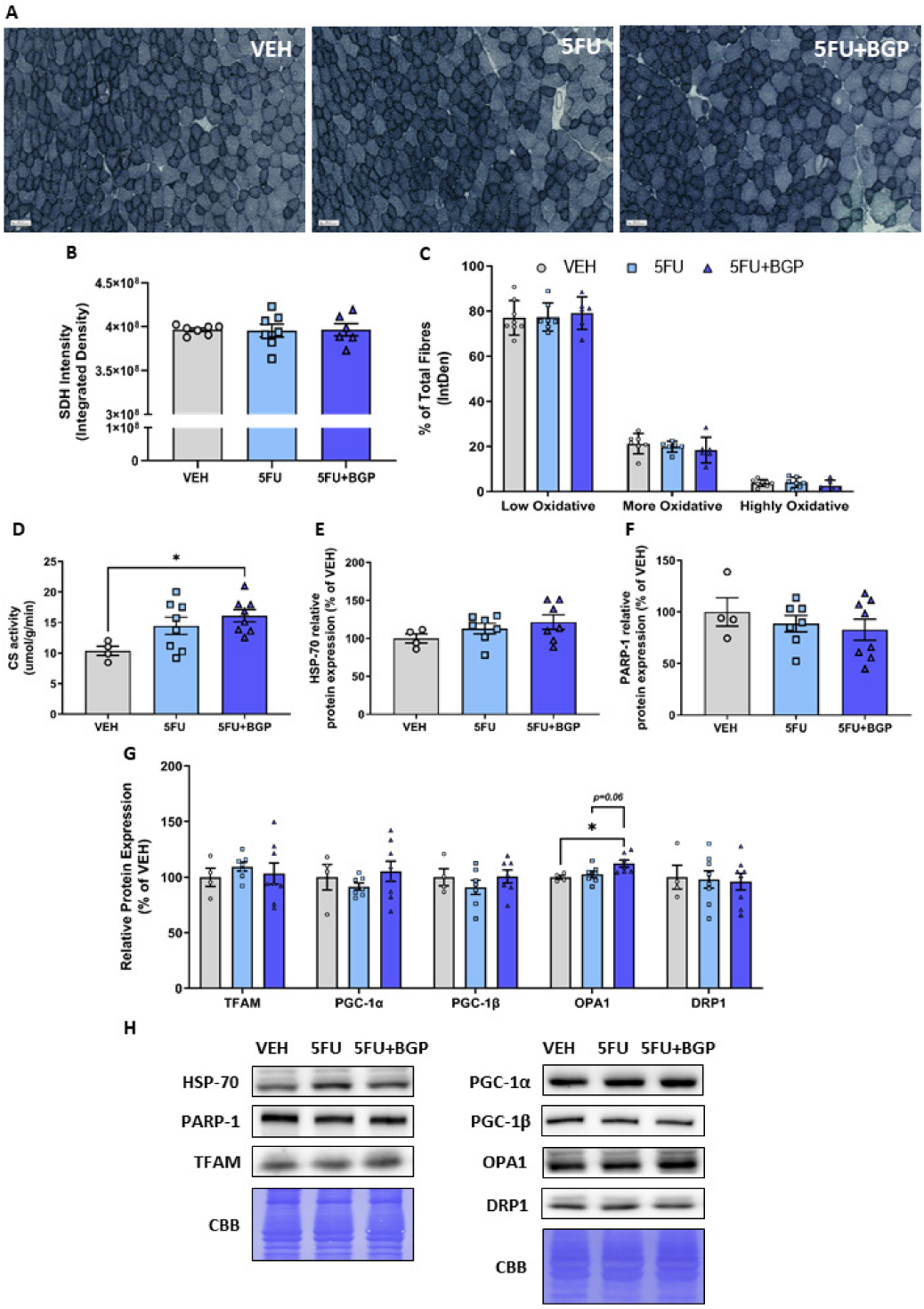

Figure 5. The effect of 5-fluorouracil (5FU) and 5FU with BGP-15 (5FU+BGP) treatment on skeletal muscle oxidative capacity and mitochondrial dynamics signalling. Succinate dehydrogenase (SDH) staining was performed on tibialis anterior (TA) cross-sections. (**A**) SDH representative images displayed, with data presented as (**B**) overall SDH intensity and (**C**) SDH intensity separated based on oxidative fibre phenotype, i.e., low oxidative, more oxidative and highly oxidative. TA muscle homogenate was analyzed for (**D**) citrate synthase (CS) activity, as a marker of mitochondrial density. Further, TA homogenate was utilized in Western blotting experiments with samples probed for (**E**) HSP-70, (**F**) PARP-1 and (**G**) a suite of proteins related to mitochondrial dynamics including; TFAM, PGC-1α, PGC-1β, OPA1 and DRP1. Protein expression was normalised to total protein derived from Coomassie Brilliant Blue (CBB) staining and presented relative to vehicle (VEH) control group. (**H**) Western blotting and CBB representative images are displayed. * = $p < 0.05$; n = 6–8 for SDH histology; n = 4 for VEH and n = 6–8 for 5FU and 5FU+BGP groups for CS activity and Western blotting. Data are mean ± SEM.

2.5. Assessment of HSP-70 Expression and Cell Viability in C2C12 Myotubes

Given that we saw no change in HSP-70 protein expression in vivo, we wanted to understand some of the potential reasons for these data. Thus, we pursued an in vitro investigation utilising differentiated C2C12 myotubes to delineate the effect of BGP-15 treatment on HSP-70 expression in both a standard and 5FU-induced chemotoxic medium. Importantly, we demonstrated that BGP-15 increased HSP-70 protein expression compared to VEH ($p < 0.05$, Figure 6A). However, in a 5FU-induced chemotoxic medium, the induction of HSP-70 by BGP-15 was blunted, thus remaining unchanged from VEH (Figure 6A). Next, we assessed cell viability, through resazurin staining, confirming that 5FU treatment induced a chemotoxic environment, compared to VEH ($p < 0.05$, Figure 6B,C). BGP-15 co-treatment displayed a modest improvement in cell viability, compared to 5FU ($p < 0.05$, Figure 6B,C). However, it was still significantly reduced compared to both VEH and BGP control groups ($p < 0.05$, Figure 6B,C). These data highlight that BGP-15 elicits pleiotropic cytoprotection, that is in part, independent of HSP-70 induction, which is likely inhibited when given alongside 5FU. These data support our in vivo data, where there was also no effect of BGP-15 on HSP-70 expression. Full-length blots are provided in Figure S3.

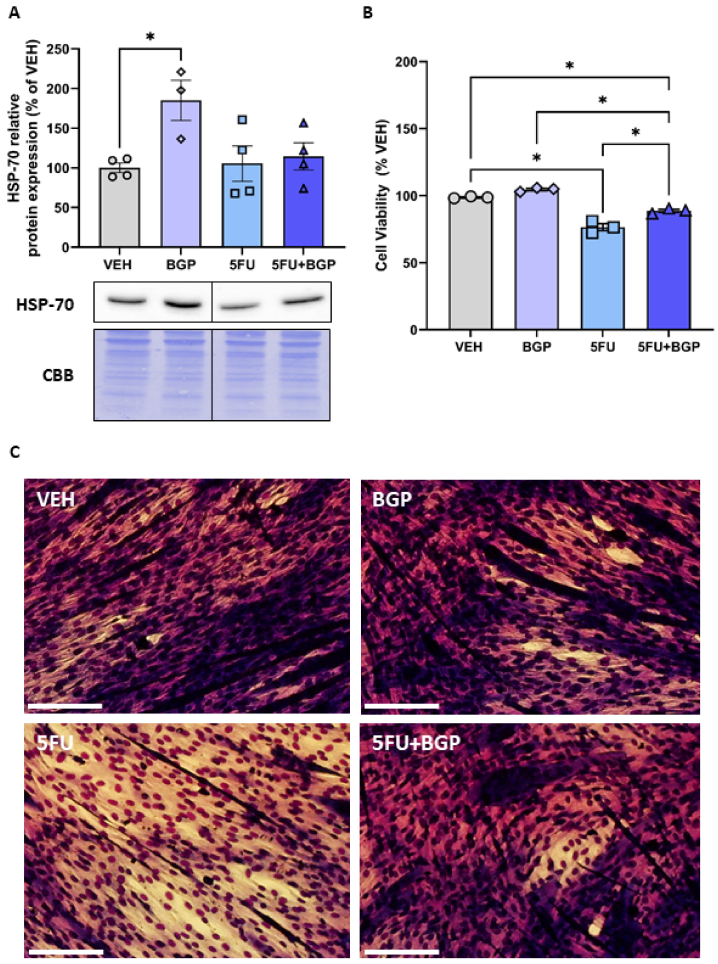

Figure 6. The effect of BGP-15 (BGP), 5-fluorouracil (5FU) and 5FU with BGP (5FU+BGP) treatment on HSP-70 expression and cell viabilityC2C12 myotubes were treated with BGP, 5FU and 5FU with BGP before being prepared as lysates for Western blotting experiments. (**A**) C2C12 lysates were then probed for HSP-70, with protein expression normalised to total protein derived from Coomassie Brilliant Blue (CBB) staining data and data presented as a percentage of the vehicle control group (VEH). (**B**) Cell viability was analyzed via the resazurin cell viability assay, with data presented as a percentage of VEH. (**C**) Representative images for the cell viability assay are displayed. Scale bar = 100 µm. * = $p < 0.05$; n = 3–4 for all C2C12 experiments. Data are mean ± SEM.

3. Discussion

The major finding of this study is that metronomic delivery of 5FU reduced the expression of key cytoskeletal proteins, desmin and dystrophin and increased the phosphorylation of p38 MAPK and NF-κB, events that are evident in other models of muscle wasting. Despite this, 5FU did not impact body composition indices or alter whole muscle mass or muscle fibre size. While our data suggest that these 5FU-mediated events are not sufficient to elicit a myopathic phenotype, they may, prime the muscle to be more susceptible to adverse effects of other constituents of multi-agent regimens, such as LV and IRI for FOLFIRI or LV and OXA for FOLFOX. Furthermore, this study found that, while BGP-15 co-therapy did not alter the 5FU-induced decrease in cytoskeletal protein abundance, it mitigated the increase in p38 MAPK and NF-κB phosphorylation, which was associated with improved mitochondrial content and fusion dynamics. Together these data suggest that while 5FU primes the muscle for myopathy, BGP-15 has pleiotropic cytoprotectant functions that protect against the activation of this molecular stress signature.

5FU treatment reduced the expression of key cytoskeletal proteins, desmin, an intermediate filament that provides stability to sarcomeres, and dystrophin, a large protein that connects the actin cytoskeleton to the sarcolemma, with the potential to compromise the structural organization of skeletal muscle and alter intracellular signalling. Previously, we have demonstrated that chemotherapeutic agent, IRI, also reduces dystrophin expression, which was associated with reduced Akt^{Ser473} phosphorylation, a direct substrate of kinase mTORC2 [12,31]. Phosphorylation of Akt^{Ser473} is a putative indicator of plasma membrane homeostasis and cytoskeletal organization [32]. As such, our finding of reduced Akt^{Ser473} phosphorylation concomitant with a reduced desmin and dystrophin protein expression, suggests that 5FU may have disrupted sarcolemmal homeostasis, cytoskeletal organization and intracellular signalling. Consistent with our previous findings, BGP-15 adjuvant therapy was not protective against the chemotherapy-induced reduction in the expression of cytoskeletal proteins [12]. Desmin and dystrophin-related myopathies are often associated with debilitating dysfunction [36,37] and myopathy is compounded in desmin and dystrophin double-knockout mice, which manifest a remarkable dystrophic phenotype with profound deterioration of sarcomere organisation and Z-line alignment [38]. Our data suggest that a critical level of desmin and dystrophin loss must occur before there is evidence of functional and structural alterations. Indeed, Baretto et al. showed that when administered over a longer duration (twice a week for 5 consecutive weeks), the 5FU-based FOLFIRI regimen reduced skeletal muscle function concurrent with aberrant skeletal muscle morphology [11], highlighting a temporal component to observing loss of function from metronomic delivery of chemotherapeutic agents. It would be of interest in future studies to evaluate the expression of key cytoskeletal proteins and sarcomere morphology in response to 5FU treatment longitudinally, to determine whether the muscles can recover or whether they retain a propensity for myopathy, which may be exacerbated, for example, by mechanical stressors such as exercise. Interestingly, we demonstrated novel evidence that BGP-15 adjuvant therapy promotes the expression of mechano-sensitive *MARP* family member, Ankrd2 [39]. We hypothesize that BGP-15 is escalating an adaptive stress response targeting tension dynamics by enhancing mechano-sensitivity within the reduced desmin and dystrophin environment. Since Ankrd2 is localized to titin filaments and Ankrd2 abundance is similarly increased in a conditional titin knockout mouse model [40], it is possible that increased mechano-sensitivity and remodelling of titin dynamics are an additional pleiotropic effect of BGP-15, which, although not warranted in this study because 5-FU did not impact contractile function, contributes to its protective effect against loss of muscle function with other chemotherapeutic agents [12].

Chemotherapeutic agents, irrespective of class, induce the activation of p38 MAPK signalling as a function of their cytotoxic nature [41]. We demonstrated that 5FU treatment increased the phosphorylation of p38 MAPK in skeletal muscle, which was consistent with findings from Barreto et al. where 5FU, administered as a constituent of the FOLFIRI chemotherapy regimen, led to enhanced p38 MAPK activity [11]. Contrary to the FOLFIRI

regimen, neither ERK1/2 nor JNK phosphorylation were increased by 5FU treatment [11]. MAPKs have been shown to exhibit specific time- and dose-dependent profiles during oxidative stress in C2C12 myoblasts [16]. Thus, we cannot rule out that ERK1/2 and JNK could have been activated at an earlier timepoint. Additionally, it is well acknowledged that p38 MAPK is positively associated with the NF-κB complex, with both targets activated in response to oxidative stress [16] and mediators of inflammatory cytokine production [19,42], although NF-κB signalling is purported to have a greater role in skeletal muscle wasting conditions (for extensive review [34]). Indeed, we showed that 5FU-induced p38 MAPK activation was associated with an increase in the phosphorylation of NF-κB subunit protein, p65, an event depicting transactivation of NF-κB, which is essential for enhancing its transcriptional activity [43]. Damrauer et al. similarly demonstrated that anti-cancer agent, cisplatin, enhances NF-κB transcriptional activity through stimulating the DNA-heterodimerization of subunits p50 and p65 in C2C12 myotubes [15]. However, chemotherapy-induced NF-κB activity in vitro reduced myotube diameter [15], while in the current study, we saw no evidence of skeletal muscle atrophy. This suggests the magnitude and persistency of NF-κB activity is important for atrophy induction, as the metronomic regimen used in our study was protective of skeletal muscle mass. Interestingly, BGP-15 mitigated the 5FU-induced increase in the phosphorylation of p38 MAPK and NF-κB subunit protein p65 in our study. Further, BGP-15 reduced the phosphorylation of MAPKs ERK 1/2 and JNK relative to 5FU. This is consistent with findings from Sarszegi et al., where BGP-15 suppressed MAPK phosphorylation, which was enhanced during imatinib (tyrosine kinase inhibitor)-induced cardiotoxicity [30]. While it is unsurprising that BGP-15 acted as a repressor of MAPK activity, it is novel that BGP-15 also inhibited the 5FU-induced activation of NF-κB. These data could suggest a negative feedback mechanism, since 5FU-induced p38 MAPK phosphorylation in vitro has previously been shown to enhance the production of inflammatory cytokines, IL-6, TNF-α and IL-1β [19], which are known stimulants of NF-κB activity [42]. Future studies are required to confirm that 5FU-induced phosphorylation of p38 MAPK and NF-κB subunit protein, p65, enhances inflammatory cytokine production and that BGP-15 has an anti-inflammatory effect in this context.

In this study, we observed no evidence of 5FU-induced alterations to oxidative capacity, mitochondrial content or mitochondrial dynamics signalling, suggesting that 5FU may require other cytotoxic-agents (e.g., the FOLFIRI regimen [11]) to perturb mitochondrial activity in vivo. This is in contrast to in vitro models where we have shown that 5FU induces mitochondrial stress in cultured C2C12 myoblasts and myotubes [20], where direct and persistent interaction between 5FU and muscle cells appears more impactful. Consistent with previous findings, we demonstrated that BGP-15 increases mitochondrial density when administered alongside chemotherapy [12]. However, in contrast, we did not observe a BGP-15-induced inhibition of PARP-1 expression in this study. Further, we did not detect a change in HSP-70 expression in vivo at the time of tissue collection, although, we did find that the addition of BGP-15 to 5FU-treated C2C12 myotubes blunted the induction of HSP-70. We hypothesize that 5FU enhances the production of pro-inflammatory cytokines [19], which have been shown to act as repressors to heat shock factor-1 transcription, inhibiting the HSP-70 adaptive stress response [44,45]. This has led our laboratory, and others, to postulate that BGP-15 acts as a cytoprotectant in response to chemical or disease-induced stress, with the underlying protective mechanisms inconsistent and largely dependent on the challenge elicited by a given stressor [27,46]. It is considered that BGP-15 may elicit cytoprotection through pleiotropic mechanisms that regulate mitochondrial quality control [47]. Indeed, we showed that BGP-15 adjuvant therapy did not affect mitochondrial biogenesis or fission signalling but did consistently promote mitochondrial fusion signalling through increased OPA1 expression (compared to VEH), which was associated with enhanced mitochondrial density.

An important, yet paradoxical, finding of this study was that 5FU treatment did not elicit any consequences on body composition indices, skeletal muscle mass or function,

despite the alterations to skeletal muscle stress signalling (i.e., p38 and NF-κB phosphorylation) that are usually associated with the induction of chemotherapy-induced cachexia and skeletal myopathy [11,15]. The lack of change to these physiological parameters from 5FU treatment may be due to the metronomic delivery of chemotherapy, which typically elicits less systemic toxicity than administration of single maximum tolerable dose (MTD) bolus or sequential daily treatments [48,49]. Metronomic delivery could activate an adaptive hormetic response which prevents the induction of skeletal myopathy in the face of low-grade stress signalling. Interestingly, when comparing to models that deliver 5FU sequentially in a shorter and more intense regimen, such as the one used in VanderVeen et al., i.e., 35 mg/kg once daily for 5 days (175 mg/kg cumulative), body mass was reduced, but there was no impact on skeletal muscle mass [13]. Further, Chen et al. utilised a similar regimen, i.e., 40 mg/kg once daily for 4 days (160 mg/kg cumulative), where there was evidence of a latent loss of body and skeletal muscle mass when harvested 4 days post final 5FU injection [14]. This highlights that 5FU-induced changes to muscle mass are dependent on the intensity of regimen and require a certain temporal component before they are physiologically exhibited. This concept is mirrored by functional studies, in which metronomic delivery of 5FU did not affect whole body grip strength but did when delivered in a short and intense regimen [50]. Given these data, we believe that metronomic 5FU may prime skeletal muscle with the molecular signature for myopathy without exerting a great enough challenge to result in physiological consequences.

There were some limitations to the study presented. Here, we utilised 6-week-old mice and treated them over 2 weeks, up to 8 weeks of age. Mice are generally considered to approach a plateau of their growth phase at 8 weeks of age, thus we treated them during this development period before measuring the impact of our interventions at sexual maturity. This might contribute to the outcome of the data, compared to conducting these interventions on sexually mature mice. However, both paediatric and adult cancer patients receive chemotherapy, and can each be impacted by cachexia. Further investigation is warranted in this model, with particular emphasis on a time-course study, involving both short-term and long-term experimental endpoints to investigate the temporal nature of the suite of proteins measured alongside the physiological parameters.

4. Materials and Methods

4.1. Animals

4.1.1. Ethical Approval

All experimental procedures were approved by the Victoria University Animal Ethics Committee (AEETH15/006) and conformed to the Australian Code of Practice for the Care and Use of Animals for Scientific Purposes.

4.1.2. Experimental Design and Treatments

Six week old male Balb/c mice were acquired from the Animal Resource Centre (ARC, Murdoch, WA, Australia) and randomly allocated to treatment groups (n = 8) upon arrival. Mice were housed on a 12 h light/dark cycle with ad libitum access to food (AIN-93G, Speciality Feeds, Glen Forrest, WA, Australia) and water supply throughout the experiments. Mice were administered either vehicle (VEH; 10% dimethyl sulfoxide (DMSO) in sterile water), 5-fluorouracil (5FU; 23 mg/kg (Sigma Aldrich, North Ryde, Australia) dissolved in 10% DMSO) or BGP-15 adjuvant therapy with 5FU (5FU+BGP; 15 mg/kg (BGP-15 donated by N-gene R&D, Australia) dissolved in 10% DMSO). The 5FU dose and regimen were used by us previously [51,52] and were effective at offsetting chemotoxicity symptoms associated with irinotecan treatment in skeletal muscle [12]. Treatments were administered via intraperitoneal injection 6 times over a 15 day period (i.e., on day 1, 3 5, 8, 10 and 12), resulting in a cumulative dose of 138 mg/kg and 90 mg/kg, of 5FU and BGP-15, respectively. The dosage and frequency of 5FU administration, with and without BGP-15, was based on previous published studies by us and our collaborators [12,51]. Repetitive chemotherapy dosing at set intervals (i.e., metronomic delivery) is compatible

with the clinical treatment of cancer in contrast to the administration of a single bolus maximum tolerated dose that is often investigated in basic science: we have discussed this approach extensively before [48]. The selected dose is equivalent to the standard human dose per body surface area [53], and has proven efficacy in mouse models of cancer [54] and elicits toxicity in other physiological systems [51,52]. The BGP-15 dose was shown to elicit skeletal muscle protection against chemotoxicity by us previously [12,29].Animals were weighed prior to the commencement of treatment (pre), on each day of treatment and at the experimental endpoint (post).

4.2. Body Composition

Echo Magnetic Resonance Imaging (echoMRI) was utilized to assess the effect of 5FU treatment and BGP-15 co-therapy on body composition indices of lean and fat mass. Live mice were placed into an echoMRI body composition analyzer (EMR-150, Echo Medical Systems, Houston, TX, USA) on day 1 (pre) and day 15 (post) of the treatment protocol, as previously described [48]. Lean and fat mass was quantified via triplicate scans spaced 30 s apart and reported as the mean of these triplicate scans.

4.3. Surgery

At the conclusion of the treatment regimen and following the final echoMRI scan, mice were deeply anaesthetised via isoflurane inhalation, before non-recovery surgery commenced. Muscles of interest were surgically excised for ex vivo analysis in the following order: (1) right *extensor digitorum longus* (EDL) and *soleus* (SOL) muscles for the assessment of contractile properties; (2) right *tibialis anterior* (TA) muscles were harvested and immediately snap-frozen for Western blotting experiments; (3) left TA muscles were weighed and prepared for histological assessment prior to snap-freezing. The remaining tissues were then harvested (i.e., the left EDL and SOL), weighed and snap-frozen.

4.4. Ex Vivo Skeletal Muscle Contractile Function

Ex vivo evaluation of skeletal muscle contractile properties were performed as previously described by us [12,55], using the predominantly fast-twitch muscle, EDL and the predominantly slow-twitch muscle, SOL. Briefly, muscles were tied with 4.0 surgical silk thread, dissected from the hindlimb and attached to a transducer in individual organ baths of a Myodynamics Muscle Strip Myograph System (DMT, Aarhus, Denmark). Each organ bath was filled with Krebs solution (118 mM NaCl, 1 mM $MgSO_4.7H_2O$, 4.75 mM KCl, 1 mM Na_2HPO, 2.5 mM $CaCl_2$, 24 mM $NaHCO_3$ and 11 mM glucose; pH 7.4) bubbled with carbogen (5% CO_2 in O_2) and maintained at a temperature of 30 °C. Data were collected and analyzed using LabChart Pro version 8.0 software (ADInstruments, Dunedin, New Zealand). Supramaximal stimulations were delivered by flanking electrodes. Optimal length (L_o) was established through sequential twitch contractions with incremental stretch, with peak twitch force (P_t) derived at L_o. Peak tetanic force (P_o) was obtained by delivering pulse trains at 350msec and 500msec for the EDL and SOL, respectively at increasing frequencies. Twitch to tetanus ratio (P_t/P_o) was assessed as an indicator of elasticity/stiffness. Specific force (sP_o) was obtained by normalising force to the physiological cross-sectional area (pCSA) as previously described [56].

4.5. Skeletal Muscle Histology

All histological experiments were completed as previously described [12,29]. To determine whether 5FU had atrophic effects on skeletal muscle and, subsequently, whether BGP-15 co-therapy could rescue any atrophy, we histologically assessed TA muscles which were cryopreserved in optimal cutting temperature compound (Sakura Finetek, Torrance, CA, USA). TA's were sectioned (10 µm, −20 °C, Leica CM1950) and mounted onto glass slides, then stained with haematoxylin and eosin (H&E), for muscle fibre size analysis, and succinate dehydrogenase (SDH), as an indicator of oxidative capacity. H&E-stained slides were processed on a Zeiss Axio Imager Z2 microscope (Carl Zeiss MicroImaging

GmbH, Göttingen, Germany), and imaged at 50x magnification, with analysis conducted as described previously [57]. SDH slides were processed the same way and imaged at 20x magnification. SDH images were analyzed in two ways: first, the whole cross-section of the TA was circled and the intensity density of the SDH stain was assessed using ImageJ; and second, the staining intensity of 600 individual fibres was measured using ImageJ with the maximum intensity density identified and used to determine a bottom, middle and top third. The percentage of fibres that fell into each third was determined and the data displayed as less oxidative (bottom third), more oxidative (middle third) and highly oxidative (top third).

4.6. Western Blotting Analyses

Western blotting was utilised to explore the effect of 5FU treatment and BGP-15 co-therapy on molecular signalling pathways surrounding cell stress, mitochondrial biogenesis and cytoskeletal structural proteins. All Western blotting protocols were completed as previously described [12]. Frozen TA muscles were homogenized using an Omni Tissue Homogenizer (TH220, Omni International, Kennesaw, GA, USA) for 20 s in ice-cold Western Immunoprecipitation Kinase (WIK) buffer (40 mM Tris, pH 7.5; 1 mM EDTA; 5 mM EGTA; 0.5% TritonX-100; 25 mM β-glycerophosphate; 25 mM NaF; 1 mM Na3VO4; 10 g/ml leupeptin; and 1 mM PMSF). Muscle homogenate was centrifuged at 3500 rpm for 5 minutes at 4 °C, before the pellet was resuspended and the muscle homogenate was frozen for future analysis. Protein concentrations were determined using a DC assay kit (Bio-Rad Laboratories, Hercules, CA, USA), to ensure equal loading on the gels. Samples were prepared with equivalent amounts of protein in either 2X SDS sample buffer (20% (*v*/*v*) glycerol; 100 mM Tris-Base, pH 6.8; 4% (*w*/*v*) SDS; 0.017% (*w*/*v*) bromophenol blue; 0.25 M dithiothreitol (DTT)), heated for 5 minutes at 95 °C, and subjected to electrophoretic separation on 7.5–12% SDS-acrylamide gels. Following electrophoretic separation, proteins were transferred to PVDF membrane, blocked with 5% not-fat milk powder in Tris-buffered saline containing 0.1% Tween 20 (TBST) for 1 hour followed by an overnight incubation at 4 °C with primary antibody dissolved in TBST containing either 1% BSA or 3% non-fat milk powder. The following primary antibodies were used: anti-phospho Akt^{Ser473} (1:3000; #4060; Cell Signalling Technology (CST)), anti-Akt (1:2000; #4691; CST), anti-Ankrd2 (1:1000; #11821-1-AP; Proteintech), anti-β-Dystroglycan (1:1000; MANDAG2 (7 D11); DSHB), anti-δ-Sarcoglycan (1:1000; ab137101; Abcam), anti-Desmin (1:1000; #5332; CST), anti-Dystrobrevin (1:500; #610766; BD Biosciences), anti-Dystrophin (1:500; ab15277; Abcam), anti-phospho ERK1/2 (1:750; #9101; CST), anti-ERK1/2 (1:1000; #9102; CST), anti-DRP1 (1:1000; #8570; CST), anti-HSP-70 (1:1000; ADI-SPA-812; Enzo Life Sciences), anti-phospho JNK (1:750; #4668; CST), anti-JNK (1:1000; #9252; CST), anti-Laminin (1:2000; L9393; Sigma-Aldrich), anti-OPA1 (1:1000; #80471; CST), anti-phospho p38 (1:750; #4511; CST), anti-p38 (1:1000; #9212; CST), anti-phospho p65 (1:750; #3033; CST), anti-p65 (1:1000; #8242; CST), anti-PARP-1 (1:1000; #9542, CST), anti-PGC-1α (1:1000; AB3242; Sigma-Aldrich), anti-PGC-1β (1:1000; ab176328; Abcam), anti-syntrophin (1:750; MA1-745; Invitrogen), anti-talin (1:200; T3287; Merck-Millipore) and anti-TFAM (1:3000; ab131607; Abcam). After overnight incubation, membranes were washed 3 separate times for 10 minutes each in TBST and then probed with a horseradish peroxidase-conjugated secondary antibody (1:5000; anti-rabbit IgG or 1:20,000; anti-mouse IgG, Vector Laboratories) in 5% not-fat milk powder in TBST for 1 hour at room temperature. Following another set of 3 separate 10-minute washes in TBST, the blots were developed with a DARQ CCD camera mounted to a Fusion FX imaging system (Vilber Lourmat, Eberhardzell, Germany) using ECL Clarity reagent (Biorad, Hercules, CA, USA). Once images were captured, the membranes were stained with Coomassie Blue and then normalised to total protein. Densitometric measurements were carried out using FusionCAPTAdvance software (Vilber Lourmat, Eberhardzell, Germany).

4.7. Citrate Synthase Activity

Citrate Synthase (CS) activity was measured as a marker of mitochondrial density [58]. Homogenized TA muscles in WIK buffer (as described above) were added to the reagent cocktail (100 mM Tris Buffer, 1 mM DTNB, 3 mM Acetyl CoA) and to initiate the reaction, oxaloacetate (10 mM) was added just prior to measuring CS activity spectrophotometrically (412 nm, 25 °C, 5 min). CS activity was calculated using the extinction coefficient of 13.6 [59] and expressed relative to muscle wet weight.

4.8. Cell Culture Experiments

4.8.1. C2C12 Cell Culture

C2C12 myoblasts (ATCC) were cultured and maintained in Dulbecco's modified Eagle's medium (DMEM) supplemented with 10% foetal bovine serum (FBS), 1% antibiotic/antimycotic, 1% Glutamax, and 1 mM sodium pyruvate (all cell culture reagents were purchased from Gibco Invitrogen, Carlsbad, CA, USA). Cells were incubated at 37 °C with 5% CO_2. To induce differentiation, cells were plated at high confluence (~90%) and changed to differentiation medium (supplemented DMEM containing 2% horse serum). Cells were maintained in differentiation medium for 4–5 days to form myotubes before commencing drug treatments. Differentiated myotubes were treated with vehicle control (VEH; DMSO), BGP-15 control (BGP; 100 mM), 5FU (1 mM) and the 5FU+BGP combination for 24 h prior to assays and protein collection.

4.8.2. Protein Collection

Cells were lysed and collected for Western blotting in radio immunoprecipitation buffer (RIPA; 1 mM EDTA, 0.5 mM EGTA, 10 mM Tris-HCl, 140 mM sodium chloride, 10% sodium deoxycholate, and 1% triton-X 100) containing protease and phosphatase inhibitors (Sigma Aldrich, St. Louis, MO, USA). The lysates were centrifuged at 13,000 rpm at 4 °C for 30 minutes. The supernatants were collected and stored at −80 °C and the pellets discarded. Western blotting was performed as described above.

4.8.3. Resazurin Cell Viability Assay

Confluent myotubes were treated with drugs of interest for up to 24 h in differentiation medium prior to resazurin viability assay (Sigma Aldrich, St. Louis, MO, USA) measurements. The resazurin assay solution was prepared at a 1:10 dilution of resazurin in DMEM differentiation medium. Once the dye was added the plates were shielded from light and stored at 37 °C with 5% CO_2 for two hours. Following the incubation period, the supernatant was transferred to an opaque 96 well plate for fluorometric reading (at 560 nm; Varioskan Flash plate reader) using SkanIt RE software (Thermo Fisher, Waltham, MA, USA). Plates containing myotubes were rinsed with ice cold PBS and fixed with 100% methanol, followed by Diff-Quick staining (Histolabs, Kew East, Australia). Plates were left to dry overnight prior to imaging with an Olympus IX81 microscope (Olympus, Tokyo, Japan) to observe morphological changes.

4.9. Statistics

Data are presented as the mean ± standard error of the mean (SEM). Data were analyzed using Graphpad prism v9 (GraphPad Software, San Diego, CA, USA). A one-way ANOVA was utilised to detect treatment differences for parametric data, while a two-way repeated measures ANOVA was used to detect differences between treatment and stimulation frequency/time for force–frequency relationships. Tukey's post hoc test was utilised for multiple comparisons testing, with an α-value of 0.05 considered significant.

5. Conclusions

This is the first study to demonstrate that metronomic delivery of 5FU reduces the expression of desmin and dystrophin, which is not affected by BGP-15. However, BGP-15 mitigated the 5FU-induced increase in p38 and NF-κB phosphorylation, which was associ-

ated with BGP-15 increasing mitochondrial density and fusion dynamics. Paradoxically, metronomic delivery of 5FU did not impact body composition indices, nor skeletal muscle mass and function. These findings suggest that the metronomic delivery of 5FU may prime skeletal muscle with a molecular signature for myopathy but does not exert a great enough challenge to result in physiological consequences within the treatment duration employed in this study. Overall, these data highlight novel mechanisms surrounding the impact of 5FU treatment and BGP-15 adjuvant therapy on skeletal muscle, supporting the need for further investigation, particularly in cancer-burdened mice to enhance the translational potential of the dataset.

Supplementary Materials: The following are available online at https://www.mdpi.com/article/10.3390/ph14050478/s1, Table S1: Organ to body mass ratios, Figure S1: Full-length Western blot images relating to the skeletal muscle homogenate data presented in Figure 3, Figure S2: Densitometry summary data from representative Western blot images, Table S2 Densitometry summary data from representative Western blot images, Figure S3: Full-length Western blot images relating to the C2C12 myotube cell lysate data presented in Figure 6.

Author Contributions: Conceptualization, E.R., D.G.C., and A.C.P.; methodology, D.G.C., C.A.T., T.C., C.A.G., A.H. and E.R.; validation, D.G.C., and T.C.; formal analysis, D.G.C., C.A.T., and T.C.; investigation, D.G.C. and T.C.; resources, E.R., C.A.G. and A.H.; data curation, D.G.C., E.R. and C.A.G.; writing—original draft preparation, D.G.C.; writing—review and editing, E.R., C.A.G., A.H. and C.A.T.; visualization, D.G.C. and E.R.; supervision, E.R., C.A.G. and A.H.; project administration, E.R.; funding acquisition, E.R., A.H. and A.C.P. All authors have read and agreed to the published version of the manuscript.

Funding: This study was funded by the former Institute of Sport, Exercise and Active Living, and Centre for Chronic Disease, program grants (both Victoria University).

Institutional Review Board Statement: The study was conducted according to the Australian Code of Practice for the Care and Use of Animals for Scientific Purposes (National Health and Medical Research Council (Australia)) and was approved by the Victoria University Animal Ethics Committee (AEETH15/006).

Informed Consent Statement: Not applicable.

Data Availability Statement: There are no archived digitally archived data sets associated with this manuscript.

Acknowledgments: The authors wish to acknowledge research assistant Nancy Pompeani and students Jordan Cook and James Sorensen who contributed to preliminary data acquisition. We would like to thank N-Gene technologies for kindly donating BGP-15. We would also like to acknowledge the Developmental Studies Hybridoma Bank (DSHB) for the use of the β-dystroglycan (MANDAG2(7D11)) antibody developed by Morris, G.E. (Wolfson Centre for Inherited Neuromuscular Disease, RJAH Orthopaedic Hospital, Oswestry, UK), which was obtained from the DSHB, created by the NICHD of the NIH and maintained at The University of Iowa, Department of Biology, Iowa City, IA 52242.

Conflicts of Interest: Dean Campelj, Cara Timpani, Tabitha Cree, Aaron Petersen, Alan Hayes and Craig Goodman declare they have no conflict of interest. Emma Rybalka is a scientific consultant to Santhera Pharmaceuticals and Epirium Bio.

References

1. Sung, H.; Ferlay, J.; Siegel, R.L.; Laversanne, M.; Soerjomataram, I.; Jemal, A.; Bray, F. Global Cancer Satistics 2020: GLOBOCAN Estimates of Incidence and Mortality Worldwide for 36 Cancers in 185 Countries. *CA Cancer J. Clin.* **2021**. [CrossRef] [PubMed]
2. Baracos, V.E.; Martin, L.; Korc, M.; Guttridge, D.C.; Fearon, K.C.H. Cancer-associated Cachexia. *Nat. Rev. Dis. Primers* **2018**, *4*, 1–18. [CrossRef] [PubMed]
3. Fearon, K.; Strasser, F.; Anker, S.D.; Bosaeus, I.; Bruera, E.; Fainsinger, R.L.; Jatoi, A.; Loprinzi, C.; MacDonald, N.; Mantovani, G.; et al. Definition and Classification of Cancer Cachexia: An International Consensus. *Lancet Oncol.* **2011**, *12*, 489–495. [CrossRef]
4. Martin, L.; Birdsell, L.; Macdonald, N.; Reiman, T.; Clandinin, M.T.; McCargar, L.J.; Murphy, R.; Ghosh, S.; Sawyer, M.B.; Baracos, V.E. Cancer Cachexia in the Age of Obesity: Skeletal Muscle Depletion is a Powerful Prognostic Factor, Independent of Body Mass Index. *J. Clin. Oncol.* **2013**, *31*, 1539–1547. [CrossRef]

5. Pin, F.; Couch, M.E.; Bonetto, A. Preservation of Muscle Mass as a Strategy to Reduce the Toxic Effects of Cancer Chemotherapy on Body Composition. *Curr. Opin. Supportive Palliat. Care* **2018**, *12*, 420–426. [CrossRef]
6. Coletti, D. Chemotherapy-induced Muscle Wasting: An Update. *Eur. J. Transl. Myol.* **2018**, *28*, 7587. [CrossRef]
7. Scheede-Bergdahl, C.; Jagoe, R.T. After the Chemotherapy: Potential Mechanisms for Chemotherapy-induced Delayed Skeletal Muscle Dysfunction in Survivors of Acute Lymphoblastic Leukaemia in Childhood. *Front. Pharmacol.* **2013**, *4*, 49. [CrossRef]
8. Longley, D.B.; Harkin, D.P.; Johnston, P.G. 5-fluorouracil: Mechanisms of Action and Clinical Strategies. *Nat. Rev. Cancer* **2003**, *3*, 330–338. [CrossRef]
9. Kennedy, B.J. 5-fluorouracil Toxicity: Old or New? *Cancer* **1999**, *86*, 1099–1100. [CrossRef]
10. Prado, C.M.; Baracos, V.E.; McCargar, L.J.; Mourtzakis, M.; Mulder, K.E.; Reiman, T.; Butts, C.A.; Scarfe, A.G.; Sawyer, M.B. Body Composition as an Independent Determinant of 5-fluorouracil-based Chemotherapy Toxicity. *Clin. Cancer Res.* **2007**, *13*, 3264–3268. [CrossRef]
11. Barreto, R.; Waning, D.L.; Gao, H.; Liu, Y.; Zimmers, T.A.; Bonetto, A. Chemotherapy-related Cachexia is Associated with Mitochondrial Depletion and the Activation of ERK1/2 and p38 MAPKs. *Oncotarget* **2016**, *7*, 43442–43460. [CrossRef]
12. Campelj, D.G.; Timpani, C.A.; Petersen, A.C.; Hayes, A.; Goodman, C.A.; Rybalka, E. The Paradoxical Effect of PARP Inhibitor BGP-15 on Irinotecan-Induced Cachexia and Skeletal Muscle Dysfunction. *Cancers* **2020**, *12*, 3810. [CrossRef]
13. VanderVeen, B.N.; Sougiannis, A.T.; Velazquez, K.T.; Carson, J.A.; Fan, D.; Murphy, E.A. The Acute Effects of 5 Fluorouracil on Skeletal Muscle Resident and Infiltrating Immune Cells in Mice. *Front. Physiol.* **2020**, *11*, 1585. [CrossRef]
14. Chen, H.; Xu, C.; Zhang, F.; Liu, Y.; Guo, Y.; Yao, Q. The Gut Microbiota Attenuates Muscle Wasting by Regulating Energy Metabolism in Chemotherapy-induced Malnutrition Rats. *Cancer Chemother. Pharmacol.* **2020**, *85*, 1049–1062. [CrossRef]
15. Damrauer, J.S.; Stadler, M.E.; Acharyya, S.; Baldwin, A.S.; Couch, M.E.; Guttridge, D.C. Chemotherapy-induced Muscle Wasting: Association with NF-κB and Cancer Cachexia. *Eur. J. Transl. Myol.* **2018**, *28*, 7590. [CrossRef]
16. Kefaloyianni, E.; Gaitanaki, C.; Beis, I. ERK1/2 and p38-MAPK Signalling Pathways, through MSK1, are Involved in NF-kappaB Transactivation during Oxidative Stress in Skeletal Myoblasts. *Cell. Signal.* **2006**, *18*, 2238–2251. [CrossRef]
17. Cai, D.; Frantz, J.D.; Tawa, N.E., Jr.; Melendez, P.A.; Oh, B.C.; Lidov, H.G.; Hasselgren, P.O.; Frontera, W.R.; Lee, J.; Glass, D.J.; et al. IKKbeta/NF-kappaB Activation Causes Severe Muscle Wasting in Mice. *Cell* **2004**, *119*, 285–298. [CrossRef]
18. Li, Y.-P.; Chen, Y.; John, J.; Moylan, J.; Jin, B.; Mann, D.L.; Reid, M.B. TNF-alpha Acts via p38 MAPK to Stimulate Expression of the Ubiquitin Ligase Atrogin1/MAFbx in Skeletal Muscle. *FASEB J.* **2005**, *19*, 362–370. [CrossRef]
19. Elsea, C.R.; Roberts, D.A.; Druker, B.J.; Wood, L.J. Inhibition of p38 MAPK Suppresses Inflammatory Cytokine Induction by Etoposide, 5-fluorouracil, and Doxorubicin without Affecting Tumoricidal Activity. *PLoS ONE* **2008**, *3*, e2355. [CrossRef]
20. Rybalka, E.; Timpani, C.A.; Cheregi, B.D.; Sorensen, J.C.; Nurgali, K.; Hayes, A. Chemotherapeutic Agents Induce Mitochondrial Superoxide Production and Toxicity but do not Alter Respiration in Skeletal Muscle in Vitro. *Mitochondrion* **2018**, *42*, 33–49. [CrossRef]
21. Barreto, R.; Mandili, G.; Witzmann, F.A.; Novelli, F.; Zimmers, T.A.; Bonetto, A. Cancer and Chemotherapy Contribute to Muscle Loss by Activating Common Signaling Pathways. *Front. Physiol.* **2016**, *7*, 472. [CrossRef] [PubMed]
22. Guttridge, D.C.; Mayo, M.W.; Madrid, L.V.; Wang, C.Y.; Baldwin, A.S., Jr. NF-kappaB-induced Loss of MyoD messenger RNA: Possible Role in Muscle Decay and Cachexia. *Science* **2000**, *289*, 2363–2366. [CrossRef] [PubMed]
23. Racz, I.; Tory, K.; Gallyas, F., Jr.; Berente, Z.; Osz, E.; Jaszlits, L.; Bernath, S.; Sumegi, B.; Rabloczky, G.; Literati-Nagy, P. BGP-15-a Novel Poly(ADP-ribose) Polymerase Inhibitor-protects Against Nephrotoxicity of Cisplatin without Compromising Its Antitumor Activity. *Biochem. Pharmacol.* **2002**, *63*, 1099–1111. [CrossRef]
24. Literati-Nagy, Z.; Tory, K.; Literati-Nagy, B.; Kolonics, A.; Torok, Z.; Gombos, I.; Balogh, G.; Vígh, L., Jr.; Horváth, I.; Mandl, J.; et al. The HSP Co-inducer BGP-15 can Prevent the Metabolic Side Effects of the Atypical Antipsychotics. *Cell Stress Chaperones* **2012**, *17*, 517–521. [CrossRef]
25. Bai, P.; Canto, C.; Oudart, H.; Brunyanszki, A.; Cen, Y.; Thomas, C.; Yamamoto, H.; Huber, A.; Kiss, B.; Houtkooper, R.H.; et al. PARP-1 Inhibition Increases Mitochondrial Metabolism through SIRT1 Activation. *Cell Metab.* **2011**, *13*, 461–468. [CrossRef]
26. Henstridge, D.C.; Bruce, C.R.; Drew, B.G.; Tory, K.; Kolonics, A.; Estevez, E.; Chung, J.; Watson, N.; Gardner, T.; Lee-Young, R.S.; et al. Activating HSP72 in Rodent Skeletal Muscle Increases Mitochondrial Number and Oxidative Capacity and Decreases Insulin Resistance. *Diabetes* **2014**, *63*, 1881–1894. [CrossRef]
27. Sapra, G.; Tham, Y.K.; Cemerlang, N.; Matsumoto, A.; Kiriazis, H.; Bernardo, B.C.; Henstridge, D.C.; Ooi, J.Y.Y.; Pretorius, L.; Boey, E.J.H.; et al. The Small-molecule BGP-15 Protects Against Heart Failure and Atrial Fibrillation in Mice. *Nat. Commun.* **2014**, *5*, 5705. [CrossRef]
28. Pető, Á.; Kósa, D.; Fehér, P.; Ujhelyi, Z.; Sinka, D.; Vecsernyés, M.; Szilvássy, Z.; Juhász, B.; Csanádi, Z.; Vigh, L.; et al. Pharmacological Overview of the BGP-15 Chemical Agent as a New Drug Candidate for the Treatment of Symptoms of Metabolic Syndrome. *Molecules* **2020**, *25*, 429. [CrossRef]
29. Sorensen, J.C.; Petersen, A.C.; Timpani, C.A.; Campelj, D.G.; Cook, J.; Trewin, A.J.; Stojanovska, V.; Stewart, M.; Hayes, A.; Rybalka, E. BGP-15 Protects Against Oxaliplatin-Induced Skeletal Myopathy and Mitochondrial Reactive Oxygen Species Production in Mice. *Front. Pharmacol.* **2017**, *8*, 137. [CrossRef]
30. Sarszegi, Z.; Bognar, E.; Gaszner, B.; Kónyi, A.; Gallyas, F., Jr.; Sumegi, B.; Berente, Z. BGP-15, a PARP-Inhibitor, Prevents Imatinib-induced Cardiotoxicity by Activating Akt and Suppressing JNK and p38 MAP Kinases. *Mol. Cell. Biochem.* **2012**, *365*, 129–137. [CrossRef]

31. Sarbassov, D.D.; Guertin, D.A.; Ali, S.M.; Sabatini, D.M. Phosphorylation and Regulation of Akt/PKB by the Rictor-mTOR Complex. *Science* **2005**, *307*, 1098–1101. [CrossRef]
32. Riggi, M.; Kusmider, B.; Loewith, R. The Flipside of the TOR Coin-TORC2 and Plasma Membrane Homeostasis at a Glance. *J. Cell Sci.* **2020**, *133*. [CrossRef]
33. Miller, M.K.; Bang, M.-L.; Witt, C.C.; Labeit, D.; Trombitas, C.; Watanabe, K.; Granzier, H.; McElhinny, A.S.; Gregorio, C.C.; Labeit, S. The Muscle Ankyrin Repeat Proteins: CARP, ankrd2/Arpp and DARP as a Family of Titin Filament-based Stress Response Molecules. *J. Mol. Biol.* **2003**, *333*, 951–964. [CrossRef]
34. Li, H.; Malhotra, S.; Kumar, A. Nuclear Factor-kappa B Signaling in Skeletal Muscle Atrophy. *J. Mol. Med.* **2008**, *86*, 1113–1126. [CrossRef]
35. Szabo, A.; Sumegi, K.; Fekete, K.; Hocsak, E.; Debreceni, B.; Setalo, G., Jr.; Kovacs, K.; Deres, L.; Kengyel, A.; Kovacs, D.; et al. Activation of Mitochondrial Fusion Provides a New Treatment for Mitochondria-related Diseases. *Biochem. Pharmacol.* **2018**, *150*, 86–96. [CrossRef]
36. Blake, D.J.; Weir, A.; Newey, S.E.; Davies, K.E. Function and Genetics of Dystrophin and Dystrophin-related Proteins in Muscle. *Physiol. Rev.* **2002**, *82*, 291–329. [CrossRef]
37. Paulin, D.; Huet, A.; Khanamyrian, L.; Xue, Z. Desminopathies in Muscle Disease. *J. Pathol.* **2004**, *204*, 418–427. [CrossRef]
38. Ferry, A.; Messéant, J.; Parlakian, A.; Lemaitre, M.; Roy, P.; Delacroix, C.; Lilienbaum, A.; Hovhannisyan, Y.; Furling, D.; Klein, A.; et al. Desmin Prevents Muscle Wasting, Exaggerated Weakness and Fragility, and Fatigue in Dystrophic MDX Mouse. *J. Physiol.* **2020**, *598*, 3667–3689. [CrossRef]
39. Kemp, T.J.; Sadusky, T.J.; Saltisi, F.; Carey, N.; Moss, J.; Yang, S.Y.; Sassoon, D.A.; Goldspink, G.; Coulton, G.R. Identification of Ankrd2, a Novel Skeletal Muscle Gene Coding for a Stretch-Responsive Ankyrin-Repeat Protein. *Genomics* **2000**, *66*, 229–241. [CrossRef]
40. Swist, S.; Unger, A.; Li, Y.; Vöge, A.; von Frieling-Salewsky, M.; Skärlén, Å.; Cacciani, N.; Braun, T.; Larsson, L.; Linke, W.A. Maintenance of Sarcomeric Integrity in Adult Muscle Cells Crucially Depends on Z-disc Anchored Titin. *Nat. Commun.* **2020**, *11*, 4479. [CrossRef]
41. Boldt, S.; Weidle, U.H.; Kolch, W. The Role of MAPK Pathways in the Action of Chemotherapeutic Drugs. *Carcinogenesis* **2002**, *23*, 1831–1838. [CrossRef]
42. Thoma, A.; Lightfoot, A.P. NF-kB and Inflammatory Cytokine Signalling: Role in Skeletal Muscle Atrophy. *Adv. Exp. Med. Biol.* **2018**, *1088*, 267–279. [CrossRef] [PubMed]
43. Christian, F.; Smith, E.L.; Carmody, R.J. The Regulation of NF-κB Subunits by Phosphorylation. *Cells* **2016**, *5*, 12. [CrossRef] [PubMed]
44. Schett, G.; Steiner, C.W.; Xu, Q.; Smolen, J.S.; Steiner, G. TNFalpha Mediates Susceptibility to Heat-induced Apoptosis by Protein Phosphatase-mediated Inhibition of the HSF1/hsp70 Stress Response. *Cell Death Differ.* **2003**, *10*, 1126–1136. [CrossRef] [PubMed]
45. Wigmore, S.J.; Sangster, K.; McNally, S.J.; Harrison, E.M.; Ross, J.A.; Fearon, K.C.H.; Garden, O.J. De-repression of Heat Shock Transcription Factor-1 in Interleukin-6-treated Hepatocytes is Mediated by Downregulation of Glycogen Synthase Kinase 3beta and MAPK/ERK-1. *Int. J. Mol. Med.* **2007**, *19*, 413–420. [CrossRef]
46. Sarnyai, F.; Szekerczés, T.; Csala, M.; Sümegi, B.; Szarka, A.; Schaff, Z.; Mandl, J. BGP-15 Protects Mitochondria in Acute, Acetaminophen Overdose Induced Liver Injury. *Pathol. Oncol. Res. POR* **2020**, *26*, 1797–1803. [CrossRef]
47. Horvath, O.; Ordog, K.; Bruszt, K.; Kalman, N.; Kovacs, D.; Radnai, B.; Gallyas, F.; Toth, K.; Halmosi, R.; Deres, L. Modulation of Mitochondrial Quality Control Processes by BGP-15 in Oxidative Stress Scenarios: From Cell Culture to Heart Failure. *Oxidative Med. Cell. Longev.* **2021**, *2021*, 6643871. [CrossRef] [PubMed]
48. Campelj, D.G.; Debruin, D.A.; Timpani, C.A.; Hayes, A.; Goodman, C.A.; Rybalka, E. Sodium Nitrate Co-supplementation does not Exacerbate Low Dose Metronomic Doxorubicin-induced Cachexia in Healthy Mice. *Sci. Rep.* **2020**, *10*, 15044. [CrossRef]
49. Kerbel, R.S.; Shaked, Y. The Potential Clinical Promise of 'Multimodality' Metronomic Chemotherapy Revealed by Preclinical Studies of Metastatic Disease. *Cancer Lett.* **2017**, *400*, 293–304, [CrossRef]
50. Sougiannis, A.T.; VanderVeen, B.N.; Enos, R.T.; Velazquez, K.T.; Bader, J.E.; Carson, M.; Chatzistamou, I.; Walla, M.; Pena, M.M.; Kubinak, J.L.; et al. Impact of 5 Fluorouracil Chemotherapy on Gut Inflammation, Functional Parameters, and Gut Microbiota. *Brain Behav. Immun.* **2019**, *80*, 44–55, [CrossRef]
51. McQuade, R.M.; Al Thaalibi, M.; Petersen, A.C.; Abalo, R.; Bornstein, J.C.; Rybalka, E.; Nurgali, K. Co-treatment With BGP-15 Exacerbates 5-Fluorouracil-Induced Gastrointestinal Dysfunction. *Front. Neurosci.* **2019**, *13*, 449. [CrossRef]
52. McQuade, R.M.; Stojanovska, V.; Donald, E.; Abalo, R.; Bornstein, J.C.; Nurgali, K. Gastrointestinal Dysfunction and Enteric Neurotoxicity Following Treatment with Anticancer Chemotherapeutic Agent 5-fluorouracil. *Neurogastroenterol. Motil.* **2016**, *28*, 1861–1875. [CrossRef]
53. Reagan-Shaw, S.; Nihal, M.; Ahmad, N. Dose Translation from Animal to Human Studies Revisited. *FASEB J.* **2008**, *22*, 659–661. [CrossRef]
54. Cao, Z.; Zhang, Z.; Huang, Z.; Wang, R.; Yang, A.; Liao, L.; Du, J. Antitumor and Immunomodulatory Effects of Low-dose 5-FU on Hepatoma 22 Tumor-bearing Mice. *Oncol. Lett.* **2014**, *7*, 1260–1264. [CrossRef]
55. Hayes, A.; Williams, D.A. Long-term Clenbuterol Administration Alters the Isometric Contractile Properties of Skeletal Muscle from Normal and Dystrophin-deficient MDX Mice. *Clin. Exp. Pharmacol. Physiol.* **1994**, *21*, 757–765. [CrossRef]

56. Brooks, S.V.; Faulkner, J.A. Contractile Properties of Skeletal Muscles from Young, Adult and Aged Mice. *J. Physiol.* **1988**, *404*, 71–82. [CrossRef]
57. Timpani, C.A.; Goodman, C.A.; Stathis, C.G.; White, J.D.; Mamchaoui, K.; Butler-Browne, G.; Gueven, N.; Hayes, A.; Rybalka, E. Adenylosuccinic Acid Therapy Ameliorates Murine Duchenne Muscular Dystrophy. *Sci. Rep.* **2020**, *10*, 1125. [CrossRef]
58. Larsen, S.; Nielsen, J.; Hansen, C.N.; Nielsen, L.B.; Wibrand, F.; Stride, N.; Schroder, H.D.; Boushel, R.; Helge, J.W.; Dela, F.; et al. Biomarkers of Mitochondrial Content in Skeletal Muscle of Healthy Young Human Subjects. *J. Physiol.* **2012**, *590*, 3349–3360. [CrossRef]
59. Srere, P.A. (CoA-acetylating)]. In *Methods in Enzymology*; Academic Press: Cambridge, MA, USA, 1969; Volume 13, pp. 3–11. [CrossRef]

Part II

The impact of anti-Acute Myeloid Leukemia chemotherapy on body composition, skeletal muscle and physical activity

Chapter 5

Cachectic muscle wasting in Acute Myeloid Leukemia: A sleeping giant with dire clinical consequences

Campelj DG, Timpani CA, Rybalka E. Cachectic muscle wasting in acute myeloid leukemia: A sleeping giant with dire clinical consequences. Submitted: Journal of Cachexia Sarcopenia and Muscle; 13/05/2021

Preface

In part 2 of this thesis, we transitioned to a more clinically compatible model of chemotherapy cachexia, utilising a multi-chemotherapeutic agent regimen. This is the normal delivery modality of chemotherapy in the clinic. Utilising a multi-agent regimen allows for the effect of drug-interactions and cumulative effects to be accounted for, which is likely an under-appreciated variable in experimental models that assess the cachectic potential of mono-chemotherapeutic agents.

We were interested to understand the impact of chemotherapy for haematological cancers on muscle cachexia. While cachexia is predominately associated with signals emitted from solid-tumor cancers [33], particularly those of the gastrointestinal system and accessory organs [34-36], cachexia is also prevalent in haematological cancers, and this might be primarily associated with the potent anti-cancer regimens used to treat them. Acute myeloid leukemia. Thus, we hypothesized that the toxicity of chemotherapy would likely be the predominant factor driving cachexia in this setting. Recently, AML has emerged as a haematological cancer where cachexia is observed [37]. The induction of cachexia during treatment with the firstline defence against AML, the '7+3' chemotherapy induction regimen (CIR) and prior to curative haematopoietic cell transplantation (HSCT), substantially reduces survivability of AML [38-40]. Here we undertook a comprehensive review of cachexia in the AML setting and the contributing factors that underly the onset of this debilitating condition.

VICTORIA UNIVERSITY

THE NEW WAY TO DO UNI

OFFICE FOR RESEARCH TRAINING, QUALITY AND INTEGRITY

DECLARATION OF CO-AUTHORSHIP AND CO-CONTRIBUTION: PAPERS INCORPORATED IN THESIS

This declaration is to be completed for each conjointly authored publication and placed at the beginning of the thesis chapter in which the publication appears.

1. PUBLICATION DETAILS (to be completed by the candidate)

Title of Paper/Journal/Book: Cachectic muscle wasting in acute myeloid leukemia: A sleeping giant with dire clinical consequences

Surname: Campelj

First name: Dean

Institute: Institute for Sustainable Industries and Liveal

Candidate's Contribution (%): 80

Status:

Accepted and in press: ☐ Date:

Published: ☐ Date:

2. CANDIDATE DECLARATION

I declare that the publication above meets the requirements to be included in the thesis as outlined in the HDR Policy and related Procedures – policy.vu.edu.au.

Dean Campelj Digitally signed by Dean Campelj Date: 2021.05.21 12:11:59 +10'00'

Signature **Date**

3. CO-AUTHOR(S) DECLARATION

In the case of the above publication, the following authors contributed to the work as follows:

The undersigned certify that:

1. They meet criteria for authorship in that they have participated in the conception, execution or interpretation of at least that part of the publication in their field of expertise;
2. They take public responsibility for their part of the publication, except for the responsible author who accepts overall responsibility for the publication;

3. There are no other authors of the publication according to these criteria;

4. Potential conflicts of interest have been disclosed to a) granting bodies, b) the editor or publisher of journals or other publications, and c) the head of the responsible academic unit; and

5. The original data will be held for at least five years from the date indicated below and is stored at the following **location(s)**:

VU Research Repository

Name(s) of Co-Author(s)	Contribution (%)	Nature of Contribution	Signature	Date
Cara A Timpani	5	Manuscript review and editing	[redacted]	18/05/21
Emma Rybalka	15	Manuscript review and editing		18/05/21

Updated: September 2019

Campelj DG, Timpani CA, Rybalka E. Cachectic muscle wasting in acute myeloid leukemia: A sleeping giant with dire clinical consequences. Submitted: Journal of Cachexia Sarcopenia and Muscle

Chapter 6

Voluntary activity exacerbates cachexia induction from the acute myeloid leukemia '7+3' chemotherapy induction regimen

Manuscript in preparation.

Preface

Following from the literature review conducted in chapter 6, we decided to evaluate the '7+3' CIR utilized in AML for its capacity to induce cachexia. The CIR is comprised of co-administration of chemotherapeutic agents, daunorubicin, an anthracycline analogue of potent DOX, and the anti-metabolite, cytarabine. These two chemotherapies have never previously been assessed for their relative impact, alone or in combination, on the induction of cachexia or skeletal muscle homeostasis *in vivo*, although some insights are available based upon *in vitro* data for daunorubicin but not cytarabine, in which muscle atrophy was observed in C2C12 skeletal myotubes [41]. We wanted to determine whether body and muscle mass could recover from the insult of the AML CIR after treatment. Thus, we assessed the time course of recovery for 14 days after the conclusion of treatment.

Additionally, we were interested in evaluating the efficacy of exercise as an adjuvant therapeutic strategy to mitigate CIR-induced cachexia. Exercise is a potent stimulus through which to naturally enhance mitochondrial density and function, and thus it may exert many of the protective properties we observed for BGP-15. The modality of exercise selected was voluntary activity, i.e. wheel running. This exercise modality has previously shown benefit to mitigate chemotherapy-induced cachexia [42]. It is also the most likely and accessible form of exercise that AML patients actively undergoing treatment would have in the clinical setting. Thus, we evaluated its protective efficacy alongside administration of the CIR.

We hypothesised that the anti-AML CIR would induce cachexia, skeletal muscle wasting and fatigue and that exercise would protect muscles from wasting during treatment.

Campelj DG, Timpani CA, Goodman CA, Rybalka E. The acute myeloid leukemia '7+3' chemotherapy induction regimen induces cachexia and impairs voluntary activity in healthy mice [Manuscript in preparation]

Chapter 7

Summary, Limitations and Future Directions

7.1 Summary of the major findings

The broad aim of this project was to evaluate the potential of an array of chemotherapeutic agents, administered as either monotherapies or in a clinically compatible multi-agent regimen, to induce cachexia and skeletal myopathy. Further, we wanted to assess the capacity of select mitoprotective adjuvant therapeutic strategies, i.e. SN, BGP-15, and, voluntary activity, to combat chemotherapy-induced cachexia.

As described in Chapter 1, chemotherapy-induced skeletal myopathy is an often-overlooked contributing factor to the induction of cachexia in the cancer setting, with attention heavily focused on the influence of cancer-host interactions. Accumulating evidence in experimental models of cachexia demonstrate that select chemotherapeutic agents rapidly induce cachectic skeletal myopathy, although the underlying mechanisms are similar [1, 25, 46, 104]. Additionally, not all chemotherapeutic agents display cachexia inducing properties, nor have they all been evaluated for their cachectic potential, either alone or in more clinically compatible multi-agent regimens. Indeed, in Part 1 of this thesis, we evaluated three different chemotherapeutic agents, i.e. DOX, IRI and 5FU, for their potential to induce cachexia [32, 50, 105]. In Part 2 of this thesis, we transitioned to a more clinically compatible multi-agent regimen, evaluating the dual delivery of chemotherapies, daunorubicin and cytarabine, constituents of the CIR utilized in AML treatment.

In Chapter 2, we demonstrated that DOX, is a potent cachexia-inducing chemotherapeutic agent – living up to its gold standard reputation [1]. This is despite administering DOX in a low-dose, metronomic regimen to lower the risk of severe systemic toxicity associated with the high-dose, single bolus protocol often described in the literature [2-10]. We demonstrated that DOX-treated mice exhibited fatigue behavior, through reduced ambulation and energy expenditure. This was likely potentiated by underlying oxidative stress as evident by the upregulation of Nrf2, a key regulator of the antioxidant response.

In Chapter 3, we evaluated the potential of IRI as a monotherapy to induce cachexia, outside of its effects as part of the well characterized regimen associated with cachexia induction, FOLFIRI, involving concomitant delivery of 5FU, LEU and IRI [25, 106-108]. Importantly, we demonstrated that IRI-induces cachectic skeletal myopathy, as highlighted by the reduction in body mass and composition indices, and skeletal muscle mass and contractile function. These findings were underscored by a reduction in protein synthesis rate and expression of the cytoskeletal protein, dystrophin. This is the first ever study to highlight that the insult of IRI may promote a type of dystrophinopathy, which has been documented in both cachectic wasting caused by cancer [109].

In Chapter 4, we evaluated the potential of 5FU administration to induce cachexia, another constituent of the FOLFIRI regimen. Interestingly, we demonstrated that 5FU does not induce cachexia, nor does it impact skeletal muscle mass or function. While these findings may be dependent on the metronomic delivery protocol [110], it highlights the notion that not all chemotherapeutic agents induce cachectic skeletal myopathy to the same extent. In particular, chemotherapeutic agents arising from the anti-metabolite class, like 5FU, show no evidence of impairing skeletal muscle mass or function, at least during a 2-week delivery regimen [111-114]. Despite the lack of physiological impact of 5FU on body and skeletal muscle mass, 5FU appeared to prime skeletal muscle for myopathy through a distinct molecular signature. This was highlighted by the increase in p38 MAPK and NF-κB phosphorylation, alongside the reduction in the expression of desmin and dystrophin in skeletal muscle. The latter findings signify that the loss of cytoskeletal proteins from chemotherapy may represent a precursor event prior to the induction of skeletal myopathy, thus uncovering a potential biomarker for early intervention.

Collectively, our studies on mono-chemotherapy agents in Part I enabled important insights but were limited in their clinical compatibility – rarely are chemotherapeutic agents delivered as monotherapies. Typically, they are administered as multi-agent regimens for

varying durations. This provides scope for potential drug interactions and compounding effects of individual drugs over the course of clinical treatment.

In Part 2 of this thesis, we were interested to evaluate the impact of the CIR utilised in AML treatment on skeletal muscle. We chose the AML treatment regimen because muscle mass is integral to treatment success and eligibility for curative HSCT, and there is broad scope for muscle mass to waste during AML treatment for multiple reasons. These include, in addition to chemotherapy and cancer factors, disuse resulting from ward confinement during AML treatment, and the pan cytopenia caused by both the malignancy, and the CIR treatment. In chapter 5, we reviewed this concept and the reasons why skeletal muscle is driven to waste in AML patients, leading to dire consequences regarding survivability. In particular, the intensity of chemotherapeutic treatment strategies, such as the universally utilised CIR, renders chemotherapy as the likely driver of cachexia in AML. It is acknowledged that additional, compounding factors are involved in the progression of this cachexia, including: myelogenous cytopenia-related factors, malnutrition, metabolic dysregulation, and instigation of the inflammatory milieu. Given the relative naivety of cachexia research in AML, we went on to investigate our primary interest in the contribution of chemotherapy as a driver of cachectic skeletal myopathy.

In chapter 6, we developed a novel model of AML CIR-induced cachexia, by administering 7-days of cytarabine concomitant with 3-days of daunorubicin. Indeed, the CIR induced significant cachexia, which was underpinned by the loss of lean and fat mass, skeletal muscle wasting and fatigue, similar to our findings in the DOX model evaluated in Chapter 2. CIR-induced cachexia did not immediately recover after chemotherapy was withdrawn, despite . the mass of the hindlimb skeletal muscles showing capacity to recover during the 2-weeks proceeding CIR treatment. Although body and lean mass did partially recover, CIR-treated animals were still considered cachectic as per the accepted definition at the conclusion of the 2-week recovery period. In this study, we also demonstrated that the CIR induces anemia, which was correlated

with the loss of lean and slow-twitch *soleus* mass. Our data suggest that anemia-related hypoxia may be a key underlying event of CIR-induced cachexia.

Collectively, *this thesis highlights the heterogenous capability of different chemotherapeutic agents to promote cachexia, and when cachexia is induced, similar sequelae are exhibited.*

The secondary aim of this thesis revolved around the evaluation of the therapeutic potential of mitoprotective adjuvant strategies to combat chemotherapy-induced cachexia. In Chapter 2, we investigated SN supplementation alongside DOX administration, given that it has previously displayed therapeutic efficacy to mitigate DOX-induced cardiomyopathy [11, 12]. SN can promote mitoprotection in a DOX-challenged environment through enhancing anti-oxidant activity to mitigate the deleterious impact from DOX-induced oxidative stress [12]. However, our group has previously established that SN promotes myopathy in skeletal muscle disease in which oxidative stress is abundant., i.e. in a murine model of Duchenne muscular dystrophy [13]. Interestingly, SN supplementation afforded no protective therapeutic potential alongside DOX, nor did it promote the onset of skeletal myopathy. This investigation suggests SN supplementation is not an appropriate therapeutic strategy to mitigate DOX-induced cachexia. We predict similar outcomes for SN supplementation as an adjuvant to any chemotherapeutic agent capable of inducing oxidative stress.

In Chapter 3 and 4 we investigated the therapeutic potential of heat-shock protein-70 (HSP-70) co-inducer and poly (ADP-ribose) polymerase-1 (PARP-1) inhibitor, BGP-15, alongside each of IRI and 5FU administration. BGP-15 displayed modest therapeutic potential alongside IRI, by mitigating the induction of cachexia and skeletal muscle myopathy. However, this protective effect was paradoxical in that BGP-15 exacerbated the IRI-induced reduction in protein synthesis, which was associated with further reduction of proteins associated with the DAPC (i.e. dystrophin and β-dystroglycan) in a step-like manner. This may depict remodeling of the contractile apparatus, cytoskeleton and/or the extracellular matrix. It is difficult to conclude from our data

whether BGP-15, when delivered alongside IRI, is beneficial for the skeletal muscular system or not, since on the one hand, BGP-15 mitigated many of the cachectic side-effects of IRI treatment, but on the other hand, it made fast-twitch muscles more prone to tearing, despite rescuing function. It was also difficult to ascertain the therapeutic efficacy of BGP-15 alongside 5FU, given that 5FU did not induce cachexia nor emit physiological consequences to skeletal muscle. BGP-15 did appear to mitigate 5FU-increased in p38 mitogen-activated protein kinase (MAPK) and nuclear factor kappa-light-chain-enhancer of activated B cells (NF-κB) phosphorylation, while increasing mitochondrial density and fusion dynamics. However, BGP-15 did not rescue the reduction in dystrophin and desmin expression from 5FU.

Finally, in Chapter 6, we evaluated the efficacy of voluntary activity alongside administration of the CIR. Interestingly, we demonstrated that voluntary activity exacerbates fat mass loss, driving cachectic wasting. This was underpinned by physical fatigue, including reduced wheel activity, energy expenditure, and, food intake. These insights suggest that rather than therapeutic, exercise therapy might actually promote cachexia during anti-cancer chemotherapy treatment. One reason for this may be that the AML CIR induces erythropenia and anemia, logically resulting in skeletal muscle hypoxia. This finding explains the physical fatigue observed in CIR-treated mice and could represent a novel driver of skeletal muscle cachexia in the AML setting.

7.2 Study Limitations

The specific limitations of each study are highlighted at the end of published/submitted experimental chapters (i.e. Chapters 2-4). Briefly, age of the mice was a key limitation given that in most of our studies, mice were still undergoing their rapid growth period at 6-weeks of age (sexual maturity achieved at approximately 8 weeks). Nevertheless, cachexia manifests across the lifespan [115], with pediatric cancer patients commonly administered chemotherapy, which can elicit lifelong impact on the skeletal muscular system [116, 117]. Thus our findings are still

pertinent and insightful. Secondly, our investigations are only conducted in male mice, thus a clear question remaints: Would the findings in this thesis be mirrored in the female population? Recently, Montalvo *et al.* highlighted sex as a confounding variable that is often overlooked in relation to DOX-induced skeletal myopathy and responsivity to exercise interventions [118]. The inclusion of female in addition to male mice could have provided valuable insights relevant to the clinical treatment of AML, albeit, AML is more prevalent in males than in females [119]. Thirdly, these investigations, while deliberately conducted in cancer-free mice to ascertain the exclusive impact of chemotherapy on the induction of cachexia, do not address the clinical paradigm in which cachexia manifests, i.e. the synergistic insult of both tumor-host interactions and chemotherapy toxicity [44]. Future studies should also ascertain the combined effect of, for example, AML and the CIR on cachexia and fatigue.

In Chapter 6, prominent limitations are observed that warrant a more complete discussion. Because of the COVID-19 pandemic and shut-down of our laboratory facilities for most of 2020, we were unable to mimic our analysis suite as per Chapters 2, 3 and 4. In particular, the ex vivo functional analyses of skeletal muscle contractile properties and the molecular investigations. Additionally, COVID-19 impacted completion of planned animal experiments, including the supplementation of mitochondrial-targeted compound, dimethyl fumarate (reviewed by our laboratory group here [120]), alongside CIR administration (for approved animal ethics application by the Victoria University Animal Ethics Committee see AEETH 20/001). To best utilise time during this period, focus was placed upon on writing and publishing the studies described in Chapters 1-5. Subsequently, there was insufficient candidature time remaining to complete the extensive array of post-mortem analyses on the tissues collected in Chapter 6. This remains a goal of future experiments.

7.3 Future Directions

The investigations undertaken in this thesis and their subsequent findings have prompted questions that warrant future scientific enquiry, including:

1. What is the influence of other chemotherapeutic agents on body mass and skeletal muscle homeostasis? Further, what is the impact of clinically compatible multi-chemotherapeutic agent regimens on body mass and skeletal muscle homeostasis? As highlighted in Chapter 1, not all agents, nor multi-agent regimens, have been evaluated for their cachectic properties. These questions denote a long-term goal of this research area, with this thesis representing a substantial knowledge gain in this effort.
2. Since, the findings of this thesis are predominately derived from younger/adolescent mice, and, that cancer is most frequently observed in the adult population, are there age-dependent effects arising from chemotherapy-induced cachexia? Further, are there long-term perturbations of chemotherapy administration to skeletal muscle homeostasis in aged mice/adult humans? Are there co-impacts on skeletal muscle from sarcopenia (the age-related decline of skeletal muscle mass and function), cancer and chemotherapy?
3. What is the underlying mechanistic interplay between chemotherapy-induced mitochondrial dysfunction and proteostasis? There is evidence that mitochondria regulate protein synthesis according to their energisation state and/or redox balance [121], thus it would be of interest to investigate these signalling cascades in response to chemotoxic stress. Further, can these signalling cascades be targeted to mitigate chemotherapy-induced skeletal muscle wasting and/or dysfunction?
4. Does chemotherapy induce a mild-dystrophinopathy? While our data highlight dystrophin as a target of multiple chemotherapeutic agents (IRI and 5FU), it is currently unclear if the reduction of dystrophin is a cause or a consequence of skeletal myopathy. Subsequently, what are the time-course changes to dystrophin protein expression and binding dynamics to other cytoskeletal structural proteins relative to chemotherapy administration? Do perturbations

in dystrophin abundance and function recover post-chemotherapy? Could dystrophin expression be targeted to protect against or treat chemotherapy-induced muscle cachexia?

5. What are the underlying mechanisms driving CIR-induced cachexia? Pertinent to the findings of this thesis, is normal dystrophin or other cytoskeletal protein expression and function perturbed from CIR administration?
6. What is the role of anemia-related hypoxia in CIR-induced cachexia? Does the synergistic insult of AML and the CIR amplify the impact of anemia-related hypoxia and/or exaggerate the induction of cachexia?

References

1. Hiensch AE, Bolam KA, Mijwel S, Jeneson JAL, Huitema ADR, Kranenburg O, et al. Doxorubicin-induced skeletal muscle atrophy: Elucidating the underlying molecular pathways. Acta Physiol (Oxf). 2019;e13400.

2. Gilliam LA, Lark DS, Reese LR, Torres MJ, Ryan TE, Lin CT, et al. Targeted overexpression of mitochondrial catalase protects against cancer chemotherapy-induced skeletal muscle dysfunction. Am J Physiol Endocrinol Metab. 2016;311:E293-301.

3. Gilliam LAA, Ferreira LF, Bruton JD, Moylan JS, Westerblad H, St Clair DK, et al. Doxorubicin acts through tumor necrosis factor receptor subtype 1 to cause dysfunction of murine skeletal muscle. Journal of applied physiology (Bethesda, Md : 1985). 2009;107:1935-42.

4. Min K, Kwon OS, Smuder AJ, Wiggs MP, Sollanek KJ, Christou DD, et al. Increased mitochondrial emission of reactive oxygen species and calpain activation are required for doxorubicin-induced cardiac and skeletal muscle myopathy. J Physiol. 2015;593:2017-36.

5. Montalvo RN, Doerr V, Min K, Szeto HH, Smuder AJ. Doxorubicin-induced oxidative stress differentially regulates proteolytic signaling in cardiac and skeletal muscle. Am J Physiol Regul Integr Comp Physiol. 2020;318:R227-r33.

6. Smuder AJ, Kavazis AN, Min K, Powers SK. Exercise protects against doxorubicin-induced markers of autophagy signaling in skeletal muscle. J Appl Physiol (1985). 2011;111:1190-8.

7. Smuder AJ, Kavazis AN, Min K, Powers SK. Exercise protects against doxorubicin-induced oxidative stress and proteolysis in skeletal muscle. J Appl Physiol (1985). 2011;110:935-42.

8. Bredahl EC, Pfannenstiel KB, Quinn CJ, Hayward R, Hydock DS. Effects of Exercise on Doxorubicin-Induced Skeletal Muscle Dysfunction. Med Sci Sports Exerc. 2016;48:1468-73.

9. Huertas AM, Morton AB, Hinkey JM, Ichinoseki-Sekine N, Smuder AJ. Modification of Neuromuscular Junction Protein Expression by Exercise and Doxorubicin. Med Sci Sports Exerc. 2020;52:1477-84.

10. Morton AB, Mor Huertas A, Hinkley JM, Ichinoseki-Sekine N, Christou DD, Smuder AJ. Mitochondrial accumulation of doxorubicin in cardiac and diaphragm muscle following exercise preconditioning. Mitochondrion. 2019;45:52-62.

11. Xi L, Zhu SG, Das A, Chen Q, Durrant D, Hobbs DC, et al. Dietary inorganic nitrate alleviates doxorubicin cardiotoxicity: mechanisms and implications. Nitric Oxide. 2012;26:274-84.

12. Zhu SG, Kukreja RC, Das A, Chen Q, Lesnefsky EJ, Xi L. Dietary nitrate supplementation protects against Doxorubicin-induced cardiomyopathy by improving mitochondrial function. J Am Coll Cardiol. 2011;57:2181-9.

13. Timpani CA, Trewin AJ, Stojanovska V, Robinson A, Goodman CA, Nurgali K, et al. Attempting to Compensate for Reduced Neuronal Nitric Oxide Synthase Protein with Nitrate Supplementation Cannot Overcome Metabolic Dysfunction but Rather Has Detrimental Effects in Dystrophin-Deficient mdx Muscle. Neurotherapeutics : the journal of the American Society for Experimental NeuroTherapeutics. 2017;14:429-46.

14. Timpani CA, Mamchaoui K, Butler-Browne G, Rybalka E. Nitric Oxide (NO) and Duchenne Muscular Dystrophy: NO Way to Go? Antioxidants (Basel). 2020;9:

15. Gilliam LA, Moylan JS, Patterson EW, Smith JD, Wilson AS, Rabbani Z, et al. Doxorubicin acts via mitochondrial ROS to stimulate catabolism in C2C12 myotubes. Am J Physiol Cell Physiol. 2012;302:C195-202.

16. Tarpey MD, Amorese AJ, Balestrieri NP, Fisher-Wellman KH, Spangenburg EE. Doxorubicin causes lesions in the electron transport system of skeletal muscle mitochondria that are associated with a loss of contractile function. Journal of Biological Chemistry. 2019;jbc.RA119.00842.

17. Baracos VE, Martin L, Korc M, Guttridge DC, Fearon KCH. Cancer-associated cachexia. Nat Rev Dis Primers. 2018;4:17105.

18. Goldberg RM, Sargent DJ, Morton RF, Fuchs CS, Ramanathan RK, Williamson SK, et al. A randomized controlled trial of fluorouracil plus leucovorin, irinotecan, and oxaliplatin

combinations in patients with previously untreated metastatic colorectal cancer. J Clin Oncol. 2004;22:23-30.

19. McQuade RM, Al Thaalibi M, Petersen AC, Abalo R, Bornstein JC, Rybalka E, et al. Co-treatment With BGP-15 Exacerbates 5-Fluorouracil-Induced Gastrointestinal Dysfunction. Front Neurosci. 2019;13:449.

20. McQuade RM, Carbone SE, Stojanovska V, Rahman A, Gwynne RM, Robinson AM, et al. Role of oxidative stress in oxaliplatin-induced enteric neuropathy and colonic dysmotility in mice. Br J Pharmacol. 2016;173:3502-21.

21. McQuade RM, Stojanovska V, Donald E, Abalo R, Bornstein JC, Nurgali K. Gastrointestinal dysfunction and enteric neurotoxicity following treatment with anticancer chemotherapeutic agent 5-fluorouracil. Neurogastroenterol Motil. 2016;28:1861-75.

22. McQuade RM, Stojanovska V, Donald EL, Rahman AA, Campelj DG, Abalo R, et al. Irinotecan-Induced Gastrointestinal Dysfunction Is Associated with Enteric Neuropathy, but Increased Numbers of Cholinergic Myenteric Neurons. Front Physiol. 2017;8:391.

23. McQuade RM, Stojanovska V, Stavely R, Timpani C, Petersen AC, Abalo R, et al. Oxaliplatin-induced enteric neuronal loss and intestinal dysfunction is prevented by co-treatment with BGP-15. British journal of pharmacology. 2018;175:656-77.

24. Sorensen JC, Petersen AC, Timpani CA, Campelj DG, Cook J, Trewin AJ, et al. BGP-15 Protects against Oxaliplatin-Induced Skeletal Myopathy and Mitochondrial Reactive Oxygen Species Production in Mice. Front Pharmacol. 2017;8:137.

25. Barreto R, Waning DL, Gao H, Liu Y, Zimmers TA, Bonetto A. Chemotherapy-related cachexia is associated with mitochondrial depletion and the activation of ERK1/2 and p38 MAPKs. Oncotarget. 2016;7:43442-60.

26. Horvath O, Ordog K, Bruszt K, Kalman N, Kovacs D, Radnai B, et al. Modulation of Mitochondrial Quality Control Processes by BGP-15 in Oxidative Stress Scenarios: From Cell Culture to Heart Failure. Oxidative Medicine and Cellular Longevity. 2021;2021:6643871.

27. Literati-Nagy Z, Tory K, Literati-Nagy B, Kolonics A, Torok Z, Gombos I, et al. The HSP co-inducer BGP-15 can prevent the metabolic side effects of the atypical antipsychotics. Cell Stress Chaperones. 2012;17:517-21.

28. Racz I, Tory K, Gallyas F, Jr., Berente Z, Osz E, Jaszlits L, et al. BGP-15 - a novel poly(ADP-ribose) polymerase inhibitor - protects against nephrotoxicity of cisplatin without compromising its antitumor activity. Biochem Pharmacol. 2002;63:1099-111.

29. Gehrig SM, van der Poel C, Sayer TA, Schertzer JD, Henstridge DC, Church JE, et al. Hsp72 preserves muscle function and slows progression of severe muscular dystrophy. Nature. 2012;484:394-8.

30. Literati-Nagy B, Tory K, Peitl B, Bajza A, Koranyi L, Literati-Nagy Z, et al. Improvement of insulin sensitivity by a novel drug candidate, BGP-15, in different animal studies. Metabolic syndrome and related disorders. 2014;12:125-31.

31. Salah H, Li M, Cacciani N, Gastaldello S, Ogilvie H, Akkad H, et al. The chaperone co-inducer BGP-15 alleviates ventilation-induced diaphragm dysfunction. Sci Transl Med. 2016;8:350ra103.

32. Campelj DG, Timpani CA, Petersen AC, Hayes A, Goodman CA, Rybalka E. The Paradoxical Effect of PARP Inhibitor BGP-15 on Irinotecan-Induced Cachexia and Skeletal Muscle Dysfunction. Cancers. 2020;12:3810.

33. Biswas AK, Acharyya S. Understanding cachexia in the context of metastatic progression. Nature Reviews Cancer. 2020;20:274-84.

34. Florescu M, Cinteza M, Vinereanu D. Chemotherapy-induced Cardiotoxicity. Maedica (Bucur). 2013;8:59-67.

35. Giglio P, Gilbert MR. Neurologic complications of cancer and its treatment. Curr Oncol Rep. 2010;12:50-9.

36. Maxwell MB, Maher KE. Chemotherapy-induced myelosuppression. Seminars in oncology nursing. 1992;8:113-23.

37. Keng MK, Sidana S, Mukherjee S, Elson P, Seastone DJ, Nazha A, et al. The Degree and Effect Of Weight Loss In Acute Myeloid Leukemia Patients Receiving Induction and Post-Remission Chemotherapy. Blood. 2013;122:3889-.

38. Ando T, Fujisawa S, Teshigawara H, Ogusa E, Ishii Y, Miyashita K, et al. Impact of treatment-related weight changes from diagnosis to hematopoietic stem-cell transplantation on clinical outcome of acute myeloid leukemia. International Journal of Hematology. 2019;109:673-83.

39. Tamaki M, Nakasone H, Nakamura Y, Kawamura M, Kawamura S, Takeshita J, et al. Body Weight Loss Before Allogeneic Hematopoietic Stem Cell Transplantation Predicts Survival Outcomes in Acute Leukemia Patients. Transplantation and Cellular Therapy. 2021;

40. Brauer D, Backhaus D, Pointner R, Vucinic V, Niederwieser D, Platzbecker U, et al. Nutritional Status at Diagnosis and Pre-transplant Weight Loss Impact Outcomes of Acute Myeloid Leukemia Patients Following Allogeneic Stem Cell Transplantation. Hemasphere. 2021;5:e532-e.

41. Amrute-Nayak M, Pegoli G, Holler T, Lopez-Davila AJ, Lanzuolo C, Nayak A. Chemotherapy triggers cachexia by deregulating synergetic function of histone-modifying enzymes. Journal of Cachexia, Sarcopenia and Muscle. 2021;12:159-76.

42. Hojman P, Fjelbye J, Zerahn B, Christensen JF, Dethlefsen C, Lonkvist CK, et al. Voluntary exercise prevents cisplatin-induced muscle wasting during chemotherapy in mice. PLoS One. 2014;9:e109030.

43. Fearon K, Strasser F, Anker SD, Bosaeus I, Bruera E, Fainsinger RL, et al. Definition and classification of cancer cachexia: an international consensus. The Lancet Oncology. 2011;12:489-95.

44. Berardi E, Madaro L, Lozanoska-Ochser B, Adamo S, Thorrez L, Bouche M, et al. A Pound of Flesh: What Cachexia Is and What It Is Not. Diagnostics. 2021;11:116.

45. Conte E, Bresciani E, Rizzi L, Cappellari O, De Luca A, Torsello A, et al. Cisplatin-Induced Skeletal Muscle Dysfunction: Mechanisms and Counteracting Therapeutic Strategies. Int J Mol Sci. 2020;21:

46. Coletti D. Chemotherapy-induced muscle wasting: an update. Eur J Transl Myol. 2018;28:7587-.

47. Ballarò R, Lopalco P, Audrito V, Beltrà M, Pin F, Angelini R, et al. Targeting Mitochondria by SS-31 Ameliorates the Whole Body Energy Status in Cancer- and Chemotherapy-Induced Cachexia. Cancers (Basel). 2021;13:

48. Alves de Lima E, Jr., Teixeira AAS, Biondo LA, Diniz TA, Silveira LS, Coletti D, et al. Exercise Reduces the Resumption of Tumor Growth and Proteolytic Pathways in the Skeletal Muscle of Mice Following Chemotherapy. Cancers (Basel). 2020;12:

49. Damrauer JS, Stadler ME, Acharyya S, Baldwin AS, Couch ME, Guttridge DC. Chemotherapy-induced muscle wasting: association with NF-κB and cancer cachexia. Eur J Transl Myol. 2018;28:7590-.

50. Campelj DG, Debruin DA, Timpani CA, Hayes A, Goodman CA, Rybalka E. Sodium nitrate co-supplementation does not exacerbate low dose metronomic doxorubicin-induced cachexia in healthy mice. Sci Rep. 2020;10:15044.

51. Bozzetti F. Forcing the vicious circle: sarcopenia increases toxicity, decreases response to chemotherapy and worsens with chemotherapy. Annals of Oncology. 2017;28:2107-18.

52. Pin F, Couch ME, Bonetto A. Preservation of muscle mass as a strategy to reduce the toxic effects of cancer chemotherapy on body composition. Curr Opin Support Palliat Care. 2018;12:420-6.

53. Argilés JM, Busquets S, Stemmler B, López-Soriano FJ. Cancer cachexia: understanding the molecular basis. Nat Rev Cancer. 2014;14:754-62.

54. von Haehling S, Anker MS, Anker SD. Prevalence and clinical impact of cachexia in chronic illness in Europe, USA, and Japan: facts and numbers update 2016. Journal of cachexia, sarcopenia and muscle. 2016;7:507-9.

55. Nakamura N, Ninomiya S, Matsumoto T, Nakamura H, Kitagawa J, Shiraki M, et al. Prognostic impact of skeletal muscle assessed by computed tomography in patients with acute myeloid leukemia. Ann Hematol. 2019;98:351-9.

56. Jung J, Lee E, Shim H, Park JH, Eom HS, Lee H. Prediction of clinical outcomes through assessment of sarcopenia and adipopenia using computed tomography in adult patients with acute myeloid leukemia. Int J Hematol. 2021;

57. Short NJ, Rytting ME, Cortes JE. Acute myeloid leukaemia. The Lancet. 2018;392:593-606.

58. Yates JW, Wallace HJ, Jr., Ellison RR, Holland JF. Cytosine arabinoside (NSC-63878) and daunorubicin (NSC-83142) therapy in acute nonlymphocytic leukemia. Cancer chemotherapy reports. 1973;57:485-8.

59. Short NJ, Konopleva M, Kadia TM, Borthakur G, Ravandi F, DiNardo CD, et al. Advances in the Treatment of Acute Myeloid Leukemia: New Drugs and New Challenges. Cancer discovery. 2020;10:506-25.

60. Loh KP, Dunne RF, Friedberg JW, Mohile SG. Integrating Assessment of Sarcopenia into Decision-making for Allogeneic Hematopoietic Cell Transplantation: Ready for Prime Time? J Natl Cancer Inst. 2019;

61. de Lima EA, de Sousa LGO, de STAA, Marshall AG, Zanchi NE, Neto JCR. Aerobic exercise, but not metformin, prevents reduction of muscular performance by AMPk activation in mice on doxorubicin chemotherapy. J Cell Physiol. 2018;233:9652-62.

62. Hulmi JJ, Nissinen TA, Rasanen M, Degerman J, Lautaoja JH, Hemanthakumar KA, et al. Prevention of chemotherapy-induced cachexia by ACVR2B ligand blocking has different effects on heart and skeletal muscle. J Cachexia Sarcopenia Muscle. 2018;9:417-32.

63. Alibhai SM, Leach M, Kowgier ME, Tomlinson GA, Brandwein JM, Minden MD. Fatigue in older adults with acute myeloid leukemia: predictors and associations with quality of life and functional status. Leukemia. 2007;21:845-8.

64. Schumacher A, Wewers D, Heinecke A, Sauerland C, Koch OM, van de Loo J, et al. Fatigue as an important aspect of quality of life in patients with acute myeloid leukemia. Leuk Res. 2002;26:355-62.

65. Schumacher A, Kessler T, Büchner T, Wewers D, van de Loo J. Quality of life in adult patients with acute myeloid leukemia receiving intensive and prolonged chemotherapy -- a longitudinal study. Leukemia. 1998;12:586-92.

66. Bryant AL, Deal AM, Battaglini CL, Phillips B, Pergolotti M, Coffman E, et al. The Effects of Exercise on Patient-Reported Outcomes and Performance-Based Physical Function in Adults With Acute Leukemia Undergoing Induction Therapy: Exercise and Quality of Life in Acute Leukemia (EQUAL). Integrative cancer therapies. 2018;17:263-70.

67. Klepin HD, Danhauer SC, Tooze JA, Stott K, Daley K, Vishnevsky T, et al. Exercise for older adult inpatients with acute myelogenous leukemia: A pilot study. Journal of geriatric oncology. 2011;2:11-7.

68. Jones LW, Alfano CM. Exercise-oncology research: past, present, and future. Acta Oncol. 2013;52:195-215.

69. Hardee JP, Counts BR, Carson JA. Understanding the Role of Exercise in Cancer Cachexia Therapy. American journal of lifestyle medicine. 2017;13:46-60.

70. Miyagi MY, Seelaender M, Castoldi A, de Almeida DC, Bacurau AV, Andrade-Oliveira V, et al. Long-term aerobic exercise protects against cisplatin-induced nephrotoxicity by modulating the expression of IL-6 and HO-1. PLoS One. 2014;9:e108543.

71. Pigna E, Berardi E, Aulino P, Rizzuto E, Zampieri S, Carraro U, et al. Aerobic Exercise and Pharmacological Treatments Counteract Cachexia by Modulating Autophagy in Colon Cancer. Scientific Reports. 2016;6:26991.

72. Bowen TS, Schuler G, Adams V. Skeletal muscle wasting in cachexia and sarcopenia: molecular pathophysiology and impact of exercise training. Journal of cachexia, sarcopenia and muscle. 2015;6:197-207.

73. Taylor SJ, Duyvestyn JM, Dagger SA, Dishington EJ, Rinaldi CA, Dovey OM, et al. Preventing chemotherapy-induced myelosuppression by repurposing the FLT3 inhibitor quizartinib. Science Translational Medicine. 2017;9:eaam8060.

74. Favier FB, Britto FA, Freyssenet DG, Bigard XA, Benoit H. HIF-1-driven skeletal muscle adaptations to chronic hypoxia: molecular insights into muscle physiology. Cellular and Molecular Life Sciences. 2015;72:4681-96.

75. Bogue MA, Philip VM, Walton DO, Grubb SC, Dunn MH, Kolishovski G, et al. Mouse Phenome Database: a data repository and analysis suite for curated primary mouse phenotype data. Nucleic acids research. 2020;48:D716-d23.

76. Rosa-Caldwell ME, Greene NP. Muscle metabolism and atrophy: let's talk about sex. Biology of Sex Differences. 2019;10:43.

77. Maral RJ, Jouanne M. Toxicology of daunorubicin in animals and man. Cancer treatment reports. 1981;65 Suppl 4:9-18.

78. Ellison RR, Holland JF, Weil M, Jacquillat C, Boiron M, Bernard J, et al. Arabinosyl cytosine: a useful agent in the treatment of acute leukemia in adults. Blood. 1968;32:507-23.

79. Nair AB, Jacob S. A simple practice guide for dose conversion between animals and human. Journal of basic and clinical pharmacy. 2016;7:27-31.

80. Even PC, Nadkarni NA. Indirect calorimetry in laboratory mice and rats: principles, practical considerations, interpretation and perspectives. Am J Physiol Regul Integr Comp Physiol. 2012;303:R459-76.

81. Timpani CA, Goodman CA, Stathis CG, White JD, Mamchaoui K, Butler-Browne G, et al. Adenylosuccinic acid therapy ameliorates murine Duchenne Muscular Dystrophy. Sci Rep. 2020;10:1125.

82. Gilliam LA, St Clair DK. Chemotherapy-induced weakness and fatigue in skeletal muscle: the role of oxidative stress. Antioxid Redox Signal. 2011;15:2543-63.

83. Dantzer R. Cytokine, sickness behavior, and depression. Immunology and allergy clinics of North America. 2009;29:247-64.

84. Muscaritoli M, Anker SD, Argilés J, Aversa Z, Bauer JM, Biolo G, et al. Consensus definition of sarcopenia, cachexia and pre-cachexia: joint document elaborated by Special Interest Groups (SIG) "cachexia-anorexia in chronic wasting diseases" and "nutrition in geriatrics". Clin Nutr. 2010;29:154-9.

85. Sartori R, Romanello V, Sandri M. Mechanisms of muscle atrophy and hypertrophy: implications in health and disease. Nat Commun. 2021;12:330.

86. Leliefeld PHC, Koenderman L, Pillay J. How Neutrophils Shape Adaptive Immune Responses. Frontiers in immunology. 2015;6:

87. Hueso T, Ekpe K, Mayeur C, Gatse A, Joncquel-Chevallier Curt M, Gricourt G, et al. Impact and consequences of intensive chemotherapy on intestinal barrier and microbiota in acute myeloid leukemia: the role of mucosal strengthening. Gut Microbes. 2020;12:1800897-.

88. Lichtman MA. A historical perspective on the development of the cytarabine (7days) and daunorubicin (3days) treatment regimen for acute myelogenous leukemia: 2013 the 40th anniversary of 7+3. Blood Cells Mol Dis. 2013;50:119-30.

89. Prado CM, Anker SD, Coats AJS, Laviano A, von Haehling S. Nutrition in the spotlight in cachexia, sarcopenia and muscle: avoiding the wildfire. Journal of Cachexia, Sarcopenia and Muscle. 2021;12:3-8.

90. Zombeck JA, Fey EG, Lyng GD, Sonis ST. A clinically translatable mouse model for chemotherapy-related fatigue. Comp Med. 2013;63:491-7.

91. Ray MA, Trammell RA, Verhulst S, Ran S, Toth LA. Development of a mouse model for assessing fatigue during chemotherapy. Comp Med. 2011;61:119-30.

92. Allen DG, Lamb GD, Westerblad H. Skeletal Muscle Fatigue: Cellular Mechanisms. Physiological Reviews. 2008;88:287-332.

93. Alibhai SMH, O'Neill S, Fisher-Schlombs K, Breunis H, Brandwein JM, Timilshina N, et al. A clinical trial of supervised exercise for adult inpatients with acute myeloid leukemia (AML) undergoing induction chemotherapy. Leukemia research. 2012;36:1255-61.

94. Sullivan KA, Grant CV, Jordan KR, Vickery SS, Pyter LM. Voluntary wheel running ameliorates select paclitaxel chemotherapy-induced sickness behaviors and associated melanocortin signaling. Behav Brain Res. 2020;399:113041.

95. Mul JD, Soto M, Cahill ME, Ryan RE, Takahashi H, So K, et al. Voluntary wheel running promotes resilience to chronic social defeat stress in mice: a role for nucleus accumbens ΔFosB. Neuropsychopharmacology. 2018;43:1934-42.

96. Banjanin S, Mrosovsky N. Preferences of mice, Mus musculus, for different types of running wheel. Laboratory animals. 2000;34:313-8.

97. Ballaro R, Beltra M, De Lucia S, Pin F, Ranjbar K, Hulmi JJ, et al. Moderate exercise in mice improves cancer plus chemotherapy-induced muscle wasting and mitochondrial alterations. FASEB J. 2019;33:5482-94.

98. Manzanares G, Brito-da-Silva G, Gandra PG. Voluntary wheel running: patterns and physiological effects in mice. Brazilian journal of medical and biological research = Revista brasileira de pesquisas medicas e biologicas. 2018;52:e7830-e.

99. Solheim TS, Laird BJA, Balstad TR, Bye A, Stene G, Baracos V, et al. Cancer cachexia: rationale for the MENAC (Multimodal-Exercise, Nutrition and Anti-inflammatory medication for Cachexia) trial. BMJ supportive & palliative care. 2018;8:258-65.

100. Slot IGM, Schols AMWJ, Vosse BAH, Kelders MCJM, Gosker HR. Hypoxia differentially regulates muscle oxidative fiber type and metabolism in a HIF-1α-dependent manner. Cellular Signalling. 2014;26:1837-45.

101. Sorensen JC, Cheregi BD, Timpani CA, Nurgali K, Hayes A, Rybalka E. Mitochondria: Inadvertent targets in chemotherapy-induced skeletal muscle toxicity and wasting? Cancer Chemother Pharmacol. 2016;78:673-83.

102. Gouspillou G, Scheede-Bergdahl C, Spendiff S, Vuda M, Meehan B, Mlynarski H, et al. Anthracycline-containing chemotherapy causes long-term impairment of mitochondrial respiration and increased reactive oxygen species release in skeletal muscle. Sci Rep. 2015;5:8717.

103. Freire PP, Fernandez GJ, de Moraes D, Cury SS, Dal Pai-Silva M, Dos Reis PP, et al. The expression landscape of cachexia-inducing factors in human cancers. J Cachexia Sarcopenia Muscle. 2020;11:947-61.

104. Moreira-Pais A, Ferreira R, Gil da Costa R. Platinum-induced muscle wasting in cancer chemotherapy: Mechanisms and potential targets for therapeutic intervention. Life Sci. 2018;208:1-9.

105. Campelj DG, Timpani CA, Cree T, Petersen AC, Hayes A, Goodman CA, et al. Metronomic 5-Fluorouracil Delivery Primes Skeletal Muscle for Myopathy but Does Not Cause Cachexia. Pharmaceuticals. 2021;14:478.

106. Barreto R, Kitase Y, Matsumoto T, Pin F, Colston KC, Couch KE, et al. ACVR2B/Fc counteracts chemotherapy-induced loss of muscle and bone mass. Sci Rep. 2017;7:14470.

107. Barreto R, Mandili G, Witzmann FA, Novelli F, Zimmers TA, Bonetto A. Cancer and Chemotherapy Contribute to Muscle Loss by Activating Common Signaling Pathways. Front Physiol. 2016;7:472.

108. Pin F, Barreto R, Couch ME, Bonetto A, O'Connell TM. Cachexia induced by cancer and chemotherapy yield distinct perturbations to energy metabolism. J Cachexia Sarcopenia Muscle. 2019;10:140-54.

109. Acharyya S, Butchbach ME, Sahenk Z, Wang H, Saji M, Carathers M, et al. Dystrophin glycoprotein complex dysfunction: a regulatory link between muscular dystrophy and cancer cachexia. Cancer Cell. 2005;8:421-32.

110. Chen H, Xu C, Zhang F, Liu Y, Guo Y, Yao Q. The gut microbiota attenuates muscle wasting by regulating energy metabolism in chemotherapy-induced malnutrition rats. Cancer Chemother Pharmacol. 2020;

111. Chen M-C, Chen Y-L, Lee C-F, Hung C-H, Chou T-C. Supplementation of Magnolol Attenuates Skeletal Muscle Atrophy in Bladder Cancer-Bearing Mice Undergoing Chemotherapy via Suppression of FoxO3 Activation and Induction of IGF-1. PloS one. 2015;10:e0143594-e.

112. Chen M-C, Hsu W-L, Hwang P-A, Chen Y-L, Chou T-C. Combined administration of fucoidan ameliorates tumor and chemotherapy-induced skeletal muscle atrophy in bladder cancer-bearing mice. Oncotarget. 2016;7:51608-18.

113. Smith RC, Cramer MS, Mitchell PJ, Capen A, Huber L, Wang R, et al. Myostatin Neutralization Results in Preservation of Muscle Mass and Strength in Preclinical Models of Tumor-Induced Muscle Wasting. Molecular cancer therapeutics. 2015;14:1661-70.

114. VanderVeen BN, Sougiannis AT, Velazquez KT, Carson JA, Fan D, Murphy EA. The Acute Effects of 5 Fluorouracil on Skeletal Muscle Resident and Infiltrating Immune Cells in Mice. Front Physiol. 2020;11:593468.

115. Couluris M, Mayer JLR, Freyer DR, Sandler E, Xu P, Krischer JP. The effect of cyproheptadine hydrochloride (periactin) and megestrol acetate (megace) on weight in children with cancer/treatment-related cachexia. J Pediatr Hematol Oncol. 2008;30:791-7.

116. Scheede-Bergdahl C, Jagoe RT. After the chemotherapy: potential mechanisms for chemotherapy-induced delayed skeletal muscle dysfunction in survivors of acute lymphoblastic leukaemia in childhood. Frontiers in pharmacology. 2013;4:49-.

117. Boland AM, Gibson TM, Lu L, Kaste SC, DeLany JP, Partin RE, et al. Dietary Protein Intake and Lean Muscle Mass in Survivors of Childhood Acute Lymphoblastic Leukemia: Report From the St. Jude Lifetime Cohort Study. Phys Ther. 2016;96:1029-38.

118. Montalvo RN, Doerr V, Nguyen BL, Kelley RC, Smuder AJ. Consideration of Sex as a Biological Variable in the Development of Doxorubicin Myotoxicity and the Efficacy of Exercise as a Therapeutic Intervention. Antioxidants (Basel). 2021;10:

119. De-Morgan A, Meggendorfer M, Haferlach C, Shlush L. Male predominance in AML is associated with specific preleukemic mutations. Leukemia. 2021;35:867-70.

120. Kourakis S, Timpani CA, de Haan JB, Gueven N, Fischer D, Rybalka E. Dimethyl Fumarate and Its Esters: A Drug with Broad Clinical Utility? Pharmaceuticals (Basel). 2020;13:306.

121. Topf U, Wrobel L, Chacinska A. Chatty Mitochondria: Keeping Balance in Cellular Protein Homeostasis. Trends Cell Biol. 2016;26:577-86.